Laser-Induced Breakdown Spectroscopy for the Characterization and Investigation of (Micro)Plastics and Their Weathering-Induced Oxidation Behavior

Dissertation

zur Erlangung des Doktorgrades
der Naturwissenschaften
(Dr. rer. nat.)
dem Fachbereich Physik
der Philipps-Universität Marburg

vorgelegt von

Caroline Coyllur Sommer

aus

Kassel

Marburg, 2023

Vom Fachbereich Physik der Philipps-Universität als Dissertation angenommen am: 29.01.2024
Erstgutachter: Prof. Dr. Martin Koch
Zweitgutachter: Prof. Dr. Jan Goldschmidt
Tag der mündlichen Prüfung: 20.02.2024
Hochschulkennziffer: 1180

Everything on me was found inside the stomachs of sea turtles - so sad

Paris Hilton

Acknowledgements

I would like to express my gratitude to all those who have made this work possible and have accompanied me along this journey. Over the past few years, I have been able to rise above myself, learned about my strengths and weaknesses, and was able to become an active member of the scientific community, which I greatly appreciate. All this would not have been possible without the help of the following people:

First and foremost, I would like to thank Prof. Dr. Martin Koch for supervising my doctoral thesis, giving me the opportunity to work in his research group, and encouraging me to pursue a career in academia. The trust he placed in me with this topic has been highly appreciated. His guidance and advice have carried me through all phases of my research. Prof. Koch's positivity and excitement for academics and research were very helpful in times of struggle. I am grateful for many fruitful discussions, the freedom to conduct my research, and the free beer at Christmas parties. I am grateful to Prof. Koch for enabling me to present my work at various international conferences over the years. These gatherings usually featured informative, inspirational, and entertaining discussions, novel ideas and concepts, as well as networking opportunities with fellow scientists. I would also like to thank Prof. Dr. Jan Goldschmidt for agreeing to be the second examiner of this work, and the other examiners of the examination board, Prof. Dr. Heinz Jänsch and Prof. Dr. Peter Lenz.

During my time as a doctoral student, I had the pleasure of working in the microplastics research group of the AG, consisting of Julia Prume, Srumika Konde, Dr. Johnny Nguyen, Dr. Stefan Brackmann, and Dr. Maximilian Schneider. Thank you for the support and the discussions about current and upcoming projects. I would also like to thank Teresa Menzel and Prof. Dr. Holger Ruckdäschel for the great collaboration in our joint research projects. Many thanks to Franzi Hüppe who accompanied me as a very good friend during my studies and my PhD and convinced me to become a part of Prof. Koch's working group. I would like to thank Maya Strobel for always brightening my mood and helping with the bureaucratic matters at the university. I am also thankful to Rüdiger Rink for his assistance with mechanical components. I appreciate the members of Prof. Wolfram Heimbrodt's working group for making their laboratories available to me so that I could conduct my research. In this context, special thanks go to Mikko Wilhelm, who taught me everything I know about experimental physics and working in a lab, and to Luise Rost for all the coffee breaks and for making me laugh in tough times. I am thankful to the Mensa crews at Lahnberge and Renthof, Jan Ornik, Alexander Jäckel, Cornelius Mach, Lara Heidrich, Jochen Taiber, Mikko Wilhelm, Luise Rost, Felix Gorka, and Alexander Schauerte. Thank you for also being too lazy to cook and keeping me company. The lunch breaks together created a great and fun working atmosphere that I will miss very much.

I was fortunate enough to supervise and work alongside driven interns and students (Nastas Bourdin, Augustine Ndukwe, Maik Wehn, Fatima Jaadi, and Katharina Lautze), whose efforts and insightful suggestions made a significant impact on this project.

Dr. Istemi Kuzu from the former AG Dehnen and Dr. Frank Noll, Dr. Hee-Cheol Kim, and Nima Heidary from AG Hampp should not be overlooked while expressing gratitude. I sincerely appreciate them for providing the FTIR system and the profilometer.

Last but not least, I would like to thank my family and my friends, especially my roommates and my Band members for all their support and essential distractions. I would like to thank especially Kevin, Franzi, Lisa, and Paula for their wonderful friendship over the years and for being there when it mattered most. To my parents: Muchas gracias por apoyarme siempre y por hacerlo todo posible para mí. I would also like to thank the federal employment agency *Bundesagentur für Arbeit* for their financial support in the writing of this work.

Leipzig, November 2023
Caroline Sommer

Contents

List of Figures

List of Tables

List of Abbreviations

ASTM	American Society for Testing and Materials
ATR	Attenuated total reflectance
BS	British Standard
CARS	Coherent anti-Stokes Raman spectroscopy
COVID-19	Coronavirus disease 2019
DIN	Deutsches Institut für Normung
DSC	Differential scanning calorimetry
EDX	Energy Dispersive X-ray-Spectroscopy
EEA	European Environment Agency
ESEM	Environmental SEM
FE-SEM	Field emission SEM
FTIR	Fourier transform infrared spectroscopy
FWHM	Full width at half maximum
GC	Gas chromatography
HDPE	High-density PE
ICCD	(Intensified) charge-coupled device
IR	Infrared
ISO	International Organization for Standardisation
LDPE	Low-density PE
LIBS	Laser-induced breakdown spectroscopy
LTE	Local thermodynamic equilibrium
MPSS	MicroPlastic Sediment Separator
MS	Mass spectrometry
Nd:YAG	Neodymium-doped yttrium aluminum garnet
PA	Polyamide
PA6	Polyamide 6 (Nylon)
PC	Polycarbonate
PCA	Principal component analysis

PCs	Principal components
PE	Polyethylene
PET	Polyethylene terephthalate
PP	Polypropylene
PS	Polystyrene
PVC	Polyvinyl chloride
py-GC-MS	Pyrolysis gas chromatography-mass spectrometry
Q-switch	Variable attenuator to influence the quality factor of the laser resonator
SEM	Scanning electron microscopy
SEM-EDX	SEM Energy dispersive X-ray spectroscopy
SNR	Signal-to-noise ratio
SUPD	Single-Use Plastic Directive
SVM	Support vector machine
TE-MCT	Thermo-electrically cooled mercury-cadmium-telluride detector
TGA	Thermal gravimetric analysis
UV light	Ultraviolet light (typically in the range of 100 nm–380 nm)

List of Symbols

$\mathbf{C_2}$	Radical diatomic carbon band (*Swan Band*)
Ca	Calcium
Cl	Chlorine
CN	Cyano radical band
Cu	Copper
C	Carbon
$\mathbf{H_\alpha}$, $\mathbf{H_\beta}$, $\mathbf{H_\epsilon}$	Spectral lines of the hydrogen atom of the Balmer series
H	Hydrogen
K	Potassium
Na	Sodium
N	Nitrogen
O	Oxygen
R	Polymer backbone
$\bullet$	denotes radical
$\Delta\lambda_{line}$	Spectral line width (FWHM)
$\Delta\lambda_{Stark}$	Stark line width (FWHM)
ΔE	Energy difference
κ	Thermal diffusivity
$\lambda_{(i,j)}$	Wavelength
π	circle constant (number Pi)
ρ	Material density
τ_ρ	Laser pulse width
$A_{(i)}$	Transition probability
B	Coefficient for ionic or neutral lines
C_p	Specific heat
CI	Carbonyl index
c	Vacuum speed of light
D_A	Ablation depth

D	Ion broadening parameter
$E_{i,j}$	Energy levels i and j
E	Laser pulse energy
f_M	Maxwellian velocity distribution function
F	Fluence/ energy density
$g_{(i,j)}$	Statistical weights/ degeneracy
h	Planck constant
I_{min}	Minimum laser irradiance (for vaporization)
I	Spectral line intensity
k	Boltzmann constant
L_v	Latent heat
M	(Ablation) mass
m	Electron mass
N_0	Total species population
N_D	Number of particles in the Debye sphere
n_e	Electron density
$N_{i,j}$	Population of energy levels
R_s	Surface reflectivity
SA	Self-absorption coefficient
sr	Steradian (unit of the solid angle)
T_0	Room temperature
T_b	Boiling temperature
t_d	Time delay
t_g	Acquisition window/ gate delay
T_g	Glass transition temperature
T	Electron excitation temperature
v	Electron speed
w	Electron broadening parameter
Z	Partition function

Chapter 1

Introduction

The increasing environmental pollution caused by plastics is undeniably a significant challenge for modern society. The original purpose of plastics, whose theory was developed by Hermann Staudinger in the early 1920s and recognized with the 1953 Nobel Prize in Chemistry [90], was to improve people's living conditions. Because of their countless advantages over other materials, such as durability, affordability, lightweight, and versatility, plastics are still considered revolutionary [190]. Given the current environmental problems related to plastic pollution, such as biodiversity loss or its impact on climate change [152], and the increasing plastic production [11], it is crucial to gain a deeper understanding of the interaction between plastics and the environment. This dissertation begins by elaborating on the weathering-induced oxidation behavior of different plastic types and its possible relevance for plastics' risk assessment. The focus of this thesis then lies in the presentation of a new identification and characterization method for (micro)plastics, which concentrates on the investigation of depth-related weathering-induced oxidation.

The importance of plastics in today's society has become particularly clear in recent years. The COVID-19 pandemic has demonstrated how indispensable plastic is in the healthcare sector and public health safety [150], and also how much it is used in private household products, such as takeaway, online shopping, and food delivery [159]. Although many of these plastic products can be avoided or replaced with sustainable alternatives, it is clear that plastic is an essential part of our lives. In 2020, the European industry generated nearly 25 million tons of plastic waste, which emitted 95 million tons of CO_2, one-third of which was due to plastic incineration [190]. In comparison, only 14 % of plastic waste was recycled and reused in Europe [190]. According to a report by the European Environment Agency (EEA) on the effects of plastics on climate and the environment, the plastics industry is expected to contribute 20 % of the world's oil consumption by 2050 (up from today's 7 %) if the predicted growth in plastic production and consumption holds true [139]. While plastic production declined in 2020 due to the COVID-19 pandemic, European production came back

with an even greater increase in 2021 compared to previous years [160]. Given that over 90 % of plastics are petroleum-based, non-biodegradable, and water-insoluble [198, 219], a rapid change in mindset is needed among manufacturers, governments, civil society, and consumers to promote sustainability and a reduction of the carbon footprint [115, 152, 159, 190].

At the political level, several goals have been formulated in recent years, such as the *European Green Deal* [67, 70], the *Circular Plastics Alliance* [44, 208], or the *Paris* [192] and *Glasgow climate agreements* [193]. Like other industries, the European plastics system must adapt to meet these goals. Many actions have already been introduced or are in the process of being implemented, such as the introduction of the *Single-Use Plastic Directive* (SUPD), the realization of various policies to increase recycling rates, the prohibition on EU member states deposing more than 10 % of their municipal solid waste in landfills after 2035, and limitations of international waste trade, such as China's ban on waste import [68, 190]. However, recent reports show that although the European plastics system is adjusting, it still needs to be faster to face the challenges of climate change and pollution [159, 160, 190]. Additional innovative approaches have been proposed to achieve faster change, such as integrating circular economy ideas in the plastics value chain or decoupling plastics from fossil fuel feedstocks [78, 109, 190]. As research continues on this solution and its implementation will take time, it remains open on how to deal with the plastic that has already entered the environment. Various organizations have been formed to address this problem. Examples include the EU-funded project *In-No-Plastic*, which focuses on preventing, removing, and reusing plastic waste from the ocean [96], or the non-profit organization *The Ocean Cleanup*, which develops and promotes technologies to remove the oceans from plastic [191].

Plastics that find their way into the environment are difficult to remove. This is because they age and break down into smaller fragments by physical, chemical, and biological processes [166, 198, 210], affecting terrestrial [56] and aquatic ecosystems [55, 170], as well as human health [48, 210]. The solid plastic fragments are commonly referred to as *microplastics* if their size is between 1 µm and 5 mm, or *nanoplastics* if they are smaller than 1 µm [71]. The former can be divided into *primary* and *secondary* microplastics, which account for 15-30 % and 70-80 % of all microplastics in the environment, respectively [109, 130]. Primary microplastics include particles produced to be of small size for commercial purposes. They are used, for instance, in toothpaste, cosmetics, or plastic nurdles (tiny lentil-sized plastic pellets from pre-production) [45, 130, 176]. Secondary microplastics refer to particles generated from large plastic debris due to environmental factors, mainly weathering caused by UV radiation [11, 45]. Both types enter the oceans through wastewater, beach litter, illegal dumping, and runoff from roads [73]. This illustrates that multiple sources are contributing to the environmental accumulation of microplastic particles.

As particle size decreases, not only does the detection and, ultimately, the removal pro-

cesses become more complicated, but also the ecological risks of plastic particles increase as more organisms can consume them. The way that microplastics interact with pollutants and accumulate in the biota is influenced by their size, form, color, and age [8, 58, 220]. As plastic items break down, the surface-to-volume ratio increases, and persistent organic and hydrophobic pollutants, trace metals, and harmful additives can be absorbed, often in amounts many times greater than in the surrounding environment [18, 77, 109, 146]. Microplastics can then serve as vectors by increasing the bioavailability of pollutants, especially in organisms, ecosystems, and food chains [8, 109]. Because of this characteristic, microplastics are frequently referred to as a *Trojan Horse* in the literature [69, 91, 93]. Additionally, often harmful additives, such as stabilizers, plasticizers, antimicrobials, or flame retardants, are intentionally added to plastics during the manufacturing process to optimize their physical attributes [84]. These additives may leak into the environment during the breakdown process since they are not covalently linked to the polymer [77, 186, 189]. For color pigments, there is the additional risk factor of aquatic organisms absorbing them, as some organisms are visual predators and tend to consume microplastics whose color resembles their food [54, 220]. It is precisely these chemicals associated with (micro)plastics, either ingested externally (e.g., pollutants) or intentionally induced (e.g., additives), that make plastics a potential hazard suspected of reducing growth and fertility [2, 108, 217], weakening the immune system [175, 214], and causing deformities in the reproductive organs of animals and humans [129].

Although physical degradation, resulting in fragmentation, increased surface area, porosity, or roughness, is primarily associated with the weathering of plastics, it is the chemical degradation that plays an integral part in assessing the potential hazard of (micro)plastics [77]. Chemical degradation, more specifically photo-oxidation, is regarded as the primary mechanism responsible for plastic degradation [12, 77, 131, 165]. Plastics can undergo chemical changes that alter their functional groups and other characteristics when exposed to ultraviolet (UV) light and oxygen [8, 77]. This can result in the production of hazardous byproducts [8, 77]. In this sense, the *age* of plastic plays an important role, as it is crucial for forming these byproducts. The longer plastics remain in the environment and are exposed to environmental effects, such as radiation or oxidation, the more likely and severe their toxicity [131]. It has also been found that aged plastics have higher concentrations of absorbed pollutants than unaged plastic particles [131]. Thus, assessing the toxicity of plastics in the environment requires careful consideration of their age. In addition, it is also suspected that age could provide information about the origin and fate of plastic particles that have been transported long distances through the air or water [147]. This could be beneficial for validating particle tracking models used to determine the behavior of plastics in the ocean or to predict their abundance [97].

However, determining the age is not easy. Only recently, a study presented for the first

time a method for estimating the age of marine polyethylene (PE) microplastics [147]. Here *age* is associated with the UV radiation exposure time. Since a plastic particle's time in the environment cannot be monitored retrospectively, the authors used the chemical bond structure of microplastics exposed to sunlight and oxygen on land and those collected from the ocean, as well as their molecular weight [147]. They converted this information into a time scale based on data from field and accelerated exposure experiments. They were then able to assign an age of up to five years to the microplastic samples. This research motivates further studies into weathering-induced oxidation.

Another recently published study also concludes that weathering-induced degradation is essential for predicting microplastics' fate in the environment [26]. Here, the authors developed a prediction model for microplastic formation based on their base polymer's mechanical and physical properties [26]. Although there are many studies on the accumulation of (micro)plastics in the environment [20, 108, 213], little is still known about the degradation rates of different polymer types [21, 34], making this study an important milestone in microplastics research. However, the study did not include UV degradation of plastics in the calculations. The authors emphasize that their results are only an approximation and that UV degradation is expected to play an important role in the emergence of microplastics in the environment [26].

To curb (micro)plastic pollution, a comprehensive understanding of the life cycle of plastic in the environment is needed. In this sense, it is essential to determine the composition of the particles, such as their base polymer and chemical additives, as well as the degradation processes and products [98]. Both are necessary to make predictions about the long-term fate of plastic waste in the future and to assess potential environmental hazards that are due to one or more of the following reasons [131]:

- toxic chemicals derived from the base polymer itself, such as residual monomers and oligomers,
- additives added to the plastic sample during manufacture or processing,
- pollutants absorbed by the plastic particles in the environment.

To date, the accumulation, transfer, and release of pollutants have been primarily decisive for the evaluation of the toxicity of plastics [131]. However, consideration should be given to relating toxicity to the age of a plastic particle, as it relates to the formation of the above-listed contaminants.

Over the years, several methods have been developed to study (micro)plastics and their weathering-induced degradation. In this context, the suitability of a method always depends on the research question. The wide variety of methods demonstrates the complexity of microplastic investigation. Mass-based and particle-based methods are used for identification

and quantification [21, 98, 109]. The former include *differential scanning calorimetry* (DSC), *thermal gravimetric analysis* (TGA), or *pyrolysis gas chromatography-mass spectrometry* (py-GC-MS), which are based on the thermal properties of a sample [94, 130]. The latter include microscopy and spectroscopic methods, such as *Raman* and *Fourier transform infrared spectroscopy* (FTIR) [98].

When determining degradation, it is not sufficient to analyze only the sample's surface, as is usually the case when characterizing morphological or chemical changes. However, a layer-by-layer analysis should be performed. Surface analysis is insufficient because degradation also occurs inside the plastic samples [134, 136], resulting in further embrittlement and fragmentation [77]. In addition, degradation is usually heterogeneous, as it depends on the environmental exposure and the homogeneity of the plastic samples [42]. Heterogeneous degradation profiles should be studied to confidently predict plastic's lifetime and evaluate the degradation processes and rates [42]. A layer-by-layer analysis can give additional insight into the weathering of plastics, as shown elsewhere [134, 136]. The degradation effect is usually investigated using FTIR or *Energy-dispersive X-ray spectroscopy* on a *scanning electron microscope* (SEM-EDX) [136, 141]. For them to perform a layer-by-layer analysis, the cross-section of a sample must first be exposed, for example, with a microtome [136, 141]. This pre-treatment makes the analysis time-consuming and laborious.

This dissertation aims to introduce a new spectroscopic method, namely laser-induced breakdown spectroscopy (LIBS), as an analytical tool for (micro)plastic identification and to advance the understanding of weathering-induced oxidation of plastic samples. Although this is a physics dissertation focusing on the physical principles and applications, the work aims to support all environmental scientists working on the problem of (micro)plastic pollution. In this context, the abundance of identification methods can be overwhelming. The present work provides a comprehensive overview of the current methods and introduces LIBS as a complementary technique where conventional methods reach their limits. LIBS is a type of atomic emission spectroscopy that can identify the sample material and simultaneously determine the chemical composition layer by layer. Its potential for plastic identification has already been demonstrated for polymer recycling and cultural heritage conservation [81, 174]. A few studies have also looked into its potential for plastic characterization, such as detecting heavy metals [39] and studying aged microplastics covered by biofilms [161]. Although several studies have investigated the application of LIBS in microplastic research in recent years (such as the two studies mentioned above), we were the first to investigate LIBS potential for microplastic identification.

This thesis includes three publications. In the first publication, LIBS is used for the first time to identify microplastics. Here, the spectral fingerprint of different plastic types is determined and compared with each other. The uniqueness of the spectra of different

plastic types is confirmed based on a concept using line intensities and multivariate analysis. Additionally, additives are detected in the spectra but these were not further characterized. The second publication extends LIBS' applicability to detect weathering-induced oxidation on polystyrene (PS) samples. For this, the oxygen peak in the spectra is used. The study shows the oxidation behavior of PS samples as a function of weathering time and penetration depth without exposing the samples' cross-section. Additionally, the influence of the antioxidant Irgafos® 168 on weathering-induced oxidation is investigated. The last publication combines the two previous studies and shows that different plastic types exhibit different oxidation and, consequently, fragmentation behavior. The presented results open up a magnitude of opportunities for (micro)plastic research and applications, such as measuring substance uptake, depth profiles for delicate samples, or analyzing samples in biological matrices. It provides a significant contribution to environmental research by advancing the development and optimization of LIBS as an analytical tool for (micro)plastics and their weathering-induced oxidation behavior.

The dissertation is written in cumulative form and structured as follows: First, a short introduction to the investigated materials, the experimental setups, the data processing, and the chemical processes involved in plastic degradation and oxidation is given. Additionally, standard analytical techniques and their challenges in analyzing (micro)plastic samples are highlighted. An examination of these methods is necessary to generate a requirement profile for the new method, which should be efficient in situations where the established methods fail. Second, LIBS is introduced to address these analytical challenges. The essential fundamental physical phenomena of this method, as well as their theoretical descriptions, are presented. The evaluation of the method, i.e., the advantages and disadvantages compared to the established methods in (micro)plastic research, is discussed. Finally, the main results are presented in concise summaries, followed by a conclusion and outlook. The original publications complete the thesis, which also includes a statement of the author's contribution. Detailed results were published in the following three peer-reviewed papers:

1. **Sommer, C.**, Schneider, L. M., Nguyen, J., Prume, J. A., Lautze, K., & Koch, M. (2021). Identifying microplastic litter with Laser Induced Breakdown Spectroscopy: A first approach. *Marine Pollution Bulletin*, 171, 112789.

2. **Sommer, C.**, Nguyen, J., Menzel, T., Prume, J. A., Ruckdäschel, H., & Koch, M. (2022). Weathering-induced oxidation: An investigation of artificially aged polystyrene samples using Laser-induced Breakdown Spectroscopy. *Polymer Testing*, 112, 107623.

3. **Sommer, C.**, Nguyen, J., Menzel, T., Ruckdäschel, H., & Koch, M. (2023). Determining weathering-induced heterogeneous oxidation profiles of polyethylene, polypropylene and polystyrene using laser-induced breakdown spectroscopy. *Chemosphere*, 140105.

Chapter 2

Background

This chapter gives a brief introduction to the materials studied and their methods. Although a comprehensive overview of plastic materials is outside the intended scope of this thesis, knowledge of their chemical and physical properties is crucial to the experiments performed and contributes to interpreting and understanding the results. For this reason, the most important properties of plastics for this study, the processing of their raw material, and the chemical processes involved in weathering-induced oxidation are discussed before addressing the analytical challenges for their identification and characterization. This chapter primarily provides the theoretical foundation of Publications 2 and 3.

2.1 Materials

The terms *plastics* and *polymers* are often used interchangeably to describe synthetic materials. However, they are not synonyms. Polymers (Greek: *poly* = many, *meros* = parts) are the raw material of plastics [66]. They are large molecules that usually consist of a large number of small molecules known as *monomers* [66, 187]. They also do not necessarily have to be turned into plastics but can occur naturally, such as cellulose or chitin. Most synthetic polymers are derived from coal, cellulose, natural gas, and, above all, petroleum [44]. The components of polymers, the monomers, are simple organic molecules that possess a double bond or at least two active functional groups [37]. Note that inorganic monomers also exist. However, since this study only deals with organic macromolecules, inorganic monomers and polymers will not be discussed.

Many polymers are synthesized from their individual monomers by a *polymerization process* [37, 66, 187]. In this context, two mechanisms are distinguished: *chain polymerization* and *step polymerization*. In chain polymerization, unsaturated monomer molecules attach to growing polymer molecules and form polymer chains in a chain reaction [66]. This requires an activated monomer, i.e., a monomer with an unpaired electron, which combines with an-

other monomer [17]. A well-known example of chain polymerization is the polymerization of the monomer *vinyl*, which leads to the formation of polyvinyl chloride (PVC) [37]. In contrast, in step polymerization, polymers are formed by a stepwise intermolecular reaction between the functional groups of the reactants [37]. This means that two molecules combine by splitting off a small molecule (usually H_2O), called *condensation reaction* [17]. This way, the initial monomer becomes a dimer, then a trimer, and so on until finally, a polymer is generated [66]. A typical example is the step polymerization of hexamethylenediamine and adipic acid to form polyamide (PA) [37]. The two polymerization processes result in polymer growth whose size terminates, for example, by destroying the site on a chain carrier at which reactions occur, e.g., by a combination of two growing radical chains [17, 37]. Due to the size and shape of the polymer molecules, polymers generally behave differently from ordinary organic substances such as alcohol or sugar. While organic substances are made up of small molecules with molecular weights typically less than a thousand amu, the molecular weight of a polymer ranges from thousands to millions of amu [37]. This difference in molecular size is associated with unique physical and chemical properties, such as flexibility or durability [37].

Plastics (Greek: *plastein* = to form, to shape) are only formed from polymers through processing [66]. For example, manufacturers use fillers and additives to make plastics resist UV radiation, be flame retardant or temperature resistant, and change their physical properties toward flexible, anti-static, or anti-microbial [37, 84, 165]. Plastics are processed in a procedure called *compounding* [37], which involves mixing and melting techniques "such as extrusion, compression, and injection molding" [201, p. 3389]. To compound additives into a polymer matrix, both are fed to either a batch mixer, e.g., an internal mixer or a two-roll mill, or to a continuous mixer, e.g., a single- or twin-screw extruder [165]. For Publication 2, the compound of polymer and additive was made by the collaborators of the University of Bayreuth using the twin-screw extruder (ZSK 26 MCC) by Coperion Werner & Pfleiderer (Stuttgart, Germany). The polymer granules are melted in the cylinder of the extruder, and the additive is dosed to produce the desired percentage. After the mixture reaches homogeneity, it is released from the extruder as a plastic strand. The plastic strand is cooled in a water bath and then granulated. During compounding and cooling, temperature, speed, and time are usually monitored to achieve special properties for the plastic product, e.g., a higher degree of crystallinity [180, 201]. Tensile bars are then produced from this compound via injection molding, i.e., the re-melted compound is injected into a mold, cooled, and the desired shape is pulled out [165, 201]. The compound is highly dependent on the properties of the polymer and additive used, so there can be significant differences when processing different types of plastics [148].

Plastics are commonly categorized into two groups: *thermoplastics* and *thermosets* [37, 60,

66]. Thermoplastics are uncross-linked polymers that can deform at elevated temperatures in a reversible process [60]. This feature has led to the popularity of thermoplastics as it allows them to be recycled and reused [37]. Thermosets consist of tightly cross-linked polymer molecules and do not soften but decompose chemically when heated [60]. This means that after production, the molecules of the polymer form an unbreakable, irreversible bond that degrades when overheated without turning into a fluid phase [27, 66]. Due to their different characteristics, thermoplastics and thermosets are manufactured and processed completely differently [148, 165]. The processing mechanism mentioned above relates to thermoplastics since these polymer types were studied in this thesis. For more information on the processing of thermosets, please refer to Chanda (2017) [37] or Olmsted and Davis (2001) [148].

An important characteristic of thermoplastics is its *lattice structure*. The lattice structure is a "topologically ordered [three-dimensional] structure[] based on one or more repeating unit cells" [216, p. 44]. It can either be a regularly repeating ordered structure, called a *crystal lattice*, or arranged without any particular long-range order, called an *amorphous lattice* [37]. Polymers can exist in both crystalline and amorphous forms. Their crystallinity can theoretically range from 0 % (completely amorphous) to 100 % (completely crystalline) [60]. However, when exhibiting crystalline morphologies, polymers always contain amorphous regions between crystallites, so 100 % crystallinity is never achieved in reality [49, 60, 180]. In this case, the more precise term *semi-crystalline lattice* is used, with crystallinity ranging from 10 % to 80 % [145]. The amorphous state is characterized by the *glass transition temperature* T_g, which is described in a later section (cf. section 2.3).

Table 2.1: Overview of plastic types used in this study (extracted from [37] and [27]).

Plastic type	Monomer	Lattice structure	Chemical formula	Structure	Usage
PE	ethylene	semi-crystalline	$(C_2H_4)_n$	aliphatic	bottles, films, sheets
PP	propylene	semi-crystalline	$(C_3H_6)_n$	aliphatic	sterilizable hospital equipment, toys
PS	styrol	amorphous	$(C_8H_8)_n$	aromatic	insulation material
PET	terephthalic acid & ethylene glycol	amorphous/ semi-crystalline	$(C_{10}H_8O_4)_n$	aromatic	bottles, clothing
PA6	amide	semi-crystalline	$(C_6H_{11}NO)_n$	aliphatic	synthetic fibers
PC	carbonate	amorphous	$(C_{16}H_{14}O_3)_n$	aromatic	lenses, screens, safety glasses
PVC	vinyl chloride	amorphous	$(C_2H_3Cl)_n$	aliphatic	water pipes, gramophone records

This study examines the most commonly used plastic types in Europe: the carbon-carbon backbone polymers polyethylene (PE), polypropylene (PP), polystyrene (PS), and polyvinyl chloride (PVC), as well as the polymers with a heteroatom in the main chain polyethylene terephthalate (PET), polycarbonate (PC), and polyamide 6 (PA6). Of the total 50.3 million tons of plastics used by European plastics converters in 2021, these plastic

types accounted for about 38.8 million tons [160]. Here, PE takes the largest share with 29.4 %, followed by PP with 19.9 % and PVC with 10.3 %. PET, PS, PA, and PC account for 8 %, 6.2 %, 1.8 %, and 1.6 %, respectively [160]. All of these plastic types are thermoplastics consisting of *aromatic* or *aliphatic* compounds. The former refers to ring-like molecules with delocalized C-C bonds, such as benzene [81]. The latter consists of single, double, or triple bonds forming a chain-like molecule [60]. The theoretical principles and concepts explained in the following sections relate exclusively to these thermoplastics.

In Publication 1, the plastic samples were solid rectangular plates, either transparent or white, measuring 3.5 x 3.5 x 0.5 cm^3, and provided by Epsotech (Jülich-Kirchberg, Germany), formerly known as Vitasheet Group. Table 2.1 provides information about the plastic types relevant to this study. Additionally, also non-plastic samples and real microplastic samples were investigated. The former consists of 14 samples: sea urchin skeleton (*Echinocardium cordatum*), common cuttlefish bone (*Sepia officinalis*), sea snail shell (*Neverita josephina*), coralline red algae (*Lithophyllum racemus*), and seagrass leaf (*Posidonia oceanica*), maple wood (*Acer platanoides*), maple bark, maple leaf, maple fruit, unknown type of wood, dandelion (*Taraxacum officinale*), moss (*Hylocomium splendens*), fine-grained sand (0.06 mm–0.2 mm, 55 % $CaCO_3$, 42 % $MgCO_3$, < 2 % SiO_2) by Erdenwerk Gregor Ziegler GmbH (Plößberg, Germany), and cellulose. The latter were extracted from sediment samples collected from the River Lahn (Marburg, Germany). The extraction process was as follows: After sampling, the sediment sample was separated into plastic and non-plastic material by density separation using the *MicroPlastic Sediment Separator* (MPSS) by Hydro-Bios Apparatebau GmbH (Altenholz, Germany), which operated for 15 h with a NaCl solution. This procedure resulted in a set of 45 plastic and non-plastic microparticles with a minimum size of 500 µm. The particles were cleaned with *Fenton's reagent* to remove all organic impurities.

For the investigation of the oxidation behavior of plastics in Publications 2 and 3, artificially aged plastic samples were produced by the collaborators of the University of Bayreuth. Here, the environmental conditions causing plastics to degrade were mimicked in a *weathering chamber*, also known as *environmental simulation* or *aging chamber* [28, 123]. Standards organizations, such as ASTM, BS, DIN, or ISO, have implemented protocols for performing accelerated weathering tests in environmental simulation chambers [28, 61, 209]. The advantage of these types of tests is that predictions can then be made about the lifetime of plastics within a reasonable test period [209] and that the influence of individual environmental factors can be systematically investigated. For the purpose of this study, different plastic types, i.e., low density (LD) PE and PP provided by LyondellBasell (Rotterdam, Netherlands), and PS with 0 %, 0.5 %, and 1 % concentrations of Irgafos® 168 provided by INEOS Styrolution Group (Frankfurt am Main, Germany), were weathered according to the ISO 4892-2:2011 standard protocol. The compound of PS and Irgafos® 168 was processed according to the

procedure described earlier. Irgafos® 168 by BASF (Ludwigshafen, Germany) is a processing stabilizer and *secondary* antioxidant based on organo-phosphite with the technical name Tris(2,4-di-tert-butylphenyl)phosphite and chemical formula $[(C_4H_9)_2C_6H_3O]_3P$. The working principle of Irgafos® 168 is explained in section 2.3. The samples provided by the collaborators of the University of Bayreuth have a size of approximately 2 x 2 x 0.7 cm^3 for PS and 1 x 4 x 0.7 cm^3 for PE and PP.

For accelerated weathering, the environmental simulation chamber Q-SUN XE-3 from Q-LAB Corporation (Westlake, OH, USA) was used, which is equipped with a Daylight-Q filter and three xenon lamps. It irradiated with 60 W/m^2 (at 300 nm–400 nm), corresponding to a total irradiance of 594 W/m^2. Relative humidity was set to 50 %, chamber temperature to 38 °C. The weathering cycle was repeated until an overall weathering time of 200 h, 400 h, 800 h, 1400 h, 2000 h, and 3200 h for the plastic samples was reached. The acceleration factor of the weathering chamber for Central Europe was calculated by the collaborators in Bayreuth as 5.2 and published by Meides et al. (2021) [134]. Consequently, the maximum weathering time of 3200 h corresponds to almost two years of outdoor weathering in Central Europe.

2.2 Instrument Details, Data Acquisition, and Data Processing

Various spectroscopic techniques were used during the course of this study, including LIBS, FTIR, and Raman spectroscopy. A detailed explanation of the theoretical background of these techniques is provided in section 2.4.3 and chapter 3. Unless otherwise indicated, the experimental setups and parameters listed below were used to collect the data described in the subsequent sections. In addition to spectroscopic techniques, microscopy and profilometer measurements were also carried out.

LIBS System

All LIBS data was obtained using the same apparatus. It consists of a second harmonic Q-switched Nd:YAG laser operating at 532 nm with a repetition rate of 10 Hz, maximum pulse energy of 200 mJ, and pulse duration of 4 ns (Brilliant b model) by Quantel laser (Les Ulis Cedex, France), notch filter (HSPF-532.0-1.0) by Kaiser Optics (Ann Arbor, MI, USA), and spectrograph (MS257) by Newport Corporation (Irvine, CA, USA) with a grating of 300 lines/mm and an entrance slit between 20 µm–30 µm, and equipped with a time-gated intensified charged-couple device (ICCD) detector (iStar DH720-18 U-03) by Andor Technology (Belfast, UK). A prism and an attenuator were inserted into the beam path to separate the second harmonic from the fundamental mode of the laser and to adjust the pulse energy, respectively. Additionally, to conduct measurements under different ambient atmospheres, a

sample chamber has been built around the sample holder. The gas flow was directed below the sample holder, and the measurements were carried out at atmospheric pressure. The components were arranged as displayed in Fig. 2.1. Objective (O) and lens (L) specifications have changed depending on the study and can be found in the corresponding publications. If not indicated differently, the pulse energy was set to 20 mJ. A white light source and a camera were also coupled into the beam path to ensure the focal plane and investigate the ablation crater.

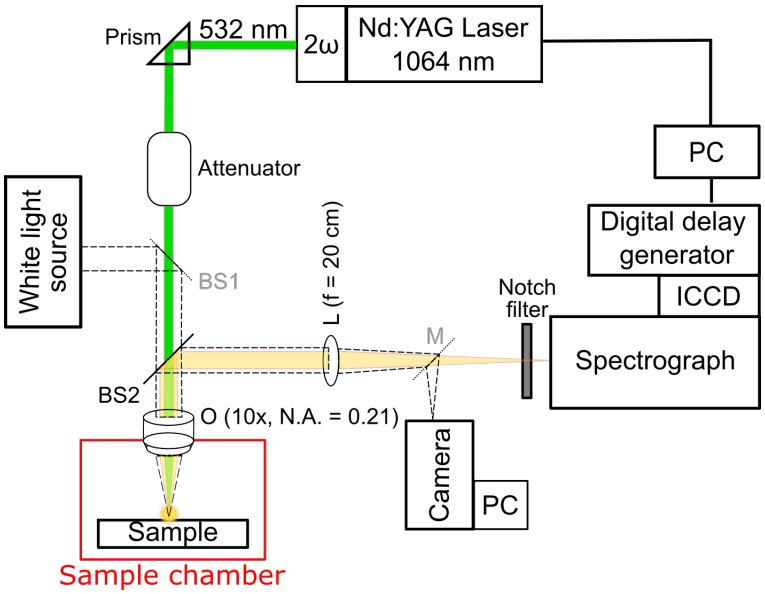

Figure 2.1: Schematic representation of the LIBS apparatus used. The green path represents the path of the laser, the yellow path represents the collected plasma light, and the dashed path represents the path of the white light. Parts of the components for the white light path (beamsplitter BS1 und mirror M) are marked in gray, which means that they were removed from the beam path during LIBS measurements. The schematic is extracted but modified from Publication 2.

The LIBS spectra were recorded in the range 300 nm–810 nm, which is consistent with previous studies [81, 174]. Note that the carbon line at 247.67 nm was not detected with the used LIBS system, as it is too deep in the UV range. The delay window of the ICCD camera was set to 100 ns when focusing on atomic signals in the spectrum and 240 ns when analyzing molecular signals. In both cases, the acquisition window was set to 1 µs. Samples were then measured multiple times (varying in frequency of occurrence depending on the study) and averaged. The flatfield and the background were recorded prior to measurements and subtracted from the original data. Depending on the study, the data were also smoothed using the Savitzky-Golay filter in the Python package *SciPy* [203], setting the mandatory filter parameters *polynomial order* and *filter window* to 5 and 11, respectively, and normalized to the noise level. Not all data was smoothed, as there is a risk of spectral information being lost. For this reason, no smoothing was performed in Publication 1 because computer-based learning algorithms were used for evaluation. These algorithms are capable of using even

slight changes in the spectroscopic data. Smoothing the data could have led to a considerable loss of important information and a poor evaluation. In Publication 3, in turn, the data was smoothed to distinguish the peaks more clearly from the noise. Here, slight changes in the spectroscopic data were less critical because the main concern was whether or not a peak was evident.

Profilometer and Microscope

In LIBS depth profiling, the assignment of the number of laser shots to depth was determined using the profilometer (cyberscan CT 100) by cybertechnologies (Eching-Dietersheim, Germany). The profilometer works according to the confocal principle using a chromatic white light sensor. A sketch of the working principle is shown in Fig. 2.2. White light is directed onto the sample and dispersed into its spectral components. The spectral components are then focused at various points along the optical axis [144]. The wavelength, whose focus is on the sample surface, i.e., whose intensity is maximum, passes through a pinhole to the spectrometer, which then records the distances via color differences [144]. In this way, the condition of the surface, e.g., cracks or craters and their corresponding depth, can be measured. The lateral resolution of the profilometer was set to 5 µm. Possible irregularities in the sample surface, e.g., slopes, were corrected by fitting a polynomial function to the surface (with the craters being removed beforehand) and then subtracting it from the data.

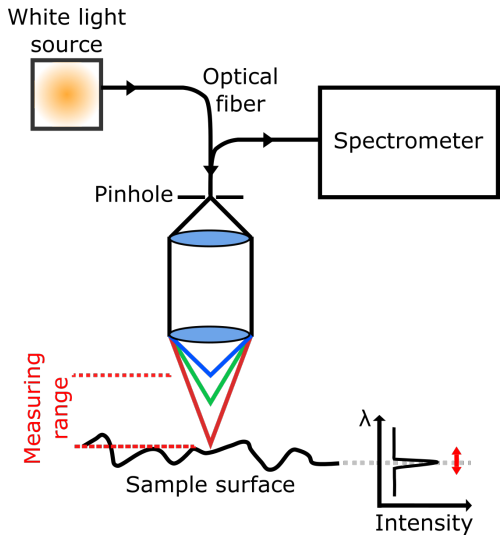

Figure 2.2: Schematic representation of the working principle of an optical confocal profilometer. The main components are a point-shaped white light source, an optical system with axial chromatism, a pinhole that allows the wavelengths to pass through, and a spectrometer. The schematic is adapted from [144] and [105].

In Publication 1, a zoom stereomicroscope (SMZ-171T) with a magnification range of 7.5x–50x by Motic Deutschland GmbH (Wetzlar, Germany) was used to examine the mi-

croplastic particles.

FTIR Systems

In this thesis, two commercially available FTIR systems were used: the Tensor 37 and the automated LUMOS II FTIR microscope, both by Bruker Optics (Ettlingen, Germany). The Tensor 37 system was used to identify real microplastic samples (Publication 1). The LUMOS II system was mainly used to determine weathering-induced oxidation (Publication 2 and Publication 3). The reason for the usage of two FTIR systems is the purchase of the LUMOS II in late 2020/early 2021. At that time, the measurements for Publication 1 had already been performed. Both systems were operated in attenuated total reflection mode (ATR) with a spectral resolution of $4\,\mathrm{cm}^{-1}$.

The Tensor 37 is equipped with a platinum-ATR unit by Bruker Optics and operated using the software OPUS 7.0, also by Bruker Optics. The samples were measured at only one spot due to the small size of the microplastic samples and recorded in the range 4000–400 cm^{-1}. The background was captured after every five measurements. The obtained spectra were then evaluated using the databases ATR-FTIR LIBRARY KIMW, BPAD-Bruker Polymer ATR Library, and BIBL ATR-FTIR- FORENSICS Library and manually verified following the procedure described in Jung et al. (2018) [103].

The LUMOS II uses a single-element thermo-electrically cooled mercury-cadmium-telluride (TE-MCT) detector and a motorized germanium ATR crystal and was operated using the software OPUS 9.5.29 by Bruker Optics. The samples were recorded in the range 4000–680 cm^{-1} with an open aperture and 30 to 50 co-added scans for various distinct sample spots. The resulting spectra were then averaged over all measurements and smoothed to account for atmospheric effects in the water and carbon dioxide spectral regions. Afterward, the spectra were baseline-corrected. Since the plastic types were known in the weathering-induced oxidation studies, no database was needed.

Raman System

Raman measurements were not part of the publications. However, the samples used were measured with both Raman and FTIR systems. As will be explained in section 2.4.3, the Raman data did not allow a systematic evaluation of weathering-induced oxidation. To illustrate this, Raman measurements are shown in section 2.4.3. These were recorded using a self-built Raman setup. It employs an Ar^+ ion laser operating at 514.5 nm (543-GS-A03) by Melles Griot (Carlsbad, CA, USA), a monochromator (Acton SpectraPro 500) with a 1200 lines/mm grating and an entrance slit of 20 µm, and a nitrogen-cooled charge-coupled Device (CCD) detector (7698-0001), both by Princeton Instruments (Trenton, NJ, USA). The laser was focused onto the sample surface with a 10x/0.25 objective. Spectral filtering

was performed with three BragGrate Notch Filters and one BragGrate Bandpass Filter, operating at 514.5 nm by OptiGrate (Oviedo, FL, USA). A white light source and a camera were also coupled into the beam path to ensure the focal plane. The CCD detector was cooled to reduce the noise level. Raman measurements were started at a detector temperature of approximately −120 °C and a noise level below 500 counts. Raman spectra of the samples were then obtained from one spot, recorded in the range 5000–500 cm^{-1}, and using an exposure time between 0.5 s–20 s, depending on the sample. The software WinSpec/32 by Princeton Instruments (Trenton, NJ, USA) was used for data acquisition and operation of the spectrometer.

Data Processing

Publication 1 used computer-based machine learning algorithms, i.e., *Principal Component Analysis* (PCA) and *Support Vector Machine* (SVM), for data analysis. To give an overview of the working principle, the methods are briefly explained. However, it should be noted that computer-based learning algorithms are used as auxiliary tools and are not the focus of this work. Their improvement was out of the scope of this thesis. Thus, a detailed mathematical explanation is omitted.

PCA helps in visualizing the data and finding patterns or outliers. In this study, various plastic samples were analyzed with characteristic peaks. If each plastic sample is to be displayed with its characteristic peaks, this may become complex. As will become apparent in Publication 1, there are 11 characteristic peaks for distinguishing and identifying plastic samples. Mathematically, the plastic samples can then be described as points in an 11-dimensional space (11 because of the number of characteristic peaks). The aim of PCA is to reduce the dimensionality of the plastic samples and display them in a new coordinate system. This means that the 22 variables (11 peak wavelengths and 11 peak intensities) are approximated by 2 or 3 variables. This is done by correlating the 11 peak wavelengths and their peak intensities. These variables are called *principal components* (PCs) and are the new coordinates of the plastic samples. They do not contain 100 % of all peak information but only parts of it and are ordered from highest to lowest significance. Nevertheless, they are structured in such a way that they provide a comprehensive representation of the data. The new axes then have no physical meaning but represent a summary of all peak wavelengths and their intensities. The dataset is distributed across the PCs based on their variance. Due to their local distribution and clustering in the diagram, the samples can be separated from each other.

SVM, in turn, is used to classify samples. It provides more precise information than PCA. In contrast to the latter, however, SVM requires prior knowledge of the polymer types. Using a training set, i.e., a set of samples whose base polymer is known (*prior knowledge*), the SVM

establishes a hyperplane that divides the known plastic samples into two classes. In this study, the classes are PE and PP, as all other polymer types can be excluded using a decision tree based on multivariate analysis and spectral line intensities, as can be seen in Publication 1. Accordingly, 20 % of the PE and PP reference samples were taken as the training set. Each plastic sample is then represented by a vector in a vector space, and the hyperplane is determined by simple linear algebra. Note that the vector space is again an 11-dimensional space, while the hyperplane is 10-dimensional (by definition, number of features - 1). When an unknown plastic sample is presented to the SVM, it classifies the sample based on the location of the sample's vector to the hyperplane previously defined with the training dataset. For more information on PCA and SVM, please refer to Jolliffe (2002) [101] and Steinwart and Christmann (2008) [185], respectively.

2.3 Fundamentals of Plastic Degradation

Due to their broad application and improper disposal, plastics are exposed to conditions for which they were initially not intended, such as UV radiation, humidity, or temperature. This causes plastics to degrade, fragment, and eventually mineralize [12]. Investigating these degradation processes can not only help to gain a deeper understanding of the material and consequently design novel plastics with better performance but also help to estimate the impact on the environment and the future of plastics when their removal from nature is not feasible. In this context, Publications 2 and 3 shed light on the degradation processes of different plastic types. To interpret the spectroscopic data correctly, a brief overview of the chemical and physical processes involved during the degradation of thermoplastics is given.

As defined by Jasso-Gastinel and Kenny (2016), any alteration in the chemical structure as well as physical attributes that result in a loss of plastic characteristics, including color, form, or solidity, under the influence of the surrounding environment or manufacturing conditions is referred to as *plastic degradation* [88, 100, 194]. Typical environmental influences are temperature, oxygen, atmospheric exposure (e.g., UV light, humidity, moisture), radiation (e.g., wavelength, intensity), and mechanical or biological stresses [15, 61, 80]. Here, chemical changes include processes such as the oxidation or hydrolysis of molecules or the breaking of chemical bonds [34, 194, 215]. Physical changes, in turn, are concerned with flaking, embrittlement, and cracking, i.e., the porosity and roughness of the sample, but also re-crystallization and densification [34, 194, 215]. If these changes occur over a longer period of time and if this time is to be taken into account in the characterization of plastics, the term *aging* is used [61]. The time it takes for plastics to degrade depends on various factors, including the base polymer type, additives, molecular structure, morphology, and, of course, the surrounding environment [5, 37, 99, 100, 215]. However, degradation always begins near

the surface and proceeds throughout the material [25, 215]. Consequently, microplastics degrade more quickly than macroplastic samples due to their increased surface-to-volume ratio [77]. In accordance with other studies, the term *weathering* or *weathering-induced degradation* will be used when environmental factors are involved in the degradation processes [49, 100, 180].

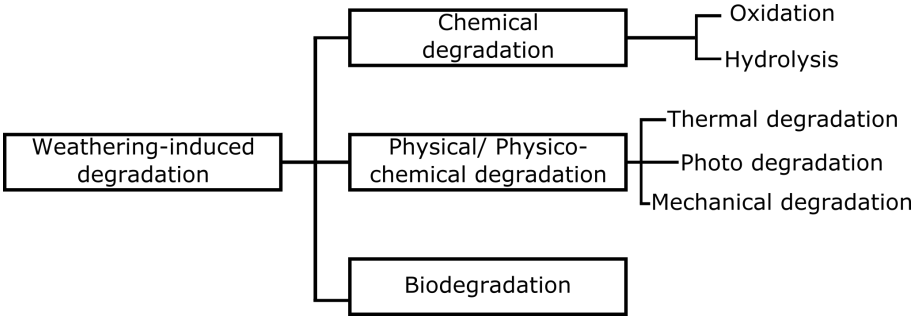

Figure 2.3: Overview of different polymer degradation processes adapted from [15] and [199].

An overview of the different mechanisms responsible for the weathering-induced degradation of plastics is seen in Fig. 2.3. The different mechanisms— chemical, physical/ physico-chemical, and biological degradation (*biodegradation*)—do not necessarily have to occur independently of each other but can occur simultaneously or be mutually dependent due to complex environmental influences [154]. The term *biodegradation* defines a process in which microorganisms in both aerobic (with oxygen) and anaerobic (without oxygen) environments produce enzymes that attack a sample's physical and chemical properties [43, 215]. However, the chemical and physical degradation of long polymer chains is generally higher than those of biodegradation, which proceeds too slowly to have a significant environmental impact [10, 15, 37, 77]. In fact, chemical reactions are primarily responsible for weathering-induced degradation of polymers, in which UV radiation and atmospheric oxygen predominate, causing chain scission [11, 77, 80, 131]. These reactions can be accelerated by higher ambient temperatures caused by the sun [200, 209, 215]. The radiation-initiated degradation process in which a molecule is degraded by absorption of a photon is called *photo-degradation* [80, 215]. When this process occurs in the presence of oxygen, it is referred to as *photo-oxidation* [215]. Consequently, the term *weathering-induced oxidation* refers to photo-oxidation induced by environmental factors. Note that oxidation does not necessarily have to occur in the presence of oxygen but can also be caused by oxidizing agents. This process can also be referred to as photo-oxidation. Here, however, the former is meant.

In general, plastics consist of carbon-based backbone chains with different functional groups (see Table 2.1) and are inherently susceptible to oxidation [33, 77]. When investigating degradability, distinguishing between plastics with carbon-carbon backbones, like PE, PP,

and PS, and plastics with carbon and heteroatoms in the main chain, like PET, is often beneficial [77]. In the former, the primary degrading agents are oxygen and UV radiation; in the latter, also biodegradation and hydrolysis are involved [77, 80]. Since in this thesis only the weathering-induced degradation of PE, PP, and PS samples is investigated, the focus is on the chemical processes of oxygen and UV radiation, i.e., photo-oxidation, and whether its effect can be measured using LIBS or not.

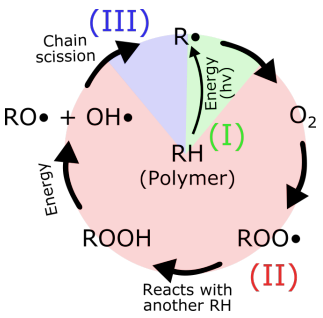

(I) Initiation:	Polymer	→	R•
(II) Propagation:	R• + O_2	→	ROO•
	ROO• + RH	→	ROOH + R•
	ROOH	→	RO• + OH•
			↓
			β-Scission
(III) Termination:	$2RO_2$	→	non radical products

Figure 2.4: Photo-oxidation cycle for carbon-carbon backbone polymers (adapted from [215]). The sequence in the illustration must be read as follows: It starts in the center, marked with a green (I); then, the absorption of a photon initiates the photo-oxidation cycle; finally, the subsequent steps proceed clockwise following the arrows. Radicals are marked with a '•'. R represents the polymer backbone, O and H stand for oxygen and hydrogen, respectively.

The photo-oxidation process consists of three steps: initiation, propagation, and termination, illustrated in Fig. 2.4 [77, 200, 215]. The references given here provide a detailed description of these steps. In the following, the explanation by Gewert et al. (2015) is used [77]: In the initiation step (I), a functional group of the polymer absorbs a photon. This functional group is called a *chromophore*. In organic molecules, as here, chromophores consist of conjugated double bonds [169], which makes aromatic compounds in particular susceptible to photo-degradation. If the photon now carries sufficient energy, a free radical (R•) is formed from the long-chain polymer molecule (RH) (green area). Thus, photo-initiation requires the presence of unsaturated chromophores to absorb radiation [77, 200]. However, photo-oxidation can also occur even if no unsaturated chromophores are present at first glance. PE and PP, for example, only have saturated bonds in their polymer backbone (C-C and C-H), which means that their binding energy is too high to be compensated by UV light [34, 77]. Consequently, they were suspected of being inert to photo-degradation [77]. Nevertheless, photo-oxidation processes occur. A common explanation is that some chromophores, in the form of impurities or structural anomalies, are created during the polymers' production, storage, or processing [77, 200]. These can enable photo-degradation to some degree. In PS, in turn, peroxide groups formed during co-polymerization and aromatic ketones of acetophenone type formed during processing act as chromophores [37].

In the propagation step (II), a peroxy radical (ROO•) is produced (red area). This occurs

through the reaction of the polymer radical (R•) with oxygen (O_2). The peroxy radical then abstracts hydrogen from the same or another polymer molecule, generating a hydroperoxide group (ROOH) (and a new macroradical (R•)). Hydroperoxides are easily photolyzed, which leads to the formation of alkyloxy (RO•) and hydroxyl (HO•) radicals [215]. Chain scission, cross-linking, branching, or the generation of oxygen-containing functional groups are the result of the propagation step.

The radical reaction finally terminates (III) when two radicals combine in a cross-linking reaction to form inert products (blue area) [77]. These products can be olefines, aldehydes, or ketones. For more detailed information on the oxidation and the formation of byproducts, please refer to the literature [77, 209, 215]. Fig. 2.4 also shows the corresponding reaction equations involved in the initiation, propagation, and termination steps of photo-oxidation.

Plastics are commonly exposed to photo-oxidation processes, as the presence of UV light and oxygen is a normal situation for them. However, oxygen can also diffuse into the plastic material independently of UV light. While photo-oxidation is a chemical process where oxygen is combined with polymer molecules, oxygen diffusion is the result of natural mechanisms that balance "the concentration gradient of a given species in a given environment" [37, p. 132]. Accordingly, diffusion into the polymer occurs when diffusing species molecules move across gaps and other spaces between polymer molecules [37]. These gaps and spaces depend on the lattice structure of the polymer, i.e., whether it is crystalline or amorphous [37]. Amorphous materials tend to have a low degree of molecular packing, while crystalline materials have a high level of molecular packing [37]. Therefore, amorphous materials are susceptible to oxygen diffusion, whereas crystalline materials are regarded as nearly impenetrable [37]. Likewise, the amorphous regions in semi-crystalline polymers are the primary recipients of oxygen.

An important influence on diffusion is when the molecular chains begin to move. This happens when the so-called *glass transition temperature* T_g is reached. [11, 37, 50]. Below this temperature, the polymer is in a solid, *glassy* state but changes to a flexible state once T_g is exceeded [180]. The glass transition temperature, thus, characterizes amorphous materials or the amorphous parts of semi-crystalline materials [180]. In the flexible state, the spaces between molecule chains grow by a factor of 2.5, which facilitates uptake [180]. Consequently, oxygen diffusion is promoted by the high mobility of the polymer chains [169].

Following oxygen diffusion and photo-oxidation, the polymer's molecular weight reduces as free radicals are released from the polymer chain, making the material brittle and more vulnerable to fragmentation from mechanical stress or crack formation [12, 77, 169, 188]. Since no mechanical stress was artificially generated in the weathering chamber, fragmentation is out of the scope of this study. However, the formation of cracks depends not only on external influences but also on the underlying lattice structure of a polymer [11, 75, 134,

136, 169]. Therefore, cracks generated by degradation processes but in the absence of outside stimuli will be discussed here. In this study, (LD)PE and PP samples, which have semi-crystalline morphology, and PS samples, which are amorphous, have been studied, and their glass transition temperature is listed in Table 2.2.

Table 2.2: Characteristic properties of PE, PP, and PS (adapted from [11]).

	LDPE	**HDPE**	**PP**	**PS**
Glass transition T_g (°C)	-100	-80	-25	+100
Crystallinity (%)	30–50	80–90	30–50	0
Oxygen resistance	Low	Low	Low	Mod.

By comparing the T_g values of PE, PP, and PS, it is evident that PS has a very high glass transition temperature, indicating that the polymer chains are less mobile at ambient temperatures. This means that oxidation occurs mainly on the sample surface because the more rigid the chains, the less oxygen penetrates inside the sample. PE and PP, in turn, have low T_g values, which means that the polymer chains in their amorphous regions are more mobile at ambient temperatures. This mobility leads to molecular rearrangements in the amorphous regions during oxidation, which increases the degree of crystallinity [169]. This phenomenon is also referred to as *chemo-crystallization* [61]. Crystallinity increases as the carbon-hydrogen bonds in the amorphous regions of the polymers are replaced by the carbonyl, vinyl, and hydroxyl compounds formed during oxidation due to chain cleavage [61]. The re-crystallized area exerts pressure on the material through its expansion or contraction between the crystallites, which leads to the formation of microcracks [136]. These cracks are not a consequence of the crystallites' deformation but are caused by the amorphous areas between them [11, 106]. As a result, the induced cracks are much more pronounced in semi-crystalline polymers than in amorphous polymers, as no pressure builds up in the latter. This feature is likely to enhance oxygen uptake and accelerate the degradation process as oxygen travels along the microcracks into deeper layers of the polymer [136]. This behavior is studied in Publication 3.

To prevent or minimize photo-oxidation, various stabilizing ingredients are added to polymers during processing [84, 165, 180]. This is necessary because oxidation of polymers occurs not only when they are exposed to harsh environmental conditions but at every stage of their life cycle, i.e., during manufacture, service, storage, and disposal. Therefore, this work investigates the effect of the antioxidant Irgafos® 168. Irgafos® is commonly used in plastics and fibers to provide thermal protection, long-term durability, and quality of polymer attributes during processing [22].

As described above, the process of oxidation involves free radicals. An agent designed to prevent oxidation should, therefore, ideally scavenge free radicals or peroxides and form stable

species so that no further reactions can occur [37]. This can be achieved in two ways: either by chain termination (*primary antioxidants*) or by hydroperoxide decomposers (*secondary antioxidants*) [37, 66, 100, 165]. The former neutralizes the peroxy radicals (ROO•) and thus prevents the formation of more free radicals [37]. The latter decomposes hydroperoxides (ROOH) into non-reactive products, which hinders process-related degradation [37, 165]. Irgafos® 168 belongs to the secondary antioxidants. Its effect is studied in Publication 2.

It can be concluded that different plastic types exhibit different oxidation rates at the sample surface and inside the sample due to their lattice structure and additives, which translates into different degradation rates. This observation indicates that the sample's surface and its interior should be examined for a comprehensive understanding of weathering-induced oxidation. The study of plastic degradation is usually done by examining the morphological or chemical changes. Morphological changes are typically investigated using a microscopic or tomographic approach, while a spectroscopic or thermal approach is used to study chemical changes [74, 134, 171]. Depth profile measurements for the evaluation of weathering-induced oxidation over the entire sample volume, in turn, are scarce and are usually performed only in combination with extensive sample pre-treatment [134, 136]. The following section presents an overview of the most common methods used to investigate the polymer base type and plastic degradation.

2.4 Analytical Techniques

To properly assess the impact of (micro)plastics on the environment and develop mitigation schemes, plastics' quantification, identification, and analysis are essential in environmental research studies. After sampling, the detection process of microplastics usually happens in three steps: first, the plastic particles are extracted from their biological matrices and purified, secondly the physical characterization of the particle is examined, and lastly, the chemical nature is determined [21, 162, 178]. The extraction and purification step typically involves density separation and sieving or filtration, followed by chemical or enzymatic digestion [21, 162]. The particles are then obtained on a filter paper and are ready for identification. However, the identification step is challenging due to the complex nature of (micro)plastic samples. Ivleva (2021) points out that there are at least five characteristics that can affect the analysis [98]:

1. The **size** range of plastic samples is broad. Even when limited to microplastic particles, the particle size varies from 1 µm to 5 mm.

2. The variety of **polymer types** and the ambiguous characteristics of non-plastic materials complicate an accurate identification.

3. Different **shapes**, such as spheres, fibers, films, or foams, behave differently in the environment and are therefore exposed to different processes.

4. The variety of **additives** inserted into the plastic samples during manufacturing (UV stabilizers, plasticizers, antioxidants, pigments, etc.) or **contaminants** absorbed by the plastic samples in the environment (persistent organic pollutants, antibiotics, heavy metals, etc.) are another obstacle in the identification process. They also complicate automatic detection using databases.

5. As plastics remain in the environment and are exposed to heat, UV radiation, or biofouling, the polymer structure degrades, leading to different stages of **aging or weathering** of plastics.

The choice of a suitable identification method depends strongly on the sample at hand and the research question [65]. For instance, mass-based information may be sufficient for the amount of plastic within an area or sample volume [98]. If, in turn, more specific information is required, e.g., transport or whereabouts of a plastics sample, a particle-based method is recommended [98]. It is assumed that the analysis of plastic particles with distinct properties can hardly be performed by a single method but rather by combining several methods [65, 98]. For this reason, improving established methods and developing new methods is of great importance in this research area.

The established methods can be divided into three categories: microscopic techniques, spectroscopic methods, and thermal analysis [21, 98, 155, 167, 178]. The first two are particle-based methods, and the latter contains mass-based methods. Advances in these techniques have led to numerous discoveries in microplastic research and are in constant competition to identify smaller particles in less time. This section presents an overview and the working principles of the methods as well as their advantages and disadvantages for identifying and analyzing (micro)plastics. This is particularly important as it helps in establishing a requirement profile for alternative techniques. Fig. 2.5 presents an outline of the methods.

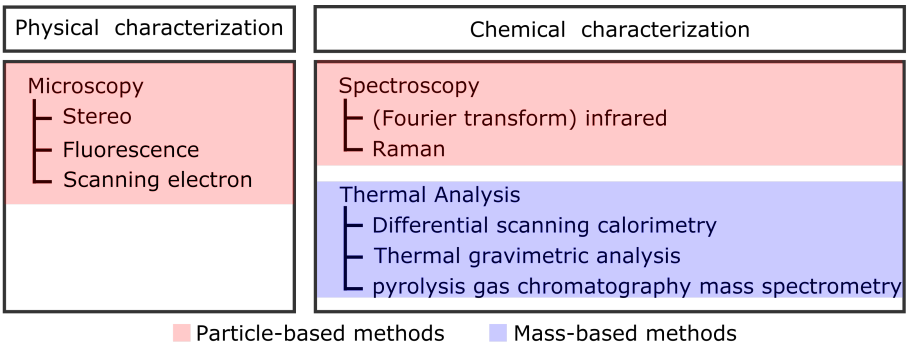

Figure 2.5: Overview of the established physical and chemical characterization methods for (micro)plastic analysis (adapted from [178]).

2.4.1 Microscopic Techniques

Visual identification is a widely used method for plastics detection [21, 94, 130]. Most prominently, *stereomicroscopy* is used to identify and quantify (micro)plastics by their physical appearance [162]. The stereomicroscope is a light microscope that provides a separate beam path for both eyes [130]. This allows the sample to be viewed from two slightly different perspectives, which results in a "stereoscopic vision" [130, p. 3]. The magnification is approximately between 8 and 50 times, so samples with a size range of hundreds of microns can be investigated [21, 130]. An example of a stereoscope image can be seen in Fig. 2.6. The plastic particles presented were extracted from their biological matrix before performing stereomicroscopy. The evaluation of color, shape, size, and morphology can provide good preliminary results in the identification of plastics [94]. In fact, degradation in the form of discoloration, cracking, and embrittlement is also readily visible in optical images [21]. An attempt was made to improve visual identification by taking into account a particle's stiffness. For this, the particles were observed under the stereomicroscope and gently squeezed with a needle [162, 178]. Nevertheless, assumptions beyond morphological structure and surface examination, such as identifying polymer type and contaminants, cannot be made [21].

The usage of stereomicroscopy is tedious, time-consuming, and subjective because each particle has to be classified individually by an experienced personnel member [94, 162]. This classification can differ from researcher to researcher, as a stereoscopic image is often ambiguous [94, 162]. For example, biofilms that have not been removed during purification [130] or discoloration due to degradation can cause the plastic particle to be mistaken for a natural particle, e.g., wood chips or leaf fragments. In this sense, the shape and structure of a plastic particle play a role in the low accuracy of the classification [94]. Moreover, it has been reported that when particles are transparent, it can even lead to error rates above 70 % [94, 182]. It is clear that the five characteristics mentioned by Ivleva (2022) that complicate microplastic identification and analysis—size, polymer type, shape, additive or contaminants, and weathering—apply and must be considered when using a stereomicroscope.

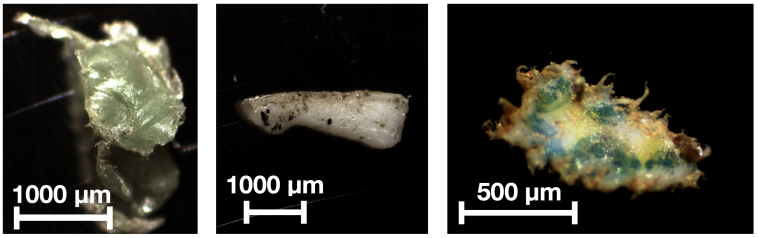

Figure 2.6: Stereomicroscopy image of microplastic particles. The particles were extracted from the River Lahn (Marburg, Germany). For determining the polymer base type, chemical analysis is required. Images were taken by colleague J. A. Prume and are used with permission.

Despite its many limitations, the main advantage of stereomicroscopy is its ease of use. A

stereomicroscope is usually the first fast-screening technique for rapidly identifying a particle's size, form, and color [21, 109, 130, 166, 221]. While it can be used as a fast and inexpensive pre-characterization method, the limitation of producing incomplete results can only be overcome in combination with chemical analysis, i.e., spectroscopy or thermal analysis [182]. For this reason, rather than being a stand-alone technique, stereomicroscopy is primarily used as a supplementary method for plastics analysis [94]. In this work, the only microscopic technique used is stereomicroscopy. Other microscopic techniques, such as *fluorescent* and *scanning electron microscopy*, will be presented below for the purpose of completeness.

In contrast to a stereomicroscope, which uses the light reflection on a sample, *fluorescence microscopy* excites a sample with a distinct wavelength and detects the fluorescence emission [94, 130]. In this case, the light source is much more intense than the white light used for a stereomicroscope [17]. Fluorescence occurs when a molecule is brought into an excited electronic state by absorption of light [17]. Then, the excited molecule collides with the surrounding molecules and travels down the vibrational levels to the lowest vibrational level of the excited electronic state [17]. This transition between the vibrational levels takes place without emitting radiation. The excited molecule remains in this state for a short amount of time (typically around 10^{-12}–10^{-6} s) until it eventually experiences spontaneous emission, releasing the remaining energy as radiation [17]. The emission of radiation is discussed in more detail in section 2.4.3. A sketch of the electronic transitions that occur during fluorescence is also presented there (cf. Fig. 2.9).

Fluorescence microscopy has been shown to reduce the error rate in microplastic detection (due to plastics' inherent fluorescent properties), reduce the size limitation when combined with imaging (due to the smaller excitation wavelength), and identify transparent plastic samples [130]. However, the laser light used to excite the sample may be hazardous and toxic due to *photobleaching*, reducing the acquisition time [130]. Photobleaching describes a process in which light photochemically destroys molecular compounds so that the electronic states are burned away, resulting in a permanent loss of fluorescence [17]. In addition, chemical additives can affect the fluorescence properties of a plastic sample and lead to misclassification [130, 158].

An auxiliary method for fluorescence microscopy is the use of the fluorescent dye *Nile Red*, which belongs to the lipophilic dyes [94, 111, 179]. The plastic particles are removed from biological matrices via density separation or chemical digestion and labeled with the dye. This procedure is called *staining* [179]. Imaging can then be used to identify and count the fluorescent particles that have been exposed to a specific light beam [94, 125]. However, this method has its limitations as some residual bio-organic materials may also be stained with dye or exhibit natural fluorescence characteristics [94, 179]. This can lead to false-positive results. In addition, a specific wavelength has to be used for excitation to generate emission

light [130].

The main disadvantage of stereomicroscopy and fluorescence microscopy is their poor resolution. This is because the wavelength of light restricts the resolution in microscopy due to the diffraction limit. This is particularly problematic when examining very small plastic particles such as nanoplastics. In contrast to these methods, electron microscopy uses electrons instead of UV or visible light to produce an image [21]. Since electrons have a much shorter wavelength than UV or visible light, high-resolution images of the morphological surface structure can be generated (resolution is in the range of a few nanometers) [94, 206]. Here, *scanning electron microscopy* (SEM) is most commonly used for (micro)plastic analysis [94, 130, 178]. An electron gun produces the electrons for an SEM image [142]. These electrons deliver energy to the electrons of the atoms in the sample, which are then released as *secondary electrons* [4]. By collecting these secondary electrons from the entire sample surface, an image is created. As the fundamentals of SEM are beyond the scope of this work, please refer to Nixon (1971) [142] and Akhtar et al. (2018) [4] for more information. Note that there are deviating methods for an SEM image. The use of secondary electrons is the most common method [4].

SEM is costly, demands a significant amount of time and effort for analysis, and does not contain information about the polymer type [130]. To accomplish the latter, an *Energy Dispersive X-ray-Spectroscopy* (EDX) detector can be installed [130]. The electrons from the electron gun collide with the electrons present in the orbitals of the sample atoms, which results in the generation of X-rays [4]. This is because the collision causes the electron to be forced out of its orbital and the free space is taken up by an electron from a higher orbital [4]. The energy difference is then released as an X-ray photon. Due to the unique orbitals of the atoms, characteristic X-rays are emitted. Note that a more detailed explanation of spectroscopy can be found in section 2.4.3, and only a brief excursion on extensions of SEM is made here.

For SEM analysis, a vacuum environment is required [4, 21]. Otherwise, the electrons can scatter with the atoms of the surrounding gas atmosphere, making this method unfavorable for in-situ field measurements. For the same reason, SEM is limited to analyzing dry samples [4]. However, there are extensions of SEM that do not require vacuum or only low vacuum and can examine wet samples, e.g., *environmental SEM* (ESEM) or *field emission SEM* (FE-SEM) [4, 38]. These come with lower resolution [38].

In conclusion, visual identification is a standard step in microplastic identification. Plastic particles smaller than 1 mm, typically not identified by the human eye, can be visualized using advanced microscopy. However, thermal or spectroscopic methods must be used to determine or systematically study polymer type, additives, toxic pollutants, or weathering effects.

2.4.2 Thermal Analysis

Although thermal analyses were not used in this work, an overview of the established methods in (micro)plastic research would not be complete without mentioning them. Therefore, the following section briefly discusses this branch of methods. Additionally, to justify a new method, the shortcomings of existing methods must be pointed out.

Temperature affects both the chemical and physical characteristics of a material [94]. These characteristics are exploited by thermal analyses, which use *thermal stability*, *thermal degradation*, or both to analyze a sample's composition [21, 94, 130, 155]. In this context, *thermal stability* refers to transitions that occur in a sample, e.g. glass transition, re-crystallization, melting, or evaporation [130], whereas *thermal degradation* refers to the decomposition of a sample in an inert atmosphere to produce smaller molecules [23]. The latter process is also referred to as *pyrolysis* when organic compounds are involved [23, 98]. Both processes are achieved by heating the sample. They are used in thermal analysis techniques such as *differential scanning calorimetry* (DSC), *thermogravimetric analysis* (TGA), or *pyrolysis-gas chromatography-mass spectrometry* (py-GC-MS) for (micro)plastics identification [94, 98, 130, 178].

DSC focuses on the thermal stability of a sample. It measures the heat flow that enters or exists a sample during heating, cooling, or an isothermal process as a function of time or temperature [23, 135]. However, the measured heat flow is not the actual value but the heat flow difference between a thermally inert reference sample and the sample under study [130]. Hence, the name *differential* scanning calorimetry [85]. The heat flow curve can then be displayed in a *thermogram* as the sample undergoes exothermic, e.g., re-crystallization, and endothermic transitions, e.g., melting, or both, resulting in increased or decreased heat flow visible in peaks [23, 135]. In this sense, DSC measures the variations in a sample's *heat capacity* [23, 135]. Since different polymer types exhibit different thermal stabilities, peaks occur at different temperatures, allowing the composition and plastic type to be determined [21, 94, 98]. DSC has additionally been used to examine the efficacy of stabilizers [151], determine oxidation [30, 171], as well as to identify morphological changes brought on by polymer degradation and aging [32]. For these analyses, only a few milligrams of the sample material are used in a single measurement [24]. In the context of this work, this technique is particularly interesting, as it could also have been used to characterize the weather-induced oxidation of plastics.

DSC is limited to the detection of semi-crystalline polymers [24, 98, 130]. This is due to the fact that the glass transition temperature, which characterizes amorphous polymers (and amorphous parts in semi-crystalline polymers), does not result in a distinct peak but in a step-like change in the heat flow curve [23]. The glass transition temperature is then typically determined from the inflection point of this step change, which, however, does not happen

instantaneously but over a temperature range [23]. This means that the glass transition temperature, which is only given as a single temperature in Table 2.2, is strictly speaking an estimate. When amorphous polymers have closely spaced or overlapping phase transition signals, they cannot be unambiguously separated from each other [24, 126]. Further heating of amorphous polymers does not lead to melting, but to chemical decomposition; a process that is not detectable by DSC, leaving the glass transition temperature as the only identification marker. In the case of semi-crystalline polymers, in turn, the thermogram shows not only the glass transition temperature but also the re-crystallization and enthalpy of fusion as distinct peaks [24]. This allows their identification [24].

In both amorphous and semi-crystalline plastics, the phase transition signals are susceptible to distortion caused by polymer branching, additives, impurities, and particle size (due to the relationship of sample size and heating rate), limiting DSC's detection capabilities [126, 135, 155]. This is particularly concerning when analyzing real (micro)plastic samples. As cited above from Ivleva (2021), environmental plastic samples exhibit a complex nature due to the wide range of polymer types, various additional substances as a consequence of processing or absorption, or different degradation processes [98]. Bitter and Lackner (2021) point out that there are three main challenges when investigating microplastics in environmental matrices using DSC: First, a variety of signals that coincide with polymer melting peaks can be obtained from organic materials; second, overlaps between peaks of different polymer types can occur; and third, mass concentrations may be below the DSC detection limit [24].

To overcome these limitations, DSC is often combined with TGA. In general, plastics decompose at temperatures around 375–500°C [21]. Once the decomposition process is initiated, pyrolysis fragments are formed and released, reducing the weight of the material [23]. In TGA, the weight loss is analyzed as a function of temperature or time in a controlled atmosphere without determining the type of component [21, 23, 94, 127]. The weight loss can then be used to draw conclusions about the sample's decomposition temperature [23, 85, 135]. TGA on its own is primarily used to measure the thermal stability, the impacts of additives, and to determine the composition of polymer products or preliminary products, e.g. pre-mixtures of additives [23]. Until recently, only PE and PP microplastic particles were identified using TGA-DSC [126]. However, Sorolla-Rosario et al. (2022) evaluated the potential of TGA-DSC to identify, distinguish, and quantify several plastic types, among them PP, PA, HDPE, LDPE, PET, PS, and PVC, using the melting, decomposition, and glass transition temperatures [183]. The authors conclude that the main limitation of this technique is the distinction between LDPE and PS, since the melting temperature of LDPE overlaps with the glass transition temperature of PS. The other samples could be clearly identified [183]. TGA-DSC has the advantage that it usually requires no sample pre-treatment,

is simple and inexpensive [183].

The pyrolysis fragments formed during the degradation of TGA can also be molecularly identified using a combination of *gas chromatography* (GC) and *mass spectrometry* (MS) [98, 155]. The procedure is used in py-GC-MS. For this, a single particle or a portion of a representative sample is placed in a pyrolysis tube [98]. The sample is then heated to a specific temperature (550–1400°C) in an inert environment [98, 117]. The gas used in the inert environment also serves as the carrier gas for the gas separation process in GC [98]. The chemical reactivity of the samples determines the pyrolytic fragments generated during decomposition [98]. In the gas separation process, the volatile pyrolytic fragments are passed through the separation column via the carrier gas [117]. Due to the polarity and vapor pressure of the fragments, the fragment molecules leave the separation column at different exit times (*retention time*) and are recorded by a detector [117]. The individual molecules are then ionized and accelerated by an electric field, separating the molecules according to their individual mass-to-charge ratios [117]. These are displayed in a pyrogram and mass spectrum.

Since each plastic type has different indicator ions and degradation products, (micro)plastics can be identified and quantified in complex environments [40, 155]. Additionally, py-GC-MS can provide information about additives in the polymer chain, thermal stability, oxidation and degradation byproducts, and is not limited to a plastic particle's size or shape [98, 117, 155]. Small sample amounts of 5–200 µg can be analyzed without any pre-treatment [157]. (Micro)plastics can be detected in biological matrices but are also often separated from them by density separation or chemical digestion and filtration [157]. py-GC-MS has become a widely used technique for simultaneous (micro)plastic identification and quantification [98, 130, 155, 157].

The main disadvantage of py-GC-MS is that it does not provide information about the physical properties of a sample under investigation. This is because py-GC-MS destroys the sample completely [94, 157]. Only the mass content of (micro)plastic samples can be specified and not the number of particles. Depending on the research question, this can be a considerable limitation. Py-GC-MS has also been found to have poor reproducibility due to sample inhomogeneity or change in the chemical nature of the sample during the measuring procedure such as catalytic events and requires complex data analysis [157]. While in theory, py-GC-MS has no particle size limitation, in practice, it is restricted to minimum particle size (approx. 50–100 µm), as the sample has to be placed inside the pyrolysis tube manually [89]. In this context, there is also a maximum size limitation, as the sample can not be bigger than the 1.5 mm diameter of the thermal desorption tubes [89, 155].

In conclusion, thermal analysis can provide information about a plastic particle's characteristics, as well as chemical composition without the need for sample pre-treatment [98].

However, thermal analysis has shortcomings. Firstly, there can be difficulties in identifying and distinguishing different plastic types when thermal properties, such as phase transition signals, degradation products, or pyrolytic fragments are too similar or are influenced by impurities in the polymer matrix. Secondly, they cannot be used to characterize the physical properties of plastics as they destroy the samples [94, 130, 178]. Lastly, thermal analysis techniques are not capable of performing depth profile analyses. Only the concentration of the absorbed substance over the entire sample can be determined, but no layer-by-layer analysis, making these methods impractical for the research in this thesis. As a result, thermal analysis is typically employed to identify chemical components or quantify (micro)plastics [94, 126, 178].

2.4.3 Spectroscopic Methods

This section covers one of the theoretical foundations of this work. Since LIBS belongs to the spectroscopic methods, the work focuses on this field. Two established spectroscopic methods were compared with LIBS and their limitations were elaborated. One of the established methods, i.e., FTIR, was used to verify the LIBS results.

Spectroscopy covers a wide range of physical methods that, with some exceptions, address how molecules or atoms scatter, absorb, or emit electromagnetic radiation [92, 121, 153]. The aim is to obtain information about the composition and properties of materials under study. When atoms or molecules interact with radiation energy, they transfer to a different *energy state* [92]. Depending on the energy of the incident radiation, electrons are brought into higher orbitals, vibrations are excited, or rotations are stimulated [153]. After a certain amount of time, the atoms and molecules return to the ground state, i.e., the stationary state at the lowest energy, and release excessive energy in the form of heat and, more importantly, radiation, i.e., as photons [121]. The energy of the photons then corresponds to the energy difference between the two energy states of the atom or molecule [153]. An exemplary sketch of the energy states and excitation of electrons can be seen in Figs. 2.9 and 3.4. Since atoms and molecules have individual energy states, the photons released during the electronic transition give an exact representation of the interacted material. This representation occurs in the form of a so-called *spectrum*. Here, the intensity distribution is given as a function of energy, i.e., frequency, wavelength, or wavenumber. In contrast to destructive thermal analysis methods, spectroscopic methods are mostly non-destructive and, when equipped with a microscope, provide additional information regarding the number, shape, and size of the plastic particles [62, 127]. In the field of microplastic research, the main limitation of spectroscopic methods is the necessity of extracting and purifying plastic particles from their biological matrices prior to measurement [62]. This step is time-consuming and laborious. For thermal analyses, in turn, this step is also common but not mandatory.

Here, the field of spectroscopy is divided into two categories: *atomic spectroscopy* and *molecular spectroscopy*. As (micro)plastic samples are long-chain carbon-based polymers with similar atomic structures (cf. Table 2.1), molecular spectroscopy is mainly used for their identification and characterization. Most prominently, Raman microspectroscopy and (FT)IR spectroscopy are used as they allow to identify the polymer base type, quantify its amount and size distribution, and characterize the shape of (micro)plastic samples [14, 41, 65, 98, 212]. Both methods are based on the interaction of radiation with molecular vibrations [98]. Therefore, the energy states to which the molecules are excited are also called *vibrational energy states*. The vibrational interactions can be theoretically described by a simple harmonic oscillator model [110]. A short overview of IR and Raman spectroscopy is given in the following. More information about their theoretical fundamentals can be found in the literature [110, 118, 187].

(FT)IR Spectroscopy

In IR spectroscopy, a molecule absorbs an infrared photon and goes from the fundamental vibrational state into an excited vibrational state [110]. However, not all molecules show infrared absorption. First, the frequency of the incident IR radiation must correspond to the frequency of the vibration, and second, the electric dipole moment of the molecule must change [153, 187]. The latter is achieved by certain expansions and contractions of chemical bonds between the atoms of a molecule. The characteristic vibrations of the molecules then result from the atomic composition, orientation, and number of bonds [153]. IR radiation can induce two types of vibrations: the chemical bond can stretch, or the bond angle can deform, i.e., bend [130]. By oscillating in different spatial directions, more complex types of stretching and bending are activated, such as *scissoring*, *rocking*, *wagging*, and *twisting* [153]. Molecules that follow this *selection rule*, i.e., their electric dipole moment changes during vibration, are called *infrared-active* [187]. Prominent infrared-active molecules are, for example, organic compounds, which is why IR spectroscopy is often used for their identification [187]. Since most polymers contain organic constituents (see Table 2.1), the infrared spectra of plastics include signals from aliphatic hydrocarbons, aromatic compounds, or oxygen-containing compounds (ethers, aldehydes and ketones, or esters) [187]. The chemical composition of an unknown plastic sample can then be determined by comparing the spectra with known plastic standard spectra in a spectral database [98, 164] or by comparison to absorption bands of polymers listed in the literature [103].

FTIR is an extension of IR spectroscopy based on the idea of interference of beams producing an interferogram [187]. The light from the excitation source is split into two separate beams that travel a different path length. Most commonly, a *Michelson interferometer* is used where different travel distances of the light beams are achieved by a movable mirror

[187]. When the beams are brought together again, constructive and destructive interference occurs depending on the travel distances. The detector then measures the intensity of the superimposed beams as a function of distance. The frequencies of the beams and the distances can be converted into each other by the mathematical *Fourier transform* [187]. Since information about the sample is contained in the frequencies of the beams, conclusions can be drawn about the sample. This means that IR and FTIR spectroscopy record the exact same signal with the main difference being the use of a spectrometer or interferometer, respectively. The interferometer enables all frequencies of the IR light emitted by the source to be scanned (wavenumber range typically between 4000–400 cm^{-1} for Mid-IR) [104, 130].

In this thesis, FTIR was used in all three publications to identify the polymer base type and characterize weathering-induced oxidation. Its findings were used to verify the LIBS results. In comparison to conventional IR spectroscopy, FTIR guarantees high performance, has a much better signal-to-noise ratio, and is significantly faster [130]. As it is an extension of IR spectroscopy, it is also non-invasive, not very destructive to environmental samples, and is less susceptible to disturbance from sample contaminants [94, 178]. However, moisture can still interfere with the sample identification, as water is infrared-active [94]. Therefore, the samples must be dried beforehand. The major disadvantage of FTIR is that pre-treatment can be very time-consuming, depending on the sample. In addition to density separation and filtration, chemical digestion of the samples is a mandatory step. Further limitations are the restriction to sample sizes above 20 µm due to the spatial resolution and to black plastic samples due to their broadband absorption of the dye carbon black [104, 212].

FTIR can operate in various modes: reflectance, transmittance, true specular reflectance/ reflection-adsorption, and attenuated total reflectance [94, 130, 212]. In this work, only the attenuated total reflectance (ATR) mode was used. Here, a crystal presses down the sample. The infrared light travels through the crystal to the sample and is totally reflected at the interface. As the light is reflected, a small portion penetrates into the sample and is absorbed [98, 163, 187]. This portion is called *evanescent wave* [17, 98]. The internally reflected light carries the absorption information and is directed to the FTIR detector, where the signal is recorded [98, 163, 187]. The absorption information comes from the fact that the evanescent wave excites vibrations in the material, which causes the reflected IR beam to lose energy at those specific wavelengths [187].

The ATR mode is used to analyze irregular plastic particles above 200–500 µm [98, 163] and has become a piece of standard equipment in modern microplastic laboratories [104]. However, this mode comes with limitations. It needs an infrared-transparent substrate, is a contact analysis method, and is not particularly well suited for large-scale examination of microplastics due to the focus on each individual particle [94, 104, 130]. Shim et al. (2017) report that it takes approximately 9 hours to scan one filter paper in this mode [178]. These

time-consuming and laborious investigations can be compensated for by using automatic mapping algorithms [178, 182]. However, this does not change the need to monitor the measurement. Particles can stick to the ATR-crystal during the measurement, which requires intervention [104].

Concerning this study, FTIR spectroscopy is an important analytical technique that can not only identify the plastic type but has also been used for evaluating the oxidation behavior of plastic [6, 202]. The amount of oxidation can be studied using the sum of the main characteristic absorption bands for oxidation or the *carbonyl index* (CI). The latter is used for a more systematic analysis as it evaluates the peak ratios. The CI is calculated by normalizing the carbonyl vibration peak C=O (1810–1690 cm^{-1}, centered at 1715 cm^{-1} [212]) to a reference bond mostly unaffected by oxidation [6]. This means:

$$CI = \frac{\text{Area under the absorption peak of the carbonyl compound}}{\text{Area under the absorption peak of the reference bond}}. \tag{2.1}$$

Here, we follow the advice of Almond et al. (2020), who compared several CI calculation methods and found equation (2.1) to be the most reliable one [6]. However, there is no standard method for calculating the CI value, which makes it difficult to compare studies. Note that since entire areas of the spectral data are used for the calculation, the areas must be selected precisely and checked for interference from other chemical processes. Otherwise, the CI value is not accurate. This is apparent in Publication 3, where a broad shoulder peak distorts the area under the reference bond. As an example, two FTIR spectra with marked carbonyl peaks are plotted in Fig. 2.7. It shows an unweathered and an artificially weathered PP sample measured with the LUMOS II system. The PP samples refer to the samples provided by the collaborators of the University of Bayreuth mentioned in section 2.1. The spectra were taken in the mid-infrared range (4000–900 cm^{-1}). It becomes evident that not only the carbonyl peak appears due to weathering, but also other areas are affected, such as the range below 1300 cm^{-1} (C-O region). These ranges can also be used to evaluate degradation.

The ability of FTIR to measure both plastic-type and degradation products makes it a powerful and versatile method in (micro)plastics research. However, the measured degradation products also complicate the use of a reference spectral database [164, 212]. Weathering-related changes in the infrared spectra, such as hydroxyl groups, alkenes, carbon double bonds, and carbonyl area, are often not taken into account when comparing or matching the spectra [178, 182, 212]. This can lead to misclassification and false negative results. Therefore, the spectra should not be simply matched with those of the reference libraries but should be evaluated by an experienced personnel member who can classify the effects in the spectrum.

In addition, FTIR is primarily a surface detection method. However, a three-dimensional

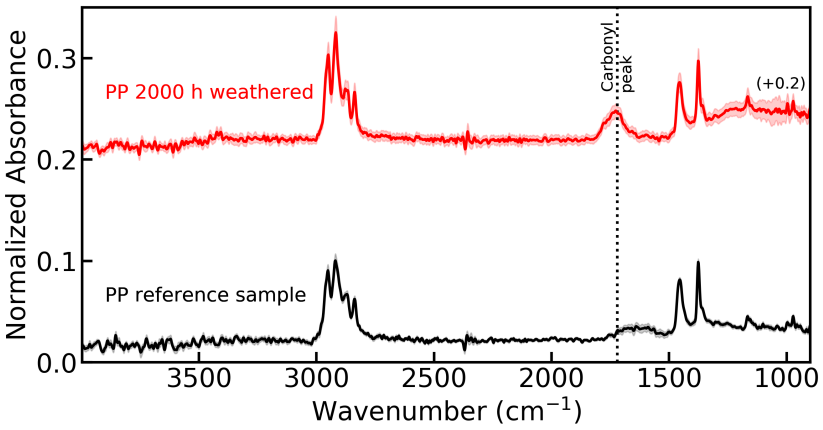

Figure 2.7: ATR-FTIR spectra of artificially weathered and unweathered PP. The spectra are the average over 16 spots (the average value is depicted as a line, and the standard deviation is depicted as a light background) and smoothed for CO_2 and hydrogen bands. The dashed line marks the carbonyl peak which is only visible in the weathered sample (red line). For visualization reasons, the data is plotted with an offset. The weathering time of 2000 h corresponds to 1.2 years of outdoor weathering in Central Europe.

analysis of the oxidation process is required to gain a better understanding of the oxygen uptake of plastics [42, 134, 136]. As mentioned in section 2.3, oxidation penetrates into the bulk of a sample and is thus responsible for microcrack formation and subsequent fragmentation. A surface detection method can still be used to perform a three-dimensional analysis when the cross-section of the sample is exposed [134]. However, exposing the cross-section is not easy to implement, depending on the sample's size and shape. Additionally, another instrument, e.g., a microtome, must be used for the analysis, which is time-consuming and costly. Therefore, alternative techniques for three-dimensional chemical imaging of weathering-induced oxidation are needed.

Raman Spectroscopy

The second most commonly used spectroscopic method for (micro)plastic identification and analysis is Raman spectroscopy [14, 212]. This method is also a surface detection technique that deals with the inelastic scattering of light by molecules [118]. In contrast to IR spectroscopy, which is based on changes in the permanent dipole moment, a molecule shows Raman absorption when the incident radiation causes a change in *polarizability* [118]. Polarizability describes the ability of the electric field of the incident laser to create a dipole in the molecule [110, 118]. A molecule that follows this *selection rule* is then called *Raman-active*. Although this difference between Raman and IR spectroscopy seems small, it plays an essential role in sample characterization, as will be apparent in the course of this section.

In Raman spectroscopy, a monochromatic light source, whose transition energy ideally does not allow fluorescence, is directed onto the sample. The Raman scattering is then

displayed as a transition of the molecule to a *virtual energy state* [110]. This state is not a stationary state that corresponds to any vibrational or electronic energy levels of the molecule but is a very short-lived quantum level ("it is not a solution of a time-independent Schrödinger equation" [124, p. 55]) [102, 110]. In that sense, a virtual state serves as a mathematical tool to determine the transition from the initial to the final state of the molecule [102, 124]. It corresponds to the energy of the light source whose electric field shifts the positive and negative charges relative to each other, which can eventually create a dipole. The interaction with the sample scatters a small portion of the light and shifts its energy relative to the laser frequency [110]. These shifts correspond to the transition energy between two vibrational states [118]. Molecules in the ground state generate lines shifted to energies lower than the laser source [118]. These lines are called *Stokes lines*. Lines shifted to higher energies are due to molecules in excited vibrational states and are called *anti-Stokes lines* [118]. Since the energy shifts depend on the structure of the different molecules in the samples, characteristic peaks are obtained. A schematic of the transitions for the Stokes and anti-Stokes shift can be seen in Fig. 2.9.

In many cases, the shifts in energy, which are traditionally measured in a unit known as *Raman shift* (cm^{-1}), also correspond precisely to the frequencies in the IR spectrum [110]. Therefore, similar results can be obtained when using Raman and IR spectroscopy. However, there are molecules whose *infrared-* and *Raman-activity* are mutually exclusive, making them undetectable by the other method [104]. In short, IR and Raman spectroscopy provide complementary results, even though the peaks have different physical origins [94, 104, 110]. In general, the more symmetric the molecule, the greater the differences between the IR and Raman spectra [110]. This becomes evident when looking at polar and nonpolar bonds in plastic samples [110]. Polar bonds are highly IR absorbing but have a weak Raman effect [110]. Nonpolar bonds, in turn, are weak or absent in IR spectroscopy but show strong Raman scattering [110]. For hydrocarbon plastic samples with a carbon chain backbone, such as PE, this means that the vibrations of the backbone can be studied using Raman spectroscopy [110]. In contrast, the vibrations of the substituents on the carbon chain, like C-H or C=O, which have polar bonds due to the differences in electronegativity, are best studied with IR spectroscopy [110].

The differences between Raman and IR spectroscopy for a plastic sample are illustrated in Fig. 2.8. Here, the Raman and FTIR spectra of an LDPE sample provided by the collaborators of the University of Bayreuth are measured in the spectral range of 4000–1000 cm^{-1}. The Raman spectrum was recorded with an exposure time of 10 s using the self-build Raman setup mentioned in section 2.2. The FTIR spectrum was recorded using the LUMOS II system. The different Raman-active and infrared-active vibration bonds of an LDPE sample are marked with dashed and dotted lines, respectively. For clarity, a list of the relevant vibration

peaks and mode assignments is provided in Table 2.3. It is evident that certain peaks are only displayed in one method, e.g., below the regions 1300 cm^{-1}, and that others match in both, e.g., C-H stretch at 2845 cm^{-1}.

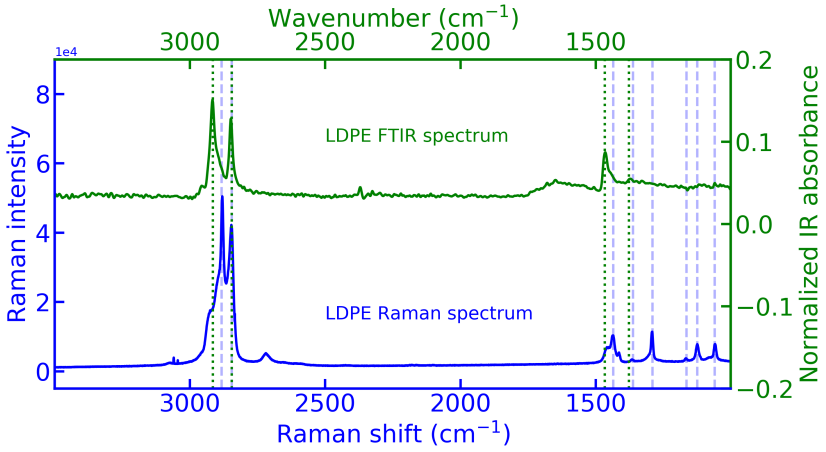

Figure 2.8: ATR-FTIR and Raman spectra of (LD)PE. The dotted and dashed lines mark the Raman and IR vibration bonds. The data is plotted with an offset. Information about the (LD)PE sample provided by the University of Bayreuth, e.g., manufacturer and size, can be found in chapter 2.1.

Table 2.3: List of major vibration modes and their assignments for ATR FTIR and Raman spectra of (LD)PE (extracted from [103], [181] and [156]).

Raman shift (cm^{-1})	Vibrational mode	IR absorption band (cm^{-1})	Vibrational mode
2883	C-H stretch	2915	C-H stretch
2845	C-H stretch	2845	C-H stretch
1440, 1460	CH_2 bend	1467	CH_2 bend
1418	CH_2 bend and CH_2 wag	1462	CH_2 bend
1375	CH_2 wag	1377	CH_3 bend
1175	CH_2 rock		
1070, 1135, 1300	C-C and CH_2 stretch and twist		

Raman spectroscopy has many advantages. It is a non-destructive and non-contact analysis method, needs only a small amount of sample material, is environmentally friendly, and has a spatial resolution down to 1 µm (much smaller than FTIR) [94, 98, 178]. In combination with confocal optical microscopy, particles with sizes of up to 300 nm can be analyzed [98]. Compared with FTIR, Raman spectroscopy has a broader spectral coverage, narrower spectral bands, a lower signal-to-noise ratio, and is insensitive towards water [94]. This enables Raman spectroscopy to investigate plastics in aqueous or biological samples [98].

However, Raman spectroscopy is used far less frequently in microplastic research than FTIR [162]. According to Prata et al. (2019), only 10 % of the reviewed studies used Raman spectroscopy [162]. This is not least due to its many weaknesses, such as long acquisition times due to the weak intensity of Raman scattering and manual spot selection [14, 94]. The

most significant limitation is the occurrence of fluorescence [14, 94, 98, 130]. (In-) organics, (micro)biological impurities, additives in the polymer chain, and, more importantly to this study, degradation products can cause fluorescence [14, 98]. These changes in the chemical composition of a sample can affect how much energy has to be put into the system for an electronic transition. As mentioned earlier, the laser energy for Raman spectroscopy is chosen so that ideally no electronic transition is activated, i.e. no fluorescence occurs. However, if the sample has changed chemically, the laser energy may now correspond to an electronic transition energy, resulting in fluorescence [98].

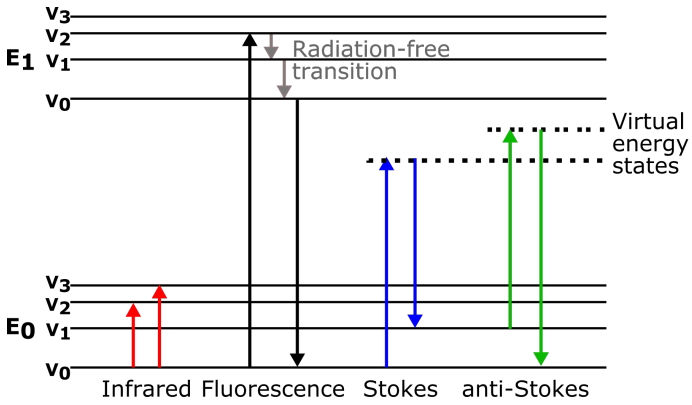

Figure 2.9: Energy states related to IR absorption, fluorescence, and Raman scattering (adapted from [122]).

The problem with fluorescence is that it interferes with the Stokes lines, which are more commonly used for analysis than anti-Stokes lines [118]. In Fig. 2.9, a schematic of the transitions for IR absorption, fluorescence, and Raman scattering is shown. It can be seen that in both fluorescence and Stokes lines, the emitted photons are shifted to the long-wavelength region of the spectrum relative to the light source [130]. The only difference is that an electronic transition occurs in fluorescence, while a vibrational state is excited in Stokes lines. Since the Stokes lines are very inefficient (1 in 10^8 photons [110]) and the fluorescence quantum yield is often orders of magnitude greater, the Raman lines are covered by the fluorescence, making sample identification and characterization much more complex [120, 130]. This phenomenon can be seen in Fig. 2.10.

Here, Raman spectra of weathered and unweathered PS samples are displayed, which were provided by the collaborators of the University of Bayreuth and were recorded in the spectral range of 4500–500 cm^{-1} at an exposure time of 1 s with the self-build Raman setup. The plot shows the fluorescence in the weathered sample. This is evident in an elevated baseline, which completely overshadows the Raman signal. Such emergence of fluorescence is an indicator of the formation of new chemical products within the sample [120]. It is obvious that fluorescent materials often cannot be detected by Raman spectroscopy, which restricts its application for real (micro)plastics. Although there are several methods to minimize fluorescence, such

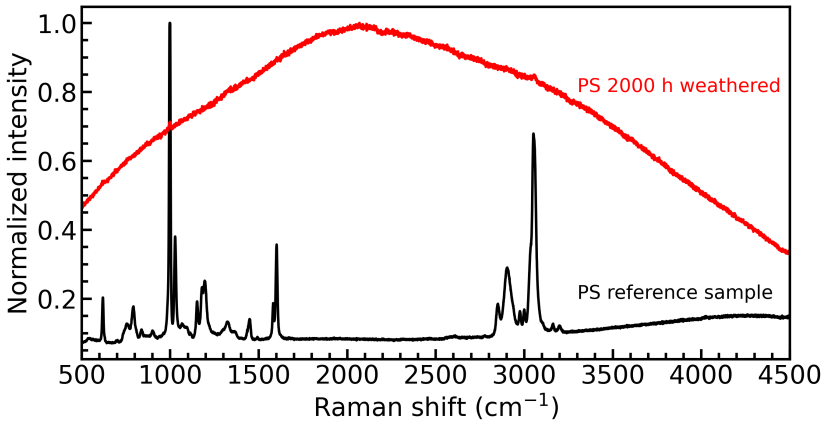

Figure 2.10: Raman spectra of artificially weathered and unweathered PS. The spectra are taken from one spot of the sample that has been measured once. The characteristic PS peaks visible in the reference spectrum (black line) are overshadowed by the increased fluorescence coming from oxidation products (red line). The data is normalized to the maximum value in the spectrum.

as nonlinear Raman techniques (e.g., coherent anti-Stokes Raman Spectroscopy (CARS)), cleaning protocols, or photobleaching, they all come with several drawbacks, as discussed by Araujo et al. (2018) [14]. Only automatic algorithms that still recognize small signatures in the data seem promising [14].

Considering the physical origin of fluorescence, i.e., the electronic transition of a molecule, the optimization of measurement parameters, such as laser wavelength and power, objective magnification, or acquisition time, is the most apparent approach to minimize its occurrence [98]. In this context, the choice of laser wavelength is crucial as the energy of the photons decreases with a longer wavelength. If the laser is exchanged with one of a larger wavelength, i.e., smaller energy, an electronic transition is often not possible, and little to no fluorescence can occur [98]. However, the intensity of the Raman effect declines with the fourth power of the laser wavelength, resulting in much weaker intensities and longer acquisition times, making identifying plastics difficult [98].

It can be concluded that Raman spectroscopy is not suitable for a systematic analysis of the weathering-induced oxidation behavior of the plastic samples used in this study. Instead, FTIR is used to validate the LIBS results for polymer identification and characterization. It should be mentioned that there are other spectroscopic methods in the field of (micro)plastic research, such as SEM-EDX, which has already been noted in section 2.4.1. Also, time-integrated [111, 149] and time-resolved photoluminescence spectroscopy [79] has recently been explored for (micro)plastic detection. However, discussing these methods in detail is beyond the scope of this work, which aims to introduce LIBS as a new and complementary technique to FTIR and Raman spectroscopy.

Evidently, the established spectroscopic methods have significant drawbacks, including a typically long acquisition time for analysis, distortion of the data based on contaminates

and weathering effects, lack of standardization, and the fact that these methods are surface detection techniques. This limits their applications. Additionally, depending on the sample, they may require excessive pre-treatment, such as chemical digestion or drying. Thermal analysis, in turn, does not require sample pre-treatment but also lacks the ability to perform layer-by-layer analysis. Here, unambiguous identification of plastics is more difficult than with spectroscopic methods due to the complex data situation and its physical restrictions. The following chapter attempts to overcome the analytical challenges of the established methods, in particular, the reduction of sample pre-treatment and depth profiling, using LIBS.

Chapter 3

Addressing Analytical Challenges using Laser-Induced Breakdown Spectroscopy

As seen, numerous techniques are available for identifying and characterizing (micro)plastics. Each of these techniques enables the investigation of various plastic properties. Although they already cover a wide range of applications, there are still some properties that are difficult to access with conventional methods. These include the direct unambiguous identification of the base polymer, determination of degradation effects, and, in particular, the systematic examination of plastic samples over their entire sample volume. This work introduces LIBS to address these analytical challenges. In this context, Publication 1 covers the identification of the base polymer. Publications 2 and 3 address the study of weathering-induced oxidation and its penetration depth. This chapter provides the theoretical background used to perform these measurements and the operation of LIBS.

LIBS is a technique of atomic emission spectroscopy that uses optical sample excitation for qualitative (e.g., determination of elements in a sample) and quantitative (e.g., determination of the elemental concentration in a sample) analysis [9, 51, 137]. It creates a plasma on the sample's surface using a focusing lens and a pulsed laser with a pulse energy of typically a few dozen to a few hundred mJ [51]. The plasma is built up by a mixture of sample material and the surrounding gas atmosphere. In the plasma state, the material splits into ions and electrons, which allows the material composition to be determined when the plasma cools down [51]. A spectrograph collects the plasma light emitted by excited ionic and atomic species and separates it according to its spectral constituents. The detector then captures the emission signal as a function of wavelength [51]. Based on the unique spectra of individual atoms, conclusions can be drawn about the elements in the plasma. Fig. 2.1 in section 2.2

shows a schematic overview of the main components used for LIBS analysis, i.e., light source, optics, spectrograph, and detector.

The term *plasma* refers to a state of matter. It is an overall neutral "local assembly of atoms, ions, and free electrons" [51, p. 23]. The transition from one state of matter to another is a phase transition at sharply defined transition boundaries, such as transition temperatures or energy densities. These phase transitions are material dependent and therefore can also be used to characterize materials, as mentioned in section 2.4.2. In LIBS, however, it is not the transition to the plasma state used as the characterization feature but the emitted *plasma light* [51, 137]. Note that the term *plasma light* used in the literature might be confusing since, strictly speaking, the emitted light is not part of the plasma, but only the after-effect of the interaction of atoms, ions, and electrons.

Due to the simple apparatus to perform LIBS measurements, this method is nowadays a well-established analytical technique [51, 137]. LIBS has a short acquisition time (in the order of µs), can be used for in-situ measurements, ablates only a small amount of sample material, requires in principle no sample pre-treatment, and can detect all elements of the periodic table only restricted by the laser energy and the sensitivity of the spectrometer. The minimum sample size measured with LIBS has not yet been evaluated. However, based on the used wavelength, it can be assumed that these are smaller particles than those detected by FTIR. The range of applications extends across all industrial sectors, from space missions [53] to food [3] and plant analyses [57, 173]. Most notably, LIBS is known for its use in combustion and metallurgical applications [57].

Unlike its simple apparatus, the physical and chemical aspects involved in LIBS are complex processes. The spectrochemical assumptions and diagnostics behind laser-induced plasmas should be reviewed before discussing LIBS' application in (micro)plastic research. Since plasma theory is challenging to quantify, especially when quantum mechanical effects have to be taken into account, only those aspects that are directly connected to the attached publications are discussed. To approach LIBS theoretically, the section is divided into three parts: First, the *light-matter interaction* is discussed, which covers the phenomenological description of the plasma formation and ablating material from solid samples, as well as plasma progression (3.1). Second, the *plasma diagnostics* are elaborated, which focuses on extracting information from the emitted plasma light where the spectral lines represent the elemental composition of the sample (3.2). Third, LIBS is discussed as a *surface and depth profile analysis* technique and the associated experimental challenges for this study are presented (3.3). The first section helps with the selection of the measurement parameters and, in combination with the third section, plays an essential role in Publications 2 and 3, as the ablated mass is decisive for depth profiling. The second section determines important plasma parameters such as *temperature* and *electron density*, the characterization of which

are necessary for understanding the physics behind laser-induced plasmas.

3.1 Laser Pulse Interaction with Solids and Plasma Formation

In LIBS, the interaction of a pulsed laser with a solid matter does not only consider the process of plasma formation but also the evaporation of matter called *laser ablation*. In the following section, both will be explained in more detail. In this context, the plasma formation, or more precisely, the transition from an insulating, neutral gas to a conducting (partially) ionized state, is referred to as *breakdown* [137]. Note that the LIBS process explained is restricted to ns-pulses, as only a Q-switched Nd:YAG laser was used in this work. The pulse duration is responsible for the dominance of thermal or ionization effects in the plasma, causing ps- or fs-pulses to result in different plasma evolution and crater formation [9]. For more information on ps- or fs-pulses, please refer to the following books and publications: [9, 51, 137, 140].

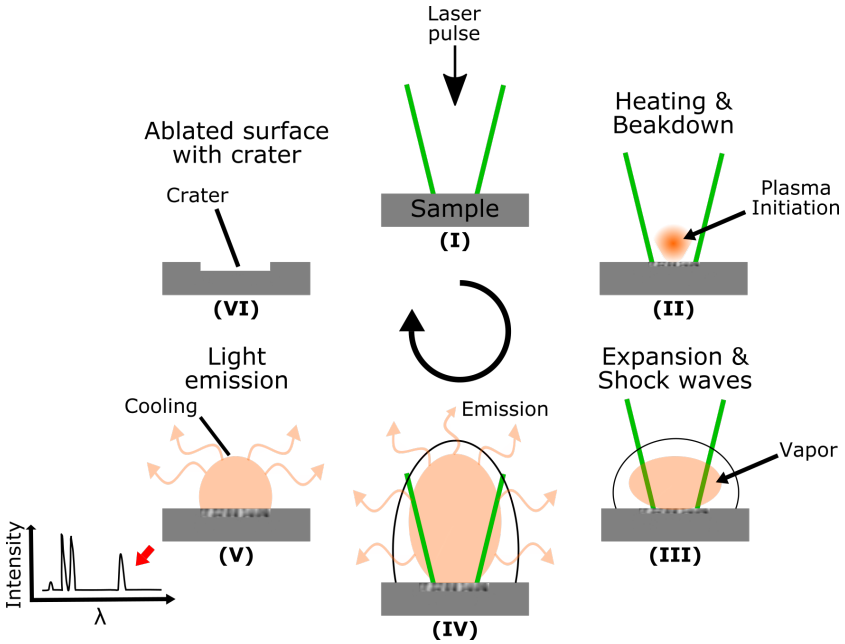

Figure 3.1: Plasma life cycle. The figure shows the multi-step LIBS process from breakdown to laser ablation, signal extraction, and crater formation for a single laser pulse. The schematic is based on [137] and [87]. Note that a chronological order has been chosen for better understanding, but some processes may occur simultaneously.

Fig. 3.1 illustrates the life diagram of the main events in laser-induced plasmas. Note that some events and their associated processes described in the following section do not necessarily have to occur in this order. They can happen simultaneously. A chronological order was used for better understanding. The life diagram will be explained in three parts: the plasma formation and expansion ((I) - (III)), the plasma's light emission ((IV)-(V)), and

the ablation crater (VI).

Plasma Formation and Expansion ((I) - (III))

In the first step, the laser is focused on the sample's surface or inside the sample (I). The energy of the laser is transferred to the material in the form of photons. Most of the energy is converted into heat by the electronic structure of the material and released via vibrations of the lattice atoms [140]. With a certain probability, the sample's atoms and electrons absorb the photons and transition to higher energy states. This will eventually break down the connections between molecules, atoms, and electrons, resulting in a(n) (ionized) gaseous state. This leads to plasma formation caused by optical excitation (II), from now on referred to as *breakdown* [51, 137]. The minimum irradiance I_{min} of a laser pulse for vaporization is given by Moenke-Blankenburg [51, 138]:

$$I_{min} = \rho L_v \sqrt{\frac{\kappa}{\tau_\rho}} \tag{3.1}$$

where L_v is the latent heat of vaporization, ρ is the density of the sample material, τ_ρ is the laser pulse width, and κ is the thermal diffusivity [51, 138].

There are two mechanisms that can cause breakdown: *multi-photon ionization* and *cascade ionization* [51, 107, 137]. In both, free electrons play a crucial role. Note that the term *free electrons* can be misleading since free electrons do not exist in solids as they do in plasmas [107, 205]. In solids, the term refers to *quasi-free* electron, i.e., electrons whose "kinetic energy is great enough ... [to] move through the liquid or solid lattice without being trapped by localized potential wells " [107, p. 158]. The term *free electrons* is used in this work for consistency with the literature [51, 107, 137, 140, 177].

Cascade ionization usually occurs in two steps. First, free electrons are generated at the beginning of the laser pulse (*cascade initiation*), and second, a high density of free electrons is built up (*cascade build-up*) [107, 140]. In the cascade initiation step, free electrons are usually created in the focal volume by multi-photon ionization or thermal ionization of impurities [107, 140]. The former describes a process in which several photons whose energy is below the ionization threshold can combine their energy to ionize an atom [107, 140]. Note that *multi-photon ionization* is also an independent breakdown mechanism, which is explained later in this section. Thermal ionization, in turn, occurs at higher gas temperatures, where molecules with sufficiently high energy can cause ionization in collision processes [137, 140]. This step usually requires a high irradiance, which the laser source provides in laser-induced plasmas. Free electrons are then the particles that operate as energy recipients, activating the cascade's build-up [137].

The initial idea of the cascade ionization is to create multiple free electrons from a single electron. In this context, the occurrence of *inverse Bremsstrahlung* is indispensable [107, 137,

177]. Inverse Bremsstrahlung refers to a process in which a free electron absorbs a photon from the incident laser pulse during a collision with an atom, ion, or molecule [9, 107, 177]. Once the energy of a free electron, gained by a collision with a heavy particle, exceeds the ionization potential of a species, the free electron can ionize a bound electron, creating two free electrons with a lower energy [107]. Repeating this process produces a large number of free electrons, i.e., a cascade, leading to breakdown. Note that the collision with a heavier particle is needed for a free electron to absorb a photon; otherwise, the energy and momentum conservation laws would not be fulfilled. A schematic of cascade ionization in breakdown formation is shown in Fig. 3.2.

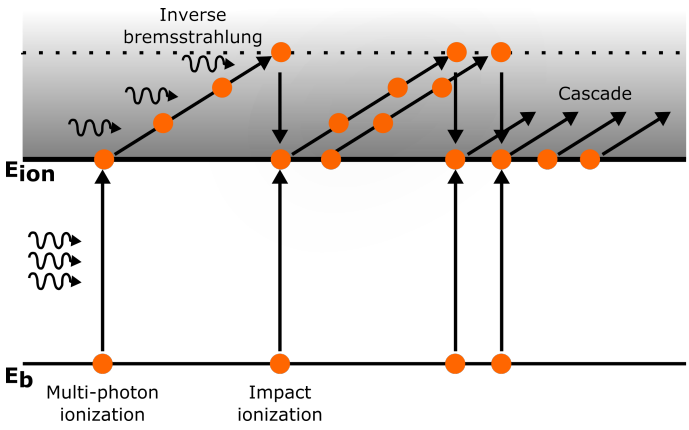

Figure 3.2: Schematic of cascade ionization in the formation of breakdown (progression from left to right). The orange circles represent electrons. $\mathbf{E_b}$ and $\mathbf{E_{ion}}$ represent a bound and the ionization state, respectively. The wavy arrows represent the incident radiation. First, a free electron is created by multi-photon ionization. Then, the energy of the free electron is increased due to inverse Bremsstrahlung. Lastly, the collision with a heavy particle creates an additional free electron. The process is repeated. The figure is adapted from [205].

The build-up of the cascade ionization is not trivial as it is a balancing act between energy gain and energy loss [177]. On the one hand, free electrons created by multi-photon ionization and higher temperatures must gain enough kinetic energy to further ionize atoms or molecules. On the other hand, collisions of free electrons with ions, atoms, or molecules can lead to the transfer of their energy and not to the generation of more charged particles [107, 137]. This means that the energy loss during these collisions must be less than the energy gain from inverse Bremsstrahlung in order for the cascade to build up [107, 177]. Additionally, since free electrons can recombine with ions during the collision process to form atoms or ions of a lower ionization stage, the recombination rate must also be lower than the ionization rate [107, 177]. Otherwise, there will not be enough free electrons to absorb the laser energy and ionize enough atoms and molecules. Therefore, a threshold value exists at which the breakdown occurs.

The second process that can cause breakdown is multi-photon ionization. This process differs from the cascade ionization process in that sense that no initiation is needed,

and the breakdown is significantly faster, meaning that the loss mechanisms are negligible [107]. Here, several photons are simultaneously absorbed, ionizing each bound electron separately [107]. There is no need for free initial "electrons, collision[,] or particle-particle interactions " [107, p. 159]. Multiphoton-ionization is a nonlinear operation, i.e., many laser photons are required to ionize a single bound electron, that only makes a notable contribution at very high irradiances [107, 140]. Although this process is generally the most common breakdown process, cascade ionization is the leading mechanism in laser-induced plasmas controlling the breakdown [177]. This is due to the rapid but linearly increasing generation of free electrons during multiphoton-ionization. Cascade ionization, in turn, starts slowly but then increases exponentially, meaning that the process eventually exceeds multiphoton ionization. For this reason, the process of cascade ionization is always referred to in the following when specifying breakdown. For the plastic samples used in this study, breakdown occurred at a power density of $5.09 \times 10^{10} \mathrm{W/cm^2}$. This value is in line with previous studies, according to which the threshold value for breakdown in solid matter is in the order of 10^{10} $\mathrm{W/cm^2}$ [9]. For the conducted experiments, however, a higher power density was used to achieve a better signal-to-noise ratio.

After the breakdown, the plasma expands almost adiabatically in all directions (III) [140]. The most fundamental characterization of a plasma is the *degree of ionization*, which describes the ratio of electrons to other species in the plasma [51]. LIBS plasmas are usually weakly ionized with a degree of ionization lower than 10% [51, 137]. This low degree might result from the fact that the recombination process grows faster than the ionization formation process with increasing ionization since it requires two charged particles to combine. Thus, more free electrons recombine with atoms or molecules than new free electrons are generated.

For the laser used in this study, the plasma is created before the end of the pulse (IV). However, the laser pulse only partially reaches the sample surface after breakdown because the plasma almost entirely absorbs it. This happens because the plasma acts like a dense medium [9, 137]. Free electrons absorb the laser energy and release it again when colliding with other species, which heats up the plasma and increases its lifetime [9, 137]. Additionally, the ions in the plasma scatter the laser light and reduce its intensity. This effect is called *plasma shielding* [9, 137]. Since the laser pulse barely reaches the sample surface, this process reduces the ablation rate, leading to molten material around the crater [9].

The Plasma's Light Emission ((IV)-(V))

This section describes the transition from event (IV) to (V) of Fig. 3.1 in more detail and defines the LIBS measurement parameters for the analysis of plastics in Publications 1, 2, and 3. Fig. 3.3 shows the time course of the plasma generated with a single laser pulse. It shows that a plasma is not a stationary phenomenon, but a constantly evolving state of matter,

leading to regions in which different species dominate (first ions, then atoms, and eventually simple molecules). At first (nanoseconds after the laser hits the sample), the ionization degree is maximum, with ions and electrons being the dominant species in the plasma. After that, the plasma begins to relax. Free electrons recombine with ions to atoms or ions of a lower ionization stage [51, 137]. This is done by plunging into an atomic or ionic energy level, releasing the excessive energy in the form of a photon. However, when electrons come into the vicinity of these species, this does not necessarily lead to recombination processes. The electrons can also be scattered, leading to a deceleration of the electrons and their release of energy [51]. This process is commonly known as *Bremsstrahlung* [51, 137, 140, 143].

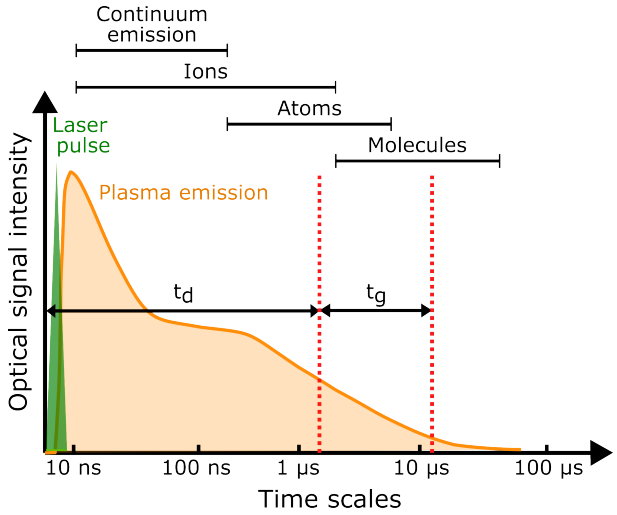

Figure 3.3: Temporal course of the emission signal from different species during plasma lifetime. The figure shows the course of the white light continuum and the periods in which ions, atoms, and molecules predominate. In a time-resolved measurement, the measurement parameters can be adjusted for the regions of interest. Here, t_d and t_g are the measurement parameters representing the gate delay time and the acquisition window, respectively. The dotted red lines show that the measurement parameters were primarily set to detect atomic and molecular emission signals. The figure is based on [137] and [72].

The recombination processes and *Bremsstrahlung* produce a *white light continuum* [51, 137]. This continuum emerges because the free electrons involved in recombination and deceleration processes generally do not have discrete energy levels. Therefore, the emitted photons have varying wavelengths and are observed as a continuum [51]. The process that generates the continuum decays more rapidly than the process of light emission by atoms and ions, as fewer and fewer free electrons are available over time. However, the white light continuum is so intense that when measured over a period of time, it can overlay the weaker emission signals from trace elements and minor species, even when it decays [137]. Particularly in the early plasma state, when a large number of free electrons is still present, it is sometimes challenging to capture element-specific radiation. Therefore, the white light continuum has to be separated using a time-resolved strategy in LIBS measurements [137].

A schematic representation of the sequence of electronic transitions that occur during the lifetime of the plasma is shown in Fig. 3.4. Before the laser hits the sample, the electrons are in the ground state (initial state). Once excited or ionized, the electrons are brought into higher electronic states or even completely detached from the atom (generation of free electrons). These transitions are called *bound-bound* or *bound-free* transitions, respectively. The shaded gray area visualizes the energy of the free electrons. After that, recombination and Bremsstrahlung occur, which generate the continuum. As seen in Fig. 3.4, these transitions are not discrete energy transitions. The discrete transitions occur during plasma relaxation, which then leads to a characteristic emission.

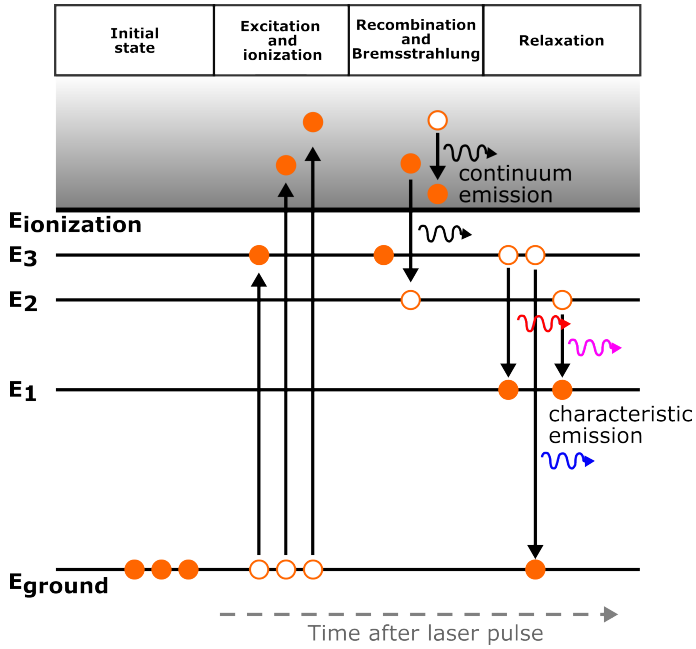

Figure 3.4: Atomic energy transitions occurring during LIBS (progression from left to right). The orange circles represent electrons. The white circles represent holes (the absence of electrons). Characteristic emission occurs during the relaxation of excited electrons to lower energy states. The figure is based on [47].

Plasma relaxation starts after the end of the laser when the plasma begins to cool down (30–100 ns after the plasma ignition) [143]. Since ions and atoms do not gain any further energy in the form of heat or light, they transition from high to low energy levels, emitting photons that correspond to the energy difference. Due to the uniqueness of these energy levels for all species, element-specific radiation is emitted during the cooling of the plasma (V).

As the plasma cools further, simple molecule radicals are formed. These are created by recombining the material atoms with each other, with the surrounding gas atmosphere, or by direct ablation [81]. Molecule radicals consist of different types of bonds and emit radiation at wavelengths that differ from those of the constituent elements [172]. This is because

the emitted radiation can be divided into rotational, vibrational, and electronic transitions according to the *Franck-Condon principle* and *Born-Oppenheimer approximation* [172, 207]. The analysis of molecule radicals is then achieved "in units of a band structure at different regions depending on the electronic energy levels and electron configuration" [172, p. 411], which offers new possibilities for the study of (micro)plastics.

Previous studies have explored the detection of diatomic radicals, such as CN or C_2, using LIBS [81, 204, 211]. As will be discussed in Publication 1, the C_2 bond plays a decisive role in the identification of plastics. The C_2 emission is caused by direct emission from the molecular fragments of the sample material or by recombination, or both [81, 211]. This means that for the detection of the C_2 bonds, "a carbon-carbon [single] bond (C-C) or [a] carbon-carbon double bond (C=C)" [211, p. 2] must be present in the investigated material, as it is the case for plastics. The CN bonds, in turn, are formed by combining with nitrogen atoms from the surrounding air [81]. These two bonds now enable vibrations between the atoms and thus absorb or emit radiation.

In Fig. 3.3, the measurement parameters t_d and t_g, which stand for the time between laser ignition and measurement (*gate delay*) and for the acquisition window (*gate window*), respectively, are adjusted in such a way that atomic and molecular signals can be recorded and most of the white light continuum is avoided. It is evident that the choice of measurement parameters significantly affects the detectable elements in the plasma. When the gate delay time is selected too short, only continuum light will be detected; is it selected too long, the ionic and atomic signals can have poor signal-to-noise ratios, but the molecular radical signals will be more present. A balance must be found. The measurement parameters in this study are determined following an approach by Grégoire et al. (2011) [81], which is displayed in Fig. 3.5.

To obtain optimum measurement parameters for the samples in this study, a PE reference sample was measured at different gate delays at a fixed gate window. Fig. 3.5 shows the signal-to-noise ratio (SNR) as a function of delay for the elements contained in organic compounds in PE. Note that the carbon line was not detected in the used LIBS system as it lies too deep in the UV range. For each delay, the gate window was set to 50 ns. The minimum gate delay was set to 100 ns. Below this value, continuum emission is expected, which is so strong that it can damage the detector. Therefore, no lower gate delays were chosen. As expected, the atomic signals H, N, and O displayed in (a) have maximum intensities at shorter delays (between 200 ns and 250 ns). The intensities of the molecular bonds displayed in (b) increase slowly, having their maximum at around 800 ns. This is surprising as previous studies show that the detection of the C_2 bond is recognizable before the CN bond due to the native origin of C_2 and the recombination origin of CN [204]. However, this observation cannot be confirmed here. On the contrary, both CN and C_2 bond emission courses in Fig.

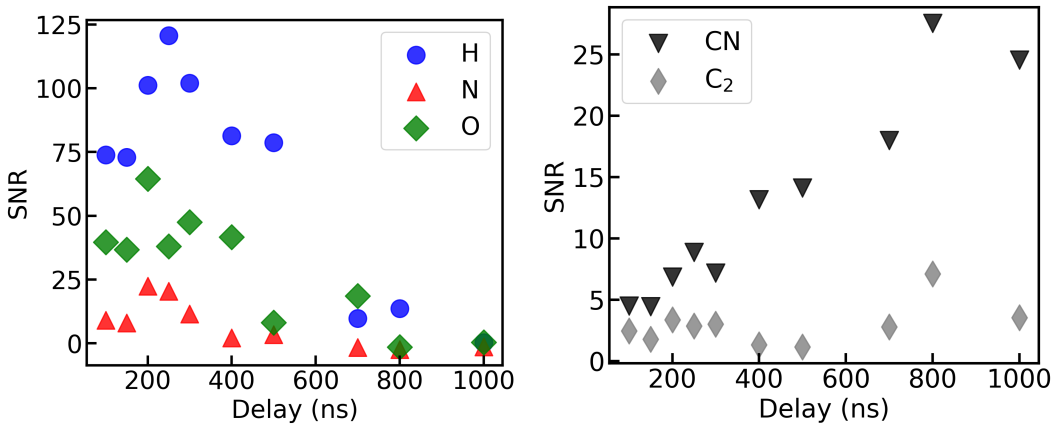

(a) Atomic signals (b) Molecular signals

Figure 3.5: Determination of measurement parameters in LIBS. The plots show the signal-to-noise ratio (SNR) for H I 656.3 nm, N I 746.8 nm, O I 777.3 nm, CN 388.3 nm, and C_2 516.5 nm as a function of delay for a PE sample. It is evident that atomic signals tend to appear earlier in the plasma than molecular signals. The evaluation procedure is based on Grégoire et al. (2011) [81]. Note that the carbon line at 247.67 nm was not detected with the used LIBS system, as it is too deep in the UV range.

3.5 (b) show an increase at later delays. It is assumed that the C_2 bond emission may be too weak to be detected at the beginning of the plasma. The strong emission of atoms then consequently overshadows the emission of the C_2 bonds. This explains why the course of CN and C_2 emissions in Fig. 3.5 (b) are similar. Additionally, the high concentration of nitrogen in the air is thought to cause the noticeably stronger CN bonds.

Based on these results, a delay of 240 ns and an acquisition window of 1 µs has been chosen as the standard measurement parameter for plastic analysis in this thesis. These parameters were also mentioned in section 2.2. Deviations from these parameters are related to the research question, e.g., if molecular signals are not part of the evaluation.

In addition to the measurement parameters, the ambient gas atmosphere is another important experimental factor that can influence the LIBS measurement. As already mentioned, the surrounding atmosphere can have a significant influence on the transmission of the produced spectral lines, e.g., in the formation of CN radicals [9, 143]. Density, pressure, and electronic configuration are additional properties of the ambient gas that affect the plasma formation [9, 143]. For instance, the ablation rate increases with increasing ambient gas density because the ambient mass limits the plasma's ability to expand, raising the temperature and plasma density close to the sample surface [143]. At the same time, the ablation rate decreases with increased ambient gas pressure [143]. This decrease is partly due to the plasma expansion, which causes the laser to no longer reach the sample surface, and partly due to the low re-condensation of the ablated mass [143]. The electronic configuration, in turn, affects the absorption of emitted radiation and can result in the absence of emission

lines in some areas of the spectrum [143].

More important to this study, however, is the impact of the chemical composition of the ambient gas. As seen with the CN molecules, new emission signals can appear in the spectrum as the entire plasma, made of a mixture of sample material and ambient gas, relaxes. In this study, all measurements were taken under air or nitrogen atmosphere and at atmospheric pressure. An example of the influence of the two atmospheres is shown in Fig. 3.6. Here, a PS sample provided by the collaborators of the University of Bayreuth has been measured in air and nitrogen atmosphere, displayed as blue and green curves, respectively. A shorter delay time (100 ns) was selected for the measurements since only atomic signals from the atmosphere were attempted to be captured. It becomes evident that the oxygen emission line at 777.3 nm is due to the surrounding air and does not originate from the sample, as it is absent in the green spectrum, i.e., in the nitrogen environment. This result is in agreement with the chemical structure of PS, which does not contain oxygen (cf. Table 2.1). Due to this strong influence, the choice of atmosphere must be made with respect to the research question. Concerning this study, the nitrogen atmosphere was chosen for detecting weathering-induced oxidation in plastic samples in Publications 2 and 3 to avoid any data distortion.

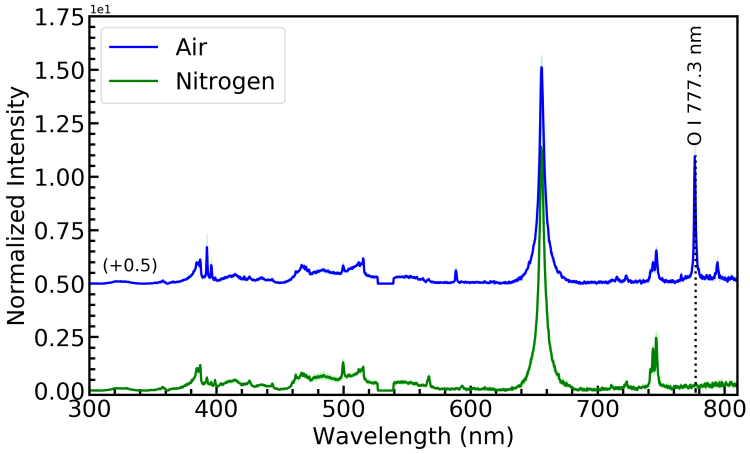

Figure 3.6: Influence of different atmospheres in LIBS. The figure shows a PS sample measured in air (blue spectrum) and nitrogen atmosphere (green spectrum). The oxygen emission line at 777.3 nm is clearly visible in the blue spectrum even though PS does not contain oxygen in its chemical structure. The same emission line is absent in the green spectrum. The plots are the average over three measurements (average is depicted as line, standard deviation as light background). The standard deviation is so small that it can hardly be noticed. For visualization reasons, the spectra are plotted with an offset. The figure is taken from the Supporting Information of Publication 3.

The Ablation Crater (VI)

The lifetime of a plasma can be up to 100 µs [51, 72, 137]. After its end, a crater is visible on the surface of the solid sample (VI). The image of a LIBS crater on a weathered PE microplastic sample is shown in Fig. 3.7. The ablated mass per pulse varies from tens to

hundreds of nanograms depending on pulse energy and duration, as well as on the focus of the lens or objective used in the setup and sample material [76]. In laser-induced plasmas, the ablated mass is not completely vaporized. Particles are also ablated that generate condensed vapor or form nanoparticles during recombination [9]. A laser pulse of energy E is then estimated to be able to vaporize a maximum mass M of

$$M = \frac{E(1 - R_s)}{C_p(T_b - T_0) + L_v} \tag{3.2}$$

where C_p is the specific heat, R_s is the surface reflectivity, T_0 is the room temperature in Kelvin, and T_b is the boiling point in Kelvin [51, 143]. The ablation depth per pulse, D_A, can also be determined. To do this, the equation has to be divided by the density of the material, and the laser pulse energy E must be replaced by the fluence F [51]. This yields

$$D_A = \frac{F(1 - R_s)}{\big(C_p(T_b - T_0) + L_v\big)\rho}. \tag{3.3}$$

Both, M and D_A are based on the assumption that all of the non-reflected laser energy enters the vaporization process [143]. In this sense, some effects are neglected, such as "losses by heat conduction; specific melting enthalpy; melt transport; recondensation of vapor; [the fact that] a part of the laser energy contributes to the expansion of the material cloud, the acceleration of the ambient gas and the formation of shock waves; [the fact that] a part is scattered and reflected by the vapor and the plasma; [and] a part contributes to the ionization and excitation of the species in the plasma" [143, p. 78]. For more information on M and D_A, and their derivation, see Noll (2012) [143].

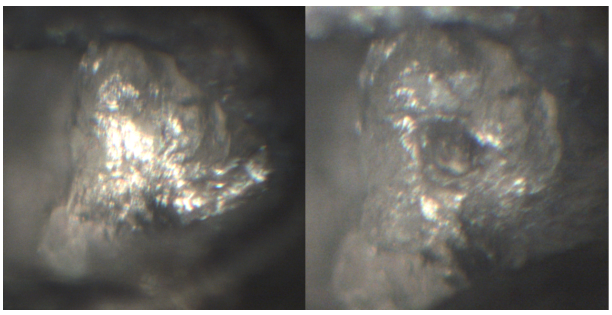

Figure 3.7: LIBS crater on a weathered PE microplastic sample. The figure shows a weathered PE microplastic sample before and after one laser shot. The crater has a size of approximately 80 µm in diameter. It shows no sharp edges, but molten material around it.

3.2 Plasma Diagnostics

In the case of an artificially generated plasma, such as laser-induced plasmas, the operator might want to evoke specific plasma properties. For example, it may be desired for the

plasma to be within a specific temperature range, as in industrial applications for coating substrates. In this work, the light emitted by the plasma should have a particular property, precisely that the measured spectral line intensities correspond to the relative concentration of the elements in the sample. To achieve this, LIBS is used to generate an *optically thin* plasma in *thermodynamic equilibrium* [51, 137]. Linking spectral information with the chemical composition of a material is not trivial. The spectral line intensities in the plasma, extracted during the event (V) in Fig. 3.1, depend not only on the corresponding element concentration in the sample but also on the plasma's characteristics and the sample's atomic transition probabilities [82]. While the previous section focused on a phenomenological description of laser-induced plasmas in plastic samples, the aim here is to determine the plasma properties, which also contributes to understanding the physics behind laser-induced plasmas. The following section explains the terms *optical density*, *thermodynamic equilibrium*, and *stoichiometric ablation*, as well as their experimental verification.

Stoichiometric Ablation

Stoichiometric ablation serves as the foundation for LIBS analysis. It describes the relationship between the composition of the sample and the composition of the observed plasma, which should ideally match [137]. This is not always the case. Vaporization of the sample material occurs at power densities $\leq 10^6$ $\mathrm{W/cm^2}$ using µs or longer laser pulses [137]. The sample material absorbs the optical energy from the laser pulse and converts it into heat, i.e., the thermal motion of the sample's constituents is accelerated [137, 218]. The constituents evaporate or sublimate when the absorbed energy surpasses the sublimation energy. The dissipation and vaporization are rapid compared to the pulse duration [35]. Elements with greater vapor pressure then accumulate in the vapor phase compared to the initial solid sample, which results in a distorted representation of the sample composition [35, 137]. This process is often referred to as *differential vaporization* in the literature [35, 137].

For laser ablation to be stoichiometric, a power density of 10^9 $\mathrm{W/cm^2}$ must be exceeded using ns or shorter laser pulses [36, 137]. This shortens the duration of the laser-material interaction and prevents the thermal energy from diffusing into the lattice [218]. Consequently, at such a high power density, an explosion occurs on the sample surface [36]. The vaporization temperature is quickly reached within the pulse duration, the material vaporizes and exerts pressure over the irradiated surface [36]. The pressure generated by the rebound of the vaporized mass prevents "the sample from further vaporizing until the underlying material reaches a critical temperature" [36, pp. 1471–1472]. Once the critical temperature is reached, the ablated mass is dissolved from the solid surface [36, 137]. Stoichiometric ablation should be the outcome of this procedure because of the quick heating and explosive ejection [35, 36, 137].

In Publications 1, 2, and 3, power densities of 7.07×10^{11} W/cm², 9.95×10^{10} W/cm², and 6.22×10^{10} W/cm² have been used, respectively. All of them are above the threshold of 10^9 W/cm². At these power densities, stoichiometric ablation continues to be satisfied because the ablated mass does not continue to increase but settles [36]. According to Chan and Russo (1991), this is probably due to a modification in laser-material interaction and plasma shielding (the plasma becomes opaque and reduces the amount of laser light reaching the sample) [36]. It can be concluded that well-chosen experimental conditions lead to stoichiometric ablation.

Thermodynamic Equilibrium

Plasma diagnostics seeks to describe the characteristics "of the assembly of atoms, molecules, electrons, and ions rather than [those of] the individual species " [51, p. 31]. In this process, *thermodynamic equilibrium* is an important pillar because, if satisfied, temperature determines many plasma properties [51, 137, 140, 143]. The term *temperature*, however, must be treated with caution. In a plasma, one cannot simply speak of only *one* temperature. The term is used to describe various energy transfers. This plays an important role because, based on the type of particles forming the plasma, a distinction between *kinetic*, *excitation*, *ionization*, and *radiative* energies and, accordingly, temperatures can be defined [137]. Only in the case of a *thermodynamic equilibrium* these energies are locally balanced and one can limit oneself to determining a *single* temperature [137, 196]. This temperature can be used to draw conclusions about the degree of ionization, the energy of the particles in the plasma, and help with the interpretation of the data, for example, if elements that are known to be part of the sample material are not visible in the spectrum. In this sense, the temperature is an important experimental parameter of laser-induced plasmas. The following section deals with the examination of thermodynamic equilibrium and the determination of the plasma parameters derived from it.

Maxwell, Boltzmann, Saha, and Planck functions theorize the distribution of kinetic, excitation, ionization, and radiative energies, respectively [137, 196]. Thus, when the plasma is in thermodynamic equilibrium, the entire system can be completely characterized using statistical mechanics [52, 143, 196]. However, thermodynamic equilibrium in a laser-induced plasma is rarely reached due to radiative losses [51, 137]. The photons emitted from the plasma lead to a discrepancy from the Planck function, affecting the equilibrium involving atoms, ions, and electrons [52, 197]. Here, it is beneficial that the non-equilibrium of photons can be ignored when processes involving other material species predominate in the plasma [137]. In such a case, the Maxwell, Boltzmann, and Saha distributions are still a perfectly adequate description [52, 137]. This new equilibrium state is referred to as *local thermodynamic equilibrium* (LTE) [51, 52, 137, 143]. In laser-induced plasmas, electron collisions are

the dominating process, which, if at least ten times larger than the radiative losses, ensure that radiative energies can be neglected [52, 82, 137]. The factor *ten* results from calculations by Griem (1963) [82].

LTE requires that equilibrium only takes place in small areas [51]. However, areas throughout the plasma can be in different LTE states, which is also attributed to the temperature distribution in the plasma itself (warmer on the inside than on the outside). The fundamental idea is that the different LTE states converge after a sufficient number of collisions [51]. This is because, the plasma then thermalizes, distributing its energy among the species and the volume [51]. Ultimately, this allows the thermodynamic equilibrium of the entire plasma to be approached. However, it should be noted that not all species achieve thermodynamic equilibrium simultaneously. Heavy species, such as atoms or ions, and light species, like electrons, balance each other faster individually, and slower together [51]. This can lead to species-dependent temperatures [51]. As a result, the plasma characteristics can be described by three parameters: the electron density n_e, the total number density of species, and the electron excitation temperature T [51, 52, 137, 143]. In most cases, however, the electron density and temperature are sufficient to characterize a plasma, as will be apparent in the examination of LTE.

To ensure LTE in a plasma, a series of tests has been developed. According to Cremers and Radziemski (2013) one of the most straightforward approaches is to show that the relative atomic emission signals of closely upper-spaced energy levels in the same multiplet are consistent with the basic hypothesis of the population of energy levels [51]. However, the validity of this approach may be limited by the re-absorption of radiation and interference with neighboring lines [51]. The most commonly used method is the McWhirter criterion [52, 133]:

$$n_e > 1.6 \cdot 10^{12} T^{\frac{1}{2}} (\Delta E)^3. \tag{3.4}$$

This criterion provides a lower limit for the electron density n_e given in cm^{-3} in LTE, with the energy difference ΔE corresponding to the selected upper and lower energy levels, and T to the temperature, expressed in eV and K, respectively. It is then found that collision mechanisms dominate over radiation processes, with very little deviation from LTE. In the following, the determination of electron density and temperature will be discussed to be able to verify LTE in Publications 1, 2, and 3.

A peak's profile sheds light on the events that take place in the plasma plume, as well as aids in determining the electron density [51, 112, 137, 140]. This is because the line profile results from many effects in the plasma, evident in *natural*, *collision*, or *Doppler broadening* [46, 51]. Neutral and collision broadening arise from collisions with neutrals, while Doppler broadening is based on the frequency shift caused by the movement of the emitted atoms (also

known as *Doppler effect*) [46, 51]. According to Cremers and Radziemski (2013), the natural broadening can be neglected because of its weak impact, leading to line widths of about one-thousandth of a nanometer [46, 51]. This resolution cannot be achieved with standard spectrometers. The Doppler broadening, in turn, results in line widths less than 0.1 nm, which also has very little effect, leaving collision broadening as the dominant mechanism [51]. When ions and electrons are involved in collisions, the collision broadening is specified as *Stark broadening* [51, 140]. Here, the electric fields induced by the fast electron movement and the slow ion movement act on the atoms in the plasma and cause them to split and shift their energy levels, broadening their emission lines [9, 51]. Hence, the Stark broadening "depends on the density of charged particles in the plasma" [16, p. 5569]. This allows the electron density to be determined [1, 63, 128, 137]. As a result, the Stark broadening of a line $\Delta\lambda_{Stark}$ is composed of the electron and ion contribution in the electric field. Miziolek, Palleschi, and Schechter (2006) express it as

$$\Delta\lambda_{Stark} = \underbrace{2w\Big(\frac{n_e}{10^{16}}\Big)}_{\substack{\text{electron}\\ \text{contribution}}} + \underbrace{3.5D\Big(\frac{n_e}{10^{16}}\Big)^{1/4}\Big[1 - B \cdot {N_D}^{-1/3}\Big]w\Big(\frac{n_e}{10^{16}}\Big)}_{\substack{\text{ion}\\ \text{contribution}}} \tag{3.5}$$

where $\Delta\lambda_{Stark}$ is given as full width at half maximum (FWHM), w is the electron broadening parameter tabulated by Griem [83], D is the ion broadening parameter, N_D is the number of particles in the *Debye sphere*, and B is a coefficient equal to 0.75 or 1.2 for neutral or ionic lines, respectively [1, 137]. The Debye sphere is given by the Debye length and represents a region in which the potential of an ion decays by the factor $1/e$ [143]. The region therefore indicates the collective interaction distance of charged particles in the plasma. In equation (3.5), the ion contribution is negligible for typical LIBS conditions since the splitting and shifting of the atomic energy levels remain constant for slow-moving ions during the relevant times, which corresponds approximately to the reciprocal of the line width in frequency units [46]. Thus, equation (3.5) reduces to:

$$\Delta\lambda_{Stark} = 2w\Big(\frac{n_e}{10^{16}}\Big). \tag{3.6}$$

From equation (3.6), the electron density n_e can be estimated by evaluating the FWHM of the observed line. This is valid because, as already mentioned, other broadening effects, such as natural or Doppler, are negligible and therefore $\Delta\lambda_{line} \approx \Delta\lambda_{Stark}$ [137]. The value for w has been calculated by Griem (1974) using a semi-empirical formula, which takes into account *quasi-static approximation* (deals with the statistical distribution of electric fields at the emitting atom or ion) and *impact approximation* (assumes that collisions do not occur simultaneously but are well-separated in time) [16, 46, 83]. It can also be determined experimentally, as shown by Konjević et al. (2002) [113]. However, due to its empirical

nature, the parameter can be associated with a high degree of uncertainty and is often unknown for atomic and especially molecular lines [46]. The value 10^{16} in equation (3.5) and (3.6) corresponds to the reference electron density for neutral atoms [128]. This calculation of the electron density is independent of the plasma state, i.e., whether LTE is satisfied or not [137]. In this study, the electron density was determined from a PE reference sample using the H_α-line of the Balmer series (H_α I 656.3 nm) and the value of w extracted from Griem (1974) [83]. The electron density was then found to be $1.17 \times 10^{18}\text{cm}^{-3}$. To confirm the LTE status, the temperature is calculated next. For this, we follow the instructions by Cremers and Radziemski (2013) [51].

The determination of the temperature is based on the *Boltzmann distribution*. Here, the temperature describes the distribution of the plasma's constituents, as well as electron velocity and the population of excited levels or ionization states [51]. The electron velocity is described by the *Maxwellian velocity distribution function* f_M:

$$f_M(v) = \Big(\frac{m}{2\pi kT}\Big)^{\frac{3}{2}} \cdot \exp\Big(\frac{-mv^2}{2kT}\Big), \tag{3.7}$$

where v is the electron speed, m is the electron mass, and k is the Boltzmann constant [51]. According to equation (3.7), the velocity distribution of the plasma's constituents drops exponentially at a given temperature, with higher velocities happening less frequently.

The Boltzmann distribution also gives the relative populations of energy levels:

$$\frac{N_j}{N_i} = \frac{g_j}{g_i} \exp\Big(-\frac{E_j - E_i}{kT}\Big), \tag{3.8}$$

where i and j refer to two levels, $N_{i,j}$ are the population of levels $E_{i,j}$, and $g_{i,j}$ are the statistical weights, also called *degeneracy*, which stands for the number of quantum states of an atom having the same energy levels [17, 51]. The spectral line intensity of a transition ($j \to i$) is given by:

$$I = \frac{hcN_0gA}{4\pi\lambda Z} \exp\Big(-\frac{E}{kT}\Big). \tag{3.9}$$

I has the unit W/sr, where sr (*steradian*) is the unit of the solid angle, c is the vacuum speed of light, h is the Planck constant, A is the transition probability, N_0 is the total species population, and Z is the partition function, which is typically considered as the ground state's statistical weight [51]. In order to determine the temperature, equation (3.9) has to be rearranged and solved for T using the natural logarithm:

$$\begin{aligned} &\overset{(3.9)}{\Rightarrow} \quad \frac{I\lambda}{gA} = \frac{hcN_0}{4\pi Z} \exp\Big(-\frac{E}{kT}\Big) \\ &\Leftrightarrow \ \ln\Big(\frac{I\lambda}{gA}\Big) = -\frac{1}{kT} \cdot E - \ln\Big(\frac{4\pi Z}{hcN_0}\Big). \end{aligned} \tag{3.10}$$

When the left side of the equation (3.10) is plotted versus E, a straight line with a slope of $-1/kT$ and the y-intercept $\ln\left(\frac{4\pi Z}{hcN_0}\right)$ is displayed. Thus, the plasma temperature is found by linear regression of the observed intensities of a sequence of lines from various excitation states of the same species. The values for A, g and E can be found in the NIST database [114]. This method is called *Boltzmann plot*. It is the standard method for determining the electron temperature using the line intensities [51, 59, 128, 137]. Fig. 3.8 shows an example of a Boltzmann plot based on the PE reference sample. Here, the slope is determined, equated to $-1/kT$ according to equation (3.10), and resolved to T. This results in a temperature of 9112.97 K $\pm$ 570.31 K for the PE reference sample.

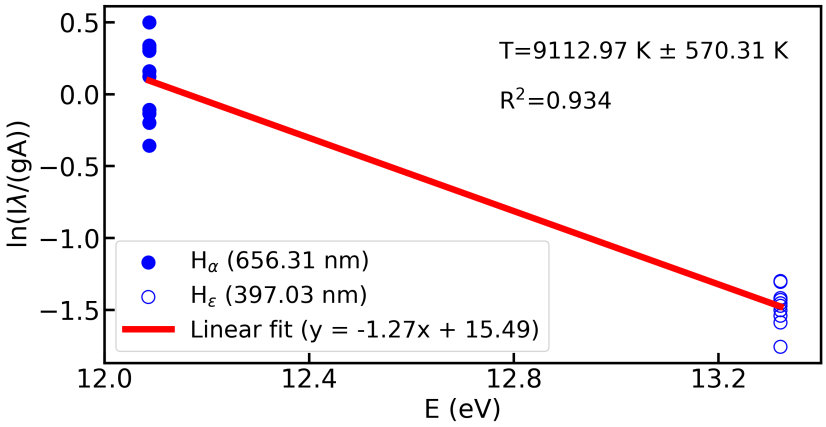

Figure 3.8: The Boltzmann plot method for the determination of electron temperature. The figure shows the linear regression of the spectral line intensities of H_α and H_ϵ for the PE reference sample. The temperature was determined using the slope of the linear fit, which has a goodness of fit of 0.934.

In combination with equation (3.4), LTE can now be confirmed for the plasmas generated in this study. This means that the collision process in the plasma predominates over the radiation losses and all species possess approximately the same *local* temperature. Knowledge of the electron density and plasma temperature enables quantitative studies of element concentrations in a sample. It can help understand "the dissociation, atomization, ionization[,] and excitation processes occurring in the plasma" [95, p. 1]. Here, the parameters are given for reproducibility purposes.

Optical Density

When the emitted radiation travels through the plasma and exits it with little to no scattering or absorption, the plasma is said to be *optically thin* [51]. However, photons are often scattered or absorbed, particularly in the cooler layers of laser-induced plasmas, e.g., at the border to the surrounding atmosphere, where most of the neutral atoms are located [1]. This observation is particularly concerning when using the peak intensity for analysis since the

spectral lines of species deform in an optically thick plasma, i.e., a plasma within which the radiation is *re-absorbed*. This kind of deformation is visible in a "flat-topped profile" [51, p. 30]. The spectral line may even exhibit a dip at the core frequency in more severe scenarios [51]. This phenomenon called *self-absorption*, is the main issue for translating line intensity to element concentration [51].

One way to check the self-absorption effect is to compare the intensity ratio of two emission lines that belong to the same species and whose upper energy levels are very close to each other. According to Agrawal et al. (2011) and equation (3.9), the ratio of the emission lines should be approximately equal to the products of the inverse ratio of their wavelengths $\lambda_{i,j}$, the ratio of their upper statistical weights $g_{i,j}$, and the ratio of their transition probabilities $A_{i,j}$ [3]. This means that the following equation should be approximately satisfied:

$$\frac{I_1}{I_2} \approx \frac{A_1}{A_2} \cdot \frac{g_1}{g_2} \cdot \frac{\lambda_2}{\lambda_1}. \tag{3.11}$$

A useful method to quantify the effect of self-absorption is the *coefficient of self-absorption* SA, introduced by El Sherbini et al. (2005) [64]:

$$SA = \left(\frac{\Delta\lambda_{line}}{2w} \frac{1}{n_e} \right)^{1/0.54} \tag{3.12}$$

where $\Delta\lambda_{line}$ is the width of an emission line suffering from self-absorption, expressed as FWHM, w is again the electron broadening parameter tabulated by Griem (1974) [83], and n_e is the electron density, estimated by an emission line believed to be free of self-absorption (usually the H_α-line, which is rarely affected from re-absorption [128]) [64].

In Publication 1, the effect of self-absorption was not determined as molecular signals were examined here. The electron broadening parameter w was tabulated by Griem (1974) only for atomic signals. Therefore, the SA could not be calculated. For Publication 2 and 3, the SA was calculated for the oxygen emission line. Here, the SA was in the range of 10^{-30}. This value is so little that one may ignore it. The plasma is, therefore, considered to be optically thin. More information about self-absorption can be found in the literature [1, 64, 116, 128].

3.3 Surface and Depth Profile Measurements

It has been shown that the laser-induced plasmas generated in this study are optically thin and in LTE, so the emitted plasma light is a valid representation of the elements in the solid samples. The plasma light can now be used for sample characterization. LIBS, like the established methods FTIR and Raman spectroscopy, is also primarily a surface analysis technique [51]. This means that the surface condition and other morphological or optical

properties of the sample are essential experimental factors. The following section discusses the obstacles encountered in surface measurements and how LIBS can be extended for depth profile analyses, the latter being considered the main analytical challenge with established methods. To begin with, the surface measurement of plastic samples is discussed.

The utility of LIBS as an atomic emission spectroscopy method for the identification and characterization of plastics is not immediately evident. As already discussed in section 2.4.3, methods based on molecular spectroscopy are commonly used due to the similar atomic structure of plastic samples. However, a time-resolved strategy can enable the analysis of molecular bands using LIBS. Fig. 3.9 shows the surface measurement of a PE reference sample from Epsotech averaged over ten distinct measuring spots. The spectrum shows that the PE sample consists of its constituent elements H and combinations of C (carbon itself is not visible as it lies too deep in the UV range), signals from the surrounding air (O and N), and signals from additives in the polymer chain (Na and K, possibly due to zinc potassium chromate and sodium bicarbonate). This simultaneous multi-element and molecular fragments detection demonstrates LIBS' potential for (micro)plastic research.

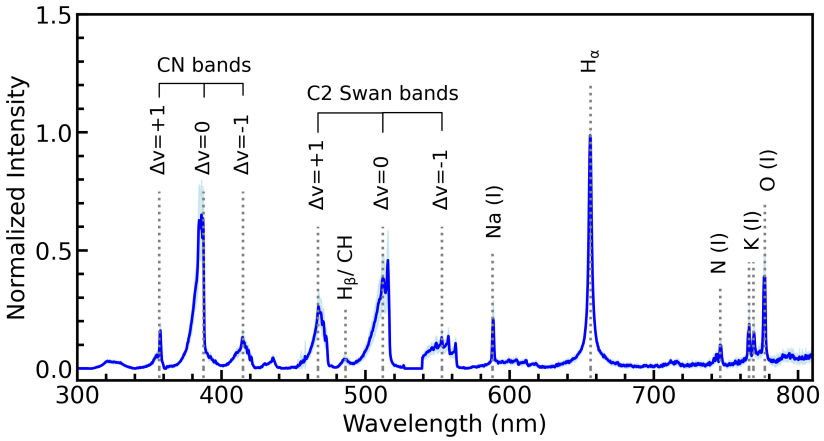

Figure 3.9: LIBS spectra of a PE reference sample. The plot shows the main atomic and molecular peaks associated with plastic samples. The peak H_β/CH stand for the overlapping peaks H_β and CH. The measurement was carried out with a reduced laser power of 6.44 mJ to keep the destruction of the sample to a minimum. The data is the average of ten measurements (average is depicted as line, standard deviation as light background) and normalized to the maximum value. Note that the difference in spectral information compared to Fig. 3.6 is due to the different pulse energy and measurement parameters. The schematic is extracted but modified from Publication 1.

Nevertheless, LIBS also faces obstacles in surface measurements that need to be taken into account. The main drawbacks of LIBS are its low sensitivity, its destructiveness (especially problematic for small microplastic samples), the significantly more complicated evaluation of the molecular data compared to vibrational spectroscopy methods, and the self-absorption effect for molecular signals, which has rarely been studied so far. However, many of LIBS' obstacles are tied to the benefits of LIBS and can be overcome by suitable experimental con-

ditions [137]. For example, LIBS does not require any sample pre-treatment. This can lead to the retention of surface contamination, which consequently also appears in the analysis [137]. Another example is that LIBS only ablates very little sample material. As a result, the measurements can vary greatly depending on the homogeneity of the sample [137]. This increases the challenge of producing accurate and reproducible results. The most severe obstacle, however, is the so-called *matrix effect*. It states that the sample's physical characteristics affect the observed signal, so a distorted perception of the elements that make up the sample matrix can occur, even though the element concentration is constant [137]. This means that in addition to processes such as non-stoichiometric ablation, the surface condition can have a negative effect on the composition of the ablated mass, e.g., when it is brittle.

In this study, the matrix effect must be checked due to the porosity of the surface caused by the weathering effects. In Publications 2 and 3 the matrix effect was scrutinized by comparing the LIBS results with FTIR measurements. As the results were in very good agreement, it was concluded that while a more porous surface allows easier removal of the material, the presence of voids in the porous material also means that less sample material can be vaporized at all. This seems to balance each other out so that the matrix effect does not play a role when comparing weathered and unweathered samples. However, this cannot be taken for granted and should always be checked. In the case of Publication 1, it cannot be ruled out that the matrix effect plays a role in data analysis. The correction of the matrix effect may improve the evaluation. However, since Publication 1 was a proof of concept, such a correction would have gone beyond the scope of the paper. The matrix effect is often corrected using calibration curves [137].

Another way to avoid the matrix effect or to reduce non-representative surface layer is to repeatedly ablate the surface with a series of laser pulses [51, 143]. Such a procedure is often referred to as a *cleaning process* [51]. It is faster than pre-treating the samples with cleaning agents and can be very effective, especially in removing chemical changes from the sample surface [51]. It has been shown that previously oxidized surfaces can be efficiently cleaned using repetitive laser pulses, roughening the underlying bulk material [51]. The removal of the oxidized layer can even be monitored using the O I 777.3 nm emission line [51].

In Publication 1, this type of cleaning was used for all samples. For the reference samples, three consecutive laser shots were fired at the surface. As seen in Fig. 3.10, the first two shots remove elements, i.e., Cu I and Ca I, on the surface that are not part of the sample interior. These impurities may originate from processing by injection molding. The molds are often coated with powder to make it easier to remove the plastic samples from them. For the microplastic samples, only one cleaning shot with a reduced laser power was used to remove any residual biological matrix. This was done to keep the destruction of the sample to a minimum.

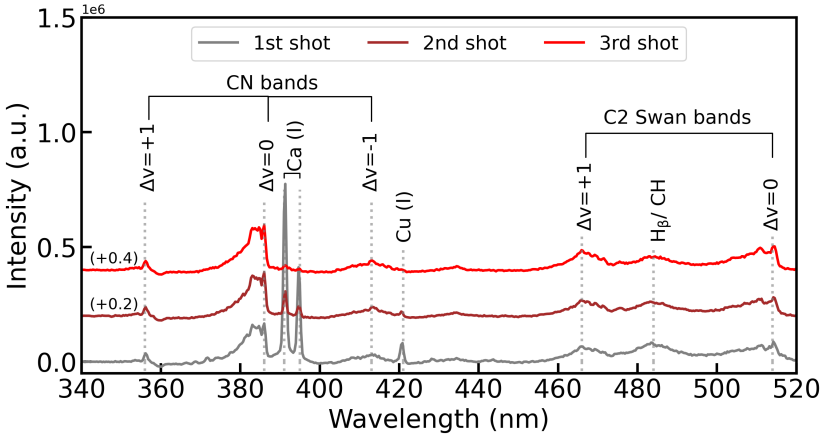

Figure 3.10: Cleaning procedure on a PET reference sample. The plot shows the measurements of three consecutive laser shots taken in the spectral range 340 nm–520 nm. While the molecular signals of PET, i.e., CN and C_2, remain almost constant, the impurities Ca I 393.38 nm, Ca I 396.83 nm and Cu I 427.49 nm are removed. The third measurement (red curve) was then used for the evaluation. Note that the peak H_β/CH stands for the overlapping peaks H_β and CH. For visualization, the spectra are plotted with an offset.

Removing and simultaneously monitoring the atomic content of a contaminated layer raises the question of whether depth profile measurements can be performed using LIBS. Such an application would give LIBS a considerable advantage over other methods since the uptake and penetration of substances are frequently investigated in environmental studies. Publication 2 and Publication 3 investigate induced oxidation and its penetration depth in plastic samples.

Since each laser shot ablates a certain amount of material and consequently drills into the sample, a depth profile should be enabled with LIBS. The amount of mass removed corresponds then to the depth resolution and depends on the morphology of the sample and the laser irradiance [132, 137]. The depth can vary widely from "a few nanometers to several micrometers " [137, p. 259]. The term *LIBS depth profiling* refers from now on to the following process: A laser pulse is repeatedly focused on a single position of a sample surface; after every third measurement, the focus is re-adjusted, i.e., the laser is moved towards the sample. Measuring the laser-induced plasma emission of each laser shot then yields depth-related spectra [132]. The depth profile is presented as a plot of emission intensities at a given wavelength as a function of pulse number or depth. The displayed intensity then corresponds to the averaged element concentration over the crater volume. An exemplary depth profile for a 2000 hours weathered PS sample is shown in Fig. 3.11.

Various methods have been used to determine atomic depth profiles. Among the established methods are X-ray photoelectron spectroscopy and Auger electron spectroscopy. However, both impose significant limitations regarding sample shape or nature, acquisition times, and resolution [31, 132]. This has led to the use of LIBS for depth profile measurements

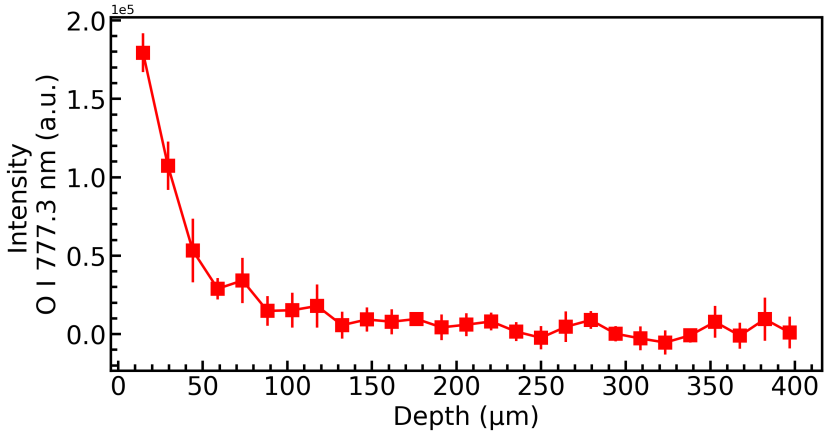

Figure 3.11: Depth profile of a PS sample weathered for 2000 hours. The plot shows the penetration depth of oxygen. Each symbol represents the average over three measurements. The plot is extracted but modified from Publication 3.

[19, 29, 31, 132]. LIBS requires almost no sample preparation, has no limitations on sample size or nature, and can perform rapid analysis in air at atmospheric pressure. However, using LIBS for depth profiling also has shortcomings. Since ablation craters are the basis of this method, the shape of the resulting profile is, in most cases, a distorted representation of the actual layers [132, 137]. This is because the laser sources have poor beam profiles that produce uneven crater bottoms and an undesirable intense mixing of layers [132, 137]. The surface roughness and the formation of the ragged crater bottoms determine the course of the depth profile and depth resolution, which consequently can be poor [137]. Thus, the measuring parameters, in particular the irradiance, must be adapted to the studied material and the required depth resolution to achieve the best possible results. Although LIBS only provides a distorted image of the depth profiles, it is often the only suitable method that enables depth measurement at all. For example, depth profile measurements are rarely performed on microplastic samples as they are often too brittle and porous to expose the cross-section with a microtome. In this case, LIBS could provide promising results as the cross-section does not even have to be exposed.

Assigning the number of laser shots to depth is one of the most challenging aspects of LIBS depth profiling [137, 184]. In this study, this has been done using the profilometer mentioned in section 2.2. To determine the depths for each shot in a depth profile rather than just the maximum depth, *line profiles* are created. Line profiles describe the following procedure: A crater with one shot is created on a distinct spot; next to it, a crater with three shots is created; next to it, a crater with six shots is created, and so on, until a series of craters of different sizes, i.e., an increasing number of laser shots, which do not overlap, is created on the sample surface. The profilometer measures these lines of shots to investigate the shot-crater relationship. Note that the number of shots in a line profile does not have to

be one, three, six, and so on, as above, but should simply be an ascending number of shots. The missing shots are then interpolated from the line profiles. The reason for this procedure is that depending on the maximum depth of the depth profile, recording and measuring a line profile is very time-consuming. Consequently, the depths are approximated. For more information on assigning the number of laser shots to depth, see Publication 2. Fig. 3.12 shows an example of a profilometer measurement of a line profile.

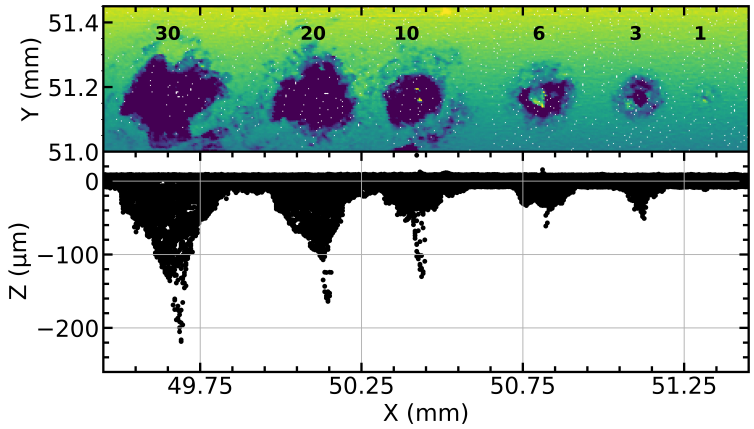

Figure 3.12: Profilometer measurement of a line profile of an 800 h weathered PS sample. The plot shows the crater depth for 1, 3, 6, 10, 20, and 30 laser shots (from right to left). In order to determine the crater size, the unevenness of the surface was fitted and straightened using a polynomial function.

Another approach to assigning crater to depth is by measuring the largest crater and assuming that each laser shot removes the same amount of material at depth. The maximum crater depth is then divided by the number of shots, which results in the respective depths being displayed equidistant from each other. This approach was used for determining the depth in Fig. 3.11 and in Publication 3. The reason for this procedure is that some of the samples were so heavily weathered that the surface was no longer a solid plane, but rather a powdery layer. As a result, craters produced by less than ten laser shots were not distinguishable from the surface damage and were not visible either with the profilometer or under the microscope. Therefore, their crater depths were estimated by the maximum crater. However, this calculation is far less accurate than the profilometer measurements, as the assumption that the crater depth increases linearly is inaccurate. As Fig. 3.12 clearly shows, the crater increases not only in depth but also in width, which means that the laser also ablates material from the crater walls inside the sample. This leads to undesirable mixing of the layers.

For craters that could be measured with the profilometer, the deviation between the actual crater depth and the calculated crater depth (depth divided by number of shots) could be up to 20 µm. The depth profiles are therefore less steep in reality but still provide insights

into the interior of the sample that would not be possible with conventional methods. When it comes to severely damaged surfaces or small sample sizes, both of which are frequently the case for microplastics, LIBS is, to the best of the author's knowledge, the only technique that can record depth profiles.

In conclusion, LIBS can become an essential tool in environmental research studies due to its ability to analyze chemical changes in a sample as a function of depth. The measurement parameters as well as experimental conditions must be set so that the generated plasma is in LTE and the spectral lines represent atomic and molecular signals that correspond to the elements in the sample material. Unlike FTIR or Raman, the samples do not have to be chemically purified for LIBS. Density separation and filtration for the extraction of microplastic samples from the biological matrix should be sufficient to enable identification. The size of the particles is limited to the crater size (in this study between 30 µm and 80 µm, depending on the pulse energy). Theoretically, particles smaller than the crater could also be analyzed. However, the sensitivity of LIBS is often a challenge because it is poor. To overcome these challenges, various experimental methods such as the introduction of a magnetic field [86], double pulses [7, 13] or ultra-fast laser ablation [119] have been developed for LIBS. In this thesis, no attempt was made to improve sensitivity. This is due to the fact that only microplastic samples with a minimum size of 500 µm were analyzed and thus could be measured several times. A sufficiently high sensitivity was then achieved by spectral accumulation. A higher sensitivity would undoubtedly improve the results but was not necessary because of the size of the samples. Out of the five characteristics affecting (micro)plastic analysis mentioned by Ivleva (2021) in section 2.2, only the size could be an issue for LIBS. In theory, polymer type, shape, additives or impurities and weathering do not play a role. The next chapter presents the results obtained with LIBS to identify the polymer base type of microplastics and study weathering-induced oxidation behavior.

Chapter 4

Summary of Results

This dissertation consists of three peer-reviewed publications evaluating LIBS' applicability for (micro)plastic samples. The aim is to introduce LIBS as a new spectroscopic technique for identifying (micro)plastics and investigating the weathering-induced oxidation behavior of plastics. The need for a new method to overcome the analytical challenges of the established methods was described in section 2.4.3. The first publication addresses the identification of real microplastic samples. The second and third publications deal with the study of weathering-induced oxidation of plastics.

4.1 Publication 1

The paper "Identifying microplastic litter with Laser Induced Breakdown Spectroscopy: A first approach" focuses on developing a method for identifying microplastics extracted from sediment samples using LIBS. It was found that current methods are time-consuming and prone to misclassification. Therefore, this publication explores the use of LIBS as a possible alternative. To the best of the authors' knowledge, this publication was the first time LIBS has been used for microplastic identification.

The study examines real microplastics of a minimum size of 500 µm from the local River Lahn, a set of reference plastic samples, and a set of non-plastic samples called *natural materials* (see section 2.1 for more information on the samples). It is found that while the spectra of natural materials and plastics can be easily distinguished from one another, the LIBS spectra of various plastic types are quite similar. However, previous studies on plastic recycling have shown that slight differences in line intensities are detectable, which are sufficient to distinguish different plastic types. This differentiation is often achieved by computer-based machine learning algorithms such as PCA or SVM [81, 140, 174, 195]. As a result, a concept based on the reference plastic samples was developed, and the uniqueness of the spectral features was elaborated.

The following 11 peaks were found to be possible identification features when comparing plastic and natural samples: molecular C_2 470 nm, C_2 512 nm, C_2 553 nm, and CN 388.3 nm, as well as atomic H_α I 656.29 nm, H_β I 486.14 nm, N I 746.8 nm, O I 777.3 nm, K I 766 nm, K I 769 nm, and Cl I 808.6 nm. The C_2 band is mainly found in plastic samples. As mentioned in section 3.1, this bond originates from the C-C and C=C linkages of the sample material itself, whereas the CN band is primarily formed by recombination processes with the surrounding atmosphere. CN can also have a native origin, as can be seen in PA6. Both plastics and natural samples show hydrogen, oxygen, and nitrogen emission lines. This is not surprising as hydrogen is expected to be a major constituent of plastics and natural materials in all sample materials used here. Oxygen and nitrogen, in turn, generally originate from the surrounding gas atmosphere. The Na and K lines were initially added for their presence in natural materials. However, these signals can also occur in plastic samples due to additives. Based on the origin of these peaks, a model for differentiating plastic types was developed.

The model is based on a decision tree that runs as follows: First, a sample is classified as plastic or natural material, which can be done based on its broad spectral differences. This difference is particularly evident in the lack of molecular bands in the spectra of natural materials. Here, the CH 485.7 nm band has also been included as it seems to separate organic from inorganic materials. However, it was not used for further analysis. Second, if the sample is classified as plastic, it is determined whether it is PVC (evident from the Cl emission line) or PET (evident in an enhanced O peak due to the oxygen heteroatom in the polymer chain). Third, if PVC and PET can be excluded, PCA is used to check the remaining samples. PCA allows the aromatic (PS and PC) and aliphatic plastic types (PA6, PE, and PP) to be easily separated from each other due to their different C_2 emission signals. Within the aromatic and aliphatic groups, PCA achieves further separation. In the aromatic group, PCA clusters PS and PC in different areas based on their different O emission lines. In the aliphatic group, PCA clusters PA6 in a different area than PE and PP due to its distinct N emission line. This leaves PE and PP for further classification, as they cannot be separated using PCA. Their chemical formula and consequently the spectral information are too similar for PCA. Finally, their classification is achieved by SVM.

The results of the reference dataset are then transferred to the sediment samples, which are composed of microplastics and natural material microparticles, to identify and, consequently, determine the base polymer type. For verification reasons, the samples were identified using FTIR. The samples were measured after one cleaning shot of the laser, i.e., the first sample layer was ablated to reduce the amount of surface contaminants (cf. Fig. 3.10). It is still found that real microplastic samples have high contamination of incorporated substances, which makes the determination of the base polymer difficult. The contamination is evident from superimposed peaks in the spectrum that do not appear in the spectra of the reference

samples. It cannot be completely ruled out that the new peaks in the spectra are due to additives in the base polymer. However, there are several matches with the peaks in the spectra of the natural materials of the sediment samples, suggesting that the overlapping peaks represent absorbed natural materials from the River Lahn.

Again, PCA was utilized to predict the base polymer type. Due to overlapping peaks, especially in the molecular band regions, the intensity values for the 11 peaks mentioned above could not be used as input variables. The contamination could have led to a bias in the analysis. For this reason, the median of the molecular peak area was calculated and used as the peak value. The results show that PCA can distinguish between plastic and natural microparticles and provides an estimate of the polymer type.

Publication 1 comes to the conclusion that LIBS could be a rapid and effective method for identifying microplastic debris. In this context, the C_2 band is crucial. LIBS offers the ability to analyze samples that, once extracted from the sediment, do not require any pre-treatment due to cleaning shots of the laser. However, further research is needed to validate and investigate the method's applicability on a larger scale.

4.2 Publication 2

The first publication leaves open whether LIBS can be used to systematically investigate peaks originating from environmental influences, contamination, or additives. The second publication addresses this question. It examines the main mechanism of polymer degradation in the environment, i.e., weathering-induced photo-oxidation, on PS samples and antioxidant-containing PS samples. It is titled "Weathering-induced oxidation: An investigation of artificially aged polystyrene samples using Laser-induced Breakdown Spectroscopy".

The results show that the artificially aged PS samples exhibit increased oxidation, which can be attributed to the effect of weathering. The results were obtained by measuring the atomic oxygen line, O I 777.3 nm with LIBS. The oxidation was also measured using the FTIR system LUMOS II. For this, the sum of the main characteristic absorbance bands (ketone, benzaldehyde, benzophenone, benzoic anhydride, carboxylate, benzoic acid dimer, benzoic acid monomer, dibenzoylmethane, dimeric acetic and formic acid, and the regions of hydroxyl, C-O, and C=O) was used to evaluate plastic oxidation over time. By comparing the two methods, the suitability of LIBS for the systematic investigation of oxidation was confirmed. Both methods show that oxidation does not grow linearly with increasing weathering; instead, it is hardly noticeable at first, rises sharply, and finally settles at 800 hours of weathering. Differences in the measurement techniques can be attributed to the crater depth and penetration depth of the IR beam in LIBS and FTIR measurements, respectively.

Two concentrations (0.5% and 1%) of the antioxidant Irgafos® 168 were added to the

PS samples to evaluate their effect on weathering-induced oxidation. The investigation of additives is particularly important as they make it difficult to correctly assess the age of plastic particles in the environment and can be responsible for the formation of toxic by-products. Irgafos® 168 is a processing stabilizer and antioxidant that inhibits the radical chain reaction of the photo-oxidation cycle by decomposing hydroperoxide groups (ROOH) formed during the propagation step (cf. Fig. 2.4). This was discussed in more detail in section 2.3. The study shows that an increased dose of Irgafos® 168 in the plastic sample hinders its oxidation. The plastic samples oxidize more slowly and less strongly. This result underlines the assumption that LIBS can also be used to analyze additives and their impact on plastic's performance in the environment.

LIBS analysis demonstrates that oxidation occurs not only on the sample surface but also penetrates into the sample. The oxygen penetration depth can, in principle, also be determined using FTIR. But for this, the cross-section has to be exposed first. Since the necessary instrumentation for this was not available, these measurements were not carried out. However, since the surface measurements from LIBS and FTIR agree well, the depth profile measurements of LIBS are assumed to be also valid. The depth profile measurements were carried out according to the procedure described in section 3.3. The measurements show heterogeneous oxidation profiles that end after approximately 50 µm inside the sample. The depth was determined using a profilometer.

In this study, important insights into the effects of weathering of PS samples are provided and the applicability of LIBS to systematically investigate chemical changes in the base polymer is demonstrated. These findings help better understand and improve plastic samples' durability and performance. Additionally, this study is an essential contribution to monitoring and understanding the degradation of plastics in the environment.

4.3 Publication 3

The third publication "Determining weathering-induced heterogeneous oxidation profiles of polyethylene, polypropylene and polystyrene using laser-induced breakdown spectroscopy" combines the previous findings and studies the oxidation behavior of different plastic types. The same measurement procedure as in Publication 2 was applied and optimized. The optimization relates to the evaluation of the data. In contrast to Publication 2, where only the peak intensity of the oxygen emission line in the LIBS spectrum was used, the sum of the pixel intensities was taken, and the data normalized to the noise level. Additionally, the CI value was calculated to evaluate the FTIR data (cf. section 2.4.3). Although the results of this new evaluation show no significant difference compared to the old evaluation, it is more robust against misinterpretations due to fluctuations in the data. It should be noted

that the CI value is not standardized which complicates the comparison of polymer oxidation studies. This study was carried out as follows: First, surface LIBS measurements were performed. Subsequently, surface FTIR measurements were recorded and used to validate the LIBS results. The results of the two measurement techniques show good agreement and are more consistent than in Publication 2. Finally, depth profiles with up to 60 laser shots were recorded with LIBS. The depth of the 60 laser shots corresponded to approximately 300 µm for PS, 700 µm for PP, and 450 µm for PE and has a depth resolution of a few micrometers. The difference in depth is due to the optical properties of the sample as well as the different levels of porosity due to the different weathering times. It should be noted that crater size and depth resolution can be further optimized, e.g., by using fs-laser pulses, which was out of the scope of this study.

This study sheds light on the different plastic properties and their importance for weathering-induced oxidation. The course of oxidation for PS has already been explained in Publication 2. The oxidation of PE and PP on the surface increases almost linearly with increasing weathering time. Remarkably, the unweathered PE reference sample shows oxygen content above zero. This concentration is suspected to be due to contamination, as it occurs in both LIBS and FTIR data. The amorphous PS samples show more oxidation on the surface during advanced weathering time compared to the semi-crystalline PE and PP samples, which is due to the chemical susceptibility of PS to photo-oxidation (PS contains unsaturated chromophores, see section 2.3). In contrast, the oxygen concentration inside the PS sample decreases rapidly (it reaches only up to 40–50 µm), while the concentration inside the PP and PE samples reaches over 600 µm and 450 µm, respectively. This difference in penetration depth is due to the formation of microcracks. As explained in section 2.3, amorphous polymers are less susceptible to surface embrittlement due to the lack of molecular rearrangements and exhibit fewer and smaller microcracks than semi-crystalline polymers. Since microcracks allow oxygen to penetrate more quickly into the bulk of the sample, oxidation takes place in deeper layers of the semi-crystalline polymers. The oxidation process spreads over the entire sample volume and complicates the evaluation of degradation rates because the samples also fragment internally. The results show significant spot-dependent fluctuations, which are attributed to the lattice structure of the plastic samples. Crystalline areas absorb less oxygen than amorphous areas because they are chemically inert. This emphasizes the importance of high spatial resolution and spatial distribution measurements.

The study concludes that LIBS is faster than conventional techniques for studying weathering-induced oxidation over the entire sample volume because no cross-section of the samples needs to be exposed. LIBS could reasonably quickly produce a three-dimensional chemical image of the sample. Further research in this direction could shed light on the fate of plastic samples in the environment, as it may provide information on their fragmentation rate.

However, further investigations are required, for example, concerning the detection limits of LIBS and possible interferences with other elements that occur in the sample material due to impurities or additives.

In the context of this work, it should be noted that the analysis of artificially aged polymers entails limitations when transferring the results and interpretations to environmental (micro)plastic samples. According to Andrady (2017), there are three main reasons for this: First, plastic fragments into smaller particles (*secondary microplastics*). This fragmentation rate highly depends on the amount and type of additives used in manufacturing. For instance, UV stabilizers and antioxidants, such as Irgafos® 168, delay the weathering process, making the determination of weathering effects variable and unreliable [11], as seen in Publication 2. In the case of real microplastics, no conclusions can be drawn about the original concentration of the additives used in manufacturing or about their leaching process [11].

Second, the fragmentation rate depends on chain scission or cross-linking reactions of the polymer molecules [11]. These are extremely difficult to predict, not least because of the heterogeneous structure of semi-crystalline polymers [11]. Therefore, instead of predicting chain and cross-linking reactions, assumptions and estimates about the fragmentation of plastics are made based on laboratory studies or small outdoor studies [26, 168]. However, mathematical modeling of scission and cross-linking processes is to date not possible.

Third, weathering does not yet result in a spectroscopic fingerprint that provides precise information about the outdoor exposure duration or exposed conditions [11]. For this, the environmental influences are still too complex. A plastic fragment provides information about the degree of degradation but no information about the original sample or the time at which the plastic fragment split off. Based on current knowledge, it is impossible to distinguish whether the measured degradation originates from a sample floating in the sea for years or from a sample that has only been lying on the beach for months.

Nevertheless, degradation studies provide essential information about the interaction between the environment and plastics. As mentioned in the introduction, only recently a new method for estimating the minimum age, i.e., minimum duration of UV exposure, of marine PE microplastics has been published [147]. Here, the authors only focused on PE samples that floated on the sea surface and therefore corresponded well with the artificially weathered samples. This means that the results of this study cannot be transferred to an ordinary microplastic particle, i.e. a particle that may have been covered by bio-films or sunk to the sea floor. Still, this study provides a first step into this direction and motivates further research. Assumptions suggest that improved technology and evaluation methods will lead to a better understanding of degradation processes, so that signatures for various environmental influences may eventually be found in the data. This would help to make statements about the duration of a plastic particle in the environment and its transport history.

Chapter 5

Conclusion

This thesis deals with the characterization and investigation of (micro)plastic samples and their weathering-induced oxidation behavior using LIBS. Weathering-induced oxidation, or more specifically photo-oxidation induced by environmental factors, is the main mechanism for the degradation of PE, PP, and PS samples, which can lead to toxic by-products from the base polymer itself or additives or the uptake of pollutants. Therefore, its examination may provide information for assessing the hazards of (micro)plastics. In this context, LIBS is being explored as an alternative technique for the examination of (micro)plastics.

As a part of this dissertation, several scientific papers were published. A concept was developed to systematically separate plastics from natural materials, identify the polymer type, and determine the extent of oxidation on the surface and inside the sample. These investigations allow a more comprehensive characterization of plastic samples, often not achieved with conventional techniques. The ability of LIBS to detect the main constituents of plastics, as well as molecular signals in combination with depth profiling capabilities, opens up a wide range of new developments and opportunities in research and applications. The aim of this work is to demonstrate the problems of identifying microplastics using conventional methods and to prove that the new proposed method, LIBS, is an efficient alternative in these areas. In doing so, a more thorough explanation of the operation of the conventional methods is necessary to understand their possibilities and limitations. Since the physics of large molecules is neither completely covered by classical nor by quantum physics, the explanation of the working principles of these methods is an important pillar of this work.

Chapter 1 introduces the topic by showing the relevance of (micro)plastic research. A rough overview of the state of research is presented, including an overview of the life circle of plastic debris. The relevance of a profound understanding of plastic identification and characterization, including the investigation of plastic degradation, is elaborated. Chapter 2 covers the background of this work in more detail. First, an overview of the materials under study is given, highlighting the chemical and physical differences between the various plastic

types. Second, the experimental setups used in this study and the data processing are presented. Lastly, the different degradation processes involved in environmental plastic samples are discussed, with particular attention to photo-oxidation. It becomes clear that the underlying lattice structure of the investigated polymer has a significant influence on oxidation. At the end of the chapter, the common analytical techniques, i.e., microscopic, thermal, and spectroscopic methods, as well as their advantages and disadvantages, are discussed.

Since the investigation of microplastic particles is multidimensional and new findings are constantly emerging that are difficult to capture using conventional methods, new techniques are essential for progress in this research field. The most common analytical challenges include long acquisition times, extensive sample pre-treatment, interference from color pigments, moisture, or organic matter, as well as the restriction to surface analysis. Chapter 3 presents LIBS for overcoming the analytical challenges of conventional methods. The chapter covers the physical principles of LIBS, specifically light-matter interaction and plasma formation, which serve as the theoretical foundation for the conducted experiments and their interpretation. LIBS utilizes the fact that the atomic composition of the sample is retained during the transition to the plasma state, which allows conclusions to be drawn about the base polymer type and oxidation. The chapter ends with applying this experimental technique for surface and depth profile analysis. To a certain extent, LIBS could be interpreted as combining the advantages of py-GC-MS and spectroscopy. The main advantage of py-GC-MS lies in the simple sample preparation due to combustion. LIBS is based on a similar idea, except that the plasma light is used for identification, not the combustion products. However, because LIBS does not require the entire sample to be incinerated but only small portions are removed, it also exhibits the advantages of spectroscopy, e.g., particle-based mass determination and the investigation of size, shape, and morphology when combined with microscopy.

Chapter 4 summarizes the results of the attached publications. First, the applicability of LIBS for microplastic research studies is demonstrated. In Publication 1, a concept is developed using the line intensities of the spectra of different plastic types and multivariate analysis to differentiate (micro)plastics from natural materials and identify the polymer base type. In this context, the C_2 bond is particularly important. When distinguishing between natural and plastic materials, atomic C, H, and O are present in both sample types. However, C_2 appears to be much more pronounced in plastic samples. Although LIBS results in a good classification for pristine plastic samples, the high contamination of real microplastic samples complicates the analysis. The results indicate that LIBS may be superior to conventional methods for characterizing environmental influences, such as the uptake of pollutants, metals, or oxygen. However, FTIR and Raman spectroscopy data analysis is much easier when identifying plastic particles, as the peaks can be assigned to unique molecular vibrations.

These vibrations are not displayed in LIBS. Here, only molecular radicals are detected, which are very similar in different plastic types. Consequently, the analysis is far more complex than FTIR and Raman analysis, where—to put it simply—only the presence of a few peaks needs to be checked.

The second and third publications take a closer look at environmental influences. First, artificially weathered amorphous PS samples with different concentrations of the antioxidant Irgafos® 168 were examined using LIBS. Afterward, the weathering behavior of the semi-crystalline plastic types PE and PP was studied and compared with the behavior of amorphous PS samples. The results show that the oxidation of the different plastic types exhibits different degrees of oxygen intensity for the same weathering time. Additionally, the oxidation does not only take place on the surface but also penetrates into the sample's interior. The non-linear penetration profile differs in decay depth and slope for the various plastic types. This proves that oxidation depends not only on the environmental conditions but also on the underlying lattice structure and microcrack formation of the plastic sample, which is in agreement with previous studies. In addition, the effect of Irgafos® 168 was examined. The additive hinders oxygen uptake until it is used up. This could be concluded from the oxygen peak in the LIBS measurements. To validate the LIBS results, all measurements on the sample surface were compared with FTIR measurements. These show similar results, confirming LIBS' suitability to detect oxidation. The necessity to study the entire sample volume is elaborated.

The presented work shows the application of LIBS for plastic characterization and investigation. In this context, LIBS provides information that is not accessible with conventional techniques. However, there is room for improvement. Better lateral and longitudinal resolution and higher sensitivity can be achieved with improved instruments. Concerning future works, this encourages investigating detection limits, matrix effects, or interference with additives and absorbed pollutants. The comparability of LIBS and FTIR data offers another perspective for future works. The oxygen intensity in the LIBS spectrum and the CI value calculated from the FTIR spectrum have shown comparable results in the present study but have physically different origins. A physical confirmation of their comparability would be a nice addition to this work.

There is no question that the most effective way to combat plastic pollution is to prevent plastic from entering the environment. As this political goal is difficult to achieve, science is left with the task of detecting plastic and removing it from the environment. The difficulty of this task is demonstrated in this thesis.

Zusammenfassung

Diese Arbeit beschäftigt sich mit der Charakterisierung und Analyse von (Mikro-)Plastikproben und deren witterungsbedingtem Oxidationsverhalten mittels laserinduzierter Plasmaspektroskopie (LIBS). Witterungsbedingte Oxidation, genauer gesagt die durch Umweltfaktoren ausgelöste Photooxidation, ist der Hauptmechanismus für die Degradierung von PE, PP und PS Proben, die zur Bildung von toxischen Nebenprodukten aus dem Basispolymer oder aus Additiven, oder zur Aufnahme von Schadstoffen führen kann. Daher kann ihre Untersuchung möglicherweise Informationen zur Bewertung der Gefahren von (Mikro-)Plastik liefern. In diesem Sinne wird LIBS als alternative Technik für die Untersuchung von (Mikro-)Plastik erforscht.

Im Rahmen dieser Dissertation wurden mehrere wissenschaftliche Publikationen veröffentlicht, in denen ein Konzept entwickelt wurde, um Kunststoffe von natürlichen Material zu unterscheiden, den Polymertypen zu identifizieren und das Ausmaß der Oxidation an der Oberfläche und im Inneren der Probe zu bestimmen. Diese Untersuchungen von LIBS ermöglicht eine umfassende Charakterisierung von Kunststoffproben, die mit herkömmlichen Techniken so nicht möglich ist. Die Fähigkeit mittels LIBS atomare und molekulare Bestandteile von Plastik durch Untersuchung der Oberfläche und tieferer Schichten nachzuweisen, eröffnet ein breites Spektrum an neuen Entwicklungen und Möglichkeiten in Forschung und Industrie. Das Ziel dieser Arbeit ist es die Probleme der Identifizierung von (Mikro-)Plastik mit herkömmlichen Methoden aufzuzeigen und nachzuweisen, dass die neue vorgeschlagendene Methode LIBS in diesen Problembereichen eine effiziente Alternative ist. Dabei ist es notwendig, auch auf die genauere Beschreibung der Wirkungsweisen der Verfahren einzugehen, da nur so deren Möglichkeiten und Beschränkungen verständlich werden. Da die Physik großer Moleküle weder vollständig von der klassischen Physik noch von der Quantenphysik abgedeckt wird, ist diese Aufgabe der Verständlichmachung der Verfahren ein wichtiger Teil der Arbeit.

Kapitel 1 zeigt die Relevanz der (Mikro-)Plastikforschung auf. Es wird ein Überblick über den Stand der Forschung gegeben, einschließlich einer Erläuterung, wie Plastikmüll in die Umwelt gelangt und welchen Prozessen es dort ausgesetzt ist. Die Bedeutung eines tiefgreifenden Verständnisses über die Degradierung von Kunststoffen, sowie deren Identifi-

zierung und Charakterisierung wird dargelegt. Kapitel 2 geht näher auf den Hintergrund der untersuchten Materialien ein. Zunächst wird ein Überblick über die untersuchten Materialien und über die Kunststoffherstellung gegeben, wobei die chemischen und physikalischen Unterschiede zwischen den verschiedenen Kunststoffarten aufgezeigt werden. Danach erfolgt die Darstellung der in dieser Studie verwendeten Versuchsaufbauten, gefolgt von einer Diskussion über die verschiedenen Abbauprozesse von Plastik in der Umwelt. Der Schwerpunkt liegt hierbei auf der Photooxidation. Es wird herausgearbeitet, dass neben der chemischen Struktur die zugrunde liegende Gitterstruktur des untersuchten Polymers einen wesentlichen Einfluss auf die Oxidation hat. Am Ende des Kapitels werden die gängigen Analysetechniken, d.h. mikroskopische, thermische und spektroskopische Verfahren, und ihre Vor- und Nachteile vorgestellt und diskutiert.

Da die Untersuchung von Mikroplastikpartikeln vielschichtig ist, kommen die herkömmlichen Methoden oft an ihre physikalischen Grenzen. Zu den bekanntesten Herausforderungen gehören lange Messszeiten, aufwändige Probenvorbehandlungen, Störung der Messung durch Farbpigmente, Feuchtigkeit oder organische Stoffe, sowie die Einschränkung auf die Oberflächenanalyse. Die Entwicklung neuer Methoden für (Mikro-)Plastikuntersuchungen ist daher essentiell um zuverlässige, vergleichbare und schneller Ergebnisse zu erzielen. Kapitel 3 stellt LIBS zur Überwindung der analytischer Herausforderungen herkömmlicher Methoden vor. Das Kapitel behandelt die physikalischen Grundlagen von LIBS, insbesondere die Licht-Materie-Wechselwirkung und Plasmabildung, welche das theoretische Fundament für die durchgeführten Experimente und deren Interpretation bildet. LIBS nutzt die Tatsache, dass die atomare Zusammensetzung der Probe beim Übergang in den Plasmazustand erhalten bleibt, wodurch Rückschlüsse auf den Typ und die Oxidation des Basispolymers gezogen werden kann. Das Kapitel endet mit der Anwendung dieser Messtechnik zur Oberflächen- und Tiefenprofilanalyse.

Kapitel 4 fasst die Ergebnisse der Publikationen zusammen. Zunächst wird die Eignung von LIBS für die Mikroplastikforschung aufgezeigt. In Publikation 1 wird ein Konzept entwickelt, das die Peakintensitäten verschiedener Kunststofftypen und eine multivariate Analyse verwendet, um Plastik von natürlichen Materialien zu unterscheiden und den Polymertyp zu identifizieren. In diesem Zusammenhang sind die C_2-Kohlenstoffbindungen besonders wichtig, da diese in Kunststoffproben deutlich stärker ausgeprägt zu sein scheinen als in natürlichen Materialien und somit ein Merkmal für Kunststoffe darstellen. Obwohl LIBS bei reinen Kunststoffproben zu einer guten Klassifizierung führt, wird die Analyse durch die starke Verunreinigung echter Mikroplastikproben erschwert. Die Ergebnisse deuten darauf hin, dass LIBS bei der Charakterisierung von Umwelteinflüssen, wie Bewitterung oder der Absorption von Schadstoffen, Metallen oder Sauerstoff, Einblicke geben kann, die außerhalb des Anwendungsbereichs von herkömmliche Methoden liegen.

Die zweite und dritte Veröffentlichung knüpfen an die erste an. Zunächst werden künstlich bewitterte amorphe PS Proben mit unterschiedlichen Konzentrationen des Antioxidationsmittels Irgafos® 168 mit LIBS untersucht. Anschließend wird das Bewitterungsverhalten der teilkristallinen Kunststofftypen PE und PP mit dem Verhalten von amorphen PS-Proben verglichen. Die Ergebnisse zeigen, dass die Oxidation der unterschiedlichen Plastiktypen bei gleicher Bewitterungszeit unterschiedlich stark ausgeprägt ist. Die Oxidation findet dabei nicht nur an der Oberfläche statt, sondern tritt auch ins Probeninnere ein. Das nicht-lineare Eindringungsprofil unterscheidet sich bei den unterschiedlichen Plastiktypen in Eindringtiefe und Verlauf. Dies macht deutlich, dass die Oxidation der Plastikproben nicht nur von den Umgebungsbedingungen, sondern auch von der zugrunde liegenden Gitterstruktur und Mikrorissbildung abhängt. Die Ergebnisse sind in Übereinstimmungen mit früheren Studien. Darüber hinaus wurden die Auswirkungen von Irgafos® 168 überprüft. Dieses Additiv verlangsamt die Sauerstoffaufnahme, was mit LIBS bestätigt werden konnte. Das belegt, dass LIBS für die Messung von Zustatzstoffen verwendet werden kann. Um die LIBS Messungen zu verifizieren, wurden alle Messungen an der Probenoberfläche mit FTIR-Messungen verglichen. Diese zeigen ähnliche Ergebnisse, was die Eignung von LIBS zum Nachweis von Oxidation bestätigt. Es wird deutlich, dass für eine umfassende Untersuchung des Oxidationsverhaltens, Messungen über das gesamte Probenvolumen notwendig sind.

LIBS liefert Informationen, die mit herkömmlichen Methoden nicht zugänglich sind. Dabei gibt es aber experimentelle Herausforderungen, welche Raum für Verbesserungen lassen. Eine bessere laterale und longitudinale Auflösung, sowie eine höhere Sensitivität können mit verbesserten Instrumenten erreicht werden. Im Hinblick auf künftige Arbeiten regt dies die Untersuchung von Nachweisgrenzen, Matrixeffekten oder Störungen durch Additive und absorbierten Schadstoffen an. Die Vergleichbarkeit von LIBS und FTIR bietet eine weitere Perspektive für künftige Arbeiten. Die Sauerstoffintensität im LIBS Spektrum und der aus dem FTIR-Spektrum berechnete CI-Wert haben in der vorliegenden Studie vergleichbare Ergebnisse erbracht. Sie sind aber physikalisch unterschiedlich begründet. Eine physikalische Bestätigung ihrer Vergleichbarkeit wäre eine schöne Ergänzung zu dieser Arbeit.

Es steht außer Frage, dass der wirksamste Weg zur Bekämpfung der Umweltverschmutzung darin liegt, dafür zu sorgen, dass Plastik gar nicht erst in die Umwelt gelangt. Da dieses politische Ziel nur schwer zu verwirklichen ist, bleibt der Wissenschaft die Aufgabe, Plastik zu entdecken und wieder aus der Umwelt zu entfernen. Die Schwierigkeit dieser Aufgabe wird in der vorliegenden Arbeit aufgezeigt. Die Aufrechterhaltung unserer Umwelt ist ein Problem, dass sich der Physik stellt.

Scientific Curriculum Vitae

Personal data

Education and scientific experience

Scientific interests

Peer-Reviewed Articles

(I) Castro-Camus, E., Ornik, J., Mach, C., Hernandez-Cardoso, G., Savalia, B., Taiber, J., ... & Koch, M. (2020). Simple ventilators for emergency use based on bag-valve pressing systems: lessons learned and future steps. *Applied Sciences*, 10(20), 7229.

(II) Sommer, C., Schneider, L. M., Nguyen, J., Prume, J. A., Lautze, K., & Koch, M. (2021). Identifying microplastic litter with Laser Induced Breakdown Spectroscopy: A first approach. *Marine Pollution Bulletin*, 171, 112789.

(III) Nguyen, J., Kesper, K., Kräling, G., Birk, C., Mross, P., Hofeditz, N., ... & Koch, M. (2021). Repurposing CPAP machines as stripped-down ventilators. *Scientific Reports*, 11(1), 12204.

(IV) Sommer, C., Nguyen, J., Menzel, T., Prume, J. A., Ruckdäschel, H., & Koch, M. (2022). Weathering-induced oxidation: An investigation of artificially aged polystyrene samples using Laser-induced Breakdown Spectroscopy. *Polymer Testing*, 112, 107623.

(V) Sommer, C., Nguyen, J., Menzel, T., Ruckdäschel, H., & Koch, M. (2023). Determining weathering-induced heterogeneous oxidation profiles of polyethylene, polypropylene and polystyrene using laser-induced breakdown spectroscopy. *Chemosphere*, 140105.

Oral Presentation at Conferences

(I) Sommer, C. (2019). *Overview on FTIR Systems.* TransMIT workshop on „Modern Spectroscopic Techniques“, Elba, Italy. https://www.transmit.de.

(II) Sommer, C., Schneider, L. M., Nguyen, J., Prume, J. A., Lautze, K., & Koch, M. (2021). *Detection of Microplastics using Laser-Induced Breakdown Spectroscopy - A first approach.* 17th International Conference on Environmental Science & Technology (CEST), Athens, Greece. https://cest.gnest.org.

(III) Sommer, C., Nguyen, J., Menzel, T., Prume, J. A., Ruckdäschel, H., & Koch, M. (2022). *LIBS: a new method for the analysis of weathering-induced oxidation on artificially aged PS samples.* Microplastic Workshop for early career researchers: Best practices and expert insights, Athens, Greece. https://ecrmpworkshop2023.ch.

(IV) Sommer, C., Schneider, L. M., Nguyen, J., Menzel, T., Prume, J. A., Lautze, K., Ruckdäschel, H., & Koch, M. (2022). *LIBS: a new method for microplastics detection and analysis.* TransMIT workshop on „Modern Spectroscopic Techniques“, Elba, Italy. https://www.transmit.de.

Poster Presentations at Conferences

(I) Sommer, C., Schneider, L. M., Nguyen, J., Prume, J. A., Lautze, K., & Koch, M. (2022). *Identifying microplastic litter with Laser-induced Breakdown Spectroscopy.* Microplastic Workshop for early career researchers: Best practices and expert insights, Athens, Greece. https://ecrmpworkshop2023.ch.

Bibliography

[1] Abdrabou, D., Schneider, L. M., Rahimi-Iman, A., Khedr, M. A., Hussein, A. M., and El-Sherbini, T. M. (2019). Study of laser-induced-plasma parameters for molybdenum targets. *Plasma Research Express*, 1(3):035004.

[2] Afreen, V., Hashmi, K., Nasir, R., Saleem, A., Khan, M. I., and Akhtar, M. F. (2023). Adverse health effects and mechanisms of microplastics on female reproductive system: a descriptive review. *Environmental Science and Pollution Research*, 30:1–14.

[3] Agrawal, R., Kumar, R., Rai, S., Pathak, A. K., Rai, A. K., and Rai, G. K. (2011). LIBS: a quality control tool for food supplements. *Food Biophysics*, 6:527–533.

[4] Akhtar, K., Khan, S. A., Khan, S. B., and Asiri, A. M. (2018). Scanning electron microscopy: Principle and applications in nanomaterials characterization. In Sharma, S. K., editor, *Handbook of Materials Characterization*, pages 113–145. Springer International Publishing.

[5] Allen, N. S. and Edge, M. (1992). *Fundamentals of polymer degradation and stabilization*. Springer Science & Business Media.

[6] Almond, J., Sugumaar, P., Wenzel, M. N., Hill, G., and Wallis, C. (2020). Determination of the carbonyl index of polyethylene and polypropylene using specified area under band methodology with ATR-FTIR spectroscopy. *e-Polymers*, 20(1):369–381.

[7] Amal, K., Elnaby, S. H., Palleschi, V., Salvetti, A., and Harith, M. A. (2006). Comparison between single-and double-pulse LIBS at different air pressures on silicon target. *Applied Physics B*, 83:651–657.

[8] Amelia, T. S. M., Khalik, W. M. A. W. M., Ong, M. C., Shao, Y. T., Pan, H.-J., and Bhubalan, K. (2021). Marine microplastics as vectors of major ocean pollutants and its hazards to the marine ecosystem and humans. *Progress in Earth and Planetary Science*, 8(1):1–26.

[9] Anabitarte, F., Cobo, A., and Lopez-Higuera, J. M. (2012). Laser-induced breakdown spectroscopy: fundamentals, applications, and challenges. *International Scholarly Research Notices*, 2012.

[10] Andrady, A. L. (1998). Biodegradation of plastics: monitoring what happens. In Pritchard, G., editor, *Plastics Additives: An AZ reference*, volume 1, pages 32–40. Springer Science & Business Media.

[11] Andrady, A. L. (2017). The plastic in microplastics: A review. *Marine Pollution Bulletin*, 119(1):12–22.

[12] Andrady, A. L., Barnes, P. W., Bornman, J. F., Gouin, T., Madronich, S., White, C. C., Zepp, R. G., and Jansen, M. A. (2022). Oxidation and fragmentation of plastics in a changing environment; from UV-radiation to biological degradation. *Science of The Total Environment*, 851:158022.

[13] Angel, S. M., Stratis, D. N., Eland, K. L., Lai, T., Berg, M. A., and Gold, D. M. (2001). LIBS using dual-and ultra-short laser pulses. *Fresenius' Journal of Analytical Chemistry*, 369:320–327.

[14] Araujo, C. F., Nolasco, M. M., Ribeiro, A. M. P., and Ribeiro-Claro, P. J. A. (2018). Identification of microplastics using raman spectroscopy: Latest developments and future prospects. *Water Research*, 142:426–440.

[15] Arutchelvi, J., Sudhakar, M., Arkatkar, A., Doble, M., Bhaduri, S., and Uppara, P. V. (2008). Biodegradation of polyethylene and polypropylene. *Indian Journal of Biotechnology*, 7.

[16] Ashkenazy, J., Kipper, R., and Caner, M. (1991). Spectroscopic measurements of electron density of capillary plasma based on stark broadening of hydrogen lines. *Physical Review A*, 43(10):5568.

[17] Atkins, P. and de Paula, J. (2014). *Atkins' Physical Chemistry*. Oxford University Press.

[18] Avio, C. G., Gorbi, S., Milan, M., Benedetti, M., Fattorini, D., d'Errico, G., Pauletto, M., Bargelloni, L., and Regoli, F. (2015). Pollutants bioavailability and toxicological risk from microplastics to marine mussels. *Environmental Pollution*, 198:211–222.

[19] Balzer, H., Hoehne, M., Noll, R., and Sturm, V. (2006). New approach to online monitoring of the al depth profile of the hot-dip galvanised sheet steel using LIBS. *Analytical and Bioanalytical Chemistry*, 385:225–233.

[20] Barnes, D. K. A., Galgani, F., Thompson, R. C., and Barlaz, M. (2009). Accumulation and fragmentation of plastic debris in global environments. *Philosophical Transactions of the Royal Society B: Biological Sciences*, 364(1526):1985–1998.

[21] Baruah, A., Sharma, A., Sharma, S. K., and Nagraik, R. (2022). An insight into different microplastic detection methods. *International Journal of Environmental Science and Technology*, 19(6):5721–5730.

[22] BASF (2023). *Irgafos® for Plastics*. www.plastics-rubber.basf.com/global/en/plastic_additives/products/antioxidants/irgafos.html. Online; accessed 27-September-2023.

[23] Bevis, J. A., Bottom, R., Duncan, J., Farhat, I., Forrest, M., Furniss, D., MacNaughton, B., Nazhat, S., Saunders, M., and Seddon, A. (2008). *Principles and Applications of Thermal Analysis*. John Wiley & Sons, Inc.

[24] Bitter, H. and Lackner, S. (2021). Fast and easy quantification of semi-crystalline microplastics in exemplary environmental matrices by differential scanning calorimetry (DSC). *Chemical Engineering Journal*, 423:129941.

[25] Blaga, A. (1980). Deterioration mechanisms in weathering of plastic materials. In *Durability of Building Materials and Components*. ASTM International.

[26] Boersma, A., Grigoriadi, K., Nooijens, M. G. A., Henke, S., Kooter, I. M., Parker, L. A., Dortmans, A., and Urbanus, J. H. (2023). Microplastic index—how to predict microplastics formation? *Polymers*, 15(9):2185.

[27] Brinson, H. F., Brinson, L. C., et al. (2008). *Polymer Engineering Science and Viscoelasticity: An Introduction*. Springer.

[28] Brown, R. P. (1991). Survey of status of test methods for accelerated durability testing. *Polymer Testing*, 10(1):3–30.

[29] Brunnbauer, L., Larisegger, S., Lohninger, H., Nelhiebel, M., and Limbeck, A. (2020). Spatially resolved polymer classification using laser induced breakdown spectroscopy (LIBS) and multivariate statistics. *Talanta*, 209:120572.

[30] Burlett, D. J. (1999). Studies of elastomer oxidation via thermal analysis. *Rubber Chemistry and Technology*, 72(1):165–173.

[31] Canel, T., Demir, P., Kacar, E., Genc Oztoprak, B., Akman, E., Gunes, M., and Demir, A. (2013). Optimization of parameters for depth resolution of galvanized steel by LIBS technique. *Optics & Laser Technology*, 54:257–264.

[32] Capitain, C., Ross-Jones, J., Möhring, S., and Tippkötter, N. (2020). Differential scanning calorimetry for quantification of polymer biodegradability in compost. *International Biodeterioration & Biodegradation*, 149:104914.

[33] Celina, M. C. (2013). Review of polymer oxidation and its relationship with materials performance and lifetime prediction. *Polymer Degradation and Stability*, 98(12):2419–2429.

[34] Chamas, A., Moon, H., Zheng, J., Qiu, Y., Tabassum, T., Jang, J. H., Abu-Omar, M., Scott, S. L., and Suh, S. (2020). Degradation rates of plastics in the environment. *ACS Sustainable Chemistry & Engineering*, 8(9):3494–3511.

[35] Chan, W.-T., Mao, X. L., and Russo, R. E. (1992). Differential vaporization during laser ablation/deposition of Bi-Sr-Ca-Cu-O superconducting materials. *Applied spectroscopy*, 46(6):1025–1031.

[36] Chan, W. T. and Russo, R. E. (1991). Study of laser-material interactions using inductively coupled plasma-atomic emission spectrometry. *Spectrochimica Acta Part B: Atomic Spectroscopy*, 46(11):1471–1486.

[37] Chanda, M. (2017). *Plastics Technology Handbook*. CRC press, 5th edition.

[38] Chang, H.-H., Cheng, C.-L., Huang, P.-J., and Lin, S.-Y. (2014). Application of scanning electron microscopy and x-ray microanalysis: Fe-sem, esem-eds, and eds mapping for studying the characteristics of topographical microstructure and elemental mapping of human cardiac calcified deposition. *Analytical and Bioanalytical Chemistry*, 406:359–366.

[39] Chen, D., Wang, T., Ma, Y., Wang, G., Kong, Q., Zhang, P., and Li, R. (2020a). Rapid characterization of heavy metals in single microplastics by laser induced breakdown spectroscopy. *Science of The Total Environment*, 743:140850.

[40] Chen, M., Liu, Y., Lin, J., and Liu, C. (2019). Characterization of a novel silicon-containing hybrid polymer by thermal curing, pyrolysis behavior, and fluorescence analysis. *Journal of Applied Polymer Science*, 136(18):47403.

[41] Chen, Y., Wen, D., Pei, J., Fei, Y., Ouyang, D., Zhang, H., and Luo, Y. (2020b). Identification and quantification of microplastics using fourier-transform infrared spectroscopy: current status and future prospects. *Current Opinion in Environmental Science & Health*, 18:14–19.

[42] Cheremisinoff, N., editor (2023). *Handbook of Polymer Science and Technology*. CRC Press.

[43] Cifuentes, I. E. M. and Öztürk, B. (2021). Exploring microbial consortia from various environments for plastic degradation. In *Methods in Enzymology*, volume 648, pages 47–69. Elsevier.

[44] Circular Plastics Alliance (2020). Executive summary - state of play for collected and sorted plastic waste in Europe, Circular Plastics Alliance. *Technical report*. Online; accessed 24-August-2023.

[45] Cole, M., Lindeque, P., Halsband, C., and Galloway, T. S. (2011). Microplastics as contaminants in the marine environment: a review. *Marine Pollution Bulletin*, 62(12):2588–2597.

[46] Cooper, J. (1966). Plasma spectroscopy. *Reports on Progress in Physics*, 29(1):35.

[47] Cote, K. G. (2018). Study of Micro-Laser-Induced Breakdown Spectroscopy (uLIBS) for Applications in Planetary Exploration.

[48] Cox, K. D., Covernton, G. A., Davies, H. L., Dower, J. F., Juanes, F., and Dudas, S. E. (2019). Human consumption of microplastics. *Environmental Science & Technology*, 53(12):7068–7074.

[49] Crawford, R. J. and Martin, P. J. (2020). *Plastics engineering*. Butterworth-Heinemann, 4th edition.

[50] Crawford, R. J. and Throne, J. L. (2002). *Rotational Molding Polymers*. William Andrew Publishing Norwich, NY.

[51] Cremers, D. A. and Radziemski, L. J. (2013). *Handbook of laser-induced breakdown spectroscopy*. John Wiley & Sons, Ltd.

[52] Cristoforetti, G., De Giacomo, A., Dell'Aglio, M., Legnaioli, S., Tognoni, E., Palleschi, V., and Omenetto, N. (2010). Local thermodynamic equilibrium in laser-induced breakdown spectroscopy: beyond the mcwhirter criterion. *Spectrochimica Acta Part B: Atomic Spectroscopy*, 65(1):86–95.

[53] De Giacomo, A., Dell'Aglio, M., De Pascale, O., Longo, S., and Capitelli, M. (2007). Laser induced breakdown spectroscopy on meteorites. *Spectrochimica Acta Part B: Atomic Spectroscopy*, 62(12):1606–1611.

[54] de Sá, L. C., Luís, L. G., and Guilhermino, L. (2015). Effects of microplastics on juveniles of the common goby (pomatoschistus microps): confusion with prey, reduction of the predatory performance and efficiency, and possible influence of developmental conditions. *Environmental Pollution*, 196:359–362.

[55] de Sá, L. C., Oliveira, M., Ribeiro, F., Rocha, T. L., and Futter, M. N. (2018). Studies of the effects of microplastics on aquatic organisms: what do we know and where should we focus our efforts in the future? *Science of The Total Environment*, 645:1029–1039.

[56] de Souza Machado, A. A., Kloas, W., Zarfl, C., Hempel, S., and Rillig, M. C. (2018). Microplastics as an emerging threat to terrestrial ecosystems. *Global Change Biology*, 24(4):1405–1416.

[57] Deguchi, Y. and Wang, Z. (2016). Industrial applications of laser-induced breakdown spectroscopy. *Plasma Sci. Technol.–Prog. Phys. States Chem. React.*

[58] do Sul, J. A. I. and Costa, M. F. (2014). The present and future of microplastic pollution in the marine environment. *Environmental Pollution*, 185:352–364.

[59] Dong, M., Mao, X., Gonzalez, J. J., Lu, J., and Russo, R. E. (2012). Time-resolved LIBS of atomic and molecular carbon from coal in air, argon and helium. *Journal of Analytical Atomic Spectrometry*, 27(12):2066–2075.

[60] Ehrenstein, G. W. (2012). *Polymeric materials: structure, properties, applications*. Carl Hanser Verlag GmbH Co KG.

[61] Ehrenstein, G. W. and Pongratz, S. (2013). *Resistance and stability of polymers*. Carl Hanser Verlag GmbH Co KG.

[62] Eisentraut, P., Dümichen, E., Ruhl, A. S., Jekel, M., Albrecht, M., Gehde, M., and Braun, U. (2018). Two birds with one stone—fast and simultaneous analysis of microplastics: microparticles derived from thermoplastics and tire wear. *Environmental Science & Technology Letters*, 5(10):608–613.

[63] El-Sherbini, A. M., Aboulfotouh, A.-N. M., Rashid, F. F., Allam, S. H., Dakrouri, A. E., and El-Sherbini, T. M. (2012). Observed enhancement in LIBS signals from nano vs. bulk ZnO targets: comparative study of plasma parameters. *World J. Nano Sci. Eng*, 2(04):181–188.

[64] El-Sherbini, A. M., El-Sherbini, T. M., Hegazy, H., Cristoforetti, G., Legnaioli, S., Palleschi, V., Pardini, L., Salvetti, A., and Tognoni, E. (2005). Evaluation of self-absorption coefficients of aluminum emission lines in laser-induced breakdown spectroscopy measurements. *Spectrochimica Acta Part B: Atomic Spectroscopy*, 60(12):1573–1579.

[65] Elert, A. M., Becker, R., Duemichen, E., Eisentraut, P., Falkenhagen, J., Sturm, H., and Braun, U. (2017). Comparison of different methods for mp detection: what can we learn from them, and why asking the right question before measurements matters? *Environmental Pollution*, 231:1256–1264.

[66] Elvers, B., editor (2016). *Ullmann's Polymers and Plastics: Products and Processes*. Wiley-VCH.

[67] European Commission (2019). Communication From The Commission To The European Parliament, The Council, The European Economic And Social Committee And The Committee Of The Regions - The European Green Deal. *Technical report*, COM/2019/640. Online; accessed 24-August-2023.

[68] European Court of Auditors (2020). Review No 4: EU action to tackle the issue of plastic waste. *Technical report*. Online; accessed 24-August-2023.

[69] Fabra, M., Williams, L., Watts, J. E. M., Hale, M. S., Couceiro, F., and Preston, J. (2021). The plastic trojan horse: Biofilms increase microplastic uptake in marine filter feeders impacting microbial transfer and organism health. *Science of the Total Environment*, 797:149217.

[70] Fetting, C. (2020). The European green deal. *ESDN report*, 53.

[71] Frias, J. P. G. L. and Nash, R. (2019). Microplastics: Finding a consensus on the definition. *Marine Pollution Bulletin*, 138:145–147.

[72] Galbács, G., editor (2022). *Laser-induced Breakdown Spectroscopy in Biological, Forensic and Materials Sciences*. Springer Nature.

[73] Galloway, T. S. and Lewis, C. N. (2016). Marine microplastics spell big problems for future generations. *Proceedings of the National Academy of Sciences*, 113(9):2331–2333.

[74] Garcea, S. C., Wang, Y., and Withers, P. J. (2018). X-ray computed tomography of polymer composites. *Composites Science and Technology*, 156:305–319.

[75] Garvey, C. J., Impéror-Clerc, M., Rouzière, S., Gouadec, G., Boyron, O., Rowenczyk, L., Mingotaud, A. F., and Ter Halle, A. (2020). Molecular-scale understanding of the embrittlement in polyethylene ocean debris. *Environmental Science & Technology*, 54(18):11173–11181.

[76] Gaudiuso, R., Dell'Aglio, M., De Pascale, O., Senesi, G. S., and De Giacomo, A. (2010). Laser induced breakdown spectroscopy for elemental analysis in environmental, cultural heritage and space applications: a review of methods and results. *Sensors*, 10(8):7434–7468.

[77] Gewert, B., Plassmann, M. M., and MacLeod, M. (2015). Pathways for degradation of plastic polymers floating in the marine environment. *Environmental Science: Processes & Impacts*, 17(9):1513–1521.

[78] Ghosh, S. K., editor (2020). *Circular Economy: Global Perspective*. Springer.

[79] Gies, S., Schömann, E.-M., Anna Prume, J., and Koch, M. (2020). Exploring the potential of time-resolved photoluminescence spectroscopy for the detection of plastics. *Applied Spectroscopy*, 74(9):1161–1166.

[80] Gijsman, P., Meijers, G., and Vitarelli, G. (1999). Comparison of the UV-degradation chemistry of polypropylene, polyethylene, polyamide 6 and polybutylene terephthalate. *Polymer Degradation and Stability*, 65(3):433–441.

[81] Grégoire, S., Boudinet, M., Pelascini, F., Surma, F., Detalle, V., and Holl, Y. (2011). Laser-induced breakdown spectroscopy for polymer identification. *Analytical and Bioanalytical Chemistry*, 400:3331–3340.

[82] Griem, H. R. (1963). Validity of local thermal equilibrium in plasma spectroscopy. *Physical Review*, 131(3):1170.

[83] Griem, H. R. (1974). *Spectral line broadening by plasmas*. Academic Press.

[84] Hahladakis, J. N., Velis, C. A., Weber, R., Iacovidou, E., and Purnell, P. (2018). An overview of chemical additives present in plastics: Migration, release, fate and environmental impact during their use, disposal and recycling. *Journal of Hazardous Materials*, 344:179–199.

[85] Haines, P. J. (2012). *Thermal Methods of Analysis: Principles, Applications and Problems*. Springer Science & Business Media.

[86] Hao, Z., Guo, L., Li, C., Shen, M., Zou, X., Li, X., Lu, Y., and Zeng, X. (2014). Sensitivity improvement in the detection of V and Mn elements in steel using laser-induced breakdown spectroscopy with ring-magnet confinement. *Journal of Analytical Atomic Spectrometry*, 29(12):2309–2314.

[87] Harmon, R. S., Hark, R. R., Throckmorton, C. S., Rankey, E. C., Wise, M. A., Somers, A. M., and Collins, L. M. (2017). Geochemical fingerprinting by handheld laser-induced breakdown spectroscopy. *Geostandards and Geoanalytical Research*, 41(4):563–584.

[88] Hawkins, W. L. (1984). Polymer degradation. In *Polymer Degradation and Stabilization*, pages 3–34. Springer Berlin Heidelberg, Berlin, Heidelberg.

[89] Hermabessiere, L., Himber, C., Boricaud, B., Kazour, M., Amara, R., Cassone, A.-L., Laurentie, M., Paul-Pont, I., Soudant, P., Dehaut, A., et al. (2018). Optimization, performance, and application of a pyrolysis-GC/MS method for the identification of microplastics. *Analytical and Bioanalytical Chemistry*, 410:6663–6676.

[90] Hermann Staudinger – Facts (2023). *NobelPrize.org*. www.nobelprize.org/prizes/chemistry/1953/staudinger/facts/. Nobel Prize Outreach AB 2023. Online; accessed 08-July-2023.

[91] Hildebrandt, L., Nack, F. L., Zimmermann, T., and Pröfrock, D. (2021). Microplastics as a trojan horse for trace metals. *Journal of Hazardous Materials Letters*, 2:100035.

[92] Hollas, J. M. (2004). *Modern Spectroscopy*. John Wiley & Sons, Ltd., 4th edition.

[93] Hu, L., Zhao, Y., and Xu, H. (2022). Trojan horse in the intestine: a review on the biotoxicity of microplastics combined environmental contaminants. *Journal of Hazardous Materials*, 439:129652.

[94] Huang, Z., Hu, B., and Wang, H. (2023). Analytical methods for microplastics in the environment: a review. *Environmental Chemistry Letters*, 21(1):383–401.

[95] Hussain, T., Gondal, M. A., and Shamraiz, M. (2016). Determination of plasma temperature and electron density of iron in iron slag samples using laser induced breakdown spectroscopy. In *IOP Conference Series: Materials Science and Engineering*, volume 146, page 012017. IOP Publishing.

[96] InNoPlastic (2023). *InNoPlastic*. www.innoplastic.eu. Online; accessed 21-September-2023.

[97] Isobe, A. and Iwasaki, S. (2022). The fate of missing ocean plastics: Are they just a marine environmental problem? *Science of the Total Environment*, 825:153935.

[98] Ivleva, N. P. (2021). Chemical analysis of microplastics and nanoplastics: Challenges, advanced methods, and perspectives. *Chemical Reviews*, 121(19):11886–11936.

[99] Jasso-Gastinel, C. F., González-Ortiz, L. J., Contreras J., R., Mendizábal M., E., and Mora G., J. (1998). The degradation of high impact polystyrene with and without starch in concentrated activated sludge. *Polymer Engineering & Science*, 38(5):863–869.

[100] Jasso-Gastinel, C. F. and Kenny, J. M., editors (2016). *Modification of Polymer Properties*. William Andrew.

[101] Jolliffe, I. T. (2002). *Principal Component Analysis*. Springer.

[102] Jorio, A., Dresselhaus, M. S., Saito, R., and Dresselhaus, G. (2011). *Raman spectroscopy in graphene related systems*. John Wiley & Sons.

[103] Jung, M. R., Horgen, F. D., Orski, S. V., Rodriguez, V., Beers, K. L., Balazs, G. H., Jones, T. T., Work, T. M., Brignac, K. C., Royer, S.-J., et al. (2018). Validation of ATR

FT-IR to identify polymers of plastic marine debris, including those ingested by marine organisms. *Marine Pollution Bulletin*, 127:704–716.

[104] Käppler, A., Fischer, D., Oberbeckmann, S., Schernewski, G., Labrenz, M., Eichhorn, K.-J., and Voit, B. (2016). Analysis of environmental microplastics by vibrational microspectroscopy: FTIR, Raman or both? *Analytical and Bioanalytical Chemistry*, 408:8377–8391.

[105] Keferstein, C. P. and Marxer, M. (2015). Berührungslos/optische Messverfahren. In *Fertigungsmesstechnik: Praxisorientierte Grundlagen, moderne Messverfahren*, pages 195–256. Springer Fachmedien Wiesbaden, Wiesbaden.

[106] Kennedy, M. A., Peacock, A. J., and Mandelkern, L. (1994). Tensile properties of crystalline polymers: linear polyethylene. *Macromolecules*, 27(19):5297–5310.

[107] Kennedy, P. K., Hammer, D. X., and Rockwell, B. A. (1997). Laser-induced breakdown in aqueous media. *Progress in Quantum Electronics*, 21(3):155–248.

[108] Khalid, N., Aqeel, M., and Noman, A. (2020). Microplastics could be a threat to plants in terrestrial systems directly or indirectly. *Environmental Pollution*, 267:115653.

[109] Kiran, B. R., Kopperi, H., and Venkata Mohan, S. (2022). Micro/nano-plastics occurrence, identification, risk analysis and mitigation: challenges and perspectives. *Reviews in Environmental Science and Bio/Technology*, 21(1):169–203.

[110] Koenig, J. L. (1999). *Spectroscopy of Polymers*. Elsevier, 2nd edition.

[111] Konde, S., Ornik, J., Prume, J. A., Taiber, J., and Koch, M. (2020). Exploring the potential of photoluminescence spectroscopy in combination with nile red staining for microplastic detection. *Marine Pollution Bulletin*, 159:111475.

[112] Konjević, N., Ivković, M., and Jovićević, S. (2010). Spectroscopic diagnostics of laser-induced plasmas. *Spectrochimica Acta Part B: Atomic Spectroscopy*, 65(8):593–602.

[113] Konjević, N., Lesage, A., Fuhr, J. R., and Wiese, W. L. (2002). Experimental stark widths and shifts for spectral lines of neutral and ionized atoms (a critical review of selected data for the period 1989 through 2000). *Journal of Physical and Chemical Reference Data*, 31(3):819–927.

[114] Kramida, A., Ralchenko, Y., Reader, J., and Team, N. A. (2022). NIST Atomic Spectra Database (version 5.10).

[115] Kumar, P. (2020). Reduce, Reuse, Recycle. Plastic and Packaging Waste in the European Green Deal and Circular Economy Action Plan. *IASS Discuss. Pap*, 10.

[116] Kunze, H.-J. (2009). *Introduction to Plasma Spectroscopy*. Springer Science & Business Media.

[117] Kusch, P. (2019). *Pyrolysis-Gas Chromatography: Mass Spectrometry of Polymeric Materials*. World Scientific.

[118] Kuzmany, H. (2009). *Solid-State Spectroscopy: An Introduction*. Springer, 2nd edition.

[119] Labutin, T. A., Lednev, V. N., Ilyin, A. A., and Popov, A. M. (2016). Femtosecond laser-induced breakdown spectroscopy. *Journal of Analytical Atomic Spectrometry*, 31(1):90–118.

[120] Lai, C. W., Schwab, M., Hill, S. C., Santarpia, J., and Pan, Y.-L. (2016). Raman scattering and red fluorescence in the photochemical transformation of dry tryptophan particles. *Optics Express*, 24(11):11654–11667.

[121] Latscha, H. P., Linti, G. W., Klein, H. A., Latscha, H. P., Linti, G. W., and Klein, H. A. (2004). Optische und spektroskopische Analysenverfahren. *Analytische Chemie: Chemie—Basiswissen III*, pages 381–443.

[122] Li, Z., Deen, M. J., Kumar, S., and Selvaganapathy, P. R. (2014). Raman spectroscopy for in-line water quality monitoring—instrumentation and potential. *Sensors*, 14(9):17275–17303.

[123] Liu, P., Shi, Y., Wu, X., Wang, H., Huang, H., Guo, X., and Gao, S. (2021). Review of the artificially-accelerated aging technology and ecological risk of microplastics. *Science of the Total Environment*, 768:144969.

[124] Long, D. A. (2002). *The Raman Effect*. John Wiley & Sons Ltd.

[125] Maes, T., Jessop, R., Wellner, N., Haupt, K., and Mayes, A. G. (2017). A rapid-screening approach to detect and quantify microplastics based on fluorescent tagging with nile red. *Scientific Reports*, 7(1):44501.

[126] Majewsky, M., Bitter, H., Eiche, E., and Horn, H. (2016). Determination of microplastic polyethylene (PE) and polypropylene (PP) in environmental samples using thermal analysis (TGA-DSC). *Science of the Total Environment*, 568:507–511.

[127] Mansa, R. and Zou, S. (2021). Thermogravimetric analysis of microplastics: A mini review. *Environmental Advances*, 5:100117.

[128] Mansour, S. A. M. (2015). Self-absorption effects on electron temperature-measurements utilizing laser induced breakdown spectroscopy (LIBS)-techniques. *Optics and Photonics Journal*, 5(3):79.

[129] Marcelino, R. C., Cardoso, R. M., Domingues, E. L. B. C., Gonçalves, R. V., Lima, G. D. A., and Novaes, R. D. (2022). The emerging risk of microplastics and nanoplastics on the microstructure and function of reproductive organs in mammals: A systematic review of preclinical evidence. *Life Sciences*, 295:120404.

[130] Mariano, S., Tacconi, S., Fidaleo, M., Rossi, M., and Dini, L. (2021). Micro and nanoplastics identification: classic methods and innovative detection techniques. *Frontiers in Toxicology*, 3:636640.

[131] Masry, M., Rossignol, S., Gardette, J.-L., Therias, S., Bussière, P.-O., and Wong-Wah-Chung, P. (2021). Characteristics, fate, and impact of marine plastic debris exposed to sunlight: A review. *Marine Pollution Bulletin*, 171:112701.

[132] Mateo, M. P., Vadillo, J. M., and Laserna, J. J. (2001). Irradiance-dependent depth profiling of layered materials using laser-induced plasma spectrometry. *Journal of Analytical Atomic Spectrometry*, 16(11):1317–1321.

[133] McWhirter, R. (1965). In Huddleston, R. H. and Leonard, S. L., editors, *Plasma Diagnostic Techniques*, chapter 5, pages 201–264. Academic Press, New York.

[134] Meides, N., Menzel, T., Poetzschner, B., Löder, M. G. J., Mansfeld, U., Strohriegl, P., Altstaedt, V., and Senker, J. (2021). Reconstructing the environmental degradation of polystyrene by accelerated weathering. *Environmental Science & Technology*, 55(12):7930–7938.

[135] Menczel, J. D. and Prime, R. B. (2009). *Thermal Analysis of Polymers: Fundamentals and Applications*. John Wiley & Sons, Inc.

[136] Menzel, T., Meides, N., Mauel, A., Mansfeld, U., Kretschmer, W., Kuhn, M., Herzig, E. M., Altstädt, V., Strohriegl, P., Senker, J., et al. (2022). Degradation of low-density polyethylene to nanoplastic particles by accelerated weathering. *Science of the Total Environment*, 826:154035.

[137] Miziolek, A. W., Palleschi, V., and Schechter, I. (2006). *Laser induced breakdown spectroscopy*. Cambridge University Press.

[138] Moenke-Blankenburg, L. (1989). *Laser Microanalysis*. John Wiley & Sons, Inc.

[139] Mortensen, L. F., Tange, I., Stenmarck, Å., Fråne, A., Nielsen, T., Boberg, N., and Bauer, F. (2021). Plastics, the circular economy and europe's environment - a priority for action. *Technical report*.

[140] Musazzi, S. and Perini, U., editors (2014). *Laser-induced Breakdown Spectroscopy: Theory and Applications*, volume 182. Springer.

[141] Nagai, N., Matsunobe, T., and Imai, T. (2005). Infrared analysis of depth profiles in UV-photochemical degradation of polymers. *Polymer Degradation and Stability*, 88(2):224–233.

[142] Nixon, W. C. (1971). The general principles of scanning electron microscopy. *Philosophical Transactions of the Royal Society of London. B, Biological Sciences*, 261(837):45–50.

[143] Noll, R. (2012). *Laser-Induced Breakdown Spectroscopy*. Springer.

[144] Nouira, H., Salgado, J. A., El-Hayek, N., Ducourtieux, S., Delvallée, A., and Anwer, N. (2014). Setup of a high-precision profilometer and comparison of tactile and optical measurements of standards. *Measurement Science and Technology*, 25(4):044016.

[145] Nurazzi, N. M., Norrrahim, M. N. F., Shazleen, S. S., Harussani, M. M., Sabaruddin, F. A., and Asyraf, M. R. M. (2023). Introduction to polymer crystallization. *Polymer Crystallization: Methods, Characterization and Applications*, pages 1–12.

[146] Ogata, Y., Takada, H., Mizukawa, K., Hirai, H., Iwasa, S., Endo, S., Mato, Y., Saha, M., Okuda, K., Nakashima, A., et al. (2009). International pellet watch: Global monitoring of persistent organic pollutants (POPs) in coastal waters. 1. initial phase data on PCBs, DDTs, and HCHs. *Marine Pollution Bulletin*, 58(10):1437–1446.

[147] Okubo, R., Yamamoto, A., Kurima, A., Sakabe, T., Ide, Y., and Isobe, A. (2023). Estimation of the age of polyethylene microplastics collected from oceans: Application to the western north pacific ocean. *Marine Pollution Bulletin*, 192:114951.

[148] Olmsted, B. A. and Davis, M. E. (2001). *Practical injection molding*. CRC Press.

[149] Ornik, J., Sommer, S., Gies, S., Weber, M., Lott, C., Balzer, J. C., and Koch, M. (2020). Could photoluminescence spectroscopy be an alternative technique for the detection of microplastics? first experiments using a 405 nm laser for excitation. *Applied Physics B*, 126:1–7.

[150] Parashar, N. and Hait, S. (2021). Plastics in the time of covid-19 pandemic: protector or polluter? *Science of the Total Environment*, 759:144274.

[151] Parra, D. F. and do Rosário Matos, J. (2002). Some synergistic effects of antioxidants in natural rubber. *Journal of Thermal Analysis and Calorimetry*, 67(2):287–294.

[152] Pathak, P., Sharma, S., and Ramakrishna, S. (2023). Circular transformation in plastic management lessens the carbon footprint of the plastic industry. *Materials Today Sustainability*, 22:100365.

[153] Pavia, D. L., Lampman, G. M., Kriz, G. S., and Vyvyan, J. A. (2014). *Introduction to Spectroscopy*. Cengage learning.

[154] Pegram, J. E. and Andrady, A. L. (1989). Outdoor weathering of selected polymeric materials under marine exposure conditions. *Polymer Degradation and Stability*, 26(4):333–345.

[155] Peñalver, R., Arroyo-Manzanares, N., López-García, I., and Hernández-Córdoba, M. (2020). An overview of microplastics characterization by thermal analysis. *Chemosphere*, 242:125170.

[156] Phan, S., Padilla-Gamiño, J. L., and Luscombe, C. K. (2022). The effect of weathering environments on microplastic chemical identification with Raman and IR spectroscopy: Part I. polyethylene and polypropylene. *Polymer Testing*, 116:107752.

[157] Pico, Y. and Barcelo, D. (2020). Pyrolysis gas chromatography-mass spectrometry in environmental analysis: Focus on organic matter and microplastics. *TrAC Trends in Analytical Chemistry*, 130:115964.

[158] Piruska, A., Nikcevic, I., Lee, S. H., Ahn, C., Heineman, W. R., Limbach, P. A., and Seliskar, C. J. (2005). The autofluorescence of plastic materials and chips measured under laser irradiation. *Lab on a Chip*, 5(12):1348–1354.

[159] PlasticsEurope (2022a). The circular economy for plastics—a european overview. *Technical report*.

[160] PlasticsEurope (2022b). Plastics – the facts 2022. *Technical report*.

[161] Pořízka, P., Brunnbauer, L., Porkert, M., Rozman, U., Marolt, G., Holub, D., Kizovskỳ, M., Benešová, M., Samek, O., Limbeck, A., et al. (2023). Laser-based techniques: Novel tools for the identification and characterization of aged microplastics with developed biofilm. *Chemosphere*, 313:137373.

[162] Prata, J. C., da Costa, J. P., Duarte, A. C., and Rocha-Santos, T. (2019). Methods for sampling and detection of microplastics in water and sediment: a critical review. *TrAC Trends in Analytical Chemistry*, 110:150–159.

[163] Primpke, S., Christiansen, S. H., Cowger, W., De Frond, H., Deshpande, A., Fischer, M., Holland, E. B., Meyns, M., O'Donnell, B. A., Ossmann, B. E., et al. (2020). Critical assessment of analytical methods for the harmonized and cost-efficient analysis of microplastics. *Applied Spectroscopy*, 74(9):1012–1047.

[164] Primpke, S., Wirth, M., Lorenz, C., and Gerdts, G. (2018). Reference database design for the automated analysis of microplastic samples based on fourier transform infrared (FTIR) spectroscopy. *Analytical and Bioanalytical Chemistry*, 410:5131–5141.

[165] Pritchard, G., editor (1998). *Plastics Additives: an AZ reference*, volume 1. Springer Science & Business Media.

[166] Priya, A., Jalil, A. A., Dutta, K., Rajendran, S., Vasseghian, Y., Qin, J., and Soto-Moscoso, M. (2022). Microplastics in the environment: recent developments in characteristic, occurrence, identification and ecological risk. *Chemosphere*, page 134161.

[167] Qiu, Q., Tan, Z., Wang, J., Peng, J., Li, M., and Zhan, Z. (2016). Extraction, enumeration and identification methods for monitoring microplastics in the environment. *Estuarine, Coastal and Shelf Science*, 176:102–109.

[168] Quik, J. T. K., Meesters, J. A. J., and Koelmans, A. A. (2023). A multimedia model to estimate the environmental fate of microplastic particles. *Science of the Total Environment*, 882:163437.

[169] Rabek, J. F. (2012). *Photodegradation of Polymers: Physical Characteristics and Applications*. Springer Science & Business Media.

[170] Redondo-Hasselerharm, P. E., Rico, A., and Koelmans, A. A. (2023). Risk assessment of microplastics in freshwater sediments guided by strict quality criteria and data alignment methods. *Journal of Hazardous Materials*, 441:129814.

[171] Riga, A., Collins, R., and Mlachak, G. (1998). Oxidative behavior of polymers by thermogravimetric analysis, differential thermal analysis and pressure differential scanning calorimetry. *Thermochimica Acta*, 324(1-2):135–149.

[172] Ryu, J.-H., Yang, J.-H., and Yoh, J. J. (2019). Novel utilization of the molecular band signal in metal oxides: understanding the aging process of pyrotechnic substances by using laser induced plasma emissions. *Optical Materials Express*, 9(2):410–422.

[173] Santos Jr., D., Nunes, L. C., de Carvalho, G. G. A., da Silva Gomes, M., de Souza, P. F., de Oliveira Leme, F., dos Santos, L. G. C., and Krug, F. J. (2012). Laser-induced breakdown spectroscopy for analysis of plant materials: a review. *Spectrochimica Acta Part B: Atomic Spectroscopy*, 71:3–13.

[174] Sattmann, R., Monch, I., Krause, H., Noll, R., Couris, S., Hatziapostolou, A., Mavromanolakis, A., Fotakis, C., Larrauri, E., and Miguel, R. (1998). Laser-induced breakdown spectroscopy for polymer identification. *Applied Spectroscopy*, 52(3):456–461.

[175] Segovia-Mendoza, M., Nava-Castro, K. E., Palacios-Arreola, M. I., Garay-Canales, C., and Morales-Montor, J. (2020). How microplastic components influence the immune system and impact on children health: Focus on cancer. *Birth Defects Research*, 112(17):1341–1361.

[176] Sewwandi, M., Keerthanan, S., Perera, K. I., and Vithanage, M. (2023). Plastic nurdles in marine environments due to accidental spillage. In *Microplastics in the Ecosphere: Air, Water, Soil, and Food*, chapter 26, pages 415–432. John Wiley & Sons, Inc.

[177] Shen, Y.-R. (1984). *Principles of nonlinear optics*. Wiley-Interscience, New York, NY, USA.

[178] Shim, W. J., Hong, S. H., and Eo, S. E. (2017). Identification methods in microplastic analysis: a review. *Analytical Methods*, 9(9):1384–1391.

[179] Shim, W. J., Song, Y. K., Hong, S. H., and Jang, M. (2016). Identification and quantification of microplastics using nile red staining. *Marine Pollution Bulletin*, 113(1-2):469–476.

[180] Shrivastava, A. (2018). *Introduction to plastics engineering*. William Andrew.

[181] Silva, D. J. d. and Wiebeck, H. (2019). Predicting LDPE/HDPE blend composition by CARS-PLS regression and confocal Raman spectroscopy. *Polímeros*, 29.

[182] Song, Y. K., Hong, S. H., Jang, M., Han, G. M., Rani, M., Lee, J., and Shim, W. J. (2015). A comparison of microscopic and spectroscopic identification methods for analysis of microplastics in environmental samples. *Marine Pollution Bulletin*, 93(1-2):202–209.

[183] Sorolla-Rosario, D., Llorca-Porcel, J., Pérez-Martínez, M., Lozano-Castello, D., and Bueno-Lopez, A. (2022). Study of microplastics with semicrystalline and amorphous structure identification by TGA and DSC. *Journal of Environmental Chemical Engineering*, 10(1):106886.

[184] St-Onge, L. and Sabsabi, M. (2000). Towards quantitative depth-profile analysis using laser-induced plasma spectroscopy: investigation of galvannealed coatings on steel. *Spectrochimica Acta Part B: Atomic Spectroscopy*, 55(3):299–308.

[185] Steinwart, I. and Christmann, A. (2008). *Support vector machines*. Springer Science & Business Media.

[186] Stringer, R. and Johnston, P. (2001). Chlorine and the environment: an overview of the chlorine industry.

[187] Stuart, B. H. (2004). *Infrared Spectroscopy: Fundamentals and Applications*. John Wiley & Sons, Inc.

[188] Summers, J. W. and Rabinovitch, E. B. (1999). Weatherability of vinyl and other plastics. In *Weathering of Plastics*, pages 61–68. Elsevier.

[189] Syberg, K., Khan, F. R., Selck, H., Palmqvist, A., Banta, G. T., Daley, J., Sano, L., and Duhaime, M. B. (2015). Microplastics: addressing ecological risk through lessons learned. *Environmental Toxicology and Chemistry*, 34(5):945–953.

[190] Systemiq (2022). Reshaping plastics: Pathways to a circular, climate neutral plastics system in europe. *Technical report*.

[191] The Ocean Cleanup (2023). *The Ocean Cleanup*. www.theoceancleanup.com. Online; accessed 21-September-2023.

[192] UNFCCC (2018). The Paris Agreement. *Technical report*, COP 21.

[193] UNFCCC (2021). Glasgow Climate Pact. *Technical report*, cp26_auv_2f_cover_decision.

[194] Utracki, L. A. and Wilkie, C. A., editors (2002). *Polymer blends handbook*, volume 1. Dordrecht: Kluwer academic publishers.

[195] Vahid Dastjerdi, M., Mousavi, S. J., Soltanolkotabi, M., and Nezarati Zadeh, A. (2018). Identification and sorting of pvc polymer in recycling process by laser-induced breakdown spectroscopy (LIBS) combined with support vector machine (SVM) model. *Iranian Journal of Science and Technology, Transactions A: Science*, 42:959–965.

[196] Van der Mullen, J. A. M. (1990). Excitation equilibria in plasmas; a classification. *Physics Reports*, 191(2-3):109–220.

[197] Van Der Mullen, J. A. M. (1990). On the atomic state distribution function in inductively coupled plasmas—II: The stage of local thermal equilibrium and its validity region. *Spectrochimica Acta Part B: Atomic Spectroscopy*, 45(1-2):1–13.

[198] Van Fan, Y., Jiang, P., Tan, R. R., Aviso, K. B., You, F., Zhao, X., Lee, C. T., and Klemeš, J. J. (2022). Forecasting plastic waste generation and interventions for environmental hazard mitigation. *Journal of Hazardous Materials*, 424:127330.

[199] Vasile, C. (1993). Degradation and decomposition. In Fatou, J. G., Vasile, C., and Seymour, R., editors, *Handbook of polyolefins, synthesis and properties*, pages 479–506. Marcel Dekker, New York.

[200] Vasile, C. (2000). *Handbook of polyolefins*. CRC press.

[201] Velásquez, E., Patino Vidal, C., Rojas, A., Guarda, A., Galotto, M. J., and Lopez de Dicastillo, C. (2021). Natural antimicrobials and antioxidants added to polylactic acid packaging films. Part I: Polymer processing techniques. *Comprehensive Reviews in Food Science and Food Safety*, 20(4):3388–3403.

[202] Vicente, J. S., Gejo, J. L., Rothenbacher, S., Sarojiniamma, S., Gogritchiani, E., Wörner, M., Kasperb, G., and Braun, A. M. (2009). Oxidation of polystyrene aerosols by VUV-photolysis and/or ozone. *Photochemical & Photobiological Sciences*, 8:944–952.

[203] Virtanen, P., Gommers, R., Oliphant, T. E., Haberland, M., Reddy, T., Cournapeau, D., Burovski, E., Peterson, P., Weckesser, W., Bright, J., et al. (2020). SciPy 1.0: fundamental algorithms for scientific computing in python. *Nature methods*, 17(3):261–272.

[204] Vivien, C., Hermann, J., Perrone, A., Boulmer-Leborgne, C., and Luches, A. (1998). A study of molecule formation during laser ablation of graphite in low-pressure nitrogen. *Journal of Physics D: Applied Physics*, 31(10):1263.

[205] Vogel, A., Noack, J., Huettmann, G., and Paltauf, G. (2002). Femtosecond-laser-produced low-density plasmas in transparent biological media: a tool for the creation of chemical, thermal, and thermomechanical effects below the optical breakdown threshold. In *Commercial and Biomedical Applications of Ultrafast and Free-Electron Lasers*, volume 4633, pages 23–37. SPIE.

[206] Wagner, J., Wang, Z.-M., Ghosal, S., Rochman, C., Gassel, M., and Wall, S. (2017). Novel method for the extraction and identification of microplastics in ocean trawl and fish gut matrices. *Analytical Methods*, 9(9):1479–1490.

[207] Wagnière, G. H. (2012). *Introduction to elementary molecular orbital theory and to semiempirical methods*, volume 1. Springer Science & Business Media.

[208] Watkins, E., Romagnoli, V., Kirhensteine, I., Ruckley, F., Kreißig, J., Mitsios, A., and Pantzar, M. (2020). Support to the Circular Plastics Alliance in Establishing a Work Plan to Develop Guidelines and Standards on Design for Recycling of Plastic Products. *Publications Office of the European Union: Luxembourg*.

[209] White, J. R. and Turnbull, A. (1994). Weathering of polymers: mechanisms of degradation and stabilization, testing strategies and modelling. *Journal of Materials Science*, 29:584–613.

[210] Wright, S. L. and Kelly, F. J. (2017). Plastic and human health: a micro issue? *Environmental Science & Technology*, 51(12):6634–6647.

[211] Xu, F., Ma, S., Zhao, C., and Dong, D. (2022). Application of molecular emissions in laser-induced breakdown spectroscopy: A review. *Frontiers in Physics*, 10:7.

[212] Xu, J.-L., Thomas, K. V., Luo, Z., and Gowen, A. A. (2019). FTIR and Raman imaging for microplastics analysis: State of the art, challenges and prospects. *TrAC Trends in Analytical Chemistry*, 119:115629.

[213] Xu, S., Ma, J., Ji, R., Pan, K., and Miao, A.-J. (2020). Microplastics in aquatic environments: occurrence, accumulation, and biological effects. *Science of the Total Environment*, 703:134699.

[214] Yang, W., Jannatun, N., Zeng, Y., Liu, T., Zhang, G., Chen, C., and Li, Y. (2022). Impacts of microplastics on immunity. *Frontiers in Toxicology*, 4:956885.

[215] Yousif, E. and Haddad, R. (2013). Photodegradation and photostabilization of polymers, especially polystyrene. *SpringerPlus*, 2(1):1–32.

[216] Zadpoor, A. A. (2019). Mechanical performance of additively manufactured meta-biomaterials. *Acta Biomaterialia*, 85:41–59.

[217] Zhang, C., Chen, J., Ma, S., Sun, Z., and Wang, Z. (2022). Microplastics may be a significant cause of male infertility. *American Journal of Men's Health*, 16(3):15579883221096549.

[218] Zhang, D. and Guan, L. (2014). 4.06. - Laser Ablation. In Hashmi, S., Batalha, G. F., Van Tyne, C. J., and Yilbas, B., editors, *Comprehensive Materials Processing*, pages 125–169. Elsevier, Oxford.

[219] Zhao, X., Cornish, K., and Vodovotz, Y. (2020). Narrowing the gap for bioplastic use in food packaging: an update. *Environmental Science & Technology*, 54(8):4712–4732.

[220] Zhao, X., Wang, J., Yee Leung, K. M., and Wu, F. (2022). Color: an important but overlooked factor for plastic photoaging and microplastic formation. *Environmental Science & Technology*, 56(13):9161–9163.

[221] Ziani, K., Ioniță-Mîndrican, C.-B., Mititelu, M., Neacșu, S. M., Negrei, C., Moroșan, E., Drăgănescu, D., and Preda, O.-T. (2023). Microplastics: a real global threat for environment and food safety: a state of the art review. *Nutrients*, 15(3):617.

Appendix

Scientific Publications

The thesis is a review of the following three publications. My contributions to each publication are indicated below.

(I) **Sommer, C.**, Schneider, L. M., Nguyen, J., Prume, J. A., Lautze, K., & Koch, M. (2021). Identifying microplastic litter with Laser Induced Breakdown Spectroscopy: A first approach. *Marine Pollution Bulletin*, 171, 112789.

- All LIBS measurements and parts of the FTIR measurements
- All of the data analysis
- Half of the writing

(II) **Sommer, C.**, Nguyen, J., Menzel, T., Prume, J. A., Ruckdäschel, H., & Koch, M. (2022). Weathering-induced oxidation: An investigation of artificially aged polystyrene samples using Laser-induced Breakdown Spectroscopy. *Polymer Testing*, 112, 107623.

- All LIBS measurements and all profilometer measurements
- Most of the data analysis
- Most of the writing

(III) **Sommer, C.**, Nguyen, J., Menzel, T., Ruckdäschel, H., & Koch, M. (2023). Determining weathering-induced heterogeneous oxidation profiles of polyethylene, polypropylene and polystyrene using laser-induced breakdown spectroscopy. *Chemosphere*, 140105.

- All measurements
- All of the data analysis
- Most of the writing

Article 1

Sommer, C., Schneider, L. M., Nguyen, J., Prume, J. A., Lautze, K., & Koch, M. (2021). Identifying microplastic litter with Laser Induced Breakdown Spectroscopy: A first approach. *Marine Pollution Bulletin*, 171, 112789.

DOI:10.1016/j.marpolbul.2021.112789
URL: https://doi.org/10.1016/j.marpolbul.2021.112789
This article was published in Marine Pollution Bulletin, Vol. 171, page 112789.

Marine Pollution Bulletin 171 (2021) 112789

Contents lists available at ScienceDirect

Marine Pollution Bulletin

journal homepage: www.elsevier.com/locate/marpolbul

Identifying microplastic litter with Laser Induced Breakdown Spectroscopy: A first approach

C. Sommer *, L.M. Schneider, J. Nguyen, J.A. Prume, K. Lautze, M. Koch

Faculty of Physics and Material Sciences Centre, Philipps University of Marburg, Marburg, Germany

ARTICLE INFO

Keywords:
Laser-Induced Breakdown Spectroscopy (LIBS)
Microplastic
Plastic identification
Sediment sample
Plastic pollution

ABSTRACT

The broad diversity of microplastic litter requires a selection of analytical techniques to reliably determine the particle's chemical composition. This study demonstrates that Laser Induced Breakdown Spectroscopy (LIBS) can identify microplastic particles based on their spectral fingerprints. By studying the spectral features of polymer reference spectra, microplastic litter can be distinguished from non-plastic materials. The results show that LIBS can be used as a fast in-situ technique for pre-characterization of the microparticle's material and is a possible tool for environmental studies on microplastics.

1. Introduction

The ever-increasing accumulation of plastic litter in natural habitats is a serious problem that is in dire need of human intervention. Accelerated by the growing popularity of plastics and the worldwide inability to enforce effective plastic recycling guidelines, it is foreseeable that plastic pollution will further emerge as a major environmental burden and eventually affect people's lives.

In recent years, micro- and nanoplastics, defined as particles with sizes less than 5 mm and larger than 100 nm, respectively (Toussaint et al., 2019), have gained a lot of attention. Almost invisible to the eye, they have been found in sediments (Van Cauwenberghe et al., 2015), in aquatic systems (Wagner et al., 2014), in air (Gasperi et al., 2018) and even in remote regions (Allen et al., 2019). Due to their small sizes, such particles can be easily ingested or absorbed by nearby organisms. Numerous studies have already found microplastics in marine life forms (Carpenter et al., 1972; Jambeck et al., 2015; Schmidt et al., 2018; Windsor et al., 2019; Wright et al., 2013) and, only recently, they have even been found in human stool (Schwabl et al., 2019) and human placenta (Ragusa et al., 2021). This is particularly concerning since microplastics can act as carriers for persistent organic pollutants (Frias et al., 2010; Rios et al., 2007; Rochman et al., 2013; Teuten et al., 2007) or heavy metals (Chen et al., 2020b) that can have detrimental effects on multiple members in the affected food web. Although long-term health effects of microplastics on humans must be studied further (Hwang et al., 2020; Smith et al., 2018), other studies have already shown that micro- and nanoplastics can affect the plant growth by either changing the soil properties (de Souza Machado et al., 2019) or through interaction with the plant's roots (Sun et al., 2020).

To address the abundance of microplastics in the environment, a complete understanding of their life cycle and their presence in different natural habitats is required. Two techniques can help shedding light onto this problem: One that determines the particle's composition, such as its base material and the presence of additional chemical agents and one that is fast and mobile so it can be used for in-situ measurements. For microplastics research, a considerable number of environmental studies use Raman spectroscopy and Fourier-transform infrared (FTIR) spectroscopy (Bellasi et al., 2020; Käppler et al., 2016; Minor et al., 2020; Primpke et al., 2017). However, both techniques come to limitations and analytical challenges when exploring real environmental samples. Raman spectroscopy, on the one hand, requires extensive data processing (Ghosal et al., 2018) and sample pre-treatment (Bläsing and Amelung, 2018) due to the fluorescent light from contaminations and color additives (Araujo et al., 2018). Additionally, it is time-consuming, since multiple scans per sample are required and the integration time per scan is of the order of seconds (Lenz et al., 2015). FTIR, on the other hand, can be used without any pre-treatment of the samples (Cincinelli et al., 2021). However, this technique is limited to dry samples with sizes above 10 μm for Midwavelength Infrared-FTIR (Primpke et al., 2017) and is limited to transparent or white samples for Near Infrared-FTIR. The limitations of both techniques make it clear that additional spectroscopic techniques are required to cover the large diversity of microplastics in the environment. Recent studies, for example, used time-integrated (Ornik et al., 2020) and time-resolved photoluminescence

* Corresponding author.
E-mail address: Caroline.sommer@physik.uni-marburg.de (C. Sommer).

https://doi.org/10.1016/j.marpolbul.2021.112789
Received 20 April 2021; Received in revised form 22 July 2021; Accepted 25 July 2021
Available online 4 August 2021

spectroscopy (Gies et al., 2020) as non-destructive methods to distinguish between plastic and non-plastic materials.

The present study proposes Laser Induced Breakdown Spectroscopy (LIBS) as an analytical tool for microplastics and introduces it as a fast and potentially mobile technique for in-situ measurements that additionally delivers promising results for the determination of the polymer type and additives. Already an established tool in areas such as forensics (Dockery and Goode, 2003), waste management (Costa et al., 2017a; Gondal and Siddiqui, 2007; Siddiqui et al., 2008), food analysis (Agrawal et al., 2011), underwater sample analysis (Guo et al., 2017) and even space exploration (De Giacomo et al., 2007), the technique extracts information about the sample's chemical composition and the molecular structure. This is done by creating a plasma on the sample's surface using laser ablation. After the plasma cools down, element-specific radiation is emitted and detected by a spectrometer. LIBS comes with multiple advantages: It requires no sample preparation, which is advantageous for in-situ studies; it can analyze samples regardless of their physical state; it is not sensitive to the sample's surface morphology; and it can effortlessly detect surface contaminants.

Despite the several advantages that come with LIBS, its potential for microplastic studies remains mostly unexplored. Only recently, Chen et al. used LIBS to study the composition of single non-plastic microparticles (Chen et al., 2020a) and to determine the concentration of heavy metals in microplastics from river samples (Chen et al., 2020b). However, its suitability for microplastic identification has not been reported yet. The present study, therefore, aims to close this gap by showing and scrutinizing, for the first time, LIBS' capability of analyzing and classifying microplastic particles. This paper is structured in three parts. At first, the capability of LIBS to distinguish between plastics and natural materials is shown by analyzing the spectra of well-defined reference macroplastics, also referred to as bulk references, as well as natural materials. In a consecutive step, a second reference set of microplastic particles as well as natural microparticles collected from a riverine environment, whose classification was given by a FTIR analysis, was measured by LIBS. Last, by comparing both sets, the influence of contamination and oxidation on LIBS' capability for identification and classification of microplastics is discussed. While both affect the signal quality compared to the macroplastic samples, LIBS is still able to distinguish natural materials from microplastics and promises a reasonable estimate of the polymer base type. In order to enable comparability with other spectroscopic techniques in future works, a standard evaluation method for data analysis in microplastic studies is used. However, it should be emphasized that the focus of the work is the principal detectability of microplastic under a developed concept with LIBS.

2. Materials and methods

2.1. Samples

The set of well-defined reference spectra included measurements of plastics and non-plastic materials. All measurements for plastics, referred to as reference plastics, were conducted on either white or transparent solid rectangular plates (provided by Vitasheet Group) with dimensions of approximately $3.5 \times 3.5 \times 0.5$ cm^3. Here, seven types of plastics were included: polyethene terephthalate (PET), polycarbonate (PC), polystyrene (PS), polyamide 6 (PA6), polyethene (PE), polypropylene (PP), and polyvinyl chloride (PVC). These base types accounted for an estimated 5.624 Mt. out of 8.288 Mt. of global plastic loss per year to the environment (Ryberg et al., 2018). Hereby, PP and PP fibers make up for 1.837 Mt., PE for 1.659 Mt., PET and PET fibers for 0.873 Mt., PA and PA fibers for 0.712 Mt., PS for 0.296 Mt., PVC for 0.234 Mt. and PC for 0.013 Mt. The rest is accounted for other polymer types from which elastomers used in tyres take the biggest share.

The reference plastics can be divided into two groups, namely aromatic plastics (for PET, PC, PS) and aliphatic plastics (for PA6, PE, PP, PVC). The difference between both groups is the presence of delocalized C—C bonds (Grégoire et al., 2011). The set of spectra for non-plastic materials, referred to as natural materials, consisted of 14 samples. Five of them were collected from the marine environment: common cuttlefish bone *(Sepia officinalis)*, coralline red algae *(Lithophyllum racemus)*, sea urchin skeleton *(Echinocardium cordatum)*, sea snail shell *(Neverita josephina)*, and seagrass leaf *(Posidonia oceanica)*. In order to obtain a larger diversity of natural materials, commercial fine-grained (0.06 - 0.2 mm) sand (Erdenwerk Gregor Ziegler GmbH, 55% $CaCO_3$, 42% $MgCO_3$, <2% SiO_2), maple wood *(Acer platanoides)*, maple bark, maple leaf, maple fruit, unknown type of wood, dandelion (*Taraxacum officinale)*, moss *(Hylocomium splendens)*, and cellulose were also added to the sample set. Neither the plastic samples nor the natural materials were subject to any kind of pretreatment, including surface smoothing and cleaning.

To test the suitability of LIBS for environmental studies, a set of microparticles were extracted from sediment samples collected from the Lahn river (Marburg, Germany). Sediments were separated from the samples by density separation with the MPSS (MicroPlastic Sediment Separator; Hydro-Bios Apparatebau GmbH), which operated for 15 h with a saturated sodium chloride solution. Since this solution is commonly used for density separation (45.6%) (Cutroneo et al., 2021), the study focuses on the plastic types that can be extracted with NaCl, namely PE, PP, PS, PA, and PC (Thomas et al., 2020). Note that PVC and PET are unlikely to extract since they are denser than the solution density (1.18- 1.19 g/ml) unless weathering effects reduce their density (Browne et al., 2011). This resulted in a set of microparticles with a minimum size of 500 μm which were subsequently examined under a stereomicroscope to collect potential plastic and non-plastic particles that were obvious to the eye. That way, a set of 45 plastic and non-plastic microparticles was collected. To separate the organic material from the microplastics Fenton's reagent was used. In Fig. 1a a selection of microparticles is presented. Fig. 1b and c show microscope images of a microplastic (PE) particle and a non-plastic microparticle, respectively.

2.2. LIBS instrument details

For this study, a LIBS system has been designed. An illustration of the built system can be found in the Supporting Information. The laser pulse was generated with a Q-switched 1064 nm Nd:YAG laser (Quantel, Brilliant b model) with a repetition rate of 10 Hz. The pulse was frequency-doubled to 532 nm delivering a maximum energy of 200 mJ with a pulse width of 4 ns. To adjust the pulse energy, an attenuator is placed in the optical pathway. A biconvex lens with a focal length of 6 cm was used to focus the laser pulse onto the sample vertically. This arrangement created a 30 μm diameter spot on the surface and an estimated power density of 7.07×10^{11} W/cm^2. For this study, the pulse energy for reference plastics, natural materials and microparticles were adjusted to 6.44 mJ. For the plastic type identification, the reference plastics were also measured with a pulse energy of 20 mJ. This was done in order to obtain the best possible reference spectra. The plots can be found in the Supporting Information.

Additionally, a notch filter (Kaiser Optics, HSPF-532.0-1.0) was placed in front of the spectrometer to block the incident laser pulse. The spectrum was recorded with a spectrometer (Newport corporation, MS257) that has a grating of 300 lines per mm, an entrance slit of 30 μm, and is equipped with a time gated intensified charge-coupled device camera (Andor, iStar DH720-18 U-03).

To investigate the crater from laser ablation and to assure focal plane, a white light source and a camera were used.

2.3. FTIR instrument details and reference library

To validate LIBS' classification of the microparticles, they have been measured with a commercially available FTIR system (Bruker, Tensor 37). The IR spectra were recorded in Attenuated Total Reflection (ATR)

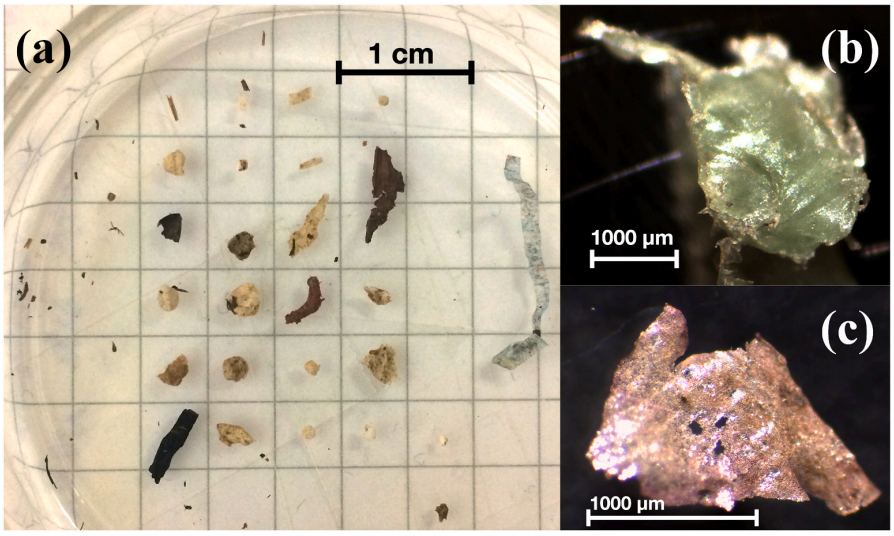

Fig. 1. Set of microplastic extracted from sediment samples. **a** shows a picture of different microparticles extracted from the sediment samples of the river Lahn (Marburg, Germany). **b** shows a microscope image of a polyethylene particle. **c** shows a microscope image of a non-plastic particle.

mode with a spectral resolution of 4 cm^{-1} in the range 4000 - 400 cm^{-1}. Following the manufacturer's suggestion, regular measurements of the background were made. Here, the background was measured after every five shots. The data acquisition and evaluation were carried out with the software OPUS 7.0 (Bruker Optics) and the databases BPAD-Bruker Polymer ATR Library, ATR-FTIR LIBRARY KIMW, and BIBL ATR-FTIR-FORENSICS Library and manually verified according to Jung et al. (2018).

All acquired data can be found in the Supporting Information.

2.4. Data acquisition and treatment

All spectra were taken at atmospheric pressure using 200 ns time delay after laser ablation and a 1 µs gate width. These parameters were chosen according to Grégoire et al. who stated that atomic signals have maximum intensities at short delays, whereas molecular bands have maximum intensities at longer delays (Grégoire et al., 2011). Since this study aims to analyze microplastics in real conditions, ambient air was used as a surrounding atmosphere, also to facilitate field applications. Additionally, recent studies come to the conclusion that air is a suitable atmosphere for analytically relevant molecular signals (Chamradová et al., 2021).

The spectral range of interest was from 300 nm to 810 nm. This range was chosen based on the results of previous works (Sattmann et al., 1998; Stefas et al., 2019) and adapted to the LIBS system used in this study. For each sample in the reference set, the spectrum was acquired by taking an average of 10 single shots on different spots on the sample's surface. Before each of these shots, two laser shots were used to get rid of any surface contaminations. For the microparticle samples, only one laser shot at a reduced laser power of 654 µJ was used for surface cleaning and one spectrum was acquired. These changes were necessary to minimize the destruction level of the sample. For all spectra, the flatfield was recorded and the continuum background was subtracted to get rid of any possible error sources. This approach was carried out to acquire reliable reference spectra, to take into consideration any possible inhomogeneity and to assure the reproducibility of the measurement.

For the data analysis, this study aims to distinguish between plastic and non-plastic microparticles. To achieve this, Principal Component Analysis (PCA) was applied, which is an unsupervised learning method commonly used in plastic research (Grégoire et al., 2011; Costa et al., 2017a, 2017b; Stefas et al., 2019). Additionally, this technique is useful to visualize the data and to identify groups and outliers. However, since this study is a proof of concept, the data analysis is not the focus of the work. There is room for improvement which has to be elaborated in future work. Yet, for the first demonstration reported in this paper, PCA proved to be sufficient. For more information on PCA, see Jolliffe (2002).

3. Results and discussion

3.1. Macroplastic identification and classification

Before stepping into the discussion of LIBS' applicability for microplastics, a concept for the detection of plastics has to be developed. For this, well-defined polymer samples were classified first using LIBS. While in general the LIBS spectra of plastic samples can be close to each other as all are based on carbon chains, previous studies have shown that a multivariate analysis or a decision tree based on the emission ratio between relevant chemical elements and molecules can distinguish different polymer types (Grégoire et al., 2011; Kim and Choi, 2019; Vahid Dastjerdi et al., 2018; Sattmann et al., 1998).

For the classification of plastics, a decision tree method has been developed based on an evaluation of the set of bulk reference spectra. It uses the relative emission strength from different elements as well as multivariate analysis similar to previous reports (Grégoire et al., 2011; Kim and Choi, 2019; Vahid Dastjerdi et al., 2018; Sattmann et al., 1998). The initial step classifies the sample as either plastic or a non-plastic material. In the case of the former, the spectrum will be examined to determine if the sample is a candidate for PVC or PET. If both types could be excluded, multivariate analysis will be applied to check if the sample is a candidate for either PA6, PS or PC. Finally, if none of these classifications applied to the sample, Support Vector Machine (SVM) is used to determine if the sample is either PE or PP.

In the following, these individual steps will be demonstrated with the set of reference spectra.

The identification of spectral lines of the measured intensities and all other spectroscopic data were obtained from the NIST atomic spectra database (Kramida et al., 2020).

3.2. Classification of plastics and non-plastics

To identify the characteristic emission lines for the classification between macroplastics and macro non-plastics, the spectra in the reference set were compared with each other. All spectra used for this can be found in the Supporting Information. As an illustration, the spectra of PE and a selection of non-plastics are shown in Fig. 2a. Visually, PE can be distinguished from non-plastics. Important peaks that can be observed in plastics are: Firstly, the atomic and ionic emission lines of its organic constituent elements, i.e. the carbon line (247.8 nm), the hydrogen lines of the Balmer series (486.14 nm and 656.29 nm), the nitrogen line (746.8 nm), and the oxygen line (777.3 nm). Secondly, the spectral lines of the inorganic elements such as the chlorine line (808.6 nm). And thirdly, diatomic molecular band of the combinations, i.e. the C2 swan band (around 470 nm, 512 nm, and 553 nm), the CN violet band (around 360 nm, 388.3 nm, and 422 nm), the CH band (around 431.27 nm, 431.7 nm, and 488.4 nm), the OH band (306.4 nm – 347.2 nm), the CO band (in UV range) and the NO band (in UV and NIR range) (Anzano et al., 2008; Banaee and Tavassoli, 2012; Costa et al., 2017b; Grégoire et al., 2011; Stefas et al., 2019; Vahid Dastjerdi et al., 2018; Wallace, 1962). Note, the carbon line, the CO band and the NO band are not detected in our setup. However, these lines did not play a significant role in the classification of plastics or at least its influence was compensated by other lines visible in the spectrum as will be shown in the course of this study.

Fig. 2a shows representatively that especially the C2 bands were enhanced in plastics compared with other natural organic samples and, as expected from their chemical composition, represent the natural fingerprint of carbon-based polymers. The present CH bands, however, seem to separate organic from inorganic materials as can be concluded from the sand and shell spectra. Both systems are included in further calculations as they contain the signature of the molecule present in the sample.

Additionally, sodium (589.15 nm) and potassium (766.49 nm and 769.89 nm) lines can be observed in plastics even though they do not belong to the base polymer matrix. These arise due to the presence of additives, such as zinc potassium chromate, which is often used in pigments or as corrosion inhibition and sodium bicarbonate, which is used in the process of plastic and polymer manufacturing (Stenmarck et al., 2017).

Finally, the emission line peaks of the molecular C2 (470 nm, 512 nm, and 553 nm), CN band (388.3 nm) and CH band (485.7 nm), as well as atomic H (486.14 nm and 656.29 nm), N (746.8 nm), O (777.3 nm), K (766 nm and 769 nm) and Cl (808.6 nm - not visible in PE) were used for further distinctions. Note, that no margin around the peaks was taken for evaluation but only the peak intensity. The K line was used since it is also very common in plants, minerals, and soil and therefore plays an important role in the separation of plastics and natural materials.

The distinction between plastic and non-plastic was also made with other plastic types. For a more analytic approach, PCA was applied on the set of reference spectra. A scatter plot of the first two principal components for all reference samples is presented in Fig. 2b. Both components explain 60.3% of the variance. Each data point corresponds to the eleven important emission lines mentioned above of a single, non-normalized spectrum from each sample. In the plot, the reference samples are divided into different groups: The five non-plastics from the marine environment are grouped as *Marine Samples* (blue, +); the seven non-plastics from plants are summarized as *Plants* (green,); *sand* (brown, ▸) and *cellulose* (black, **c**) are assigned to individual groups; and all plastics are grouped as *Reference Plastics* (red, ⬢). An evaluation of the data distribution shows that plastics and non-plastics can be clearly separated.

3.3. Plastic type identification

The polymer base type can be identified using a decision tree. For this, the normalized emission line intensities for chlorine and oxygen are presented as box plots in Fig. 3a and b, respectively. Note, that for this analysis the spectra were taken with a pulse energy of 20 mJ and have been normalized to the maximum value to enable a more comparable analysis of the data. The following observations were made: As the polymer types selected for this study in summary made up over 90% of the global primary waste generation in 2015 (Geyer et al., 2017) and among these only PVC contains chlorine in its base polymer, a clear classification based on the chlorine emission line is possible (sensitivity: 98%, specificity: 98% within the used polymer data set for a threshold at 0.026 (cf. Fig. 3a)). Other polymers containing chlorine such as PE-C can be neglected as they are not decisive for the generation of waste and thus

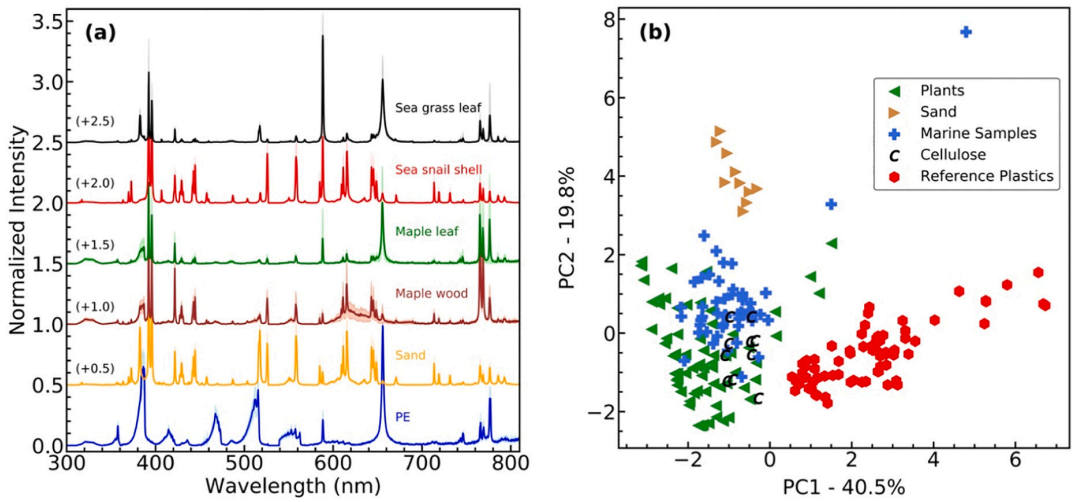

Fig. 2. Comparison between LIBS spectra from reference macroplastic samples and natural materials. **a** shows a comparison of representative LIBS spectra between different natural materials and the reference spectrum of PE. The data clearly illustrates the distinction between plastic and non-plastic macro samples. The spectra are the average over ten shots (average is depicted as line, standard deviation as light background). For better visualization, the spectra are plotted with an offset and normalized to the maximum value of each spectrum. **b** shows a PCA involving more plastic and non-plastic macro reference samples and types. In this figure all data were acquired with a laser power of 6.44 mJ. An even better separation is possible when using 20 mJ (cf. Supporting Information Fig. SI. 4).

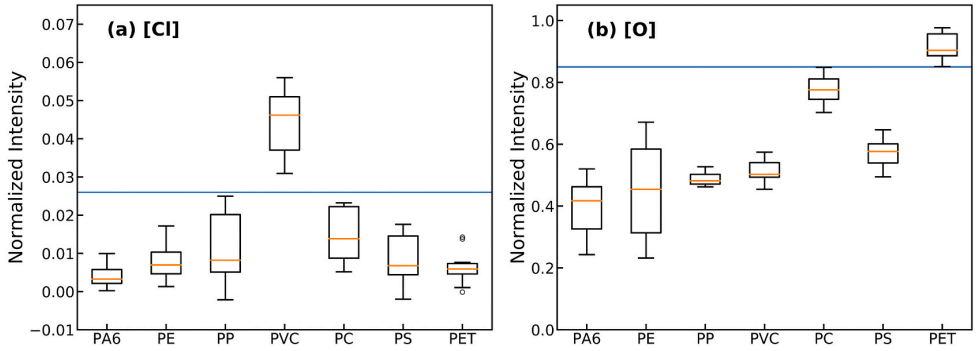

Fig. 3. Comparison of emission lines for different plastic types. **a** shows a box plot of emission line intensity for chlorine as a function of plastic-type. **b** shows a box plot of emission line for oxygen as a function of plastic type. For the plots, each spectrum was normalized by the maximum intensity in their data. The solid line illustrates a threshold to classify a sample candidate as PVC (0.026 in (a)) or as PET (0.85 in (b)).

also not for the generation of (secondary) microplastics. Beyond that, chlorine is also commonly used for flame retardants (Stenmarck et al., 2017) but their expected chlorine concentration is lower, which is why this issue can also be neglected.

Similarly, PET can be identified using the emission line for oxygen (sensitivity: 99%, specificity: 93% within the used polymer data set for a threshold at 0.85 (cf. Fig. 3b)) due to the presence of ester bonds in the molecular structure (Kim and Choi, 2019). Again, this result only applies to the limited dataset used in this study. Polymers containing a lot of oxygen, such as PMMA, could falsely be classified as PET in that way. However, since PMMA accounts only for 0.54% of the entire plastic waste in Germany according to the data by Conversio Market and Strategy GmbH (2018), such possible misclassifications are unlikely.

As a result, both plastic types can be identified by defining a threshold value shown as a solid line in Fig. 3a and b. It should be noted that the results improved for oxygen when calculating the signal-to-noise ratio whereas, due to the clear separation, such a step is redundant for chlorine.

To distinguish between the remaining plastic types, i.e. PE, PP, PA6, PS and PC, PCA was applied on the set of selected emission lines. Like in Fig. 2b, a scatter plot of the first two principal components for the remaining plastic types is presented in Fig. 4a. Here, both principal components capture 59.6% of the explained variance with each data point representing a single, non-normalized spectrum of a sample. In the distribution in Fig. 4a, all data points for PS (orange, ⬟), PC (purple, ●) and PA6 (red, ▼) form separate clusters, whereas those for PE (blue, ▲) and PP (green,) form a single cluster. This shows that aromatic plastic types, i.e. PS and PC, and aliphatic types, i.e. PA6, PE, PP, can be distinguished from each other. The reason for this is the inherent higher emission line intensity for C2 in aromatic samples due to the presence of delocalized C—C bonds in their molecular structure as can be seen in Fig. 4b (Grégoire et al., 2011). Since PA6 can be distinguished from PE and PP, a final step remains to distinguish both plastic types from each other. To achieve this, a SVM model was generated and applied on 10 spectra for PE and 10 spectra for PP. The model was fit on 80% of the dataset, whereas the remaining 20% served as a test dataset to evaluate the model. The linear kernel function was used since the correct classification rate with this model for the test data was 95% ± 9.9% for ten training runs with new randomly generated training-test split per run. The methods were used as implemented in the Python library Scikit-learn (Pedregosa et al., 2011). Any noise in the spectra was negligible compared to the relevant peaks mentioned earlier. However, on closer inspection, it became clear that the reference plastics are not free from additives (cf. shoulder and side peaks in PS (Fig. 4b)). These did not interfere with the classification.

It has to be noted that the base material classification can also be performed using a single step multivariate analysis together with a machine learning approach (Lasheras et al., 2010; Vahid Dastjerdi et al.,

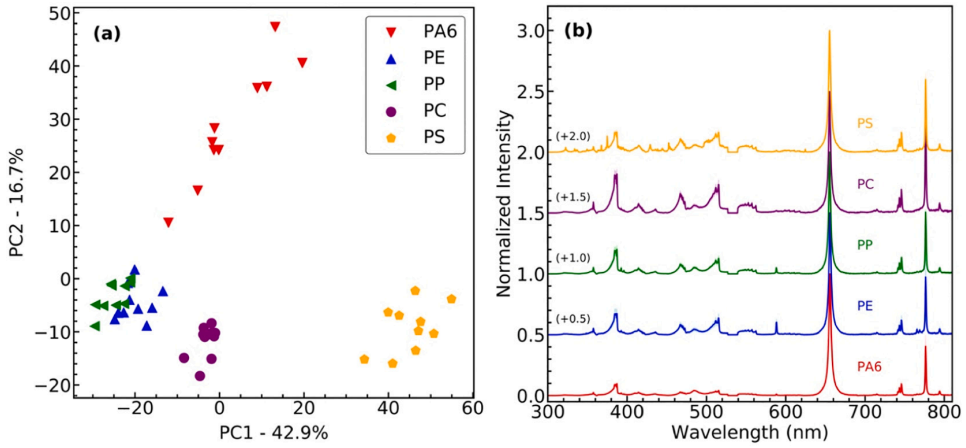

Fig. 4. Plastic type identification for PS, PC, PA6, PE, and PP. **a** shows a PCA with the first two principal components separating the plastic types into four clusters. **b** shows the reference spectra of the microplastic samples measured at 20 mJ. The spectra are the average over ten shots (average is depicted as line, standard deviation as light background). For better visualization, the spectra are plotted with an offset and normalized to the maximum value of each spectrum.

2018). However, the current approach gives more insight into the actual decision criteria. In addition, the goal of this paper is to present a first approach and concept of identifying microplastics using LIBS and not to develop a single step method for the classification of macroplastic samples. The results obtained with this model are also applicable for the data taken at 6.44 mJ. They are qualitatively reproducible and comparable.

3.4. Identification of microplastics and natural microparticles

An examination of the 45 extracted microparticles (MP) with FTIR revealed that 29 of them were plastics (16 PS, ten PE, two PP, and one PA6) and 16 natural materials. The spectrum of two representative microparticles made of PE and their reference spectrum are presented together with a natural material microparticle in Fig. 5. When comparing the spectra of real microplastics with their clean and well-defined reference counterparts, one observes that the particles split into two groups. One subset that closely resembles the spectra of the references (PE-MP 1) and another one that in addition shows various additional spectral features which even overshadow the polymer fingerprint at first sight (PE-MP 2) (cf. Fig. 5). Many of the additional peaks are also visible in the spectrum of the natural material particle (NM-MP) complicating a distinction between microplastic and non-plastic microparticles. The peaks were associated with Ca (393.38 nm, 396.83 nm and 422.69 nm), Fe (358.1 nm, 373.6 nm, 382.1 nm, and 557.8 nm), Ti (429.99 nm, 498.17 nm, 499.10 nm, 499.95 nm, 500.72 nm, and 501.4 nm) and Mn (403.18 nm, 446.04 nm). Part of the contribution of the Fe lines may come from the separation process. However, on a closer look, it stands out that the Swan band system is more enhanced in the plastic samples than in the natural material particle, providing a possible indicator for the presence of plastic. If the eleven important peaks mentioned above are used to distinguish between plastic and non-plastic, many effects of the contamination are eliminated. The particles presented in Fig. 5. are then separable based on their spectral feature given by these eleven peaks.

This observed complexity can be foreseen as biological contamination, interdiffused substances and oxidation/degradation of the polymer matrix can be expected (Brunnbauer et al., 2020). These effects can make a separation between microplastics and natural microparticles more difficult as especially the C2 swan band system decreases over time due to polymer degradation according to Brunnbauer et al. (2020). However, the influence does not seem to have a great negative impact on this study. The present data, which comes from particles that have aged in the Lahn river for an indefinite period of time, is still separable into microplastics and natural material as will be shown in the next paragraph. Brunnbauer et al. (2020) also points out that this decline of signal is a general problem of microplastic identification and is also found in FTIR bands (Brunnbauer et al., 2020). But LIBS has a decisive advantage over FTIR: Due to laser ablation, it can be used for depth profile analysis regardless of the optical properties of the sample's material. A depth profile of the contamination could be established by using low laser energies. The C2 swan bands can then be a possible indicator for the aging or weathering of microplastics. Analyzing these processes can give an insight in the change of the chemical properties of plastics in the environment. Therefore, more methods for microplastic identification and its analysis as well as its impact on the environment need to be established. Beyond that, better data are expected for measurements in deeper layers of the microplastic samples from which the base polymer type can presumably be determined.

In order to quantify the increased complexity and variance of real microplastics, the spectra from various microplastics and microparticles from sediment samples were acquired and a PCA was performed to visualize the data. To ensure that the molecular signal is evaluated for the bands and not the atomic signals of the contamination overlapping with the bands, the broad peaks were cut out of the spectrum with a certain margin (CN: 383 nm – 387 nm, C2($\Delta\nu = +1$): 458 nm – 475 nm, CH: 480 nm – 491 nm, C2($\Delta\nu$=0): 495 nm – 518 nm, C2($\Delta\nu$=-1): 540 nm – 563 nm) and the median of this area together with the emission intensities of N, H_α, H_β, K, O, and Cl were used as input.

Fig. 6 shows the first two principal components capturing 53.4% of the explained variance. The natural microparticles form a cluster which shows little overlap with the set of data points characterizing the microplastic particles. The plastic types PE and PS also seem to divide into different areas, which indicates that the base polymer type could be determined. For PP and PA6, however, no statements can be made since the amount of data points is sparse. Additionally, the PS samples show more contamination than the PE samples resulting in higher K lines. Since PS is often used in form of foam/ styrofoam more contamination

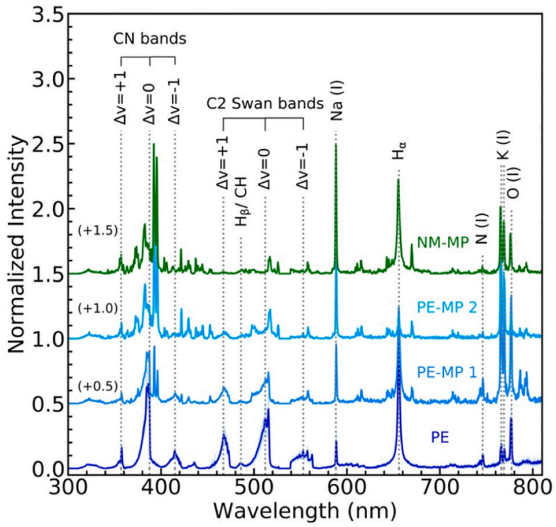

Fig. 5. Comparison of LIBS spectra from microparticles of sediment samples (NM-MP, PE-MP 1 and 2) and bulk reference spectra (PE). The plot shows the significance of the Swan band system for distinguishing NM-MP (natural material) and PE-MPs (polyethylene). For visualization, the spectra are plotted with an offset and normalized to the maximum value.

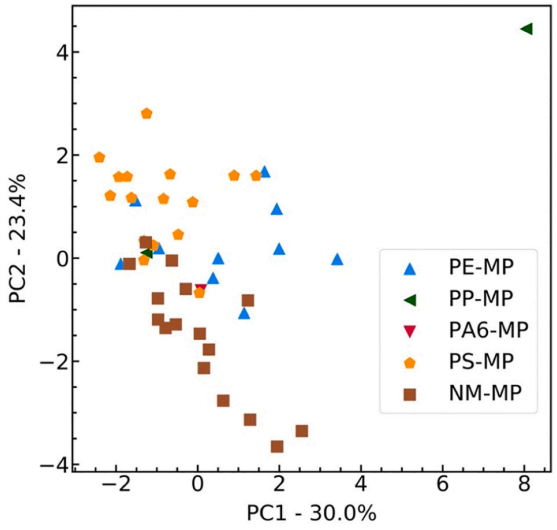

Fig. 6. PCA for microparticle samples. The scatter plot of the first two principal components indicates a separation between plastic type (PE-MP, PP-MP, PA6-MP, and PS-MP) and natural material (NM-MP).

enters the sample compared to solid HDPE pieces. Still a separation from the natural microparticles, which were mainly attributed to wood after a visual verification, is possible. Wood consists largely of cellulose ($C_{12}H_{20}O_{10}$). Its characterization in the PCA is therefore mainly based on the atomic signals of oxygen, hydrogen and carbon (the latter is not measured in our system). The molecular signal of the C2 swan band seem to build little to no clusters for natural microparticles.

In combination with Fig. 5 it becomes clear that a separation between microplastics and natural material can only be based on the C2 swan band system. Since atomic signals originating from contamination on the sample's surface overlap with the molecular bands (cf. Fig. 5), it is recommended to calculate the median of the spectral signal. This way no wrong signal is evaluated as spectral fingerprint of the sample. When working with environmental samples, this is of special importance. Nevertheless, further samples should be examined for an even more robust analysis. For that, it should be noted that some plastic types occur significantly more frequently in the environment than others and not all plastics, such as PVC and PET, could be included due to their high density compared to the NaCl solution. Therefore, the use of NaCl explains the lack of PET or PVC particles and the high frequency of PE and PS in the sample set. Though, once extracted from the sediment with other solutions such as potassium formate (ZZobkov et al., 2020), PVC and PET can be identified by their spectra as shown in Fig. 3.

Finally, it can be said that LIBS seems to be capable of identifying microplastics reliably without any sample preparation with the concept developed in this study. By using cleaning shots to eliminate non-plastic material on the sample's surface, removing most of the spectral data, calculating the median for the molecular signal and finally working only with eleven peaks, most of the effects originating from contaminants and additives were eliminated. The previous results from the PCA support that this approach leads to possible classification of microplastic particles. This concept could be implemented into advanced data processing methods, which, however, is out of the scope of this study.

4. Conclusion and outlook

This work was the first approach on in-situ analysis of microplastics by LIBS. It demonstrated that LIBS can be used to separate plastic from natural materials and identify the base polymer type. We have developed a concept to classify macroplastics commonly found in plastic waste and distinguish them from natural materials. Similar to other studies, this concept was based on a combination of line intensities from different elements and multivariate analysis.

When LIBS is applied to real microplastics, a distinction between natural microparticles and microplastics is possible using the concept developed with macroplastic samples. Here, the C2 swan band system is not only essential for the detection of plastics collected from the environment but also the width of its spectral signal helps to separate plastic from non-plastic material. To take into account the differences of atomic and molecular signals, the median of the spectral range of molecular signals was calculated instead of using the peak intensity. Furthermore, with this concept, PE and PS formed partially distinct clusters. This promises that LIBS is also able to give reasonable estimates for microplastic particles even if the signal is deteriorated by contamination and oxidation of the polymer matrix. Nonetheless, a bigger sample set is needed to confirm and quantify the polymer matrix.

Considering the potential of LIBS for rapid identification (less than one second per scan), its mobile usage, its applicability for depth profile analyzes including studies on toxic pollutants, and the minimal destruction due to a small number of laser shots (up to single-shot LIBS) and a reduced laser power (the ablated amount is in the order of tens to hundreds of nanograms (Gaudiuso et al., 2010)), makes this a strong and promising method for the detection of microplastics, especially for in-situ measurements in field studies. For heterogeneous samples bigger than the laser spot raster scanning systems can be implemented to obtain an accurate composition of the sample. In combination with optical microscopy, one can optimize this method for detecting even smaller particles as demonstrated by Fichet et al. (2006).

CRediT authorship contribution statement

Caroline Sommer: Conceptualization, Methodology, Investigation, Software, Formal analysis, Visualization, Validation, Data curation, Writing – Original Draft, Writing – Review & Editing. **Maximilian Schneider:** Conceptualization, Supervision, Methodology, Writing – Original Draft, Writing – Review & Editing. **Johnny Nguyen:** Conceptualization, Supervision, Software, Writing – Original Draft, Writing – Review & Editing. **Julia Prume:** Resources, Writing – Review & Editing. **Katharina Lautze:** Resources, Writing – Review & Editing. **Martin Koch:** Conceptualization, Project administration, Writing – Review & Editing.

Declaration of competing interest

The authors declare that they have no known competing financial interests or personal relationships that could have appeared to influence the work reported in this paper.

Acknowledgements

We want to thank the Federal Institute for Materials Research and Testing (BAM) and the Vitasheet Group for providing reference samples. We thank Mikko Wilhelm for support and introducing to the laboratory.

Data availability

The data is available at the repository for research data of the Philipps-University Marburg.

Appendix A. Supplementary data

Supplementary data to this article can be found online at https://doi.org/10.1016/j.marpolbul.2021.112789.

References

Agrawal, R., Kumar, R., Rai, S., Pathak, A.K., Rai, A.K., Rai, G.K., 2011. LIBS: a quality control tool for food supplements. Food Biophys. 6, 527–533. https://doi.org/10.1007/s11483-011-9235-y.

Allen, S., Allen, D., Phoenix, V.R., Le Roux, G., Durántez Jiménez, P., Simonneau, A., Binet, S., Galop, D., 2019. Atmospheric transport and deposition of microplastics in a remote mountain catchment. Nat. Geosci. 12, 339–344. https://doi.org/10.1038/s41561-019-0335-5.

Anzano, J., Lasheras, R.-J., Bonilla, B., Casas, J., 2008. Classification of polymers by determining of C1:C2:CN:H:N: O ratios by laser-induced plasma spectroscopy (LIPS). Polym. Test. 27, 705–710. https://doi.org/10.1016/j.polymertesting.2008.05.012.

Araujo, C.F., Nolasco, M.M., Ribeiro, A.M.P., Ribeiro-Claro, P.J.A., 2018. Identification of microplastics using raman spectroscopy: latest developments and future prospects. Water Res. 142, 426–440. https://doi.org/10.1016/j.watres.2018.05.060.

Banaee, M., Tavassoli, S.H., 2012. Discrimination of polymers by laser induced breakdown spectroscopy together with the DFA method. Polym. Test. 31, 759–764. https://doi.org/10.1016/j.polymertesting.2012.04.010.

Bellasi, A., Binda, G., Pozzi, A., Galafassi, S., Volta, P., Bettinetti, R., 2020. Microplastic contamination in freshwater environments: a review, focusing on interactions with sediments and benthic organisms. Environments 7, 30. https://doi.org/10.3390/environments7040030.

Bläsing, M., Amelung, W., 2018. Plastics in soil: analytical methods and possible sources. Sci. Total Environ. 612, 422–435. https://doi.org/10.1016/j.scitotenv.2017.08.086.

Browne, M.A., Crump, P., Niven, S.J., Teuten, E., Tonkin, A., Galloway, T., Thompson, R., 2011. Accumulation of microplastic on shorelines woldwide: sources and sinks. Environmental science & technology. 45 (21), 9175–9179. https://doi.org/10.1021/es201811s.

Brunnbauer, L., Mayr, M., Larisegger, S., Nelhiebel, M., Pagnin, L., Wiesinger, R., Limbeck, A., 2020. Combined LA-ICP-MS/LIBS: powerful analytical tools for the investigation of polymer alteration after treatment under corrosive conditions. Sci. Rep. 10 (1), 1–10. https://doi.org/10.1038/s41598-020-69210-9.

Carpenter, E.J., Anderson, S.J., Harvey, G.R., Miklas, H.P., Peck, B.B., 1972. Polystyrene Spherules in Coastal Waters. Science (80-.). 178, 749–750. doi:10.1126/science.178.4062.749.

Chamradová, I., Pořízka, P., Kaiser, J., 2021. Laser-induced breakdown spectroscopy analysis of polymers in three different atmospheres. Polym. Test. 96, 107079 https://doi.org/10.1016/j.polymertesting.2021.107079.
Chen, D., Huang, Z., Wang, T., Ma, Y., Zhang, Y., Wang, G., Zhang, P., 2020a. Highthroughput analysis of single particles by micro laser induced breakdown spectroscopy. Anal. Chim. Acta 1095, 14–19. https://doi.org/10.1016/j.aca.2019.10.018.
Chen, D., Wang, T., Ma, Y., Wang, G., Kong, Q., Zhang, P., Li, R., 2020b. Rapid characterization of heavy metals in single microplastics by laser induced breakdown spectroscopy. Sci. Total Environ. 743, 140850 https://doi.org/10.1016/j.scitotenv.2020.140850.
Cincinelli, A., Scopetani, C., Chelazzi, D., Martellini, T., Pogojeva, M., Slobodnik, J., 2021. Microplastics in the Black Sea sediments. Sci. Total Environ. 760, 143898 https://doi.org/10.1016/j.scitotenv.2020.143898.
Conversio Market & Strategy GmbH, 2018. Stoffstrombild kunststoffe in deutschland 2017. Retrieved from. https://www.conversio-gmbh.com/res/Summary_Material_Flow_Analysis_Plastics_Germany_2017_EN.pdf.
Costa, V.C., Aquino, F.W.B., Paranhos, C.M., Pereira-Filho, E.R., 2017a. Identification and classification of polymer e-waste using laser-induced breakdown spectroscopy (LIBS) and chemometric tools. Polym. Test. 59, 390–395. https://doi.org/10.1016/j.polymertesting.2017.02.017.
Costa, V.C., Aquino, F.W.B., Paranhos, C.M., Pereira-Filho, E.R., 2017b. Use of laser-induced breakdown spectroscopy for the determination of polycarbonate (PC) and acrylonitrilebutadiene-styrene (ABS) concentrations in PC/ABS plastics from e-waste. Waste Manag. 70, 212–221. https://doi.org/10.1016/j.wasman.2017.09.027.
Cutroneo, L., Reboa, A., Geneselli, I., Capello, M., 2021. Considerations on salts used for density separation in the extraction of microplastics from sediments. Mar. Pollut. Bull. 166, 112216 https://doi.org/10.1016/j.marpolbul.2021.112216.
De Giacomo, A., Dell'Aglio, M., De Pascale, O., Longo, S., Capitelli, M., 2007. Laser induced breakdown spectroscopy on meteorites. Spectrochim. Acta Part B At. Spectrosc. 62, 1606–1611. https://doi.org/10.1016/j.sab.2007.10.004.
de Souza Machado, A.A., Lau, C.W., Kloas, W., Bergmann, J., Bachelier, J.B., Faltin, E., Becker, R., Görlich, A.S., Rillig, M.C., 2019. Microplastics can change soil properties and affect plant performance. Environ. Sci. Technol. 53, 6044–6052. https://doi.org/10.1021/acs.est.9b01339.
Dockery, C.R., Goode, S.R., 2003. Laser-induced breakdown spectroscopy for the detection of gunshot residues on the hands of a shooter. Appl. Opt. 42, 6153. https://doi.org/10.1364/AO.42.006153.
Fichet, P., Lacour, J. L., Menut, D., Mauchien, P., Rivoallan, A., Fabre, C., ... & Boiron, M. C. (2006). Micro LIBS technique. Laser-Induced Breakdown Spectroscopy. Cambridge University Press, Cambridge, 539–555. doi:10.1017/CBO9780511541261.017.
Frias, J.P.G.L., Sobral, P., Ferreira, A.M., 2010. Organic pollutants in microplastics from two beaches of the portuguese coast. Mar. Pollut. Bull. 60, 1988–1992. https://doi.org/10.1016/j.marpolbul.2010.07.030.
Gasperi, J., Wright, S.L., Dris, R., Collard, F., Mandin, C., Guerrouache, M., Langlois, V., Kelly, F.J., Tassin, B., 2018. Microplastics in air: are we breathing it in? Curr. Opin. Environ. Sci. Heal. 1, 1–5. https://doi.org/10.1016/j.coesh.2017.10.002.
Gaudiuso, R., Dell'Aglio, M., Pascale, O. De, Senesi, G.S., Giacomo, A. De, 2010. Laser induced breakdown spectroscopy for elemental analysis in environmental, cultural heritage and space applications: a review of methods and results. Sensors 10, 7434–7468. https://doi.org/10.3390/s100807434.
Geyer, R., Jambeck, J.R., Law, K.L., 2017. Production, use, and fate of all plastics ever made. Sci. Adv. 3 (7), e1700782 https://doi.org/10.1126/sciadv.1700782.
Ghosal, S., Chen, M., Wagner, J., Wang, Z.-M., Wall, S., 2018. Molecular identification of polymers and anthropogenic particles extracted from oceanic water and fish stomach – a raman micro-spectroscopy study. Environ. Pollut. 233, 1113–1124. https://doi.org/10.1016/j.envpol.2017.10.014.
Gies, S., Schömann, E.M., Anna Prume, J., Koch, M., 2020. Exploring the potential of time-resolved photoluminescence spectroscopy for the detection of plastics. Appl. Spectrosc. 74 (9), 1161–1166. https://doi.org/10.1177/0003702820933282.
Gondal, M.A., Siddiqui, M.N., 2007. Identification of different kinds of plastics using laserinduced breakdown spectroscopy for waste management. J. Environ. Sci. Heal. Part A 42, 1989–1997. https://doi.org/10.1080/10934520701628973.
Grégoire, S., Boudinet, M., Pelascini, F., Surma, F., Detalle, V., Holl, Y., 2011. Laser-induced breakdown spectroscopy for polymer identification. Anal. Bioanal. Chem. 400, 3331–3340. https://doi.org/10.1007/s00216-011-4898-2.
Guo, J., Lu, Y., Cheng, K., Song, J., Ye, W., Li, N., Zheng, R., 2017. Development of a compact underwater laser-induced breakdown spectroscopy (LIBS) system and preliminary results in sea trials. Appl. Opt. 56, 8196. https://doi.org/10.1364/AO.56.008196.
Hwang, J., Choi, D., Han, S., Jung, S.Y., Choi, J., Hong, J., 2020. Potential toxicity of polystyrene microplastic particles. Sci. Rep. 10, 7391. https://doi.org/10.1038/s41598-020-64464-9.
Jambeck, J.R., Geyer, R., Wilcox, C., Siegler, T.R., Perryman, M., Andrady, A., Narayan, R., Law, K.L., 2015. Plastic waste inputs from land into the ocean. Science 347 (6223), 768–771. https://doi.org/10.1126/science.1260352.
Jolliffe, I., 2002. Principal Component Analysis. Springer Verlag, New York.
Jung, M.R., Horgen, F.D., Orski, S.V., Rodriguez, V., Beers, K.L., Balazs, G.H., Lynch, J. M., 2018. Validation of ATR FT-IR to identify polymers of plastic marine debris, including those ingested by marine organisms. Mar. Pollut. Bull. 127, 704–716. https://doi.org/10.1016/j.marpolbul.2017.12.061.
Käppler, A., Fischer, D., Oberbeckmann, S., Schernewski, G., Labrenz, M., Eichhorn, K.-J., Voit, B., 2016. Analysis of environmental microplastics by vibrational microspectroscopy: FTIR, raman or both? Anal. Bioanal. Chem. 408, 8377–8391. https://doi.org/10.1007/s00216-016-9956-3.
Kim, E., Choi, W.Z., 2019. Real-time identification of plastics by types using laser-induced breakdown spectroscopy. J. Mater. Cycles Waste Manag. 21, 176–180. https://doi.org/10.1007/s10163-018-0780-z.
Kramida, A., Ralchenko, Y., Reader, J., Team, N.A, 2020. NIST atomic spectra database (version 5.8).
Lasheras, R.J., Bello-Gálvez, C., Anzano, J., 2010. Identification of polymers by libs using methods of correlation and normalized coordinates. Polym. Test. 29 (8), 1057–1064. https://doi.org/10.1016/j.polymertesting.2010.07.011.
Lenz, R., Enders, K., Stedmon, C.A., Mackenzie, D.M.A., Nielsen, T.G., 2015. A critical assessment of visual identification of marine microplastic using raman spectroscopy for analysis improvement. Mar. Pollut. Bull. 100, 82–91. https://doi.org/10.1016/j.marpolbul.2015.09.026.
Minor, E.C., Lin, R., Burrows, A., Cooney, E.M., Grosshuesch, S., Lafrancois, B., 2020. An analysis of microlitter and microplastics from Lake Superior beach sand and surfacewater. Sci. Total Environ. 744, 140824 https://doi.org/10.1016/j.scitotenv.2020.140824.
Ornik, J., Sommer, S., Gies, S., Weber, M., Lott, C., Balzer, J.C., Koch, M., 2020. Could photoluminescence spectroscopy be an alternative technique for the detection of microplastics? First experiments using a 405 nm laser for excitation. Appl. Phys. B Lasers Opt. 126, 15. https://doi.org/10.1007/s00340-019-7360-3.
Pedregosa, F., Varoquaux, G., Gramfort, A., Michel, V., Thirion, B., Grisel, O., Blondel, M., Prettenhofer, P., Weiss, R., Dubourg, V., Vanderplas, J., Passos, A., Cournapeau, D., Brucher, M., Perrot, M., Duchesnay, É., 2011. Scikit-learn: machine learning in python. J. Mach. Learn. Res. 12, 2825–2830.
Primpke, S., Lorenz, C., Rascher-Friesenhausen, R., Gerdts, G., 2017. An automated approach for microplastics analysis using focal plane array (FPA) FTIR microscopy and image analysis. Anal. Methods 9, 1499–1511. https://doi.org/10.1039/C6AY02476A.
Ragusa, Antonio, et al. 2021 "Plasticenta: First evidence of microplastics in human placenta." Environment International 146: 106274. doi:10.1016/j.envint.2020.106274.
Rios, L.M., Moore, C., Jones, P.R., 2007. Persistent organic pollutants carried by synthetic polymers in the ocean environment. Mar. Pollut. Bull. 54, 1230–1237. https://doi.org/10.1016/j.marpolbul.2007.03.022.
Rochman, C.M., Hoh, E., Hentschel, B.T., Kaye, S., 2013. Long-term field measurement of sorption of organic contaminants to five types of plastic pellets: implications for plastic marine debris. Environ. Sci. Technol. 130109073312009 https://doi.org/10.1021/es303700s.
Ryberg, M.W., Laurent, A., Hauschild, M., 2018. Mapping of global plastics value chain and plastics losses to the environment: with a particular focus on marine environment. http://hdl.handle.net/20.500.11822/26745.
Sattmann, R., Monch, I., Krause, H., Noll, R., Couris, S., Hatziapostolou, A., Miguel, R., 1998. Laser-induced breakdown spectroscopy for polymer identification. Appl. Spectrosc. 52 (3), 456–461.
Schmidt, C., Krauth, T., Wagner, S., 2018. Correction to export of plastic debris by Rivers into the sea. Environ. Sci. Technol. 52, 927. https://doi.org/10.1021/acs.est.7b06377.
Schwabl, P., Köppel, S., Königshofer, P., Bucsics, T., Trauner, M., Reiberger, T., Liebmann, B., 2019. Detection of various microplastics in human stool. Ann. Intern. Med. 171, 453. https://doi.org/10.7326/M19-0618.
Siddiqui, M.N., Gondal, M.A., Redhwi, H.H., 2008. Identification of different type of polymers in plastics waste. J. Environ. Sci. Heal. Part A 43, 1303–1310. https://doi.org/10.1080/10934520802177946.
Smith, M., Love, D.C., Rochman, C.M., Neff, R.A., 2018. Microplastics in seafood and the implications for human health. Curr. Environ. Heal. Reports 5, 375–386. https://doi.org/10.1007/s40572-018-0206-z.
Stefas, D., Gyftokostas, N., Bellou, E., Couris, S., 2019. Laser-induced breakdown spectroscopy assisted by machine learning for plastics/polymers identification. Atoms 7, 79. doi:10.3390/atoms7030079.
Stenmarck, Å., Belleza, E.L., Fråne, A., Busch, N., 2017. Hazardous substances in plastics: –ways to increase recycling. Nordic Council of Ministers. https://doi.org/10.6027/TN2017-505.
Sun, X.-D., Yuan, X.-Z., Jia, Y., Feng, L.-J., Zhu, F.-P., Dong, S.-S., Liu, J., Kong, X., Tian, H., Duan, J.-L., Ding, Z., Wang, S.-G., Xing, B., 2020. Differentially charged nanoplastics demonstrate distinct accumulation in Arabidopsis thaliana. Nat. Nanotechnol. 15, 755–760. https://doi.org/10.1038/s41565-020-0707-4.
Teuten, E.L., Rowland, S.J., Galloway, T.S., Thompson, R.C., 2007. Potential for plastics to transport hydrophobic contaminants. Environ. Sci. Technol. 41, 7759–7764. https://doi.org/10.1021/es071737s.
Thomas, D., Schütze, B., Heinze, W.M., Steinmetz, Z., 2020. Sample preparation techniques for the analysis of microplastics in soil—a review. Sustainability. 12 (21), 9074. https://doi.org/10.3390/su12219074.
Toussaint, B., Raffael, B., Angers-Loustau, A., Gilliland, D., Kestens, V., Petrillo, M., RioEchevarria, I.M., Van den Eede, G., 2019. Review of micro- and nanoplastic contamination in the food chain. Food Addit. Contam. Part A 36, 639–673. https://doi.org/10.1080/19440049.2019.1583381.
Vahid Dastjerdi, M., Mousavi, S.J., Soltanolkotabi, M., Nezarati Zadeh, A., 2018. Identification and sorting of PVC polymer in recycling process by laser-induced breakdown spectroscopy (LIBS) combined with support vector machine (SVM) model. Iran. J. Sci. Technol. Trans. A Sci. 42, 959–965. doi:10.1007/s40995-016-0084-x.
Van Cauwenberghe, L., Devriese, L., Galgani, F., Robbens, J., Janssen, C.R., 2015. Microplastics in sediments: A review of techniques, occurrence and effects. Mar. Environ. Res. 111, 5–17. doi:10.1016/j.marenvres.2015.06.007.
Wagner, M., Scherer, C., Alvarez-Muñoz, D., Brennholt, N., Bourrain, X., Buchinger, S., Fries, E., Grosbois, C., Klasmeier, J., Marti, T., Rodriguez-Mozaz, S., Urbatzka, R.,

Vethaak, A.D., Winther-Nielsen, M., Reifferscheid, G., 2014. Microplastics in freshwater ecosystems: what we know and what we need to know. Environ. Sci. Eur. 26, 12. https://doi.org/10.1186/s12302-014-0012-7.

Wallace, L., 1962. Band-head wavelengths of C2, ch, cn, co, nh, no, 02, oh, and their ions. Astrophys. J. Suppl. Ser. 7, 165. http://adsabs.harvard.edu/pdf/1962ApJS....7.165W.

Windsor, F.M., Tilley, R.M., Tyler, C.R., Ormerod, S.J., 2019. Microplastic ingestion by riverine macroinvertebrates. Sci. Total Environ. 646, 68–74. https://doi.org/10.1016/j.scitotenv.2018.07.271.

Wright, S.L., Thompson, R.C., Galloway, T.S., 2013. The physical impacts of microplastics on marine organisms: a review. Environ. Pollut. 178, 483–492. https://doi.org/10.1016/j.envpol.2013.02.031.

Zobkov, M, Zobkova, M, Galakhina, N, Efremova, T, 2020. Method for microplastics extraction from Lake sediments. MethodsX 7 (101140). https://doi.org/10.1016/j.mex.2020.101140. In this issue.

Supporting Information

S1 Experimental Setup

Fig. SI.1 shows an illustration of the built LIBS system. The optical pathway to generate the plasma on the sample's surface is highlighted in green. After the attenuator, a prism is used to secure that the 532 nm second harmonic beam is well separated from the 1064 nm fundamental mode. For the present work, the laser pulse was focused on the sample vertically. To achieve this, mirrors M2, M3, M4 and the beamsplitter BS2 are mounted on a breadboard guiding the laser beam accordingly. The optical path to acquire the sample's spectrum is highlighted in pink.

To investigate the crater and to assure focal plane, a white light source and a camera are also coupled into the setup. To achieve this, a beamsplitter BS1 and mirror M5 are inserted into the pathway, mounted on a flipped mount to remove them easily for measurements. The optical path is shown in dashed lines.

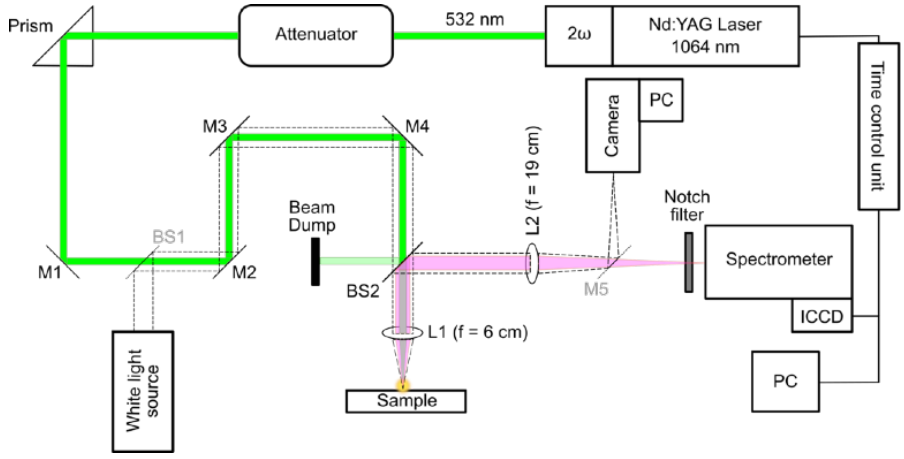

***Fig. SI.1* | Illustration of built LIBS system used for sample identification.**

S2 Data Acquisition and Corrections

The raw data has been corrected for the continuum background and the flatfield of the ICCD in a first step. Afterwards, the spectral intensities were corrected for the spectral response function of the lenses, the notch filter, the grating as well as the camera sensitivity.

Due to the width of the grating, the range of the spectrometer per acquisition was limited. To cover the range from 300 nm to 810 nm, the spectral ranges from 300 nm to 532 nm, 532 nm

to 700 nm, and 700 nm to 810 nm had to be taken and matched together. Therefore, three shots were needed to acquire the complete spectrum of a sample. This procedure was repeated 10 times per sample on different spots on the sample's surface and ultimately averaged. The corrected data was then normalized to the global maximum of the three ranges before averaging. Since the H_α-line is mostly the line with the highest intensity for the reference samples, this results in a standard deviation of zero for this peak. The normalized data were used for visualization reasons and comparing ratios. However, PCA and SVM were performed on automatically scaled non-normalized data (scaled data has zero mean and unit variance) in order to retrieve all information in the data set.

S3 LIBS - Reference Spectra

The LIBS spectra for the plastic reference samples from Vitasheet, which have been used to classify different polymer types are shown in Fig. SI. 2a. As expected by their chemical similarities, the spectra have a quite common shape, but as proven in the manuscript reasonable differences which make them distinguishable.

In order to check reliability and reproducibility of the approach, a second reference sample set provided by the German Federal Institute for Material Research and Testing (BAM) has been analyzed. As these samples are in the form of pellets with a rough surface, generally a bigger experimental variance is expected as can be seen in Fig. SI. 2b.

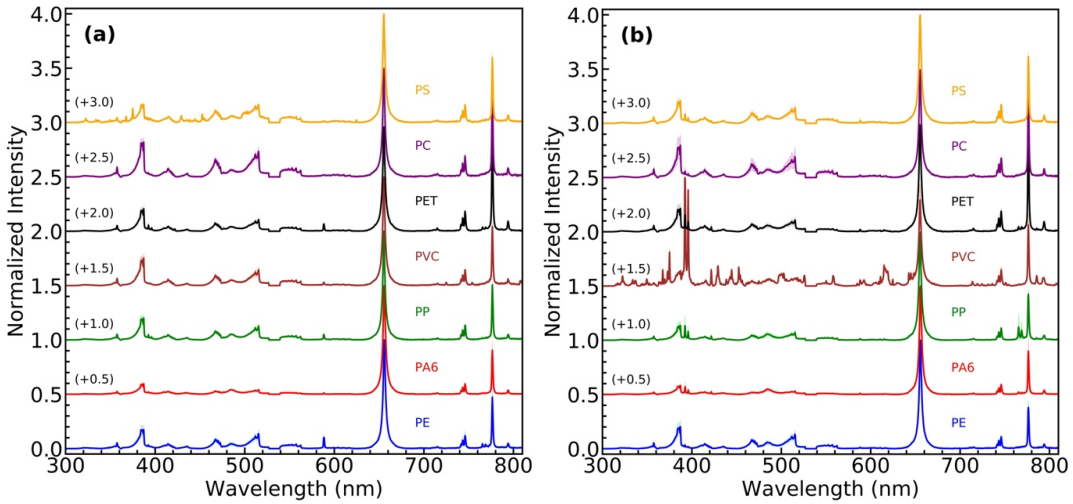

***Fig. SI.2* | LIBS spectra for the plastic reference. a** shows samples from Vitasheet. **b** shows samples from BAM. Both sets were measured with a pulse energy of 20 mJ. The spectra are the average over ten shots

(average is depicted as line, standard deviation as light background). For better visualization, the spectra are plotted with an offset and normalized to the maximum value of each spectrum.

Except for PVC and PS, the spectra are comparable to the Vitasheet results. Both samples show a clear influence of additives by the emergence of shoulders and additional side peaks. But since only the eleven important emission lines were used for the classification, additional peaks in the spectrum can be set aside. It is also noticeable that the BAM samples show more Ca-lines (393.41 nm and 396.87 nm) which should not be so strongly present in the spectra due to the two cleaning shots before measurement. This concludes that the BAM samples contain a higher concentration of additives like calcium carbonate ($CaCO_3$).

The spectra were analyzed similar to Fig. 3 and Fig. 4a of the main manuscript. Besides the bigger errorbars due to the minor changes in focus at the pellets, the results are qualitatively reproducible and comparable to the Vitasheet set.

The LIBS spectra for the natural materials are presented in Fig. SI. 3a. They were measured with a laser power of 6.44 mJ and compared with the reference plastics measured at the same power. The spectra of the latter are presented in Fig. SI. 3b. As discussed in the main manuscript the significantly higher C2 swan bands (around 470 nm, 513 nm, and 553 nm) of the plastic samples provides a good distinction between plastic and non-plastic materials.

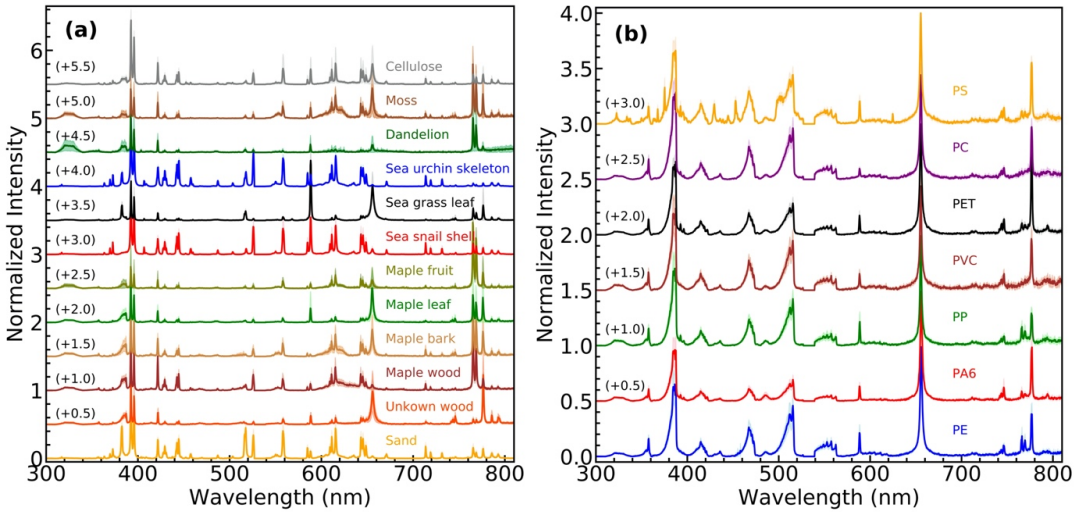

***Fig. SI.3* | LIBS spectra for the natural material and plastic references. a** shows natural material samples from the marine environment and flora as well as sand and cellulose. **b** shows samples from Vitasheet. Both sets were measured with a pulse energy of 6.44 mJ. For better visualization, the spectra are plotted with an offset and normalized to the maximum value.

For a more analytic approach to classifying plastics and non-plastics, PCA can be applied on the set of natural materials and the reference spectra measured at 20mJ. The natural materials could not be measured with this laser power since the detector would have been overloaded. All data shows the highest intensity measured in their respective energy (6.44 mJ for natural material, 20mJ for plastic samples). A scatter plot of the first two principal components for all reference samples is presented in Fig. SI. 4. Both components explain 69 % of the variance. Each data point corresponds to a single, non-normalized spectrum of a sample. As in the main manuscript, the reference samples are divided into different groups: the five non-plastics from the marine environment are grouped as *Marine Samples* (blue, ✚); the seven non-plastics from plants are summarized as *Plants* (green, ◀); sand (brown, ▶) and cellulose (black, **c**) are assigned to individual groups; and all plastics are grouped as *Reference Plastics* (red, ⬢). An evaluation of the data distribution shows that plastics and non-plastics can be clearly separated.

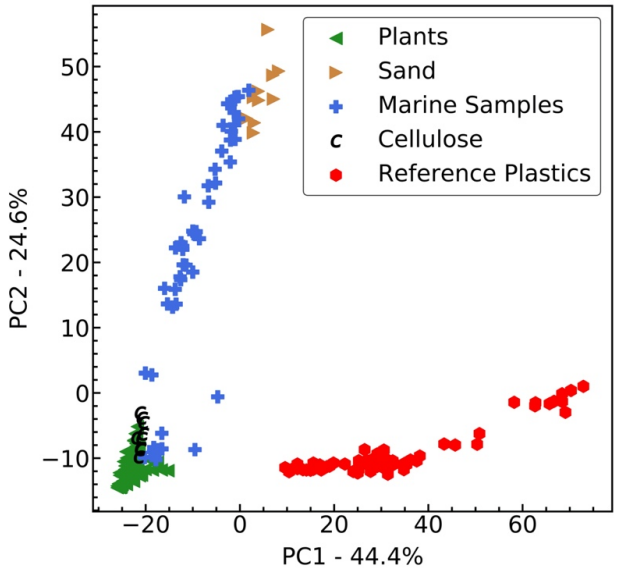

***Fig. SI4* | Comparison between LIBS Spectra from Reference Macroplastic Samples and Natural Materials**. The PCA involves all plastic and non-plastic macro samples mentioned above. The reference plastics were acquired with a laser power of 20 mJ. The natural materials were aquired with a laser power of 6.44 mJ.

S4 LIBS spectra of microparticles

The LIBS spectra of a representative set of the microparticles extracted from the Lahn river are shown in Fig. SI. 5. Some microplastic samples are heavily contaminated but still show

the spectral fingerprint of plastics. The natural microparticles, however, show mostly no C2 swan bands. Microparticle 6 and 8 show slight C2 signals complicating their analysis. Such misclassifications are possible due to the organic components in the natural materials. They also appear in FTIR analyzes as can be observed in Fig. SI. 6b. Microparticle 4 shows slight peaks for PA6 (around 3000 cm^{-1} and 1500 cm^{-1}). However, the particle does not have sufficient peaks for the database to assign a plastic type. In such cases optical verification is helpful as the sample's elasticity and its wear of the edges can provide information about the material.

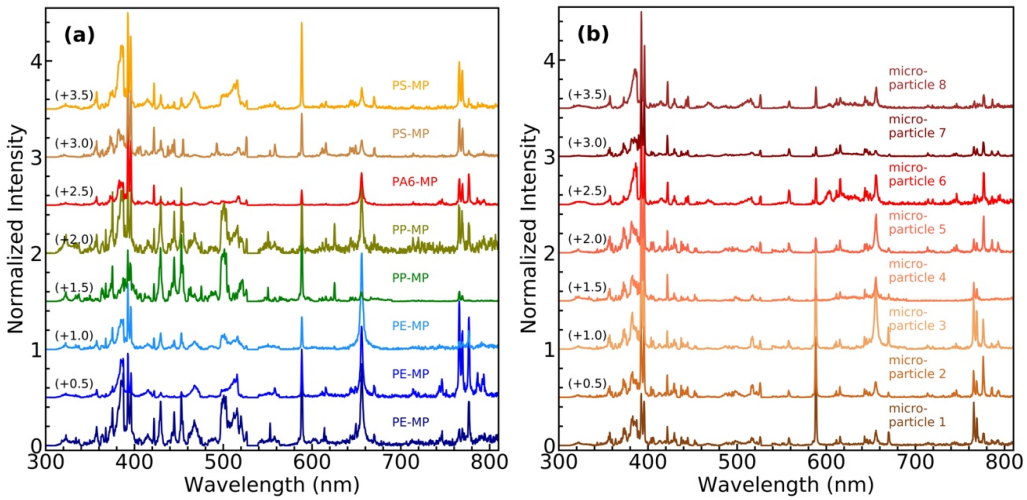

***Fig. SI.5* | LIBS spectra of the microparticles extracted from sediment samples. a** shows spectra of microplastic particles. **b** shows spectra and non-plastic particles. All microparticles were measured with a laser power of 6.44 mJ.

S5 FTIR Spectra of the microparticles

The FTIR spectra which have been used to check and identify the classification of the extracted microparticles are shown in Figure SI.6a (plastics) and Figure SI.6b (non-plastics).

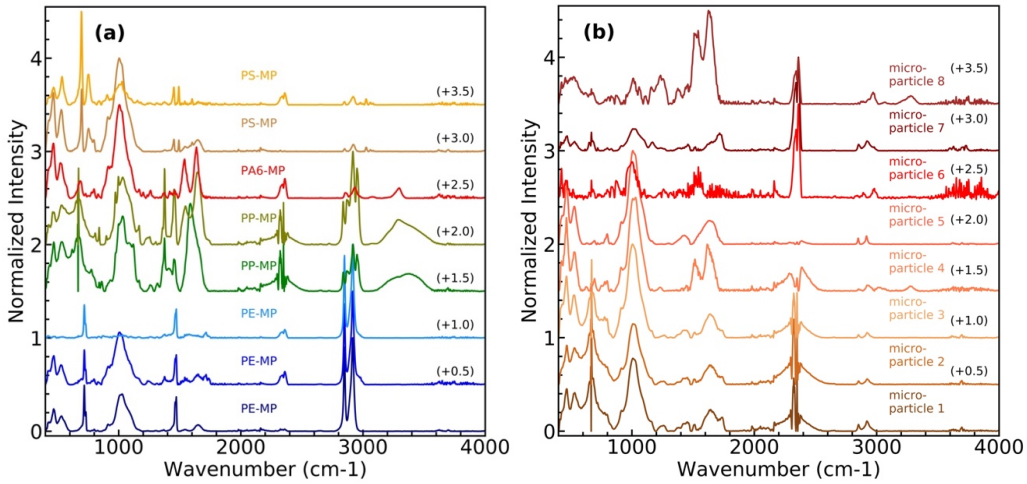

***Fig. SI.6* | FTIR spectra of the microparticles extracted from sediment samples. a** shows spectra of microplastics particles. **b** shows spectra of non-plastic particles.

For the identification of microparticles, the databases BPAD-Bruker Polymer ATR Library, ATR-FTIR LIBRARY KIMW, and BIBL ATR-FTIR-FORENSICS Library were used as well as a manual verification according to Jung et al. (2018) was carried out.

S6 References

Anzano, J., Lasheras, R.-J., Bonilla, B., Casas, J., 2008. Classification of polymers by determining of C1:C2:CN:H:N:O ratios by laser-induced plasma spectroscopy (LIPS). Polym. Test. 27, 705–710. https://doi.org/10.1016/j.polymertesting.2008.05.012.

Costa, V.C., Aquino, F.W.B., Paranhos, C.M., Pereira-Filho, E.R., 2017b. Use of laser-induced breakdown spectroscopy for the determination of polycarbonate (PC) and acrylonitrilebutadiene-styrene (ABS) concentrations in PC/ABS plastics from e-waste. Waste Manag. 70, 212–221. https://doi.org/10.1016/j.wasman.2017.09.027.

Jung, M. R., Horgen, F. D., Orski, S. V., Rodriguez, V., Beers, K. L., Balazs, G. H., ... & Lynch, J. M., 2018. Validation of ATR FT-IR to identify polymers of plastic marine debris, including those ingested by marine organisms. *Marine Pollution Bulletin*, *127*, 704-716.https://doi.org/10.1016/j.marpolbul.2017.12.061.

Kramida, A., Ralchenko, Y., Reader, J., Team, N.A., 2020. NIST Atomic Spectra Database (version 5.8).

Article 2

Sommer, C., Nguyen, J., Menzel, T., Prume, J. A., Ruckdäschel, H., & Koch, M. (2022). Weathering-induced oxidation: An investigation of artificially aged polystyrene samples using Laser-induced Breakdown Spectroscopy. *Polymer Testing*, 112, 107623.

DOI:10.1016/j.polymertesting.2022.107623
URL: https://doi.org/10.1016/j.polymertesting.2022.107623
This article was published in Polymer Testing, Vol. 112, page 107623.

Polymer Testing 112 (2022) 107623

Contents lists available at ScienceDirect

Polymer Testing

journal homepage: www.elsevier.com/locate/polytest

Weathering-induced oxidation: An investigation of artificially aged polystyrene samples using Laser-induced Breakdown Spectroscopy

Caroline Sommer [a,*], Johnny Nguyen [a], Teresa Menzel [b], Julia A. Prume [a,c], Holger Ruckdäschel [b], Martin Koch [a]

[a] Faculty of Physics and Material Sciences Centre, Philipps-University Marburg, 35037 Marburg, Germany
[b] Department Polymer Engineering, University of Bayreuth, 95447 Bayreuth, Germany
[c] Bayreuth Graduate School of Mathematical and Natural Sciences (BayNAT), University of Bayreuth, 95447 Bayreuth, Germany

ARTICLE INFO

Keywords:
Laser-induced Breakdown Spectroscopy
Weathering-induced oxidation
Polystyrene
Plastic degradation
Surface and depth profile analysis

ABSTRACT

This study discusses weathering-induced oxidation of polystyrene with and without different concentrations of the antioxidant Irgafos using Laser-induced Breakdown Spectroscopy (LIBS). By examining the spectral feature of oxidation and due to laser ablation, a systematical analysis of the oxygen content on the sample's surface and its penetration depth could be conducted. The results show that LIBS can be used as a fast technique for the quantification of weathering-induced oxidation.

1. Introduction

Plastic litter is a rapidly emerging health hazard that is in dire need for global action [1–4]. Most prominently, it is associated with waste in our marine environment which accounts for roughly 8 MT of the global plastic litter produced annually [1]. Once released in the open water, they are exposed to harsh conditions, such as sunlight exposure and mechanical stress. Such conditions are in stark contrast to those intended for most consumer plastic products. As a result, their material properties deteriorate with time which promotes fragmentation where a material breaks up into smaller pieces. Particles with sizes less than 5 mm, commonly termed as secondary microplastics [5], are particularly concerning as they have already been detected in multiple types of organisms including the human body [6–10]. This is precisely why we urgently need assessments of the long-term effects of (secondary micro-) plastics on our ecosystem and mitigation schemes to keep their potential detrimental effect to a minimum. Both, however, require a much better understanding of the interaction between plastics and the environment that could ultimately help make plastics more biodegradable and thus contribute to a reduction in plastic litter.

Plastic degradation in our environment is the result of numerous physical, chemical and biological processes that can occur over time scales of months and years [11]. Studying these processes is not straightforward as they can also vary with the chemical composition of the starting material [12]. Studies on degradation usually analyze the influence of the most essential environmental process on a selection of plastic litter types by recreating them in the lab. By adjusting the environmental parameters, the plastic degradation times, which usually take years, can be shortened to a few months [13,14]. This enables us to investigate degradation in a shortened time frame. The results of the discovered degradation processes could be important in the predictions on the long-term fate of plastic litter in the future.

Plastic degradation can be studied by characterizing the morphological or chemical changes induced by the environment. For morphological measurements, tools such as scanning electrode microscopy [15,16], atomic force microscopy [17] and X-ray computed tomography [18] are available. These tools can help us assessing the fragmentation sizes and rates that occur for certain environmental factors. To study molecular changes, non-destructive tools such as spectrophotometry [19], Fourier-transform infrared spectroscopy (FTIR) [20], nuclear magnetic resonance spectroscopy [16,21] and energy-dispersive X-ray spectroscopy [16] have already been employed. Such measurements can relate degradation processes with changes in the molecular structure that promote fragmentation or even the generation of toxic byproducts [12]. Overall, we see that findings on plastic degradation are typically acquired with tools that investigate the sample surface or the entire sample volume. A better understanding of degradation, however, requires a layer-by-layer analysis of the examined sample [22,23]. Such an analysis can be achieved with tools such as X-ray photoelectron spectroscopy, laser-ablation-inductively coupled plasma mass spectrometry (LA-ICP-MS) and mass spectrometry (GD-MS) [22,24]. Yet, these tools require specific sample shapes or long acquisition times or they have

* Corresponding author.
E-mail address: caroline.sommer@physik.uni-marburg.de (C. Sommer).

https://doi.org/10.1016/j.polymertesting.2022.107623
Received 23 February 2022; Received in revised form 6 April 2022; Accepted 2 May 2022
Available online 12 May 2022

poor resolutions [22]. Additionally, studies on degradation of plastic litter samples collected from the environment require an identification of the plastic type as a mandatory step [23]. Amongst those tools just mentioned only a few are used to investigate the plastic type of the sample.

A suitable candidate that can potentially identify the sample material and determine the chemical composition layer-by-layer simultaneously is laser-induced breakdown spectroscopy (LIBS). It is a type of atomic emission spectroscopy that gains information on the sample composition by generating a plasma on its surface. As the plasma decays, element-specific radiation is emitted and detected by a spectrometer. As a result, this technique is sensitive to almost all elements in the periodic table and hence, suitable to detect chemical changes and contamination. LIBS is commonly used for the investigation of metals [22,25–27] but it has already been demonstrated as a tool for depth profile studies [22,24,28]. Its potential for plastic identification has already been demonstrated for pristine plastic samples [29–31] and for microplastics [32]. Only few studies, however, have looked into its potential for plastic sample characterization [29–33]. Here, LIBS proved to be suitable to detect external elements in plastics such as encapsulated heavy metals [34,35] and remnants of corrosive gases [36]. To date, plastic degradation studies that use the layer-by-layer analysis capabilities of LIBS remain scarce. To the best of our knowledge, such studies have only been conducted by Brunnbauer et al. who investigated the degradation of artificially aged paint samples (a mixture of inorganic pigment and an organic polymeric binder) by evaluating the intensity of C2 and O with sample depth in an inert gas [36] and a spatially resolved classification of a multilayer system of 5 different synthetic polymers [37]. In the former, they show that the degradation of the paint samples become less pronounced with increasing sample depth. Although this proves that LIBS can be used to study degradation processes, it remains open if LIBS is sensitive enough to study different degradation stages of plastic litter which comprises of materials such as polystyrene (PS). Such an analysis can give an insight on the minimum time required for an environmental influence to induce chemical products inside the sample that could eventually escape.

Our study aims to close this gap by looking into the oxidation of different PS samples that were weathered with a standardized protocol [38]. PS is particularly interesting as weathering can generate one of the highest number of micro- and nanoparticles [39] which is essential for plastic litter mitigation studies. Additionally, PS is due to its carbon–carbon backbone susceptible to photo-oxidation, which is believed to be the most important abiotic degradation pathway in aerobic outdoor environments [12]. By evaluating the intensity of O with depth for PS at different weathering incubation times, we observe weathering-induced oxidation effects after around 400 h of artificial weathering. Thanks to the capability of LIBS to evaluate the sample composition with depth, we found potential additional insights on weathering-induced oxidation for PS that are not visible with surface detection methods. These results make LIBS stand out as a method that not only can identify plastic but also quantify the chemical composition inside the sample.

2. Materials and methods

2.1. Materials and accelerated weathering

This study used a series of commercially available, amorphous PS samples (INEOS Styrolution Group, Styrolution PS 158N) which contains 0 %, 0.5 % and 1 % concentrations of Irgafos 168, an antioxidant and processing stabilizer based on organophosphite. According to the manufacturer, this grade contained no additional additives besides 600 ppm of zinc stearate. For the accelerated weathering trials, type 1 A tensile bars were produced according to ISO 527-2 [40] via injection molding (Arburg GmbH, Arburg Allrounder 470H 1000-170).

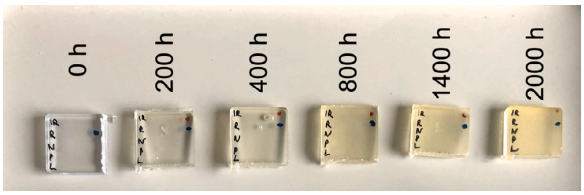

Fig. 1. A series of artificially weathered PS samples after different weathering times.

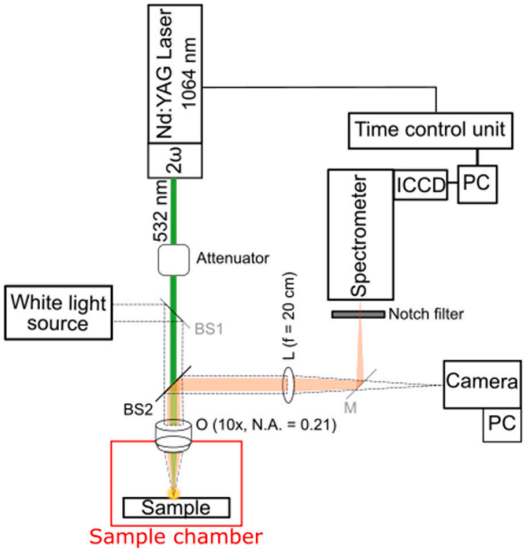

Fig. 2. Illustration of the built LIBS system used for measurements in different atmospheres.

The tensile bars were exposed to controlled accelerated weathering conditions following the standard ISO 4892-2:2011 [38]. For the weathering, an industrial test chamber (Q-LAB Corporation, Q-SUN XE-3) was used. To mimic the irradiation spectra of sunlight, the chamber was equipped with 3 xenon arc lamps and Daylight-Q filters. Following the standard, the irradiance intensity in the wavelength range 300–400 nm was set to 60 W/m^2. During the 102 min dry phase, the chamber temperature and relative humidity were set to 38 ° C and 55 %, respectively. During the stage of 18 min distilled water spraying, the temperature and the humidity were not controlled. For the analysis, samples after 200, 400, 800, 1400, and 2000 h of exposure were generated. A set of PS samples in different aging states is presented in Fig. 1.

2.2. Experimental setup

Fig. 2 shows the schematic of the experimental setup used to study the oxidation of plastics. A second harmonic Q-switched Nd:YAG laser (Quantel, Brilliant b model) with a repetition rate of 10 Hz, laser wavelength of 532 nm, pulse duration of 4 ns and maximum energy of 200 mJ was used as a radiation source. The laser pulse to generate the plasma on the sample's surface followed the pathway highlighted in green. First, it passed an attenuator, where its energy can be modified to adjust the ablation volume on the sample. After that, the pulse was focused vertically on the sample using a 10 x objective lens (O).

This arrangement created an approximately 80 μm diameter spot on the surface with an estimated power density of 9.95 × 10^{10} W/cm^2. A sample chamber was build around the sample holder to conduct measurements in an environment other than air. For this study, nitrogen

gas was used with a purity of 99.999 %. The relative humidity inside the chamber was between 0 %-10 %.

The optical path to acquire the sample's spectrum is highlighted in orange. A notch filter (Kaiser Optics, HSPF-532.0-1.0) was placed in front of the spectrometer to remove the incident laser pulse from the emitted light. The spectrum was recorded with a spectrometer (Newport corporation, MS257) that has a grating of 300 lines/mm and an entrance slit of 30 μm. It was equipped with a time-gated intensified charged-couple device (ICCD) camera (Andor, iStar DH720-18 U-03).

To investigate the ablation crater associated with LIBS measurements and to assure focal plane, a white light source and a camera were used. For this purpose, a detachable beamsplitter (BS1) and mirror (M) were integrated in the setup. The sample was then observed through the dashed optical pathway. To measure the depth of the crater, a profilometer was used (cyberTECHNOLOGIES, cyberSCAN CT 100). The lateral resolution was set to 5 μm.

For validation, FTIR measurements were conducted with a standalone FTIR microscope (Bruker, LUMOS II), operated with the spectroscopy software OPUS (version 8.5.29). The system was equipped with a single-element thermo-electrically cooled mercury-cadmium-telluride (TE-MCT) detector and a motorized germanium attenuated total reflection (ATR) crystal. The latter was applied to measure the samples with medium pressure.

2.3. Spectral acquisition

All LIBS spectra were acquired under the following conditions. The focal plane was set on the sample's surface, the pulse energy was adjusted to 20 mJ and the delay and gate width of the ICCD camera were set to 100 ns and 1000 ns, respectively. These settings were chosen in accordance to a report by Grègoire et al. which states that short delay widths produce signals with high signal-to-noise ratios for atomic signals while larger widths improve the ratio for molecular signals [30]. For this study, the delay width was optimized for the oxygen emission line. Since the C2 swan band system is also an important characterization parameter for plastics [32], the gate width was set to a higher value. Note that further optimizations of this parameter may be possible, but were not in the scope of this study.

The spectra were recorded in the spectral range 300 nm – 800 nm. This range was chosen based on the results of previous works [29,31,32]. Prior to a measurement, each sample was cleaned with 2-propanol. The measurements were performed in air or in nitrogen gas at atmospheric pressure where the gas flow was directed under the sample holder. The nitrogen gas prevented the air from interacting with the plasma and thus, interfering with the spectral signal.

To study weathering-induced oxidation on the sample's surface, a single-shot spectrum was acquired on 8 different sample locations. Measurements of the sample depth profile were acquired from 8 different spots that are separated by at least 200 μm. Each spot was hit 12 times by the laser pulse and the focal plane was adjusted after 3 consecutive shots. For the evaluation, the spectrum corresponding to a shot number, from now on referred to as layer, was averaged over all spots and their corresponding standard deviation was calculated. The depth of the layers was determined from the measurements by extracting the maximum depth in the crater area. Potential irregularities of the sample's surface, e.g. bumps or tilts, were also accounted for by fitting the surface with a polynomial function and subtracting it from the data.

For all spectra, the flatfield was recorded and the continuum background was subtracted to get rid of any possible error sources. This approach assured reliable and reproducible data and took any possible inhomogeneities into consideration that occur during the acquisitions.

For FTIR measurements, the sample and the background spectra were recorded with open aperture, 30 co-added scans, and a resolution of 4 cm^{-1} in the mid-infrared spectral range of 4000 cm^{-1}– 680 cm^{-1}. For each sample, one measurement was performed consisting of four replicated spots which were arranged in a square grid with distances of about 500 μm between each spot. The resulting spectra were averaged and processed for atmospheric influences in the spectral areas of carbon dioxide and water.

Table 1
List of relevant emission lines in the LIBS spectrum for PS [30–33,41].

Chemical species	Wavelength (nm)
C (I)	247.8
H	486.14, 656.29
O (I)	777.3
C2	470, 516.3, 553
CN	360, 388.3, 422
Ca (I)	422.69
Ca (II)	393.38, 396.83
Fe	557.8
K (I)	766.49, 769.89
Na (I)	589.15
N (I)	746.8

Table 2
List of absorption bands in ATR-FTIR spectrum formed by the oxidation processes in PS [36,42,43].

Functional group	Absorption band (cm^{-1})
ketone	1725
benzoic anhydride	1725, 1785
benzaldehyde	1704
benzophenone	1690
carboxylate	1553
benzoic acid dimer	1698
benzoic acid monomer	1732
dibenzoylmethane	1515, 1605
dimeric acetic and formic acid	1710
hydroxyl region	3000–3600
C-O region	1100–1200
C=O region	1732

2.4. Spectral line identification

The characteristic peaks for the spectral fingerprint of plastics in LIBS are the atomic and ionic emission lines of the hydrogen Balmer series, the carbon line and the oxygen line, as well as the diatomic molecular bands of the C2 swan band and the CN violet band [30–33]. In addition, peaks coming from additives within the sample or from contamination on the sample's surface such as calcium, iron, sodium, nitrogen and potassium are also inevitable. For the characterization of weathering-induced oxidation of PS, this work will only focus on the oxygen emission line at 777.3 nm. Note that the carbon line is not detected with this setup as it lies in the deep UV range. All relevant peaks are summarized in Table 1.

For the evaluation with FTIR, the main and secondary absorption bands formed by the oxidation processes in PS are used as reported by numerous studies [36,42,43] and summarized in Table 2. The sum of the intensities of all these absorption bands was calculated and used as input. Here, we follow the same approach as Brunnbauer et al. [36].

3. Results and discussion

3.1. Influence of atmospheres on laser-induced plasma

When conducting LIBS measurements in an environment other than vacuum, additional contributions from the environment to the emission spectrum are possible. These contributions must be considered first before conclusions can be drawn from the spectral data. Since this study focuses on the presence of oxygen in the sample, conducting measurements in ambient air may not be wise because of possible contributions from the surrounding oxygen. To further look into this, the spectrum of weathered PS measured in ambient air is evaluated first. Fig. 3a shows the spectra of two PS samples after 0 h (red) and 2000 h (blue) of weathering measured in air. The superposition reveals additional peaks in the spectrum for 2000 h weathered PS compared to untreated PS. The additional peaks not belonging to the

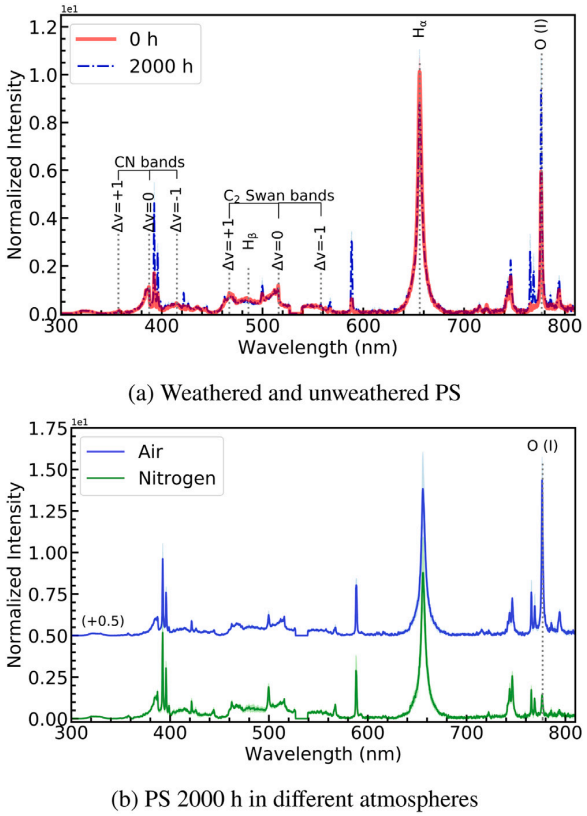

Fig. 3. LIBS spectra from PS 0 h and PS 2000 h in different atmospheres. (a) shows the samples PS 0 h and PS 2000 h measured in air. Apart from the peaks coming from additives, the aging seems to only have influenced the oxygen peak from the characteristic plastic peaks (CN, C2, H, O). (b) shows sample PS 2000 h measured in air and nitrogen atmosphere. It shows that the oxygen peak is highly influenced by air. The spectra are the average over 3 measurements (average is depicted as line, standard deviation as light background). For better comparability, the spectra are normalized to C2 ($\Delta v = 0$). In (b) the spectra are plotted with an offset.

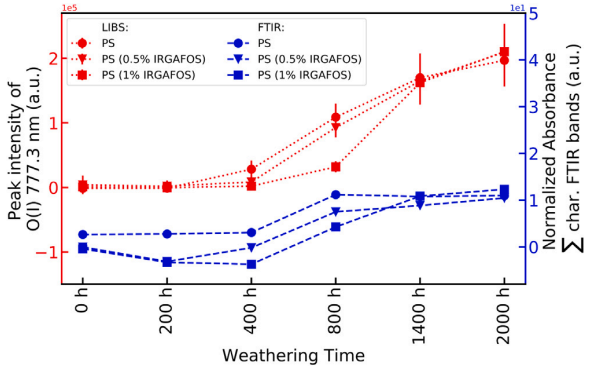

Fig. 4. Course of oxidation at different weathering times. The plot shows the detected oxidation level for LIBS (oxygen intensity at 777.3 nm is shown on the left axis) and FTIR (sum of characteristic peaks representing the spectral fingerprint of chemical processes generated by oxidation is shown on the right axis). Each LIBS data point is the average over 8 measurements (average is depicted as a symbol, standard deviation as line). Each FTIR data point is the average over 4 measurements and normalized to CO_2 and hydrogen bands.

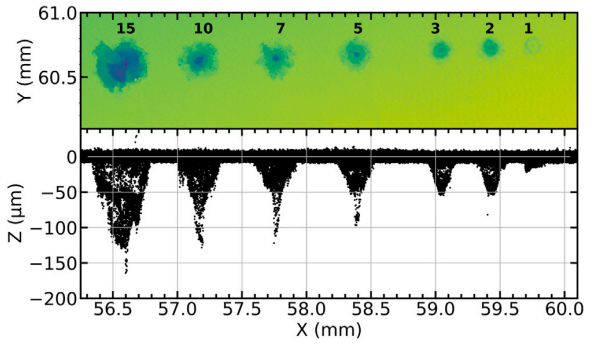

Fig. 5. Surface measurement from 2000 h weathered PS (1% Irgafos) The plot shows the crater depth from 1 to 15 shots. In addition it shows the embrittlement of the sample's surface. In order to determine the crater depth precisely, the unevenness of the surface was fitted and straightened using a polynomial function.

polymer matrix of PS are listed in the second half of Table 1. These occurrences originate from contaminations on the porous surface which develop during the weathering treatment. A comparison of the oxygen peak at 777.3 nm for both samples shows an increase in intensity for 2000 h weathered PS which implies a higher oxygen content due to weathering. Yet, the measurements raise the question of why the unweathered sample (red) shows an oxygen peak at all when there is no oxygen in its chemical structure. Fig. 3b helps to shed light on this issue. The plot shows the 2000 h weathered sample measured in air and in nitrogen. Depending on the atmosphere, the oxygen peak is more than 6 times more intense. This demonstrates the significant influence of air on the oxygen peak. Therefore, it is advised not to use air as surrounding atmosphere for weathering-induced oxidation. Nitrogen, however, appears to be a more suitable atmosphere for oxidation measurements and is additionally a more sustainable alternative as opposed to inert gases used elsewhere [36]. These findings agree with other previous reports that the surrounding sample environment can bias the observations [44,45]. Therefore, this work will not quantify the influences of different gases on the spectra.

Note that although contaminations are present in weathered samples, the spectral fingerprint for PS can still be identified in the spectrum (see Fig. 3a and Table 1). This underlines the suitability of LIBS as an identification method for plastic materials.

3.2. Oxygen intensity with regard to weathering time

As mentioned earlier, weathering-induced oxidation is studied with LIBS by evaluating the oxygen intensity in different samples. This raises the question if the results are comparable to already established methods. In the following, LIBS measurements on the sample surface for different weathering times are compared to those measured with FTIR. The spectral data acquired with the latter can be found in the supplements.

Fig. 4 shows surface measurements with LIBS (dotted, red) and FTIR (dashed, blue) for PS, PS (0.5 % Irgafos) and PS (1 % Irgafos) at different weathering times. In the LIBS procedure, the oxygen intensity increases after 400 h of weathering. Before that, the oxidation is hardly observable. At 800 h, the measurements for PS (1 % Irgafos) stand out since the increase of the oxygen peak is clearly lower than in the other samples. Reason for this may be due to the higher concentration of Irgafos. However, after 800 h the oxygen peak increases rapidly and reaches a value comparable to the one of the other samples. As Irgafos slows down the weathering-induced oxidation of PS by decomposing the generated hydroperoxide or by limiting the formation of peroxide radicals by trapping the oxygen present into the bulk of the polymer [46], the oxidation can only be delayed as long as the additive is not used up. After 800 h, this seems to have occurred and the oxygen

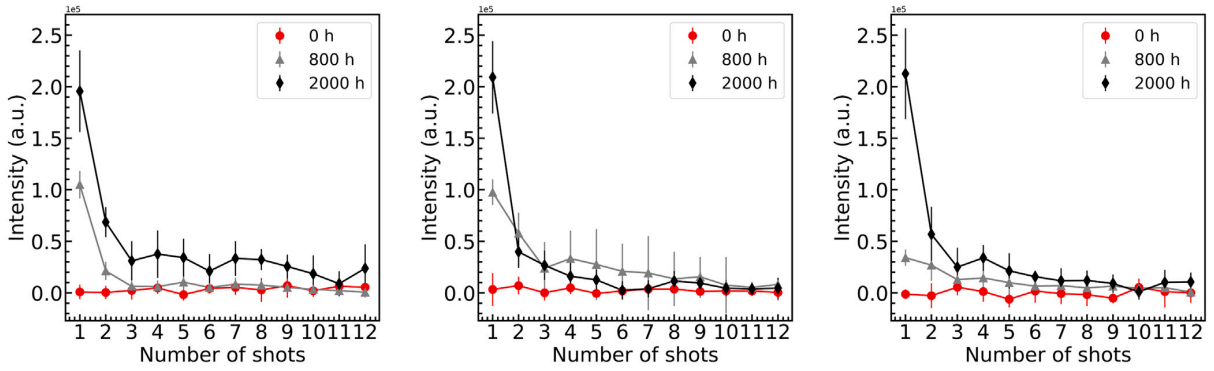

Fig. 6. Oxygen intensity with depth for different samples up to 2000 h of weathering time. The plot shows the decrease of the oxygen intensity with increasing number of shots inside the sample. 12 shots correspond to a depth of approximately (111.39 ± 9.97) µm.

content increases steeply. Note that the contribution of Irgafos to the oxygen intensity in the LIBS signal is negligible due to the small amount of Irgafos compared to the reaction coming from photo-oxidation. It should also be mentioned that the analysis of the oxidized form of Irgafos is not the focus of this work and we refer to [46] for more details on this topic.

In the FTIR measurements the absorbance increases after 400 h of weathering and starts to saturate for weathering times larger than 1400 h. Potential reasons for this saturation have already been discussed in [16]. It is explained that the oligomers derived from polymer chains become shorter and their polarities become high enough so that they dissolve in water and are rinsed out during the cleaning protocol [16]. However, in the LIBS measurements this saturation has not been observed. This may be due to the fact that LIBS measures at larger depths than FTIR. One LIBS shot has an ablation depth of approximately (23.53 ± 4.91) µm, compared to a maximum penetration depth of 6 µm for ATR-FTIR. Accordingly, in LIBS the oxygen content is averaged over a larger volume. Since some of the ketone groups in the surface are rinsed out, saturation occurs in FTIR measurements [16], while LIBS includes oxidation that occur in deeper layers which do not rinse out easily. This could explain the difference in the data from 800 h onwards in Fig. 4. It can be said that the trend of the course of oxidation received from the LIBS measurements are in good agreement with the FTIR results.

The comparison shows that the use of ATR-FTIR as a sole characterization method raises questions that need further explanation, such as the saturation observed earlier. Here, LIBS can provide additional details because of its larger penetration depth and thus, both techniques may complement each other. Furthermore, for weathering-induced oxidation the evaluation in LIBS is more convenient than in FTIR, since the former only needs to analyze one peak while the latter has to identify and include all relevant absorption bands.

3.3. Depth profile analysis

In the following, depth profiles of PS, PS (0.5 % Irgafos) and PS (1 % Irgafos) at 3 different weathering times (0 h, 800 h, and 2000 h) are generated using LIBS.

In order to evaluate the depth of the crater after each laser shot, referred to as layer, a pattern with 1, 2, 3, 5, 7, 10 and 15 shots was generated. This profile was made under the same conditions as the depth profile measurements described in chapter 2.3. Fig. 5 shows an example of a profilometer measurement for the craters corresponding to a different number of laser shots. The plot reveals that the ablation depth increases with the number of shots. With this measuring procedure a total depth of (111.39 ± 9.97) µm for 12 layers were achieved. The thick strip of data points around the height Z = 0 µm illustrates the increased surface roughness due to weathering.

Fig. 6 shows the propagation of the oxidation into the samples PS, PS (0.5 % Irgafos) and PS (1 % Irgafos). The oxygen intensity for the unweathered samples (red, ●) remains unchanged regardless of whether measurements are taken on the surface or inside the sample. The depth profiles indicate that the oxidation for a weathering time of 800 h for all samples (gray, ▲) extends into the second layer with a depth of approximately (51.23 ± 11.21) µm. For samples that were weathered for 2000 h (black, ♦), the oxidation penetrates into the third layer with a depth of approximately (57.98 ± 6.36) µm. This proves that the oxygen content as well as its penetration depth varies with weathering time. The influence of the additive concentration can be observed by evaluating the oxygen intensity in the second layer. In PS the oxygen intensity for 800 h and 2000 h are clearly distinguishable (see Fig. 6(a)). However, the oxygen intensity for PS (0.5 % Irgafos) and PS (1 % Irgafos) for a weathering time of 800 h and 2000 h are within the scope of their error bars equal in the second layer. Even though the penetration depth is the same for all samples, the trend of the oxygen peak in PS with additives appears to be flatter than in PS with no additives for a weathering time of 800 h. At 2000 h, however, no influence of the oxidation process is visible which could be due to the fact that the additive has already been used up (see Fig. 6). This may imply that oxidation penetrates less intense into the samples with higher concentration. Such a behavior is in agreement with the findings of Gijsman et al. who showed that the oxidation-depth profile of PA with an antioxidant is much flatter than for PA without the antioxidant [47]. Overall, the results illustrate that LIBS is sufficiently sensitive to perform a layer-by-layer analysis to identify changes in the sample's chemical structure due to weathering-induced oxidation.

4. Conclusion

The low biodegradability of plastic does not only lead to an accumulation of plastic litter in the environment but also to its exposure to various weathering and aging processes. In this study, we focus on weathering-induced oxidation for polystyrene (PS) samples. The aim was to systematically study this effect on the sample's surface and its depth profile at different weathering times (0 h, 200 h, 400 h, 800 h, 1400 h, 2000 h) using LIBS as an analytical tool.

During the course of this study, 3 sets of samples with different additive concentrations were analyzed in nitrogen gas. It was shown that ambient gas can have strong effects on LIBS measurements. Therefore, an atmosphere that does not contain oxygen is recommended for measuring the degree of weathering-induced oxidation. In this context,

nitrogen has proven to be a cost-efficient alternative compared to inert gases.

The PS samples used in this study showed increased oxygen peaks with weathering time starting from 400 h in the LIBS spectra. Similar results were also obtained with FTIR. There, increased absorption bands formed by oxidation processes were detected from 400 h onwards compared to unweathered samples. This confirms that LIBS is sensitive enough to measure oxidation on the sample's surface. Due to laser ablation, LIBS is also capable of depth profile analysis and therefore, the penetration depth of the oxidation could be evaluated. In the weathered samples increased oxygen peaks were detected up to (57.98 ± 6.36) μm. The addition of Irgafos appears to hinder the penetration of oxygen with weathering time until the additive has been used up. Overall, these results illustrate that LIBS could provide valuable insights on the degradation of plastics in the environment that are not visible with common analytical tools.

To date, most studies on plastic pollution use FTIR, which has established itself as a non-destructive tool for (micro-) plastic identification [48–51]. It derives details on the chemical structure of the sample by looking at interactions between infrared light and functional groups in a molecule. To conduct a layer-by-layer analysis similar to our study but with FTIR, the sample must be prepared, e.g. with a microtome, to expose the sample's cross-section which can be more difficult as the sample size decreases, e.g. for microplastics. In comparison, LIBS primarily evaluates the emission signals from atoms that belong to the target material. While this technique is minimal destructive due to laser ablation, a layer-by-layer analysis does not require any sample preparation. Both can, therefore, be considered as complementary spectroscopic techniques that determine and validate the properties of the sample. This motivates further research on LIBS' application on degraded plastic litter samples from the environment as well as the comparability of the results measured with LIBS and FTIR. Additionally, a larger sample set should be evaluated in order to obtain statistically meaningful results.

In conclusion, considering LIBS' ability to combine plastics identification, trace element detection and, as shown in the present study, the detection of weathering-induced-oxidation, this technique has the potential to establish itself as a promising identification and analysis tool for plastic litter.

CRediT authorship contribution statement

Caroline Sommer: Conceptualization, Methodology, Investigation, Software, Formal analysis, Visualization, Validation, Writing – original draft, Writing – review & editing. **Johnny Nguyen:** Conceptualization, Methodology, Supervision, Software, Formal analysis, Investigation, Writing – original draft, Writing – review & editing. **Teresa Menzel:** Resources, Writing – review & editing. **Julia A. Prume:** Investigation, Validation, Writing – review & editing. **Holger Ruckdäschel:** Project administration, Writing – review & editing. **Martin Koch:** Project administration, Writing – review & editing.

Declaration of competing interest

The authors declare that they have no known competing financial interests or personal relationships that could have appeared to influence the work reported in this paper.

Data availability

The data is available from the corresponding author.

Acknowledgments

We thank Dr. Frank Noll and Dr. Hee-Cheol Kim for providing their expertise for the profilometer measurements and Felix Gorka for support and helping interpreting the FTIR data.

Funding

Part of this project was funded by the Deutsche Forschungsgemeinschaft (DFG, German Research Foundation) - Project Number 391977956 - SFB 1357, subproject C01. Open Access funding was provided by the Open Acess Publication Fund of Philipps-Universität Marburg with support of the Deutsche Forschungsgemeinschaft (DFG, German Research Foundation).

Appendix A. Supplementary data

Supplementary material related to this article can be found online at https://doi.org/10.1016/j.polymertesting.2022.107623.

References

[1] H. Ritchie, M. Roser, Plastic pollution, Our World in Data (2018).
[2] C.M. Rochman, M.A. Browne, A.J. Underwood, J.A. van Franeker, R.C. Thompson, L.A. Amaral-Zettler, The ecological impacts of marine debris: unraveling the demonstrated evidence from what is perceived, Ecology 97 (2) (2016) 302–312.
[3] A.D. Vethaak, H.A. Leslie, Plastic debris is a human health issue, Environ. Sci. Technol. 50 (13) (2016) 6825–6826.
[4] C.M. Rochman, M.A. Browne, B.S. Halpern, B.T. Hentschel, E. Hoh, H.K. Karapanagioti, L.M. Rios-Mendoza, H. Takada, S. Teh, R.C. Thompson, Classify plastic waste as hazardous, Nature 494 (7436) (2013) 169–171.
[5] B. Toussaint, B. Raffael, A. Angers-Loustau, D. Gilliland, V. Kestens, M. Petrillo, I.M. Rio-Echevarria, G. Van den Eede, Review of micro- and nanoplastic contamination in the food chain, Food Addit. Contamin.: A 36 (5) (2019) 639–673.
[6] L.G.A. Barboza, C. Lopes, P. Oliveira, F. Bessa, V. Otero, B. Henriques, J. Raimundo, M. Caetano, C. Vale, L. Guilhermino, Microplastics in wild fish from North East Atlantic Ocean and its potential for causing neurotoxic effects, lipid oxidative damage, and human health risks associated with ingestion exposure, Sci. Total Environ. 717 (2020) 134625.
[7] M. Haave, A. Gomiero, J. Schönheit, H. Nilsen, A.B. Olsen, Documentation of microplastics in tissues of Wild Coastal animals, Front. Environ. Sci. 9 (2021).
[8] A.J. Jamieson, L.S.R. Brooks, W.D.K. Reid, S.B. Piertney, B.E. Narayanaswamy, T.D. Linley, Microplastics and synthetic particles ingested by deep-sea amphipods in six of the deepest marine ecosystems on Earth, R. Soc. Open Sci. 6 (2) (2019) 180667.
[9] A.A. Koelmans, N.H. Mohamed Nor, E. Hermsen, M. Kooi, S.M. Mintenig, J. De France, Microplastics in freshwaters and drinking water: Critical review and assessment of data quality, Water Res. 155 (2019) 410–422.
[10] A. Ragusa, A. Svelato, C. Santacroce, P. Catalano, V. Notarstefano, O. Carnevali, F. Papa, M.C.A. Rongioletti, F. Baiocco, S. Draghi, E. D'Amore, D. Rinaldo, M. Matta, E. Giorgini, Plasticenta: First evidence of microplastics in human placenta, Environ. Int. 146 (2021) 106274.
[11] A.L. Andrady, Microplastics in the marine environment, Mar. Pollut. Bull. 62 (8) (2011) 1596–1605.
[12] B. Gewert, M.M. Plassmann, M. MacLeod, Pathways for degradation of plastic polymers floating in the marine environment, Environ. Sci.: Processes Impacts 17 (9) (2015) 1513–1521.
[13] A.S. Maxwell, W.R. Broughton, G.D. Dean, G.D. Sims, Review of Accelerated Ageing Methods and Lifetime Prediction Techniques for Polymeric Materials, NPL Report, National Physical Laboratory, 2005.
[14] P. Liu, Y. Shi, X. Wu, H. Wang, H. Huang, X. Guo, S. Gao, Review of the artificially-accelerated aging technology and ecological risk of microplastics, Sci. Total Environ. 768 (2021) 144969.
[15] B. Suresh, S. Maruthamuthu, M. Kannan, A. Chandramohan, Mechanical and surface properties of low-density polyethylene film modified by photo-oxidation, Polymer J. 43 (4) (2011) 398–406.
[16] N. Meides, T. Menzel, B. Poetzschner, M.G.J. Löder, U. Mansfeld, P. Strohriegl, V. Altstaedt, J. Senker, Reconstructing the environmental degradation of polystyrene by accelerated weathering, Environ. Sci. Technol. (2021).
[17] N. Ojha, N. Pradhan, S. Singh, A. Barla, A. Shrivastava, P. Khatua, V. Rai, S. Bose, Evaluation of HDPE and LDPE degradation by fungus, implemented by statistical optimization, Sci. Rep. 7 (1) (2017) 39515.
[18] S. Garcea, Y. Wang, P. Withers, X-ray Computed tomography of polymer composites, Compos. Sci. Technol. 156 (2018) 305–319.
[19] C.P. Ward, C.J. Armstrong, A.N. Walsh, J.H. Jackson, C.M. Reddy, Sunlight converts polystyrene to carbon dioxide and dissolved organic carbon, Environ. Sci. Technol. Lett. 6 (11) (2019) 669–674.

[20] M. Celina, D. Ottesen, K. Gillen, R. Clough, FTIR emission spectroscopy applied to polymer degradation, Polym. Degrad. Stab. 58 (1–2) (1997) 15–31.
[21] N. Peez, M.-C. Janiska, W. Imhof, The first application of quantitative 1H NMR spectroscopy as a simple and fast method of identification and quantification of microplastic particles (PE, PET, and PS), Anal. Bioanal. Chem. 411 (4) (2019) 823–833.
[22] T. Canel, P. Demir, E. Kacar, B.G. Oztoprak, E. Akman, M. Gunes, A. Demir, Optimization of parameters for depth resolution of galvanized steel by LIBS technique, Opt. Laser Technol. 54 (2013) 257–264.
[23] N.P. Ivleva, Chemical analysis of microplastics and nanoplastics: Challenges, advanced methods, and perspectives, Chem. Rev. 121 (19) (2021) 11886–11936.
[24] M.P. Mateo, G. Nicolas, V. Pinon, A. Yanez, Improvements in depth-profiling of thick samples by laser-induced breakdown spectroscopy using linear correlation, Surf. Interf. Anal. Int. J. Devot. Dev. Appl. Tech. Anal. Surf. Interfaces Thin Films 38 (5) (2006) 941–948.
[25] H. Balzer, M. Hoehne, R. Noll, V. Sturm, New approach to online monitoring of the Al depth profile of the hot-dip galvanised sheet steel using LIBS, Anal. Bioanal. Chem. 385 (2) (2006) 225–233.
[26] S. Couris, A. Hatziapostolou, D. Anglos, A. Mavromanolakis, C. Fotakis, Laser-induced breakdown spectroscopy (LIBS) applications in environmental issues, in: ALT'96 International Symposium on Laser Methods for Biomedical Applications, vol. 2965, International Society for Optics and Photonics, 1996, pp. 83–87.
[27] V. Dwivedi, A. Marín-Roldán, J. Karhunen, P. Paris, I. Jõgi, C. Porosnicu, C. Lungu, H. van der Meiden, A. Hakola, P. Veis, CF-LIBS quantification and depth profile analysis of Be coating mixed layers, Nucl. Mater. Energy 27 (2021) 100990.
[28] G. Galbács, A critical review of recent progress in analytical laser-induced breakdown spectroscopy, Anal. Bioanal. Chem. 407 (25) (2015) 7537–7562.
[29] R. Sattmann, I. Monch, H. Krause, R. Noll, S. Couris, A. Hatziapostolou, A. Mavromanolakis, C. Fotakis, E. Larrauri, R. Miguel, Laser-induced breakdown spectroscopy for polymer identification, Appl. Spectrosc. 52 (3) (1998) 456–461.
[30] S. Grégoire, M. Boudinet, F. Pelascini, F. Surma, V. Detalle, Y. Holl, Laser-induced breakdown spectroscopy for polymer identification, Anal. Bioanal. Chem. 400 (10) (2011) 3331–3340.
[31] D. Stefas, N. Gyftokostas, E. Bellou, S. Couris, Laser-induced breakdown spectroscopy assisted by machine learning for plastics/polymers identification, Atoms 7 (3) (2019) 79.
[32] C. Sommer, L. Schneider, J. Nguyen, J. Prume, K. Lautze, M. Koch, Identifying microplastic litter with laser induced breakdown spectroscopy: A first approach, Mar. Pollut. Bull. 171 (2021) 112789.
[33] M.V. Dastjerdi, S.J. Mousavi, M. Soltanolkotabi, A.N. Zadeh, Identification and sorting of PVC polymer in recycling process by laser-induced breakdown spectroscopy (LIBS) combined with support vector machine (SVM) model, Iran. J. Sci. Technol. Trans. A Sci. 42 (2) (2018) 959–965.
[34] X. Chen, S. Ali, L. Yuan, F. Guo, G. Huang, W. Shi, X. Chen, Characterization and source analysis of heavy metals contamination in microplastics by Laser-Induced Breakdown Spectroscopy, Chemosphere 287 (2022) 132172.
[35] D. Chen, T. Wang, Y. Ma, G. Wang, Q. Kong, P. Zhang, R. Li, Rapid characterization of heavy metals in single microplastics by laser induced breakdown spectroscopy, Sci. Total Environ. 743 (2020) 140850.
[36] L. Brunnbauer, M. Mayr, S. Larisegger, M. Nelhiebel, L. Pagnin, R. Wiesinger, M. Schreiner, A. Limbeck, Combined LA-ICP-MS/LIBS: powerful analytical tools for the investigation of polymer alteration after treatment under corrosive conditions, Sci. Rep. 10 (1) (2020) 12513.
[37] L. Brunnbauer, S. Larisegger, H. Lohninger, M. Nelhiebel, A. Limbeck, Spatially resolved polymer classification using laser induced breakdown spectroscopy (LIBS) and multivariate statistics, Talanta 209 (2020) 120572.
[38] ISO 4892-2:2011, Plastics — Methods of exposure to laboratory light sources — Part 2: Xenon-arc lamps, International Organization for Standardization, 2011.
[39] S. Lambert, M. Wagner, Characterisation of nanoplastics during the degradation of polystyrene, Chemosphere 145 (2016) 265–268.
[40] ISO 527-2:2012, Plastics — Determination of Tensile Properties — Part 2: Test Conditions for Moulding and Extrusion Plastics, Technical Report, International Organization for Standardization, Geneva, CH, 2012, p. 11.
[41] A. Kramida, Y. Ralchenko, J. Reader, N.A. Team, NIST Atomic Spectra Database (version 5.9), National Institute of Standards and Technology, Gaithersburg, 2021, http://dx.doi.org/10.18434/T4W30F.
[42] C. Sandt, J. Waeytens, A. Deniset-Besseau, C. Nielsen-Leroux, A. Réjasse, Use and misuse of FTIR spectroscopy for studying the bio-oxidation of plastics, Spectrochim. Acta A 258 (2021) 119841.
[43] B. Mailhot, J.L. Gardette, Polystyrene photooxidation. 1. Identification of the IR-absorbing photoproducts formed at short and long wavelengths, Macromolecules 25 (16) (1992) 4119–4126.
[44] M. Dong, X. Mao, J.J. Gonzalez, J. Lu, R.E. Russo, Time-resolved LIBS of atomic and molecular carbon from coal in air, argon and helium, J. Anal. At. Spectrom. 27 (12) (2012) 2066.
[45] S.J. Mousavi, M.H. Farsani, S.M.R. Darbani, A. Mousaviazar, M. Soltanolkotabi, A.E. Majd, CN and C 2 vibrational spectra analysis in molecular LIBS of organic materials, Appl. Phys. B 122 (5) (2016) 106.
[46] K. Fouyer, O. Lavastre, D. Rondeau, Direct monitoring of the role played by a stabilizer in a solid sample of polymer using direct analysis in real time mass spectrometry: the case of irgafos 168 in polyethylene, Anal. Chem. 84 (20) (2012) 8642–8649.
[47] P. Gijsman, W. Dong, A. Quintana, M. Celina, Influence of temperature and stabilization on oxygen diffusion limited oxidation profiles of polyamide 6, Polym. Degrad. Stab. 130 (2016) 83–96.
[48] A. Bellasi, G. Binda, A. Pozzi, S. Galafassi, P. Volta, R. Bettinetti, Microplastic contamination in freshwater environments: A review, focusing on interactions with sediments and benthic organisms, Environments 7 (4) (2020) 30.
[49] A. Käppler, D. Fischer, S. Oberbeckmann, G. Schernewski, M. Labrenz, K.-J. Eichhorn, B. Voit, Analysis of environmental microplastics by vibrational microspectroscopy: FTIR, Raman or both? Anal. Bioanal. Chem. 408 (29) (2016) 8377–8391.
[50] E.C. Minor, R. Lin, A. Burrows, E.M. Cooney, S. Grosshuesch, B. Lafrancois, An analysis of microlitter and microplastics from lake superior beach sand and surface-water, Sci. Total Environ. 744 (2020) 140824.
[51] S. Primpke, C. Lorenz, R. Rascher-Friesenhausen, G. Gerdts, An automated approach for microplastics analysis using focal plane array (FPA) FTIR microscopy and image analysis, Anal. Methods 9 (9) (2017) 1499–1511.

Appendix

FTIR spectra

The FTIR spectra that have been used for evaluating the LIBS results are presented in Fig. 7. The sum of the marked values (dotted lines and grey region) can be found in Table 2 and are used as input for Fig. 4.

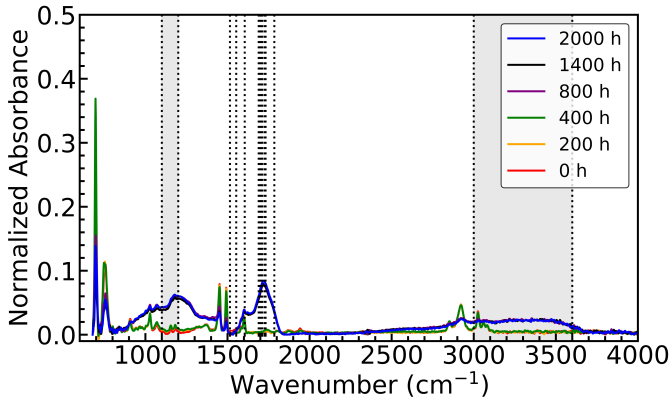

(a) PS

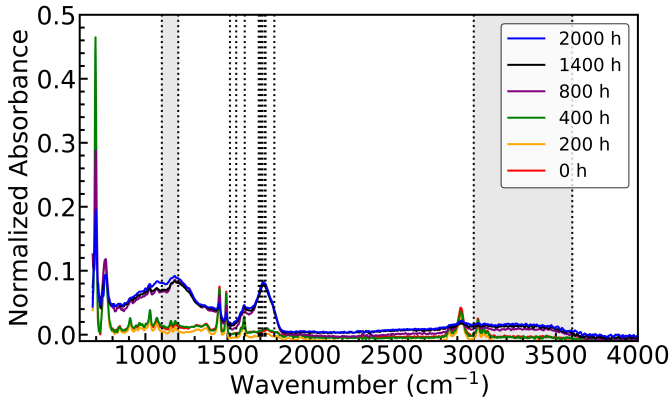

(b) PS (0.5 % Irgafos)

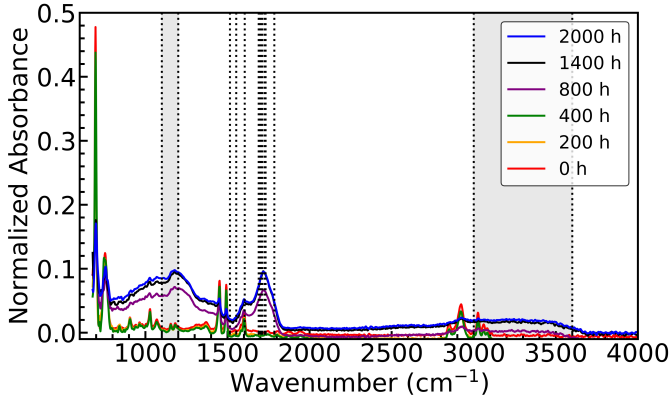

(c) PS (1 % Irgafos)

Figure 7: FTIR spectra of weathered PS with different concentrations of Irgafos. The dotted lines and the grey regions marked the used values for evaluation. They correspond to the values listed in Table 2.

Article 3

Sommer, C., Nguyen, J., Menzel, T., Ruckdäschel, H., & Koch, M. (2023). Determining weathering-induced heterogeneous oxidation profiles of polyethylene, polypropylene and polystyrene using laser-induced breakdown spectroscopy. *Chemosphere*, 140105.

DOI:10.1016/j.chemosphere.2023.140105
URL: https://doi.org/10.1016/j.chemosphere.2023.140105
This article was published in Chemosphere, page 140105.

Chemosphere 343 (2023) 140105

Contents lists available at ScienceDirect

Chemosphere

journal homepage: www.elsevier.com/locate/chemosphere

Determining weathering-induced heterogeneous oxidation profiles of polyethylene, polypropylene and polystyrene using laser-induced breakdown spectroscopy

Caroline Sommer [a,*], Johnny Nguyen [a], Teresa Menzel [b], Holger Ruckdäschel [b], Martin Koch [a]

[a] Faculty of Physics and Material Sciences Centre, Philipps-University Marburg, 35037, Marburg, Germany
[b] Department Polymer Engineering, University of Bayreuth, 95447, Bayreuth, Germany

HIGHLIGHTS

- Heterogeneous plastic degradation is related to the plastic's lattice structure.
- Degradation processes should be studied over the entire sample volume.
- LIBS can conduct three-dimensional chemical mapping without exposing the cross-section.
- PE, PP and PS samples have been studied for different weathering times.

GRAPHICAL ABSTRACT

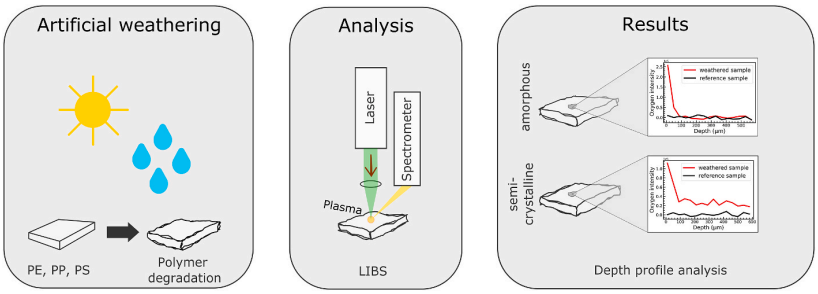

ARTICLE INFO

Handling Editor: Michael Bank

Keywords:
Laser-induced Breakdown Spectroscopy
Heterogeneous plastic degradation
Depth profile and surface analysis
Weathered plastics
Amorphous polymers
Semi-crystalline polymers

ABSTRACT

Weathering-induced polymer degradation is typically heterogeneous which plays an integral part in fragmentation. Despite that, the current selection of techniques to investigate such heterogeneities, especially beneath the sample surface, is sparse. We introduce Laser-induced Breakdown Spectroscopy (LIBS) as an analytical tool and evaluate its performance for depth profiling. Three types of polymers were selected (polyethylene, polypropylene, and polystyrene) that were aged under controlled conditions. We demonstrate that LIBS can detect heterogeneous oxidation on the surface and inside the samples. The results reveal that different oxidation behaviors are linked to the sample's lattice structure and the subsequent formation of microcracks. This implies that LIBS is beneficial to give additional insights into the weathering and degradation behavior of environmentally relevant plastics.

1. Introduction

Improperly discarded plastic products are exposed to an environment that is vastly different from the one when those items were still in use. The exposure to factors, such as extended UV light irradiation, abrasions, and humidity fluctuations, promotes polymer degradation which inevitably leads to fragmentation (Barnes et al., 2009). With decreasing size, those fragments become more susceptible to

* Corresponding author.
E-mail address: caroline.sommer@physik.uni-marburg.de (C. Sommer).

https://doi.org/10.1016/j.chemosphere.2023.140105
Received 15 March 2023; Received in revised form 31 July 2023; Accepted 6 September 2023
Available online 13 September 2023
0045-6535/

microorganisms that could initiate a cascade of effects and ultimately influence entire ecosystems (Lim, 2021; MacLeod et al., 2021). Mitigating the detrimental effects of plastic debris is not simple, as their long-term fate is poorly understood. Such knowledge, however, is essential for any environmental risk assessment.

Our current knowledge of weathering-induced polymer degradation is mostly derived from accelerated weathering experiments where representative plastic samples are studied in controlled environments (Plohl et al., 2022; Meides et al., 2022). This approach revealed the underlying photochemical processes for selected plastic types (Yousif and Haddad, 2013; Grause et al., 2020; Chamas et al., 2020; Rodriguez et al., 2020; Lee and Li, 2021; Andrady et al., 2022) and a better understanding of mechanisms that promote fragmentation (Plohl et al., 2022; Meides et al., 2022; Menzel et al., 2022). Studying samples from the environment, in turn, can also be beneficial as they may reveal additional insights that should be looked into further. Recently, Scott et al. investigated the degradation of print cartridges from a cargo spill and compared it to pristine and unexposed cartridges (Scott et al., 2022). By studying the morphology and chemical composition of the sample surface, they reported a strong heterogeneous degradation distribution that was linked to the additive TiO_2. However, it remains open if these observations can be extended to the entire sample volume. Studies on artificially-aged samples showed that degradation can be present inside the sample (Menzel et al., 2022; Meides et al., 2021). This suggests that the heterogeneity on the surface may continue into the sample and, therefore, play a part in polymer degradation. Here, artificially-aged plastics can help studying the evolution of these heterogeneities systematically. Looking at the chemical changes inside the sample, however, is a major challenge in environmental research studies.

Molecular changes linked to plastic degradation, such as weathering-induced oxidation, are commonly studied with techniques based on infrared (IR) spectroscopy (Gillen and Clough, 1989). Since those techniques examine the sample surface or thin, IR-transparent layers, investigating degradation over the entire volume requires extensive sample preparations to expose the cross-section (Nagai et al., 2005; Rivaton et al., 2002; Bokria and Schlick, 2002; Motyakin and Schlick, 2002). Typically, this is achieved by using a microtome to cut out layers from the sample. Depending on the sample size and shape, it may also be necessary to stabilize the sample in a resin (Gardette, 1995) which raises concerns about sample contamination that could interfere with the data interpretation. One technique that omits this preparation is Fourier-transformed infrared (FTIR) spectroscopy in attenuated total reflection (ATR) mode. Here, the sample is in contact with a crystal and the angle of the incident light is varied to examine the sample at distances up to 5 μm below the sample surface (Scott et al., 2022; Gillen and Clough, 1989). Such penetration depths are much lower compared to the sample sizes present in the environment which can be up to a few centimeters. Alternative techniques are, therefore, desirable that do not require an exposure of the sample's cross-section and can acquire measurements at greater depths with respect to the sample's original shape.

Recently, laser-induced breakdown spectroscopy (LIBS) has been used to study the chemical composition of weathered polymers, such as aged microplastics covered by biofilms (Pořízka et al., 2023), artificially aged paint samples (Brunnbauer et al., 2020) and artificially weathered polystyrene (PS) (Sommer et al., 2022). The latter study demonstrated that LIBS is sufficiently sensitive to study photo-oxidation in polystyrene without the need to expose its cross-section and to detect the ability of the additive Irgafos 168 to slow down weathering-induced oxidation in PS. For degradation studies on the sample surface, the results were comparable to those acquired with FTIR. LIBS, however, has the additional advantage that degradation can be systematically studied at different depths beyond 5 μm without exposing the cross-section. This motivates further studies into weathering-induced chemical changes for different types of plastic as their development could be beneficial for understanding their long-term fate in our environment. In the present study, we investigated the degradation of three common plastic types, namely PS, polyethylene (PE), and polypropylene (PP) that were weathered by following an ISO standard protocol. Our study reveals plastic-type-dependent responses to weathering on the sample surface and in the sample volume. They are related to the formation of microcracks and the materials lattice structure which for PE and PP is semi-crystalline and for PS amorphous. The results underline LIBS' capabilities to study weathering-induced molecular changes over the sample volume and on its surface. It can, therefore, provide additional insights into plastic degradation that complement our current understanding of the life cycle of plastic debris.

2. Materials and methods

2.1. Materials and aging of plastics

For this study, we chose three commercially available polymers with different physical and chemical structures. PS (Styrolution PS158 N) delivered by INEOS Styrolution Group (Frankfurt am Main, Germany) represents an amorphous polymer type, whereas PE (Lupolen, 1800P) and PP (Moplen HP526J), both delivered by LyondellBasell (Rotterdam, Netherlands), have a semi-crystalline structure. Furthermore, the selected grade for PP contains low amounts of antioxidative additives. This additive has been studied in (Meides et al., 2022). For all polymer types, ISO 527-2 type 1A tensile bars were injection molded (Arburg Allrounder 470H 1000-170, Arburg GmbH, Loßburg, Germany) and subsequently exposed to artificial weathering in a Q-SUN XE-3 (Q-LAB Corporation, Westlake, OH) equipped with three xenon arc lamps. The weathering conditions correspond to the ISO 4892–2:2011 with a constant irradiance set to 60 W/m^2 at 300 nm − 400 nm and a chamber temperature of 38 °C. All PS samples were collected after 200, 400, 800, 1400, and 2000 h of total exposure. The PE and PP samples were collected after 200, 400, 800, 1400, 2000, and 3200 h of total exposure.

2.2. Laser-induced breakdown spectroscopy (LIBS)

LIBS is a type of atomic emission spectroscopy that uses the light emitted from a plasma for material characterization. For this purpose, an energetic, pulsed laser beam is focused onto the sample which couples its energy into the material. As it gets excited and evaporates, the plasma is formed with the surrounding atmosphere. While the plasma is cooling down, element-specific light is emitted which can be resolved with a spectrometer and thus, allows us to track specific elements in the material. Since for our study, we are interested in chemical changes due to weathering-induced oxidation, we focus on the light emitted by the oxygen in the sample. The lifetime of the plasma is typically between 0.5 μs and 10 μs, which makes LIBS a fast detection method (Noll and Noll, 2012). In principle, this method can be applied to all samples regardless of their state of aggregation. For solid samples, a permanent crater is formed which typically corresponds to an ablated mass of tens to hundreds of nanograms (Gaudiuso et al., 2010). Because of that, LIBS is a minimal destructive method. By repeating the measurement on the same crater, we generate a bigger and deeper hole, which allows us to evaluate the chemical composition at different depths. Note that repeated measurements on the same location do not affect the aging of polymers. This is due to the fact that laser ablation only changes the physical properties of the material under study (plasma formation) and not its atomic composition.

Fig. 1 illustrates the built LIBS system that was used in this study. The system utilized a 532 nm Q-switched Nd-YAG laser (Quantel, Brilliant b model) that operated at 12.5 mJ with a pulse duration and a repetition rate of 4 ns and 10 Hz, respectively. These settings produced a laser pulse with a spot size of approximately 80 μm and a fluence of around 6.22×10^{10} W/cm^2. To collect the light emitted from the plasma, we used an optical arrangement that consisted of a 10 × -objective, a lens (f = 20 cm), and a beam splitter BS (Thorlabs, EBS1). The spectrum was

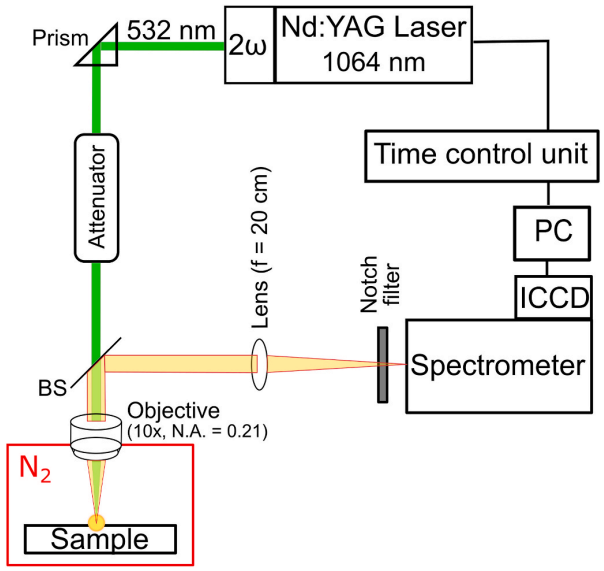

Fig. 1. Illustration of the LIBS system.

acquired with a spectrometer (Newport Corporation, MS257) that has a grating of 300 lines/mm, an entrance slit of 20 μm and a wavelength range of 300 nm–800 nm. It was attached to a time-gated intensified charge-coupled device (ICCD) camera (Andor, iStar DH720-18 U-03), where the gate delay and the gate width were set to 100 ns and 1000 ns, respectively. These settings were particularly chosen to maximize the atomic signal that corresponds to the oxygen in the sample. They were derived from another study that reported that atomic signals are emitted earlier from the plasma while molecular signals appear later (Grégoire et al., 2011). Note that these parameters could be further optimized which is out of the scope of this study.

Since the light emitted from the plasma also includes signals from elements in the ambient air, additional precautions were necessary to remove the oxygen from the air. For that reason, we conducted all measurements in nitrogen gas which has proven to be beneficial in previous studies (Sommer et al., 2022; Dong et al., 2012; Mousavi et al., 2016). The gas used had a purity of 99.999% and the gas flow was directed under the sample holder. The humidity inside the chamber was kept between 0 % and 15% and the measurements were conducted at atmospheric pressure. The influence of air and nitrogen atmosphere on the LIBS data can be found in the supporting information. Here it becomes evident that the nitrogen atmosphere is sufficient to remove any residual oxygen in the sample chamber, as the oxygen line is absent in unweathered samples. To confirm that the measured oxygen intensities were not influenced by the atmosphere, an example of a distorted oxygen line in air is also shown. This difference in influence explains why the choice of ambient atmosphere is dependent on the research question.

2.3. Spectral acquisition with LIBS

Prior to the measurements, all samples were cleaned with 2-propanol and then fixed on the sample holder that was mounted perpendicular to the incident laser beam. For the surface analyses, a single-shot spectrum was taken from ten different sample spots. The depth profile measurements were conducted on three distinct spots. For such measurements, the maximum achievable depth is limited by the capabilities of the LIBS system to focus the laser pulse to the bottom of the ablated hole. These capabilities, in turn, depend on the width and depth of the generated hole. For example, by increasing the width of the hole, which could be achieved by increasing the system's spot size, it is possible to increase the maximum penetration depth of the system. This, however, would decrease the lateral and longitudinal resolution which is not in favor of studying heterogeneous weathering. With our system, we achieved 60 shots for each sample location and readjusted the focal plane after every three consecutive shots. For the evaluation, we adopt the same procedure described in our previous study: for each shot number, we take the corresponding spectrum of each spot and calculate the mean value and the standard deviation (Sommer et al., 2022).

The flat field was calculated and included for all spectra. In addition, the continuum background of the plasma light was fitted using a 4th-degree polynomial function and subtracted from the data. This way the vicinity of the emission line of interest is set to zero and the data are compared to each other in dependence of the continuum. This approach eliminates systematic errors in the setup and assures reproducible data during the acquisitions. After that, we eliminated any excessive noise in the signal by smoothing each spectrum with the Savitzky-Golay filter in the Python package *SciPy* (Virtanen et al., 2020). For this procedure, we set the mandatory filter parameters *filter window* and *polynomial order* to 11 and 5, respectively. The smoothing step was necessary to avoid any evaluation of the noise by mistake. Since for each acquired spectrum, the atomic peaks were larger than the noise intensity, the risk of a peak disappearing by smoothing is low. Additional details on the effects of smoothing on the LIBS data and the data used for the surface analysis can be found in the supporting information. For better comparability, all data were normalized to the noise level by calculating the signal-to-noise ratio.

2.4. Crater depth characterisation

To relate the shot number to a depth in the sample, we used a profilometer (cybertechnologies, cyberscan CT 100) to measure the surface of an area with ablation craters. The lateral resolution was set to 5 μm. The depth of a crater was then determined by extracting the maximum depth in the crater area. We accounted for possible irregularities linked to the sample surface, e.g. bumps or tilts, as follows: first, we removed all craters from the measurement; then, we fitted a polynomial function to the remaining surface data; and finally, we used the fit to correct the unaltered measurement.

2.5. Fourier-transform infrared spectroscopy (FTIR)

The FTIR measurements were conducted with a standalone FTIR system (Bruker, LUMOS II) that comes with its own software (OPUS, version 8.5.29). The system has a single-element thermo-electrically cooled mercury-cadmium-telluride detector and a motorized germanium attenuated total reflection (ATR) crystal. We operated the system in ATR mode and, for clarity, shall refer to the acquired data as FTIR data. The sample and background spectra were acquired in the mid-infrared spectral range (4000 cm^{-1}-680 cm^{-1}) with an open aperture, 50 co-added scans, and a resolution of 4 cm^{-1}. Each sample was measured at 16 different spots. The resulting spectrum for a sample was averaged over the spectra of all spots and smoothed for atmospheric effects in the spectral regions of carbon dioxide and water. After that, we applied a baseline correction to account for the noise originating from the surrounding environment of the molecule (Walfridson and Kuttainen Thyni, 2022). Our implementation of the correction was as follows: for each peak of interest, we selected the minimum and maximum wavenumber that encloses the peak. Next, we fitted a linear function to the pair of data and subtract the interpolated values from the measurements in that range. Spectral values that, as a result, became negative were set to zero. The samples were measured with *medium pressure* which is a setting in the software.

2.6. Spectral line identification

To determine the oxygen content in PE, PP, and PS from the LIBS

spectra, we use the atomic transition lines for oxygen that are listed in the NIST atomic spectra database (Kramida et al., 2021). We chose peak O I 777.3 nm for the qualitative analysis with LIBS due to its robust transition probability and line strengths in the nitrogen atmosphere. This is in accordance with previous studies (Brunnbauer et al., 2020; Sommer et al., 2022; Davari et al., 2017). The sum of pixel intensities between 775.5 nm and 778 nm was calculated and used as input value for the analysis.

For the FTIR data, the extent of oxidation was evaluated using the carbonyl index (CI). However, since there is currently no standard method to calculate the CI value, it was necessary to select a method beforehand (Walfridson and Kuttainen Thyni, 2022). Various studies suggested to use a specified area under the band normalized to a reference bond that is mostly unaffected by the oxidation process (Walfridson and Kuttainen Thyni, 2022; Almond et al., 2020; Vicente et al., 2009). We, therefore, use the following equation for calculating CI:

$$CI = \frac{\text{Area under the absorption peak of the carbonyl compound}}{\text{Area under the absorption peak of the reference bond}}$$

For all samples, the spectral region of the carbonyl (C═O) vibration peak is set to 1850 cm^{-1}-1650 cm^{-1}. For PE and PP, the methylene (CH_2) scissoring peak in the range 1500 cm^{-1}-1420 cm^{-1} has been used as the reference bond (Almond et al., 2020). For PS, we only use the maximum intensity of the methylene peak at 1451 cm^{-1}. This was necessary because in this region a broad shoulder peak (CO) originating from weathering distorts the area under the methylene peak (Vicente et al., 2009).

All FTIR spectra used in this study can be found in the supporting information.

3. Results and discussion

Our goal is to use LIBS to investigate weathering-induced oxidation in different plastic types. We start by investigating the oxidation on the sample surface and afterwards, evaluate its progression into the sample. The surface measurements of LIBS are compared with corresponding FTIR measurements in order to validate LIBS as an oxygen detection method. Once the LIBS measurements are confirmed, we can assume that the results are valid for the depth profile analysis.

3.1. Surface analysis

Fig. 2 shows the oxidation level on the surface as a function of weathering duration for all plastic types. The oxygen intensities extracted from the LIBS spectra are highlighted as red dotted lines. Amongst all plastic types, the measurements corresponding to PS (●) immediately stand out. Prior to 200 h of weathering, we detect little to no oxygen uptake on the surface. Once the weathering time exceeds 200 h, the oxygen peak intensity increases. Between 400 h and 800 h, we observe a steep increase in the peak intensity after which it saturates to a constant level. This characteristic behavior reflects the structural changes in the polymer chains of the sample. During oxidation, those chains break down which form hydroxy, peroxo, keto, carboxy, and vinyl defects (Meides et al., 2021; Shi et al., 2019; Vaillant et al., 1994). These defects can only be formed while the backbone of the polymer is still intact. Therefore, once the backbone is completely degraded, the polymer is completely oxidized and the sample can no longer absorb oxygen. In our data, this stage is reached when the oxygen level is saturating.

In comparison to PS, the surface oxidation of PE (■) and PP (▼) is less pronounced. For PE, we see a steady increase in the oxygen intensity after 400 h of weathering which appears to saturate after 2000 h. Our data also reveals a statistically significant amount of oxygen in the unweathered sample that could be related to surface contamination. This will be apparent in the latter part of our analysis. For PP, the oxygen peak intensity increases almost linearly with increasing weathering time until the sample has been weathered for 1400 h. Note that due to increasing surface embrittlement of the PP samples as a result of weathering, shot-to-shot fluctuations become more likely. This results in increased error bars, as it is visible for 1400 h, 2000 h and 3200 h weathered PP. Within the error bars, the oxygen intensity saturates. Following our measurements for all plastic types, PS samples are significantly more oxidized on the surface than the PE and PP samples. This behavior is related to the underlying structure of each plastic type. In general, materials with crystalline structures are chemically inert. Consequently, they absorb less oxygen and, as a result, degrade slower (Patterson and Bailey, 2007; Sastri and Sastri, 2010; Plackett et al., 2011). With respect to our samples, PE and PP have a partly crystalline and partly amorphous lattice structure while PS is amorphous. Consequently, more oxidation occurs in the latter compared to the former two

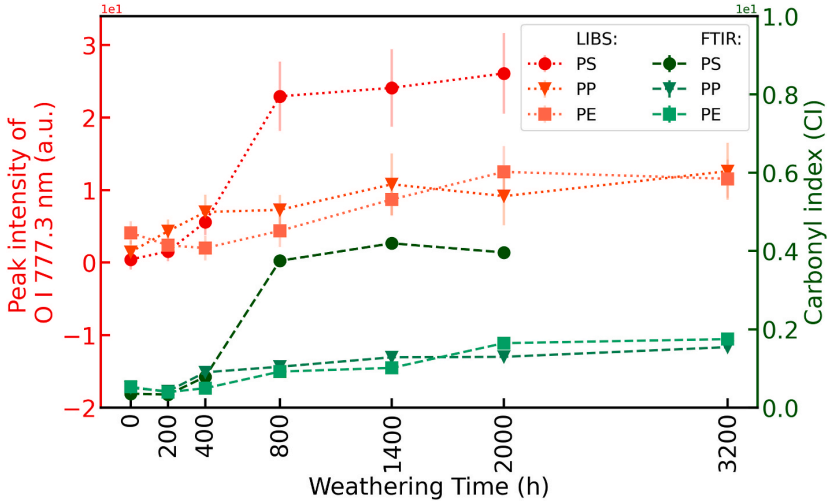

Fig. 2. Oxygen intensity for different weathering times. The plot shows the degree of oxidation detected in the LIBS measurements (oxygen intensity around 777.3 nm is displayed on the left axis) and the FTIR measurements (the sum of carbonyl compounds normalized to a reference bond is displayed on the right axis). With increasing weathering time, the oxidation on the surface of all samples progresses. Each LIBS data point is an average of ten measurements. Each FTIR data point is the average of 16 measurements. The average value is depicted as a symbol while the standard deviation is represented as a line.

plastic types. The data suggests that LIBS may also be used to extract information on the degree of crystallinity. However, this is out of the scope of this study.

To validate our insights from the LIBS measurements, we also conducted FTIR measurements on the samples. In Fig. 2, the CI values calculated from the FTIR spectra are highlighted as green dashed lines. The elevated CI value for the unprocessed PE confirms our previous observation with LIBS even though the elevation is not as clear as in the measurements with LIBS. Still, this suggests an effect that is related to external contamination. Looking further, the surface oxidation of PS compared to PE and PP is more pronounced in the FTIR data than in the LIBS data and we observe differences in the oxidation levels at 200 h. The reason for these observations is the different sampling depth which is larger for LIBS than for FTIR (Sommer et al., 2022). With LIBS, the ablation depths of one laser shot for PS, PE, and PP are (14.04 ± 4.50) µm, (25.05 ± 5.68) µm and (36.25 ± 9.57) µm, respectively. Note that the crater depth was averaged over all weathering stages. This leads to a higher deviation, since the crater depends on the structural robustness of each plastic type, which can change with increasing weathering time. The crater depth for 60 laser shots, given separately for different weathering times, can be found in the supporting information. FTIR, in turn, has a maximum penetration depth of 5 µm. The oxygen content in LIBS is, therefore, averaged over a larger volume. Since it can be expected that oxidation penetrates into the samples, LIBS detects oxygen that lies in deeper layers. As we will see in the course of this study, oxygen penetrates into deeper layers for PE and PP samples than for PS. Therefore, we see differences when comparing the absolute values between LIBS and FTIR measurements.

Overall, both techniques reveal a similar trend in the samples which suggests that both techniques are comparable. This confirms that LIBS is suitable to study surface oxidation on different sample types. Note that further research is required to evaluate the comparability of the oxygen intensity in the LIBS spectrum with the CI value extracted from the FTIR spectrum due to their physically different origins.

3.2. Depth profile analysis

Fig. 3 summarizes the measured depth profiles of oxygen for all plastic types at three different weathering stages. Each plot shows the oxygen peak intensity as a function of the number of shots which represents the depth for a specified plastic type. The red data points (■) represent the samples with the largest weathering time, i.e. 3200 h for PP and PE, and 2000 h for PS. The orange data set (▲) corresponds to samples weathered for 800 h and the black data set (●) refers to the unweathered plastics.

Fig. 3 (a) summarizes the depth profiles acquired for PP. The depths corresponding to 60 shots, given separately for all weathering stages and plastic types, can be found in the supporting information. Here, 60 shots averaged over all weathering stages have an approximate depth of 412 µm. For the unweathered sample, the oxygen content for all layers is consistently around zero which confirms that no oxidation took place in the sample. Once the sample has been weathered for 800 h, we detect oxygen up to the ninth layer of the sample. The drop in the oxygen intensity appears to be non-linear which provides evidence that weathering-induced oxidation into the sample is heterogeneous. The depth profile for the sample weathered for 3200 h reveals that this trend continues where oxygen can now be detected up to the 60th layer.

Fig. 3 (b) shows the depth profiles acquired for PS. The depth for 60 shots averaged over all weathering stages is approximately 266 µm. As before, the depth profile of the unweathered sample shows no evidence of any oxidation in the sample volume. While the oxygen peak intensities on the surface of both weathered samples are identical, we do see an elevated oxygen peak intensity inside the 2000-h-weathered sample. In both samples, we do not detect any oxygen beyond the seventh layer which is in contrast to our observations for PP.

Fig. 3 (c) sums up the depth profiles measured for PE. Here, the depth for 60 shots averaged over all weathering stages corresponds to approximately 272 µm. In the unweathered sample, we observe that the oxygen peak intensity on the surface drops to zero after the first shot. This immediate drop supports our hypothesis that the oxygen content of the unweathered PE sample has been contaminated, as the contamination only occurs on the surface. For all weathered samples, we observe oxygen penetrating into the sample. After 800 h of weathering, oxygen can be detected until the 25th layer. In the 3200-h-weathered sample, oxygen is clearly detectable up to the 60th layer. In comparison to PP, the decrease in oxygen intensity in the weathered samples is slower. This illustrates clearly the benefits of analyzing the sample at different depths as they may provide hints for some anomalies in a measurement.

In addition to the lattice structure, one contribution that promotes different responses of polymers to weathering is the formation of microcracks. These morphological structures can facilitate oxygen uptake, as it can directly reach deeper layers which is much faster than diffusing through the solid material. The formation of microcracks in PE and PS has already been extensively studied elsewhere (Menzel et al., 2022; Meides et al., 2021). For PE, microcracks appear after 1400 h of weathering while for PS, the mechanical and surface embrittlement correlate (Menzel et al., 2022; Meides et al., 2021). Once microcracks are formed, their length and depth increase with progressive weathering time. Menzel et al. reported that PS is less prone to surface embrittlement than PE due to its amorphous structure. On the one hand, the amorphous structure of PS has a low mobility of polymer chains due to its high glass transition temperature (T_g) of 100 °C. The more rigid the chains, the more oxidation takes place on the surface and not inside the samples, as oxygen diffusion is hindered by the low mobility of polymer chains (Rabek, 2012). The polymer chains in PE, on the other hand, are highly mobile (T_g < room temperature) which results in molecular rearrangement in the amorphous regions and subsequent chemo-crystallization into crystalline units. These rearrangements result in stress-induced crack formation on the surface of PE. Consequently, these cracks are much more pronounced than the ones in PS (Menzel et al., 2022). Transferring these findings to our study, we observe that less oxygen is absorbed in PE and PP compared to PS due to their semi-crystalline structure. This is reflected in Figs. 2 and 3 where the intensities relative to each other are different. However, due to the microcracks, oxygen travels deeper into the sample which results in oxidation in deeper layers. This explains why PE and PP show oxidation inside the sample compared to PS where oxidation only is detectable to the ninth layer. In the latter case, oxygen diffusion through the solid structure in order to reach these layers is hindered by low chain mobility. For PE and PP, oxygen diffusion into deeper layers is promoted along the cracks and by high chain mobility, reducing the reaction rate in the surface-near layers.

The influence of the semi-crystalline structure of PE and PP is also visible in their corresponding depth profiles in Fig. 3 (a) and (c). Compared to PS (Fig. 3 (b)), each data point has much larger error bars which indicate that the depth profiles between different spots vary. In PE and PP, the detected oxygen content depends on the lattice structure that is present on the selected spot which is either amorphous or crystalline. As a result, the oxygen content is strongly location dependent and thus, can lead to broad fluctuations between the measurements. For PS, these fluctuations are barely observed since the lattice structure for different spots is always amorphous. In conclusion, the fluctuations highlight LIBS' capability to study the heterogeneity of weathering-induced oxidation in plastics. These heterogeneities can be attributed to the lattice structure of the samples and their ability to form microcracks.

4. Conclusion

The investigation of heterogeneous plastic degradation is not only caused by different environmental conditions but also related to the underlying lattice structure and microcracks formation of each plastic

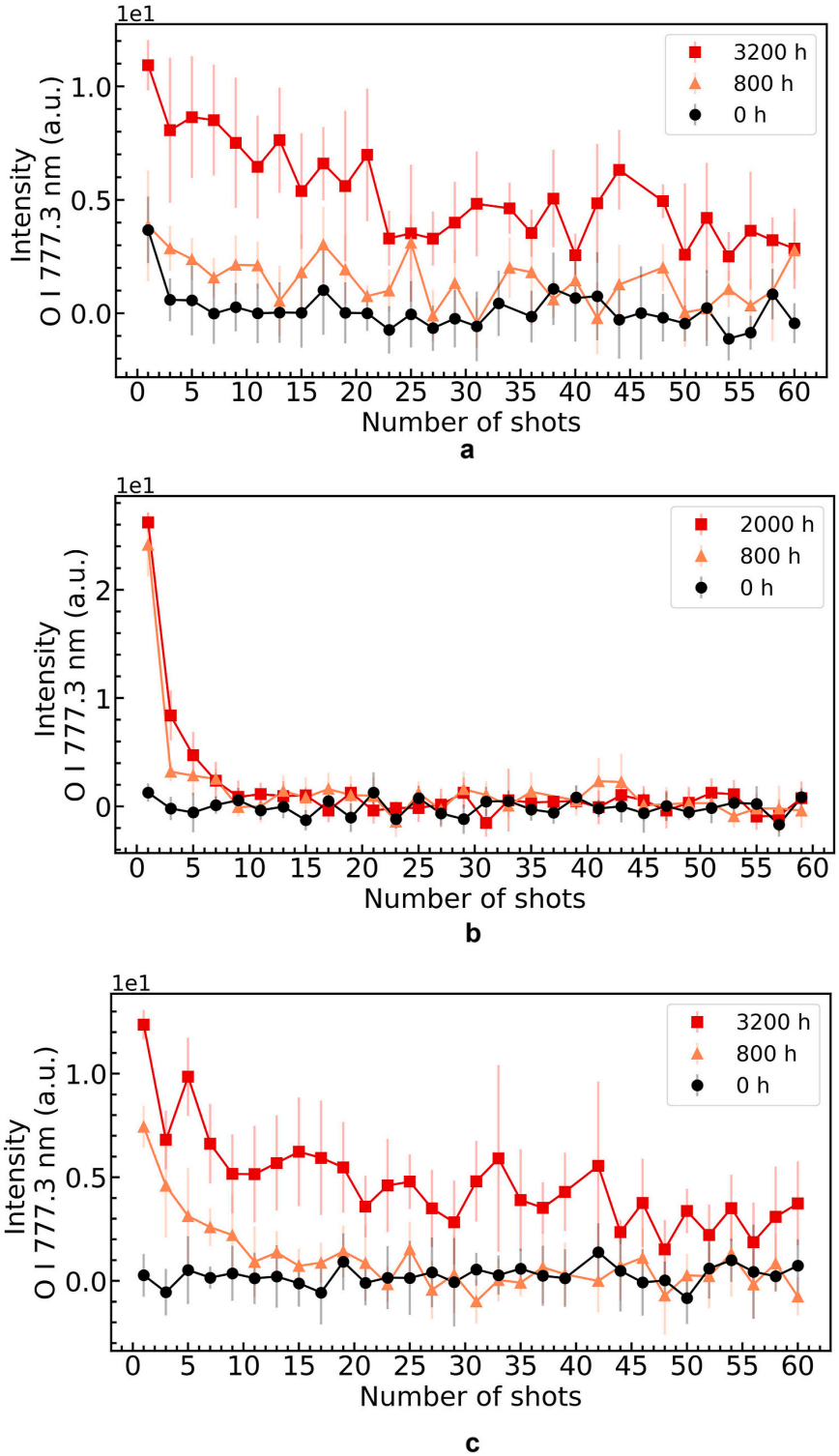

Fig. 3. Heterogeneous oxidation profiles for different plastic types up to 3200 h of weathering. (a), (b), and (c) show the oxygen intensity with an increasing number of shots for PP, PS, and PE, respectively. For visualization reasons, every second laser shot was omitted from the plot. The complete depth profiles can be found in the supporting information. Each data point is the average over three measurements. The average is depicted as a symbol and the standard deviation as a line. Please note that the removal of a layer and consequently the depth progression is not uniform, since the crater is not only increased in depth but also in width with each shot (cf. supporting information).

type. It implies that the degradation processes, including fragmentation, are not limited to the sample surface but rather over the entire volume. This adds another layer of complexity to the assessment of the fate of plastic debris. In this study, we demonstrated the capabilities of LIBS for depth profiling of artificially weathered plastics. This method could be extended in the future to obtain a three-dimensional chemical imaging. We found significant location-dependent fluctuations, which highlights the importance to study degradation with sufficiently high spatial resolution. Here, our results confirm the conclusions reported in other studies which underline the suitability of LIBS as a complementary technique.

Our results show the changes in the oxygen content of weathered plastics with a depth resolution of a few micrometers. The fact that no cross-section of the samples had to be exposed for depth profile analysis of several hundred micrometers makes this method much faster than conventional procedures. Note that the crater size and, consequently the depth resolution, are system dependent and thus, can be further optimized.

As a validation step, the LIBS measurements were compared to FTIR measurements on the surface of the samples. This comparison showed that analyzing sample oxidation with LIBS is more practical than an evaluation with FTIR. FTIR lacks a standard method to calculate the CI value which complicates evaluations and comparisons between different studies on weathering-induced oxidation of polymers (Almond et al., 2020).

In conclusion, this study makes an important contribution to environmental research by shedding light on the different aging processes inside various plastic types. These heterogeneous processes on the surface and in the sample are essential for understanding weathering-induced changes, such as size evolution, degradation rate, and degradation state. This encourages further research, e.g. measuring heterogeneous oxidation profiles of microplastic particles, which can provide additional hints on their fate, as well as detection limits, matrix effects or interferences by additives. Such studies have, to our knowledge, not been conducted yet.

Funding

Part of this project was funded by the Deutsche Forschungsgemeinschaft (DFG, German Research Foundation) - Project Number 391977956 - SFB 1357, subproject C01.

CRediT authorship contribution statement

Caroline Sommer: Investigation, Conceptualization, Methodology, Software, Formal analysis, Visualization, Writing – original draft, Writing – review & editing. **Johnny Nguyen:** Writing – original draft, Writing – review & editing, Conceptualization. **Teresa Menzel:** Resources, Validation, Conceptualization, Writing – review & editing. **Holger Ruckdäschel:** Project administration, Writing – review & editing. **Martin Koch:** Project administration, Writing – review & editing.

Declaration of competing interest

The authors declare that they have no known competing financial interests or personal relationships that could have appeared to influence the work reported in this paper.

Data availability

Data will be made available on request.

Acknowledgments

We thank Dr. Frank Noll, Dr. Hee-Cheol Kim and Nima Heidary for providing their expertise for the profilometer measurements.

Appendix A. Supplementary data

Supplementary data to this article can be found online at https://doi.org/10.1016/j.chemosphere.2023.140105.

References

Almond, J., Sugumaar, P., Wenzel, M.N., Hill, G., Wallis, C., 2020. Determination of the carbonyl index of polyethylene and polypropylene using specified area under band methodology with atr-ftir spectroscopy. E-Polymers 20, 369–381.
Andrady, A., Barnes, P., Bornman, J., Gouin, T., Madronich, S., White, C., Zepp, R., Jansen, M., 2022. Oxidation and fragmentation of plastics in a changing environment; from uv-radiation to biological degradation. Sci. Total Environ. 851, 158022 https://doi.org/10.1016/j.scitotenv.2022.158022.
Barnes, D.K.A., Galgani, F., Thompson, R.C., Barlaz, M., 2009. Accumulation and fragmentation of plastic debris in global environments. Phil. Trans. Biol. Sci. 364, 1985–1998. https://doi.org/10.1098/rstb.2008.0205.
Bokria, J.G., Schlick, S., 2002. Spatial effects in the photodegradation of poly (acrylonitrile–butadiene–styrene): a study by atr-ftir. Polymer 43, 3239–3246. https://doi.org/10.1016/S0032-3861(02)00152-0.
Brunnbauer, L., Mayr, M., Larisegger, S., Nelhiebel, M., Pagnin, L., Wiesinger, R., Schreiner, M., Limbeck, A., 2020. Combined la-icp-ms/libs: powerful analytical tools for the investigation of polymer alteration after treatment under corrosive conditions. Sci. Rep. 10, 1–10.
Chamas, A., Moon, H., Zheng, J., Qiu, Y., Tabassum, T., Jang, J.H., Abu-Omar, M., Scott, S.L., Suh, S., 2020. Degradation rates of plastics in the environment. ACS Sustain. Chem. Eng. 8, 3494–3511. https://pubs.acs.org/doi/10.1021/acssuschemeng.9b06635. doi:10.1021/acssuschemeng.9b06635.
Davari, S.A., Hu, S., Pamu, R., Mukherjee, D., 2017. Calibration-free quantitative analysis of thin-film oxide layers in semiconductors using laser induced breakdown spectroscopy (libs). J. Anal. Atomic Spectrom. 32, 1378–1387.
Dong, M., Mao, X., Gonzalez, J.J., Lu, J., Russo, R.E., 2012. Time-resolved libs of atomic and molecular carbon from coal in air, argon and helium. J. Anal. Atomic Spectrom. 27, 2066–2075.
Gardette, J.-L., 1995. Heterogeneous photooxidation of solid polymers. Angew. Makromol. Chem. 232, 85–103. https://doi.org/10.1002/apmc.1995.052320106.
Gaudiuso, R., Dell'Aglio, M., De Pascale, O., Senesi, G.S., De Giacomo, A., 2010. Laser induced breakdown spectroscopy for elemental analysis in environmental, cultural heritage and space applications: a review of methods and results. Sensors 10, 7434–7468.
Gillen, K.T., Clough, R.L., 1989. Techniques for monitoring heterogeneous oxidation of polymers. Marcel Dekker, Inc., Handbook Polym. Sci.Technol. 2, 167–202.
Grause, G., Chien, M.-F., Inoue, C., 2020. Changes during the weathering of polyolefins. Polym. Degrad. Stabil. 181, 109364 https://doi.org/10.1016/j.polymdegradstab.2020.109364.
Grégoire, S., Boudinet, M., Pelascini, F., Surma, F., Detalle, V., Holl, Y., 2011. Laser-induced breakdown spectroscopy for polymer identification. Anal. Bioanal. Chem. 400, 3331–3340.
Kramida, A., Ralchenko, Y., Reader, J., Team, N.A., 2021. NIST Atomic Spectra Database. https://doi.org/10.18434/T4W30F. URL:, version 5.9. https://physics.nist.gov/asd.
Lee, Q.Y., Li, H., 2021. Photocatalytic degradation of plastic waste: a mini review. Micromachines 12, 907. https://doi.org/10.3390/mi12080907.
Lim, X., 2021. Microplastics are everywhere — but are they harmful? Nature 593, 22–25. http://www.nature.com/articles/d41586-021-01143-3. doi:10.1038/d41586-021-01143-3.
MacLeod, M., Arp, H.P.H., Tekman, M.B., Jahnke, A., 2021. The global threat from plastic pollution. Science 373, 61–65. https://doi.org/10.1126/science.abg5433.
Meides, N., Menzel, T., Poetzschner, B., Löder, M.G., Mansfeld, U., Strohriegl, P., Altstaedt, V., Senker, J., 2021. Reconstructing the environmental degradation of polystyrene by accelerated weathering. Environ. Sci. Technol. 55, 7930–7938.
Meides, N., Mauel, A., Menzel, T., Altstädt, V., Ruckdäschel, H., Senker, J., Strohriegl, P., 2022. Quantifying the fragmentation of polypropylene upon exposure to accelerated weathering. Microplastics and Nanoplastics 2, 23. https://doi.org/10.1186/s43591-022-00042-2.
Menzel, T., Meides, N., Mauel, A., Mansfeld, U., Kretschmer, W., Kuhn, M., Herzig, E.M., Altstädt, V., Strohriegl, P., Senker, J., et al., 2022. Degradation of low-density polyethylene to nanoplastic particles by accelerated weathering. Sci. Total Environ. 826, 154035.
Motyakin, M.V., Schlick, S., 2002. Thermal degradation at 393 k of poly(acrylonitrile-butadiene-styrene) (abs) containing a hindered amine stabilizer: a study by 1d and 2d electron spin resonance imaging (esri) and atr–ftir. Polym. Degrad. Stabil. 76, 25–36. https://doi.org/10.1016/S0141-3910(01)00262-2.
Mousavi, S., Hemati Farsani, M., Darbani, S., Mousaviazar, A., Soltanolkotabi, M., Eslami Majd, A., 2016. Cn and c 2 vibrational spectra analysis in molecular libs of organic materials. Appl. Phys. B 122, 1–16.
Nagai, N., Matsunobe, T., Imai, T., 2005. Infrared analysis of depth profiles in uv-photochemical degradation of polymers. Polym. Degrad. Stabil. 88, 224–233. https://doi.org/10.1016/j.polymdegradstab.2004.11.001.
Noll, R., Noll, R., 2012. Laser-induced Breakdown Spectroscopy. Springer.
Patterson, J.D., Bailey, B.C., 2007. Solid-state Physics: Introduction to the Theory. Springer Science & Business Media.
Plackett, D., Siró, I., 2011. 18 - polyhydroxyalkanoates (phas) for food packaging. In: Lagarón, J.-M. (Ed.), Multifunctional and Nanoreinforced Polymers for Food Packaging. Woodhead Publishing, pp. 498–526. https://doi.org/10.1533/

9780857092786.4.498. URL: https://www.sciencedirect.com/science/article/pii/B9781845697389500185.
Plohl, O., Sep, N., Zemljic, L.F., Vujanovic, A., Colnik, M., Fan, Y.V., Škerget, M., Klemeš, J.J., Cucek, L., Valh, J.V., 2022. Fragmentation of disposed plastic waste materials in different aquatic environments. Chem. Eng. Transact. 94, 1249–1254. https://www.cetjournal.it/index.php/cet/article/view/CET2294208. doi:10.3303/CET2294208.
Pořízka, P., Brunnbauer, L., Porkert, M., Rozman, U., Marolt, G., Holub, D., Kizovskỳ, M., Benešová, M., Samek, O., Limbeck, A., et al., 2023. Laser-based techniques: novel tools for the identification and characterization of aged microplastics with developed biofilm. Chemosphere 313, 137373.
Rabek, J.F., 2012. Photodegradation of Polymers: Physical Characteristics and Applications. Springer Science & Business Media.
Rivaton, A., Mailhot, B., Soulestin, J., Varghese, H., Gardette, J., 2002. Comparison of the photochemical and thermal degradation of bisphenol-a polycarbonate and trimethylcyclohexane–polycarbonate. Polym. Degrad. Stabil. 75, 17–33. https://doi.org/10.1016/S0141-3910(01)00201-4.
Rodriguez, A., Mansoor, B., Ayoub, G., Colin, X., Benzerga, A., 2020. Effect of uv-aging on the mechanical and fracture behavior of low density polyethylene. Polym. Degrad. Stabil. 180, 109185 https://doi.org/10.1016/j.polymdegradstab.2020.109185.
Sastri, V.R., 2010. Chapter 9 - other polymers: styrenics, silicones, thermoplastic elastomers, biopolymers, and thermosets. In: Sastri, V.R. (Ed.), Plastics in Medical Devices, Plastics Design Library. William Andrew Publishing, Boston, pp. 217–262. https://doi.org/10.1016/B978-0-8155-2027-6.10009-1. URL: https://www.sciencedirect.com/science/article/pii/B9780815520276100091.
Scott, J.W., Turner, A., Prada, A.F., Zhao, L., 2022. Heterogeneous weathering of polypropylene in the marine environment. Sci. Total Environ. 812, 152308 https://doi.org/10.1016/j.scitotenv.2021.152308.
Shi, Y., Qin, J., Tao, Y., Jie, G., Wang, J., 2019. Natural weathering severity of typical coastal environment on polystyrene: experiment and modeling. Polym. Test. 76, 138–145.
Sommer, C., Nguyen, J., Menzel, T., Prume, J.A., Ruckdäschel, H., Koch, M., 2022. Weathering-induced oxidation: an investigation of artificially aged polystyrene samples using laser-induced breakdown spectroscopy. Polym. Test. 112, 107623.
Vaillant, D., Lacoste, J., Dauphin, G., 1994. The oxidation mechanism of polypropylene: contribution of 13c-nmr spectroscopy. Polym. Degrad. Stabil. 45, 355–360.
Vicente, J.S., Gejo, J.L., Rothenbacher, S., Sarojiniamma, S., Gogritchiani, E., Wörner, M., Kasperb, G., Braun, A.M., 2009. Oxidation of polystyrene aerosols by vuv-photolysis and/or ozone. Photochem. Photobiol. Sci. 8, 944–952.
Virtanen, P., Gommers, R., Oliphant, T.E., Haberland, M., Reddy, T., Cournapeau, D., Burovski, E., Peterson, P., Weckesser, W., Bright, J., van der Walt, S.J., Brett, M., Wilson, J., Millman, K.J., Mayorov, N., Nelson, A.R.J., Jones, E., Kern, R., Larson, E., Carey, C.J., Polat, İ., Feng, Y., Moore, E.W., VanderPlas, J., Laxalde, D., Perktold, J., Cimrman, R., Henriksen, I., Quintero, E.A., Harris, C.R., Archibald, A.M., Ribeiro, A. H., Pedregosa, F., van Mulbregt, P., 2020. SciPy 1.0 contributors, SciPy 1.0: fundamental algorithms for scientific computing in Python. Nat. Methods 17, 261–272. https://doi.org/10.1038/s41592-019-0686-2.
Walfridson, M., Kuttainen Thyni, E., 2022. Automation of Carbonyl Index Calculations for Fast Evaluation of Microplastics Degradation.
Yousif, E., Haddad, R., 2013. Photodegradation and photostabilization of polymers, especially polystyrene: review. SpringerPlus 2, 398. https://doi.org/10.1186/2193-1801-2-398.

Supporting Information

S1. Influence of atmosphere on O I 777.3 nm emission line

In order to account for the oxygen concentration remaining in the sample chamber when flooded with nitrogen and its influence on the spectroscopic data, an unweathered PS sample was measured in air and in a nitrogen atmosphere. The results are presented in Fig. S1. The blue and green spectra represent the measurements in air and nitrogen, respectively. Since PS does no contain any oxygen in its chemical structure, an oxygen peak at 777.3 nm is not expected in the data. However, an emission line at this wavelength is clearly visible in the measurements in air (marked with a dotted black line). This line originates from the surrounding air which interacts with the plasma. When the unweathered PS sample is measured in nitrogen, the oxygen emission line disappears. We conclude that any remaining oxygen content in the sample chamber when flooded with nitrogen does not affect our results and can be neglected.

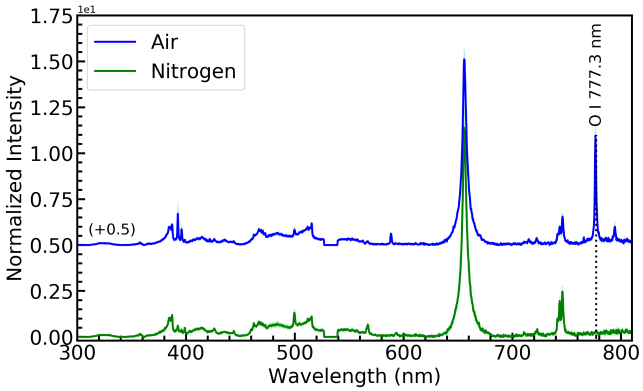

Figure S1: LIBS spectra of an unweathered PS sample measured in air and nitrogen atmosphere. The plot shows that the O I 777.3 nm emission line (dotted black line) is highly influenced by the surrounding atmosphere. The spectra are the average over 3 measurements (the average is depicted as a line, and the standard deviation as light background). For better comparability, the spectra are normalized to C2 ($\Delta\nu = 0$) and plotted with an offset.

S2. Smoothing of LIBS spectra

Smoothing can have strong effects on data as it eliminates outliers from data sets to make patterns more noticeable. However, it can also lead to the elimination of usable data points. To ensure that this is not the case, we compare smoothed and unsmoothed data. Fig. S2 shows the LIBS spectra of a PP sample weathered for 200 hours. The plot shows that the oxygen peak, marked with a dotted black line, is so pronounced that smoothing only helps to separate peak from noise, making the pattern more distinct. The smoothing parameters were set according to the instructions in chapter 2.3. They were chosen so that the noise does not completely disappear. In this way, small fluctuations in the peaks are still visible.

The smoothed LIBS data used for the surface analysis can be seen in the next section.

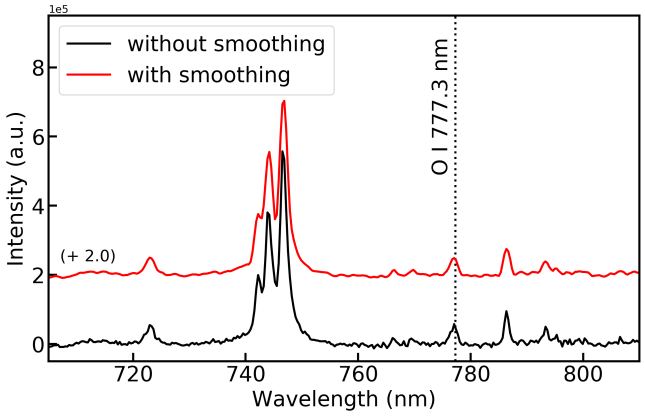

Figure S2: Smoothing effect on a 200 hours weathered PP sample. The plot shows the amount of noise reduction due to smoothing. The dotted black line marks the oxygen emission line. Both spectra are background subtracted and the average over 3 measurements. The black spectrum is unsmoothed. The red spectrum is smooth according to the instructions in chapter 2.3. For visualization reasons, the data is plotted with an offset.

In order to evaluate the effect of smoothing, signal-to-noise ratios (SNR)

were calculated. The SNR was calculated according to the following definition: $SNR = (I_{\text{signal}} - I_{\text{background}})/N_{\text{background}}$, where $N_{\text{background}}$ is the standard deviation of the background signal. The values can be found in table S1. Depending on the weathering time, the sample noises varies, increasing with weathering time. Table S1 supports our statement that smoothing has no negative impact on our data, in particular it does not cause an oxygen peaks to disappear. In general it can be said that the SNR increases with smoothing, while the error remains more or less constant.

	PE		**PP**		**PS**	
	without smoothing	with smoothing	without smoothing	with smoothing	without smoothing	with smoothing
0 h	3.1 ± 1.7	4.0 ± 1.5	1.3 ± 1.8	1.6 ± 1.7	0.3 ± 1.2	0.3 ± 1.1
200 h	1.7 ± 1.7	2.3 ± 1.5	3.4 ± 2.0	4.4 ± 1.8	1.3 ± 1.8	1.9 ± 1.6
400 h	1.6 ± 1.6	2.1 ± 1.8	5.0 ± 2.0	6.9 ± 2.2	5.1 ± 2.3	7.2 ± 2.4
800 h	3.2 ± 1.9	4.3 ± 1.8	5.4 ± 2.1	7.3 ± 2.1	18 ± 4	25 ± 4
1400 h	6.6 ± 2.5	8.8 ± 2.9	8 ± 4	11 ± 5	20 ± 5	27 ± 5
2000 h	9.0 ± 2.4	12.2 ± 2.4	6.7 ± 3.3	9 ± 4	20 ± 4	28 ± 4
3200 h	8.8 ± 2.9	11.6 ± 3.1	9.0 ± 3.2	12 ± 4	-	-

Table S1: Signal-to-noise ratio (SNR) for smoothed and unsmoothed data. The values correspond to the mean value and standard deviation for the SNR from three measurements on the sample's surface.

S3. LIBS spectra

In Fig. S3 the processed LIBS data for the surface analysis (cf. Fig. 2) is presented. It is noticeable that the oxygen peak is not the only peak that varies with weathering time. In the range below 770 nm, peak fluctuations are visible. These peaks were assigned to K I 766.5 nm and K I 769.9 nm and may be due to surface contamination. Note that the fluctuations of potassium or other peaks in the spectrum do not affect the analysis since only the area around the oxygen emission line was used for analysis.

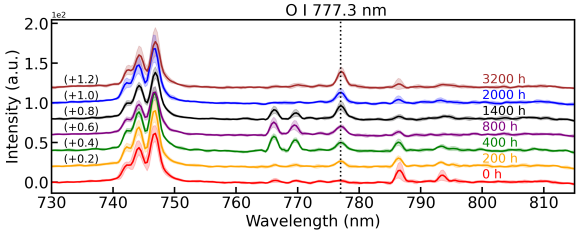

(a) PP

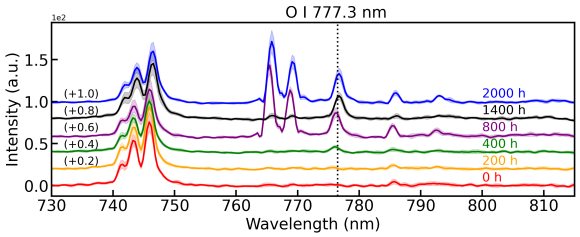

(b) PS

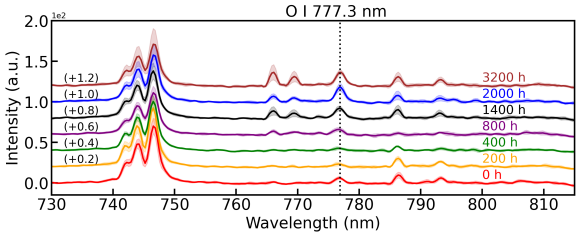

(c) PE

Figure S3: LIBS spectra of weathered PP, PS, and PE samples. The spectra are the average over 10 spots (the average value is depicted as a line, the standard deviation is depicted as a light background), background subtracted and smoothed according to section 2.3. The dotted black lines mark the oxygen emission line. For visualization reasons, the data is plotted with an offset.

S4. Oxygen intensity as a function of depth

	PE		PP		PS	
	60 shots	layer	60 shots	layer	60 shots	layer
0 h	190.4 ± 12.5	3.2 ± 0.2	220.4 ± 19.4	3.7 ± 0.2	282.2 ± 42.3	4.7 ± 0.2
800 h	180.6 ± 29.3	3.0 ± 0.5	327.0 ± 12.7	5.4 ± 0.5	276.0 ± 19.5	4.6 ± 0.5
2000 h	-	-	-	-	240.3 ± 41.0	4.0 ± 0.2
3200 h	447.0 ± 12.9	7.5 ± 0.2	687.2 ± 44.9	10.0 ± 0.2	-	-

Table S2: Maximum ablation depth for 60 laser shots for all samples. The values represent the mean value and standard deviation that were calculated from three measurements per sample. The values are given in µm.

Table S2 summarizes the maximum ablation depth in µm for 60 laser shots on each plastic sample that was included in this study. The craters corresponding to 60 shots have been measured using a profilometer. For each sample, we calculated the mean and standard deviation of three ablation craters according to section 2.4. The approximate layer thickness per shot was also calculated and is given in table S2.

Following Brunnbauer et al., the approximated layer thicknesses are used as depth per shot [1]. Note that these thicknesses are significantly smaller than the shot depths given in chapter 3.1. This is because the depth progression is not uniform. The crater increases not only in depth but also in width with each shot. In addition to that, the crater also depends on sample properties, such as texture, reflectivity, hardness, etc., which may vary inside the sample. To include all influences for the crater depths would go beyond the scope of this work, which is why the simplified approach of Brunnbauer et al. was chosen [1]. A plot showing oxygen intensity as a function of depth is given below. Please note that only 60 shots were taken for each sample. Deeper layers can be reached for the more weathered samples because the surface embrittlement

increases with the weathering time.

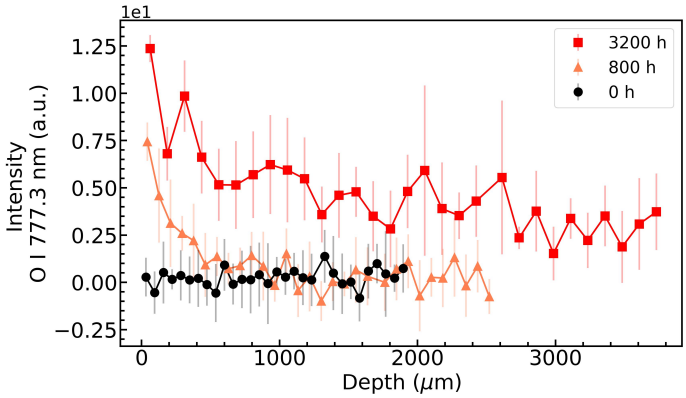

(a) PP

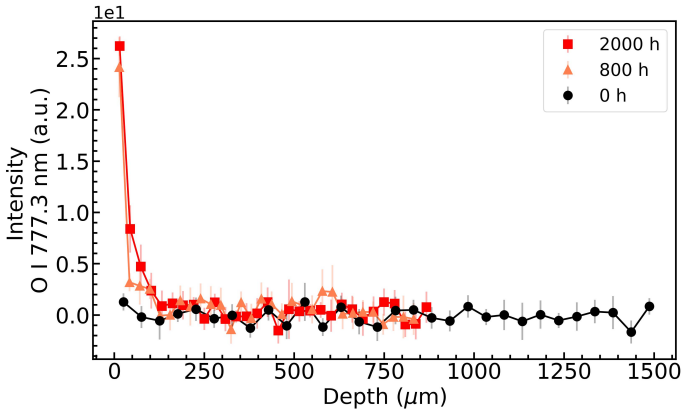

(b) PS

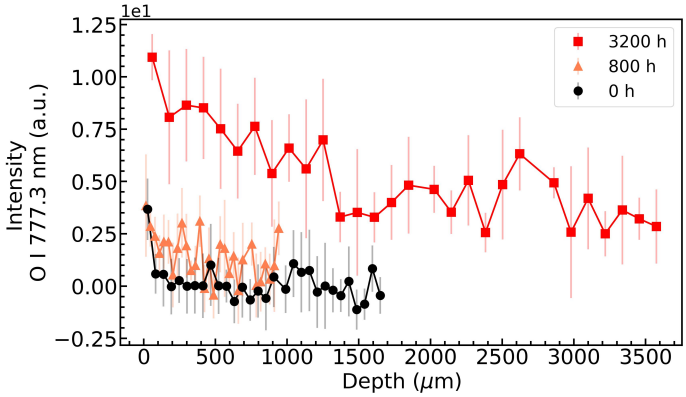

(c) PE

Figure S4: Oxygen intensity as a function of depth for PP, PS, and PE. The plot shows the course of oxidation with increasing depth. For visualization reasons only every second layer is displayed. The layer thickness are extracted from table S2.

S5. Depth profiles

In Fig. S5, the depth profiles of PP, PS, and PE are displayed. This figure is a supplement to Fig. 3 that shows all measurements inside the sample.

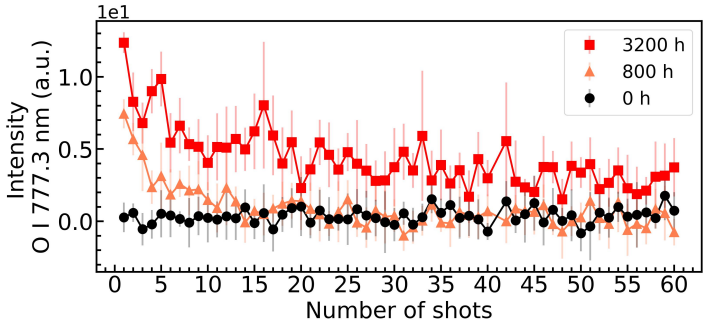

(a) PP

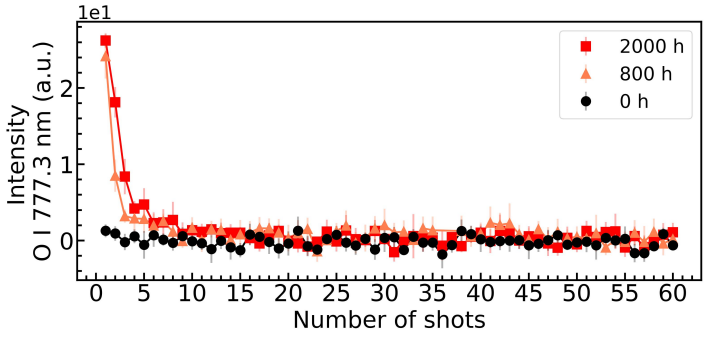

(b) PS

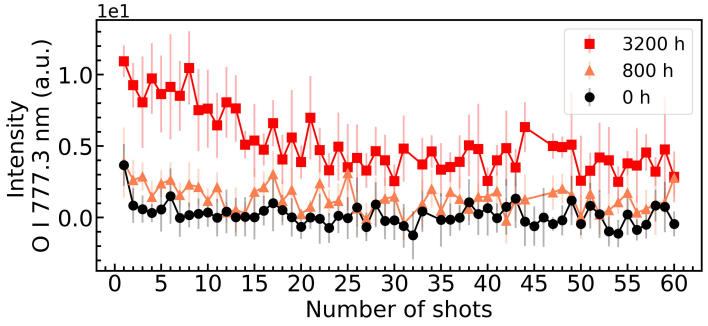

(c) PE

Figure S5: Depth profile of PP, PS, and PE with all shots. The plot shows the course of oxidation with an increasing number of shots inside the samples.

S6. Alternative evaluation of the LIBS data

The LIBS data can also be evaluated using the maximum value of the peak area between 775.5 nm and 778 nm. The evaluation follows the same procedure as described in chapter 2.3 with the difference that only the peak maximum is used as input value and no signal-to-noise ratio is calculated. The corresponding surface and depth profile analyses can be seen in Figs. S6 and S7.

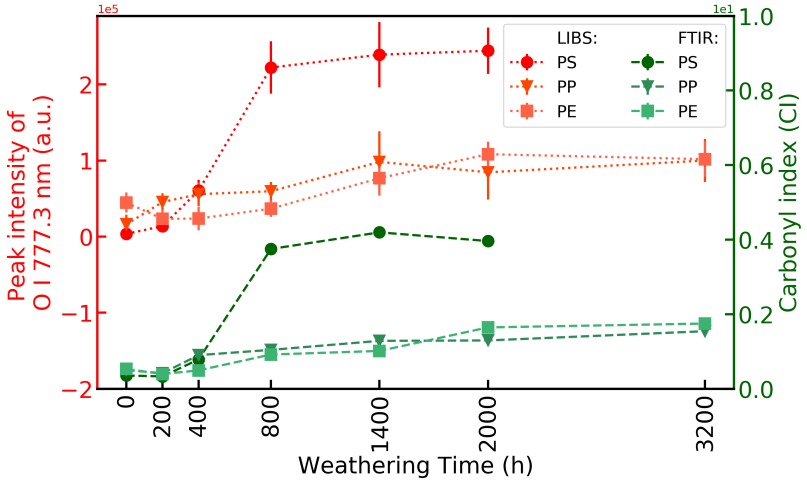

Figure S6: Oxygen intensity for different weathering times. The plot shows the degree of oxidation detected in the LIBS measurements (oxygen intensity at 777.3 nm is displayed on the left axis) and the FTIR measurements (the sum of carbonyl compounds normalized to a reference bond is displayed on the right axis). With increasing weathering time, the oxidation on the surface of all samples progresses. Each LIBS data point is an average of ten measurements. Each FTIR data point is the average of 16 measurements. The average value is depicted as a symbol while the standard deviation is represented as a line.

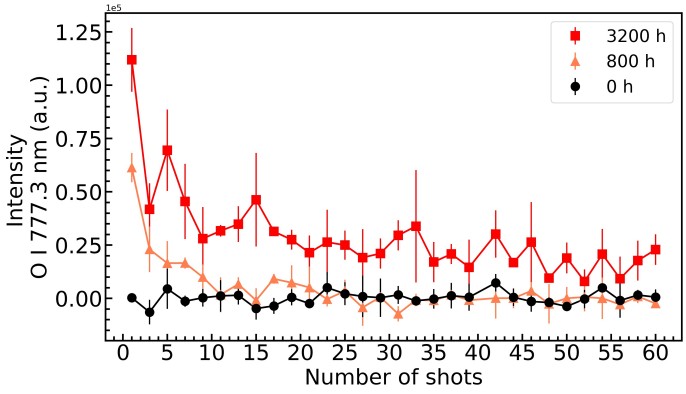

(a) PP

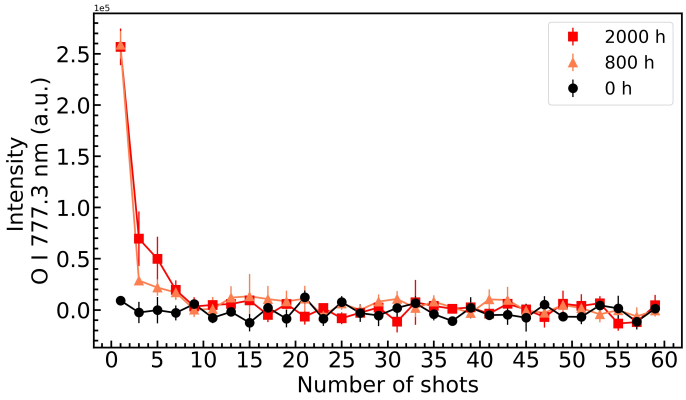

(b) PS

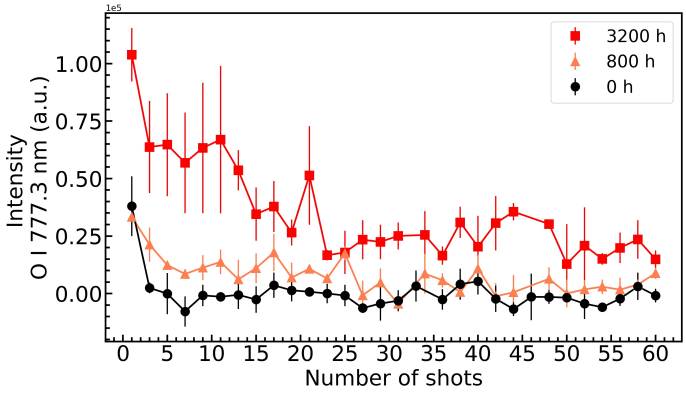

(c) PE

Figure S7: Heterogeneous oxidation profiles for different plastic types up to 3200 hours of weathering. (a), (b), and (c) show the oxygen intensity with an increasing number of shots for PP, PS, and PE, respectively. For visualization reasons, every second laser shot was omitted from the plot. The complete depth profiles can be found in the supporting information. Each data point is the average over three measurements. The average is depicted as a symbol and the standard deviation as a line.

S7. FTIR spectra

The FTIR data that is used for validating the LIBS measurements are presented in Fig. S8. The CI value has been calculated as described in chapter 2.6. For the grey areas, the sum of the data has been calculated and used as a value for the corresponding peak. Note that in the carbonyl region for PE, the unweathered sample shows a small increase. This small increase is in accordance with the LIBS results (cf. chapter 3.1).)

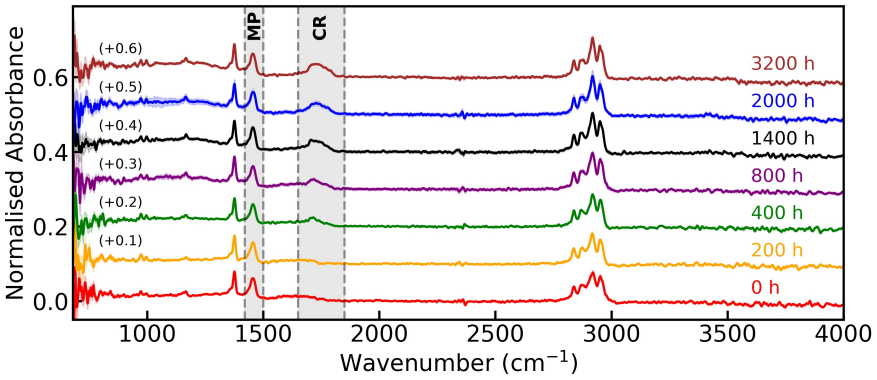

(a) PP

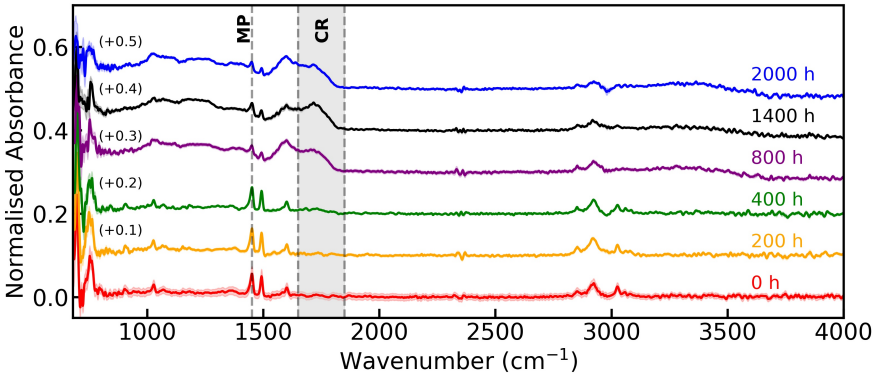

(b) PS

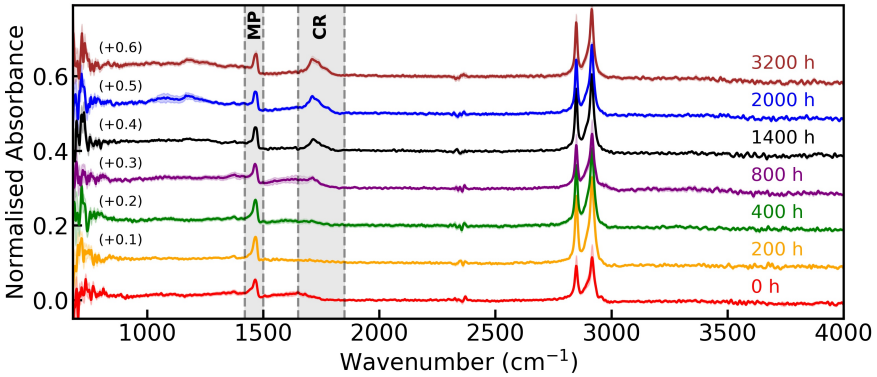

(c) PE

Figure S8: FTIR spectra of weathered PP, PS, and PE samples. The spectra are the average over 16 spots (the average value is depicted as a line, and the standard deviation is depicted as a light background) and smoothed for CO_2 and hydrogen bands. The dashed lines and the grey areas mark the values used for the analysis (cf. section 2.6). Here, MP and CR stand for methylene peak and carbonyl region, respectively. For visualization reasons, the data is plotted with an offset.

References

[1] L. Brunnbauer, M. Mayr, S. Larisegger, M. Nelhiebel, L. Pagnin, R. Wiesinger, M. Schreiner, A. Limbeck, Combined la-icp-ms/libs: powerful analytical tools for the investigation of polymer alteration after treatment under corrosive conditions, Scientific Reports 10 (2020) 1–10.